EMIM2010 is the 5th annual meeting of the European Society for Molecular Imaging - **ESMI**. The EMIM2010 is also the final meeting of the European network of excellence DiMI - Diagnostic Molecular Imaging, and is organised in collaboration with the ESR - European Society of Radiology, the European network of excellence CliniGene – Clinical Gene Transfer and Therapy, and is also supported through COST actions D38 and BM0607 – the European cooperation in science and technology.

committees

5th EMIM EXECUTIVE COMMITTEE

Andreas H. Jacobs, ESMI President
Renata Mikołajczak, Local Organiser
Clemens W.G.M. Löwik, ESMI Vice President
Bertrand Tavitian, ESMI Past President
Silvio Aime, ESMI Secretary
Simone Mergui, ESMI Treasurer

LOCAL ORGANIZING COMMITTEE

Iliana Chwalinska, Warsaw (P)
Eugeniusz Dzuik, Warsaw (P)
Izabela Kozlowicz-Gudzinska, Warsaw (P)
Leszek Krolicki, Warsaw (P)
Renata Mikolajczak, Warsaw (P)

5th EMIM SCIENTIFIC COMMITTEE

Ludwig Aigner, Salzburg (A)
Silvio Aime, Torino (I)
Veerle Baekelandt, Leuven (B)
Hervé Boutin, Manchester (Uk)
Harald Carlsen, Oslo (N)
John Clark, Edinburgh (Uk)
Marion Dejong, Rotterdam (Nl)
Silvana Del Vecchio, Naples (I)
Frédéric Dollé, Orsay (F)
Eugeniusz Dzuik, Warsaw (Pl)
Cornel Fraefel, Zuerich (Ch)
Jorgen Frokiaer, Aarhus (Dk)
Nicolas Grenier, Bordeaux (F)
Denis Guilloteau, Tours (F)
Uwe Haberkorn, Heidelberg (D)
Mathias Höhn, Cologne (D)
Andreas H. Jacobs, Münster (D)
Fabian Kiessling, Aachen (D)
Izabela Kozlowicz-Gudzinska, Warsaw (P)
Leszek Krolicki, Warsaw (Pl)
Tony Lahoutte, Jette (B)
Adriaan Lammertsma, Amsterdam (Nl)
Bengt Långstrom, (S)
Clemens W.G.M. Löwik, Leiden (Nl)
Helmut R. Maecke, Freiburg (Ch)
Adriana Maggi, Milano (I)
Serge Maitrejean, Paris (F)
Renata Mikolajczak, Warsaw (P)
Chrit Moonen, Bordeaux (F)
Klaas Nicolay, Eindhoven (Nl)
Vasilis Nziachristos,Munich (D)
Sabina Pappata, Naples (I)
David Parker, Durham (Uk)
Bernd PIchler, Tübingen (D)
Anna Planas, Barcelona (E)
Juha Rinne, Turku (Fin)
Jorge Ripoll, Heraklion (Gr)
Markus Rudin, Zürich (Ch)
Michael Schäfers, Münster (D)
Markus Schwaiger, Munich (D)
Bertrand Tavitian, Orsay (F)
Eva Tóth, Orleans (F)
Annemie Van Der Linden, Antwerp (B)
David Wyper, Glasgow (Uk)

5th EMIM Young Investigator Award SELECTION COMMITTEE

Veerle Baekelandt
Hervé Boutin
Peter Brader
John Clark (Chair)
Frédéric Dollé
Nicolas Grenier
Fabian Kiessling
Adriaan Lammertsma
Renata Mikolajczak
Chrit Moonen
Klaas Nicolay
Markus Schwaiger
Bertrand Tavitian (Chair)
Eva Tóth
David Wyper

content – per topic

overview oral presentations – per title

Day 0 - Wednesday May 26, 2010

Day 1 - Thursday May 27, 2010

Day 2 - Friday May 28, 2010

Parallel Session 5: NEUROSCIENCE II

Parallel Session 6: CARDIOVASCULAR I - together with the ESR

Parallel Session 7: PROBES II - together with the EANM

Parallel Session 8: Gene and cell based therapies - together with CliniGene

ESMI Plenary Lecture 4 by Hans-Jürgen Wester

Plenary Session on Current Contribution of Imaging Technologies to Drug Development

Day 3 - Saturday May 29, 2010

ESMI Plenary Lecture by Jagat Narula

Parallel Session 9: CARDIOVASCULAR II

Parallel Session 10: CANCER II - supported by COST actions

Welcome to the 5th EMIM in Warsaw, Poland

Dear Colleagues,

on behalf of the ESMI as well as the other organising and contributing societies and networks it is our great pleasure to welcome you to Warsaw, Poland, for the 5th European Molecular Imaging Meeting. EMIM 2010 brings together top European scientists from 3 societies, 2 European Networks of Excellence (NoEs) and 2 COST actions. With great honour we may state that your fellow attendees represent not only colleagues from all over Europe, but also Asia and the US.

The societies and networks with primary responsibility for organising the meeting are:

- European Society for Molecular Imaging – ESMI
- NoE Diagnostic Molecular Imaging – DiMI
- European Cooperation in Science and Technology – COST Actions D38 and BM0607
- European Society of Radiology – ESR
- We also gratefully acknowledge the contribution from the following participating organisations:
- European Association of Nuclear Medicine – EANM
- NoE Clinical Gene Transfer and Therapy – Clinigene

All these organisations were working together, with input from a scientifically complementary scientific steering committee, to develop a strong scientific programme which integrates developments in imaging technologies and molecular imaging agents with applications for drug development, basic science investigations, and clinical translation with special emphasis in the main disease burdens of our society such as cancer, cardiovascular disease and neurodegeneration.

We developed the 5th EMIM scientific programme primarily on the outstanding strength of submitted abstracts. About 150 abstracts were submitted, reviewed and scored. Then, each of the concurrent session co-chairs reviewed the scored abstracts which were considered relevant to their particular sessions. Session co-chairs selected abstracts for oral presentation based on average abstract score, session content and structure. Attention was also paid to diversity of disciplines and geographical distribution. From this effort 39 abstracts were integrated into the Parallel as well as Plenary Sessions that bring attendees from different disciplines together for a comprehensive examination of the role of molecular imaging in particular biomedical problems. 21 of these oral abstract presentations will be held by Young Investigator Award (YIA) applicants. The YIA selection committee is going to select the best 3 YIA presentations to be held again during the final Plenary Session on Saturday where then THE Young Investigator Awardee will be announced. Furthermore, special attention has been put on seven guided poster walks which have been scheduled on Thursday and Friday afternoon with no other competing sessions in order to enhance the knowledge exchange of experienced and young researchers. Each of the guided poster walks will be chaired by two chairs and will result in one poster award. The seven Poster Awards will also be offered during the Closing Ceremony on Saturday.

We are especially proud and thankful that Prof. Dr. Christopher Contag will give the inaugural lecture, entitled, *"Point-of-care microscopy: molecular imaging with cellular resolution"*. In addition, we have planned 5 exciting plenary lectures, covering topics on probe design, systems biology, cancer, neuroinflammation, and atherosclerosis. Furthermore, we have dedicated one Plenary Session each to Excellent, Late Breaking, and YIA Abstracts as well as to Current Contribution of Imaging Technologies to Drug Development.

We would like to take this opportunity to acknowledge the support of this year's sponsors of the conference, especially recognizing the continued interest and support from DG Research of the European Commission. Moreover we would like to thank YOU for participating in this year's EMIM and making it possible by your attendance. We hope you will enjoy the conference. If this is not your first time attending an EMIM conference then welcome back and we hope you will establish new contacts and continue to expand your network of scientific excellence. Please help first-time attendees to meet others and generally make people feel at home. Regardless whether this is your first time with us or not we will endeavour to have you come back again in the future.

As in previous years our intention is that this high-level meeting will foster the coherence of a sustainable European Molecular Imaging Community with the common goal to translate fundamental research discoveries into medical application and health benefit for the European Society.

Sincerely,

The 5th European Molecular Imaging Meeting Executive Committee

Andreas H. Jacobs, ESMI President
Renata Mikołajczak, Local Organiser
Clemens W.G.M. Löwik, ESMI Vice President
Bertrand Tavitian, ESMI Past President
Silvio Aime, ESMI Secretary
Simone Mergui, ESMI Treasurer

Dear Colleagues,

it is a pleasure for me to welcome you to the 5th European Molecular Imaging Meeting in Warszawa. With an impressive history of previous successful meetings, this time the European Society of Molecular Imaging decided in favour for Poland, the country belonging to East as well as to Central Europe.
In some way this *in-between-situation* is also characteristic for the field of MI: the discipline MI is not defined by a profession, no one is automatically a MI professional. Molecular Imaging is multidisciplinary. This makes it on the one hand difficult: we have to define ourselves and the direction of our research; it forces us to look beyond our bench and own disciplines. On the other hand this is also the advantage of MI: it means at any time to be in process, be in cross-communication and stay open-minded.

Me and my colleagues involved in the organisation of this meeting believe that it will strengthen Molecular Imaging research activities within Eastern and Central Europe, as well as between the various disciplines working in the broad field of MI.

The efforts of the ESMI to provide a platform for exchange have started to lead into the formation of a European MI community. This is just the beginning of our common efforts and with our activities and willingness for cross-interaction we can further establish this development.
We hope that the familiar arrangement of the meeting venue will create a friendly atmosphere and provide a maximum of opportunities for you to meet friends and exchange views. Enjoy the interesting scientific programme of invited talks, oral and poster presentations as well as the technical exhibition. I also want to say thanks to the companies who are supporting this meeting and the MI community; especially to those who come to Warszawa.

Do not forget that Warszawa is a lively city, with a number of historical sites, museums and parks. We are also in the year of Chopin; you can find a lot of information about his music and places he used to live. Take some time to immerse yourself in the history of the city.

On behalf of local organizing committee I wish your visit to Warszawa will be informative, interesting and enjoyable.

Sincerely,

Renata Mikołajczak, Local Organiser

Dear Ladies and Gentlemen,

It is my great pleasure to welcome you to the 5th annual meeting of the European Society for Molecular Imaging. In my capacity as president of the European Society of Radiology I would like to thank the organisers of this important event that has been organised in close cooperation with the ESR for their kind invitation.

It is an honour to be here today as the ESR has supported the creation of the European Society for Molecular Imaging from the very beginning and many ESR representatives have been and are still represented in this organisation. We are looking forward to enhancing the successful cooperation between the European Society for Molecular Imaging and the European Society of Radiology in the future.

Realising the importance of molecular imaging, latest research discoveries in this field and possible translations into medical practice, I will reinforce the topic of molecular imaging within the European Society of Radiology during my presidency and make sure that the work of all ESR bodies is coordinated with a special focus on this issue.

I would also like to take this opportunity to invite you all to attend ECR 2011 from March 3 to 7 in Vienna, Austria. The ESR would be most happy to welcome you at its annual meeting.

I thank you for having taken the time to be with us in Warsaw this week and I wish you a most successful meeting.

Sincerely,

Professor Maximilian F. Reiser, ESR President

Why Warsaw?

Warsaw, the capital of Poland, a captivating city with a distinctive atmosphere and definitely worth visiting. Warsaw is a perfect embodiment of changes that have taken place in Poland in the past 20 years. It is a city of many faces - a contrasting blend of historical and socrealist buildings neighbouring post-modern skyscrapers, of cosy cafes and vibrant clubs, of historical Żoliborz and artistic Praga district, but most of all it is a thriving European capital. Whether you come to Warsaw on a business trip, for a conference, or as a tourist, Warsaw will definitely exceed your expectations.

Novotel Warsawa Centrum

Marszałkowska 94/98, 00-510 Warszawa

Tel: +48 22 596 25 48 | Fax: +48 22 596 01 22

The Novotel Warsawa Centrum hotel provides excellent conference facilities. Close to the iconic Palace of Culture and Science and 500 m from the railway station with a convenient connection to the airport. The plenary lectures will take place in ROZA and IRYS, the parallel sessions will take place in ROZA or IRYS. Visit the exhibition in LILIA, FREZJA as well as in the FOYER; and get in communication! The poster sessions will take place in PROMENADA. You are mostly welcome to view the posters also besides of the "official" poster sessions.

How to get there

From OKECIE Airport, take bus route No.175 to Centrum. From Warszawa Centralna railway station take tram No.7, 8, 9, 22, 24 or 25 to Centrum (one stop). Via the E30, E77 or E67 highways, head in the direction of Centrum. By metro, alight at Centrum.

Airport : WARSZAWA OKECIE AIRPORT
Railway Station : WARSZAWA CENTRALNA STATION

The Gala dinner will take place on Friday May 28, 2010 at Zamojski Palace Warsaw 2, Foksal street. Zamojski Palace is within walking distance. Looking forward to meeting you there.

Floor plan

1. GEHC
2. ART
3. BIOSCAN/PHILIPS
4. ZINSSER ANALYTIC
5. CaliperLS
6. MR solutions
7. Carestream
8. BRUKER
9. VISUALSONICS
10. SIEMENS
11. BIOSPACE LAB
12. LOT-Oriel
13. CT Imaging
14. SEDECAL
15. VisEn
16. LI-COR
17. SKYSCAN/MILabs
18. Polatom
19. information

This meeting would not have been possible without your support.

WMIC 2010 Speakers

Keynote Address by Shizuo Akira, MD, PhD

Professor of Department of Host Defense, Research Institute for Microbial Diseases and Director of the WPI Immunology Frontier Research Center (WPI-IFReC), Osaka University

Featured Plenary Speakers

Kevin Brindle, PhD
Professor, Dept of Biochemistry
University of Cambridge

Robert J. Gropler, MD
Chief, Cardiovascular Imaging Center,
Mallinckrodt Institute of Radiology

Gregory Lanza, MD, PhD
Professor of Medicine
Div. of Cardiovascular Diseases
Washington University School of Medicine

Herman P. Spaink, PhD
Professor of Molecular Cell Biology
Leiden University

Jun Takahashi, MD, PhD
Associate Professor
Center for iPS Cell Research and Application (iCeMS)
Kyoto University, Japan

Scientific Sessions

Preliminary List. For full list, visit our website.

In Vivo Studies
* Clinical Studies
* Translational Studies
* Animal Models

Imaging Instrumentation and Methodology
* Hybrid & Multimodality Imaging
* Magnetic Resonance Imaging
* Optical and Opto-acoustic Imaging
* PET/SPECT/CT Imaging
* Ultrasonic Imaging & Drug Delivery

Development/Novel Use of Imaging Probes
* CT
* MRI
* Multi-modality
* Optical and Photoacoustic
* PET/SPECT
* Ultrasound

Imaging Disease/Organ Processes
* Cancer
* Cardiovascular System
* Central Nervous System
* Immune System

Drug and/or Radiation Therapy
* Image Guided Therapy
* Monitoring Therapy
* Novel Therapy Development

REGISTER NOW
September 8-11, 2010
Kyoto, Japan
www.WMICmeeting.org

The Society for Molecular Imaging · AMI Academy of Molecular Imaging · FASMI · esmi European Society for Molecular Imaging · ISMRM International Society for Magnetic Resonance in Medicine · RSNA · SNM Advancing Molecular Imaging and Therapy

	Wednesday - 26 May 2010		Thursday - 27 May 2010		Friday - 28 May 2010		Saturday - 29 May 2010	
room	ROZA	IRYS	ROZA	IRYS	ROZA	IRYS	ROZA	IRYS
08:00-09:00			Registration		Registration			
09:00-10:00			ESMI Plenary Lecture 1 by Violaine Sée (Liverpool, UK)		ESMI Plenary Lecture 3 by Theodorus W.J.Gadella (Amsterdam, The Netherlands)		ESMI Plenary Lecture 5 by Klaas Nicolay (Eindhoven, The Netherlands)	
10:00-10:30			Coffee break & Exhibition		Coffee break & Exhibition			
10:30-12:00			PS 1: Cancer I - together with ESR	PS 2: Neuroscience I	PS 5: Neuroscience II	PS 6: Cardiovascular I - together with ESR	PS 9: Cardiovascular II	PS 10: Cancer II - together with COST
12:00-13:00			Lunch break & Exhibition				Break	
13:00-14:30			PS 3: Technology	PS 4: Probes I - together with COST	PS 7: Probes II	PS 8: Gene and Cell Based Therapies - together with CliniGene	12:30-13:30 ESMI Plenary Session and Closing Ceremony	
14:30-16:00	Registration		Guided Poster Session 1 with Coffee break		Guided Poster Session 2 with Coffee break			
16:00-17:00			ESMI Plenary Lecture 2 by Francesca Odoardi (Goettingen, Germany)		ESMI Plenary Lecture 4 by Hans-Jürgen Wester (Munich, Germany)			
17:00-18:00			ESMI Plenary Session on Excellent, Late Breaking and YIA Abstracts		ESMI Plenary Session on Current Contribution of Imaging Technologies to Drug Development			
18:00-19:30	Open Ceremony and Inaugural Lecture by Christopher H. Contag (Stanford, USA)				ESMI Executive Committee meets Industry			
19:00			Sightseeing Tour					
19:30	Opening Reception and Exhibition				Gala Dinner at Zamojski Palace Warsaw 2, Foksal street			

Day 0 - Wednesday May 26, 2010

	ROZA	IRYS	GERBERA
09:00-12:00	Exhibitor's set up		DiMI WP Meetings (Closed Meetings)
14:00-18:00	**Registration**		
	Posters set up Speaker's documents set up		
13:00-15:00			ESMI Executive Committee (Closed Meeting)
15:00-17:00			ESMI Council Meeting (Closed Meeting)
18:00-19:30	**Opening Ceremony and Inaugural Lecture**		
	Mariusz Klubczuk plays Chopin: *Nocturne B flat Minor Op.9 No 1; Mazurka C Major Op.24 No 2* Welcome – **Andreas H. Jacobs** (ESMI President) Welcome – **Renata Mikolajczak** (EMIM Local Organiser) Welcome – **Andrzey Siemaszko** (NCP in Poland for EU research) Welcome – **Maximilian Reiser** (ESR President) Announcement of ESMI Award 2010, **John Clark** (ESMI Award Winner 2009) **Mariusz Klubczuk** plays Chopin: *Etude C sharp Minor Op. 25 No 7; Etude A Minor Op. 25 No 12* Inaugural lecture by **Christopher H. Contag** (Stanford, USA) *Point-of-Care Microscopy: Molecular Imaging with Cellular Resolution*		
19:30-21:00	**Opening Reception and Exhibition**		

Day 1 - Thursday May 27, 2010

	ROZA	IRYS	GERBERA
08:00-08:45			DiMI SMB (Closed Meeting)
08:00-09:00	**Registration**		
09:00-10:00	**ESMI Plenary Lecture 1 by Violaine Sée (Liverpool, UK)** *Transcription factors dynamics: from discrete pulses to oscillatory pattern to control gene expression* Co-Chairs: Clemens WGM Löwik (Leiden, The Netherlands), Leszek Krolicki (Warsaw, Poland)		
10:00-10:30	**Coffee break & Exhibition**		YIA Selection Committee (Closed Meeting)
10:30-12:00	**Parallel Session 1: Cancer I (together with ESR)** Co-Chairs: Markus Schwaiger (Munich, Germany), Peter Brader (Vienna, Austria)	**Parallel Session 2: Neuroscience I** Co-Chairs: Annemie van der Linden (Antwerp, Belgium), David Wyper (Glasgow, UK), Hervé Boutin (Manchester, UK)	
10:30-10:45	Multimodal imaging approaches for cell-cell interaction Steffen Maßberg, (Munich, Germany)	[11C](R)-PK11195- a tricky tracer. Do we really need it to image microglial activation? Alex Gerhard (Manchester, UK)	
10:45-11:00	Molecular imaging for monitoring treatment with protein kinase inhibitors Wolfgang Weber (Freiburg, Germany)	YIA Applicant's Presentation: Preclinical imaging of the type 1 cannabinoid receptor in neurodegenerative diseases Cindy Casteels (Leuven, Belgium)	
11:00-11:15	Potentials of imaging biomarkers inpatients Bernard Van Beers (Paris, France)	YIA Applicant's Presentation: Longitudinal non-invasive detection of amyloid plaques by combined molecular, functional and morphological imaging in transgenic mouse models of alzheimers disease, Florian C. Maier (Tübingen, Germany)	
11:15-11:30	YIA Applicant's Presentation: Pre-clinical screening of anti - her2 nanobodies for molecular imaging of breast cancer Ilse Vaneycken (Brussels, Belgium)	Serotonergic neurotransmission in early Alzheimer's disease, Steen G. Hasselbalch (Copenhagen, Denmark)	
11:30-11:45	YIA Applicant's Presentation: [18f]-fdg/[18f]-flt-pet and bioluminescence imaging of therapy response in b-cell lymphoma mice treated with cytotoxic and antiproliferative agents, Marijke De Saint-Hubert (Leuven, Belgium)	Qualitative and quantitative assessment of florbetapir f-18 pet (18f-av45) amyloid deposition PET imaging - validation by pathology. preliminary report Grzegorz Romanowicz (Gdańsk, Poland)	
11:45-12:00	tf-pimonidazole: an hypoxia marker suitable for *in vivo* 19f mrs imaging Arend Heerschap (Nijmegen, The Netherlands)	YIA Applicant's Presentation: In-vivo imaging of a mouse traumatic brain injury model using dual-isotope quantitative SPECT/CT Domokos Máthé (Budapest, Hungary)	
12:00-13:00	**Lunch break**		TOPIM2011 committee (Closed meeting)

	ROZA	IRYS	GERBERA
13:00-14:30	**Parallel Session 3: Technology** Co-Chairs: Jorge Ripoll (Heraklion, Greece), Markus Rudin (Zürich, Switzerland)	**Parallel Session 4: Probes I (together with COST action D38)** Co-Chairs: Eva Jakab-Tóth (Orléans, France), Silvio Aime (Torino, Italy)	
13:00-13:15	Molecular analysis of adaptive immune function through microscopic and mesoscopic imaging Jens Stein (Bern, Switzerland)	The alignment of target-specific lipoCEST MRI contrast agents Sander Langereis (Eindhoven, The Netherlands)	
13:15-13:30	Magnetic resonance imaging – from structure to molecular interactions Markus Rudin (Zürich, Switzerland)	Lanthanide-based *in vivo* luminescence imaging Stephane Petoud (Orléans, France and Pittsburgh, US)	
13:30-13:45	Imaging modalities: PET/SPECT Sibylle Ziegler (Munich, Germany)	New perspectives for imaging molecules and metabolism *in vivo* Rolf Gruetter (Lausanne, Switzerland)	
13:45-14:00	*In vivo* fluorescence kinetic imaging for improved contrast and studies of temporal and quantitative biodistribution James Mansfield (Cambridge, UK)	YIA Applicant's Presentation: *In vivo* biodistribution of radiolabeled matrix metalloproteinase-2 activatable cell penetrating peptides Sander Van Duijnhoven (Eindhoven, The Netherlands)	
14:00-14:15	Cerenkov radiation imaging of a xenograft murine model of mammary carcinoma Federico Boschi (Verona, Italy)	YIA Applicant's Presentation: Bioresponsive mri contrast agents based on self-assembling beta-cyclodextrin nanocapsules Jonathan Martinelli (Alessandria, Italy)	
14:15-14:30	A system for 4d (3d+kinetics) molecular imaging in bioluminescence and fluorescence Serge Maitrejean (Paris, France)	Photochemical activation of endosomal escape of MRI-gd-agents in tumor cells Eliana Gianolio (Torino, Italy)	
14:30-16:00	**Guided Poster Session 1 with Coffee break (see page 110)** **Poster Walk 1: Imaging Cancer Biology (P001-P012) & (P105-P106)** Co-Chairs: Fabian Kiessling (Aachen, Germany), Markus Rudin (Zürich, Switzerland) **Poster Walk 2: Technology & Data Analysis Methods (P070-P078) & (P097-P104)** Co-Chairs: Serge Maitrejean (Paris, France), Adriaan Lammertsma (Amsterdam, The Netherlands) **Poster Walk 3: Molecular Neuroimaging (P034-P047) & (P107)** Co-Chairs: Sabina Pappata (Naples, Italy), Andreas H. Jacobs (Münster, Germany) **Poster Walk 4: Probe Design (P058-P069)** Co-Chairs: Frédéric Dollé (Orsay, France), Helmut Maecke (Freiburg, Germany)		
16:00-17:00	**ESMI Plenary Lecture 2 by Francesca Odoardi (Göttingen, Germany)** *Immune surveillance and autoimmunity: how encephalitogenic T cells enter their target organ* Co-Chairs: Renata Mikolajczak (Warsaw, Poland), Chrit Moonen (Bordeaux, France)		
17:00-18:00	**Plenary Session on Excellent, Late Breaking, and Young Investigator Award Abstracts** Co-Chairs: Renata Mikolajczak (Warsaw, Poland), Chrit Moonen (Bordeaux, France)		
17:00-17:10	Exendin-4 derivatives labeled with radiometals for the detection of insulinoma: a "from bench to bed approach" Damian Wild (Freiburg, Germany)		
17:10-17:20	YIA Applicant's Presentation: Assessment of hif transcriptional activity in a mouse tumor model using gpi anchored avidin- a novel protein reporter for *in vivo* imaging Steffi Lehmann (Zürich, Switzerland)		
17:20-17:30	YIA Applicant's Presentation: A leukocyte ligand of vascular adhesion protein-1 as an imaging tool in PET Anu Autio (Turku, Finland)		
17:30-17:40	YIA Applicant's Presentation: Clinical translation of ex vivo sentinel lymph node mapping for colorectal cancer using invisible near-infrared fluorescence light Merlijn Huttemann (Leiden, The Netherlands)		
17:40-17:50	YIA Applicant's Presentation: Development of strategies for *in vivo* MRI and optical imaging of neural stem cells distribution for the treatment of traumatic spinal cord injury Ramona Lui (Milano, Italy)		
17:50-18:00	Validation of bone marrow-derived stromal cell graft position by colocalisation of histology, bioluminescence and magnetic resonance imaging Nathalie de Vocht (Antwerp, Belgium)		
18:15-18:45	DiMI General Assembly (Closed Meeting)		
19:00-20:00	DiMI WP Meeting (Closed Meeting)		DiMI WP Meeting (Closed Meeting)

Day 2 - Friday May 28, 2010

	ROZA	IRYS	GERBERA
08:00-08:45	DiMI WP Meeting (Closed Meeting)		ESMI Exec. Com. & ESMI Council Meeting (Closed Meeting) together with Treasurer
08:00-09:00	**Registration**		
09:00-10:00	**ESMI Plenary Lecture 3 by Theodorus W.J. Gadella Jr. (Amsterdam, Netherlands)** *New probe-based strategies for quantitative microscopy of signaling dynamics in single cells* **Co-Chairs:** Vasilis Nziachristos (Munich, Germany), Bengt Långström (Uppsala, Sweden)		
10:00-10:30	**Coffee break & Exhibition**		
10:30-12:00	**Parallel Session 5: Neuroscience II** Co-Chairs: Markus Rudin (Zürich, Switzerland), Veerle Baekelandt (Leuven, Belgium), Mathias Hoehn (Cologne, Germany)	**Parallel Session 6: Cardiovascular I (together with ESR)** Co-Chairs: Tony Lahoutte (Mons, Belgium), Nicolas Grenier (Bordeaux, France)	
10:30-10:45	Potential to use transgenic animals for imaging of neurological diseases Ludwig Aigner (Salzburg, Austria)	Potentials of new contrast agents for vascular molecular imaging in patients Philippe Douek (Lyon, France)	
10:45-11:00	Specific cell labeling with imaging reporters *in vivo* by viral vectors: the challenges Veerle Baekelandt (Leuven, Belgium)	Protease specific nanosensors in atherosclerosis Eyk Schellenberger (Berlin, Germany)	
11:00-11:15	YIA Applicant's Presentation: Optimization of an MRI method to measure microvessel density: application to monitor angiogenesis after stroke Philipp Boehm-Sturm (Cologne, Germany)	YIA Applicant's Presentation: Imaging of inflamed carotid artery atherosclerotic plaques with the use of 99mtc-hynic-il-2 scintigraphy in the end-stage renal disease patients Marta Opalinska (Krakow, Poland)	
11:15-11:30	MRI study of intra-arterial bone marrow-derived macrophage administration after acute focal ischemic stroke in rats Adrien Riou (Lyon, France)	Uptake of 68ga-chloride in atherosclerotic plaques of ldlr-/-apob100/100mice Johanna Silvola (Turku, Finland)	
11:30-11:45	YIA Applicant's Presentation: Inactivated paramagnetic tissue plasminogen activator predicts thrombolysis outcome following stroke Maxime Gauberti (Caen, France)	YIA Applicant's Presentation: Hybrid imaging using dual energy µct and fmt for characterization of atherosclerotic plaques in apoe -/- mice Felix Gremse (Aachen, Germany)	
11:45-12:00	Matrix metalloproteinase-9 – a possible therapeutic target in intractable epilepsy Grzegorz Wilczynski (Warsaw, Poland)	YIA Applicant's Presentation: Long circulating emulsion based CT contrast agents Anke De Vries (Eindhoven, The Netherlands)	
12:00-13:00	**Lunch Break**		ESMI Training Committee (Closed Meeting)
13:00-14:30	**Parallel Session 7: Probes II (together with EANM)** Co-Chairs: Frédéric Dollé (Orsay, France) , Denis Guilloteau (Tours, France)	**Parallel Session 8: Gene and Cell Based Therapies (together with Clinigene)** Co-Chairs: Ludwig Aigner (Salzburg, Austria), Cornel Fraefel (Zürich, Switzerland)	
13:00-13:15	Application of microfluidics to the ultra-rapid preparation of fluorine-18 and carbon-11 labelled compounds Philip Miller (London, UK)	Everything but not cell replacement with neural stem cell transplants Stefano Pluchino (Milano, Italy)	
13:15-13:30	Radioligand for in vivo measuring neurotransmitters release, Christer Halldin (Stockholm, Sweden)	Mesenchymal Stem Cell Transplantation: An Option to Promote Remyelination? Ludwig Aigner (Salzburg, Austria)	
13:30-13:45	18F-tracers for Amyloid plaques Denis Guilloteau (Tours, France)	Viral vector-mediated transcriptional targeting of dendritic cells for antigen-specific tolerance induction in EAE/MS Christiane Dresch (Zürich, Switzerland)	
13:45-14:00	YIA Applicant's Presentation: Chelators for radiocopper: biological/ pharmacokinetic differences of [tyr3,thr8]octreotide conjugates, Abiraj Keelara (Basel, Switzerland)	Delivery of a bioluminescent transgene to a tumor via bone marrow engraftment and local control of gene expression by non invasive local hyperthermia Pierre-Yves Fortin (Bordeaux, France)	
14:00-14:15	[11c]SOMADAM: potential sert ligand for PET studies and comparison with [11c]MADAM Fabienne Gourand (Caen, France)	YIA Applicant's Presentation: Dendritic cell labelling with paramagnetic nanoparticles and 111in-oxine for in vivo magnetic resonance imagingand scintigraphic imaging Cristina Martelli (Milan, Italy)	
14:15-14:30	MR imaging of extracellular redox by a thiolsensitive gd(iii)-do3a derivative Giuseppe Digilio (Torino, Italy)	YIA Applicant's Presentation: The type 2 cannabinoid receptor as a new PET reporter gene for the brain Caroline Vandeputte (Leuven, Belgium)	

	ROZA	IRYS	GERBERA
14:30-16:00	**Guided Poster Session 2 with Coffee break (see page 110)** **Poster Walk 5: Imaging in Cancer & Drug Development (P013-P030)** Co-Chairs: Peter Brader (Graz, Austria), Nicolas Grenier (Bordeaux, France) **Poster Walk 6: Imaging in Other Diseases (P031-P033) & (P079-P091)** Co-Chairs: Bertrand Tavitian (Orsay, France), John Clark (Edingburgh, UK) **Poster Walk 7: Imaging-guided Gene and Cell based and Targeted Therapies (P048-P057) & (P092-P096)** Co-Chairs: Ludwig Aigner (Salzburg, Austria), Adriana Maggi (Milano, Italy)		
16:00-17:00	**ESMI Plenary Lecture 4 by Hans-Jürgen Wester (Munich, Germany)** *Molecular Imaging of CXCR4 Receptors* Co-Chairs: Adriana Maggi (Milano, Italy), Adriaan Lammertsma (Amsterdam, The Netherlands)		
17:00-18:00	**Plenary Session on Current Contribution of Imaging Technologies to Drug Development** Co-Chairs: Adriana Maggi (Milano, Italy), Adriaan Lammertsma (Amsterdam, The Netherlands)		
17:00-17:15	Evaluation of the temporal window for drug delivery following ultrasound mediated membrane permeability enhancement Matthieu Lepetit-Coiffe (Bordeaux, France)		
17:15-17:30	Integrisense: a novel near-infrared fluorescent probe for a_vb_3 integrin and its applications in drug discovery Cyrille Sur, Merck Research Laboratories (Westpoint, USA)		
17:30-17:45	Harnessing the power of bioluminescence to cross the *in vitro–in vivo* divide John Watson, PROMEGA (Madison, Wisconsin, USA)		
17:45-18:00	*In vivo* imaging in drug discovery: the example of application in the development of novel estrogenic compounds Andrea Biserni, TOP Srl (Milano, Italy)		
18:00-19:00			**ESMI Executive Committee meets Industry (Closed Meeting)**
19:30	**Gala Dinner at Zamojski Palace**		

Day 3 - Saturday May 29, 2010

	ROZA	IRYS	GERBERA
08:00-08:45	ESMI General Assembly (Closed Meeting)		
09:00-10:00	**ESMI Plenary Lecture 5 by Klaas Nicolay** (Eindhoven, The Netherlands) *Multi-modality molecular imaging of atherosclerosis, usingtargeted contrast agents* Co-Chairs: Uwe Haberkorn (Heidelberg, Germany), Helmut Maecke (Freiburg, Germany)		
10:00-10:30	**Coffee break & Exhibition**		YIA Selection Committee
10:30-12:00	**Parallel Session 9: Cardiovascular II** Co-Chairs: Klaas Nicolay (Eindhoven, The Netherlands), Michael Schäfers (Münster, Germany)	**Parallel Session 10: Cancer II(with COST action BM0607)** Co-Chairs: Marion de Jong (Rotterdam, The Netherlands), Fabian Kiessling (Aachen, Germany)	
10:30-10:45	Advances in contrast-enhanced MRI of the mouse heart Gustav Strijkers (Eindhoven, The Netherlands)	Cancer Imaging Uwe Haberkorn (Heidelberg, Germany)	
10:45-11:00	Molecular imaging of $\alpha_v\beta_3$ integrin expression with 18F-galacto-RGD after experimental myocardial infarction: comparison with left ventricular remodeling and function Antti Saraste (Turku, Finland/Munich, Germany)	Controlled Drug Delivery under Image guidance Holger Grüll (Eindhoven, The Netherlands)	
11:00-11:15	Existing and emerging animal models mimicking cardiovascular disease and their relevance for molecular imaging Michael Schäfers (Münster, Germany)	Targeted radionuclide imaging and therapy (COST Action BM0607), Marion de Jong (Rotterdam, The Netherlands)	
11:15-11:30	Imaging of matrix metalloproteinase activity in vulnerable human carotid plaques with multispectral optoacoustic tomography Daniel Razansky (Munich, Germany)	Targeting cancer stem cells using radiolabeled sonic hedgehog, Izabela Tworowska (Houston, USA)	
11:30-11:45	C-jun n-terminal kinase promotes inflammation at atherosclerosis-prone sites by enhancing expression and activity of nf-κb transcription factor Paul Evans (London, UK)	YIA Applicant's Presentation: Evaluation of the photosensitizer bremachlorin for photodynamic treatment of breast cancer bone metastasis Pieter Van Driel (Leiden, The Netherlands)	
11:45-12:00	YIA Applicant's Presentation: Absolute quantification in small animal pinhole gated myocardial perfusion SPECT Lode Goethals (Brussels, Belgium)	*In vivo* targeting of hek-hsst2/3/5 xenografts by 111in-labeled [(dota)ser1,leu8,trp22,tyr25]-ss-28 in scid mice Theodosia Maina (Athens, Greece)	
12:00-12:30	**Break**		YIA Selection Committee
12:30-13:30	**ESMI Plenary Session and Closing Ceremony and Young Investigator Award Presentations** **Young Investigator Awards & Poster Awards Ceremony** Co-Chairs: John Clark (Edinburgh, UK), Bertrand Tavitian (Orsay, France)		

MY NOTES

Do not forget:

Join the next ESMI Winter Conference – TOPIM2011:

HOT TOPIC 2011: Emerging image-guided methods in Medicine

Jan. 16-21, 2011 in Les Houches, France &

further information/pre-registration

send mail to office@ e-smi.eu

WWW.E-SMI.EU

20

Christopher H. Contag

Dr. Contag is an Associate Professor of Pediatrics in the Division of Neonatal and Developmental Medicine, and a member of the BioX faculty at Stanford University. He is the Director of the Stanford Infrared Optical Science and Photomedicine Program, director of Stanford's Center for Innovation in *In Vivo* Imaging (SCI3) and co-director of the Molecular Imaging Program at Stanford (MIPS). Dr. Contag received his B.S. in Biology from the University of Minnesota, St. Paul in 1982; and earned his Ph.D. in Microbiology from the University of Minnesota, Minneapolis in 1988. He was a postdoctoral fellow at Stanford University from 1990-1994, and joined the faculty in Pediatrics at Stanford in 1995 with a joint appointment in Microbiology and Immunology and a courtesy appointment in Radiology.

Dr. Contag is a pioneer in the emerging field of molecular imaging and is developing imaging approaches aimed at revealing molecular processes in living subjects and advancing therapeutic strategies through imaging. His laboratory develops macroscopic and microscopic optical imaging tools and uses imaging to assess tissue responses to stress, reveal immune cell migration patterns, understand stem cell biology and advance biological therapies. He is a founding member, and a past president, of the Society for Molecular Imaging, and for his fundamental contributions in imaging, is a recipient of the Achievement Award from the Society for Molecular Imaging. Dr. Contag is a scientific founder of Xenogen Corp. – now Caliper LifeSciences. He is also a founder of ConcentRx Corp.

Selected References

- Cao, Y-A, Stevenson, DKS, Weissman, I, Contag, CH. 2008. Heme Oxygenase-1 Deficiency leads to disrupted response to acute stress in stem cells and progenitors. Blood. 112: 4494-4502
- Banaszynski, LA, Sellmyer, MA, Thorne, SH, Contag, CH, Wandless, TJ. 2008. Chemical control of protein stability and function in living mice. Nature Med. 14 (10):1123-7.
- Wender, PA, Goun, EA, Jones, LR, Pillow, TH, Rothbard, JB, Shinde, R, Contag, CH. 2007. Real-time analysis of uptake and bioactivatable cleavage of luciferin-transporter conjugates in transgenic reporter mice. Proc Nat Acad Sci, USA. 104(25):10340-5.
- Thorne SH, Negrin, RS, Contag, CH. 2006. Synergistic antitumor effects of immune cell-viral biotherapy. Science. 311:1780-1784.
- Cao, Y-A, Wagers, A, Beilhack, A, Dusich, J, Bachmann, MH, Negrin, RS, Weissman, IL, Contag, CH. 2004. Shifting foci of hematopoeisis during reconstitution from single stem cells. Proc. Natl. Acad. Sci. USA. 101(1):221-226.
- Hardy, JK, Chu, P, Gibbs, K, Contag, CH. 2004. Extracellular replication of Listeria monocytogenes in the gall bladder. Science. 303(5659): 851-853
- Contag, CH and Bachmann, MH. 2004. The writing is on the vessel wall. Nature. 429:618-620.
- Shachaf, CM, Kopelman, A, Arvanitis, C, Beer, S, Mandl, S, Bachmann, MH, Borowsky, AD, Ruebner, B, Cardiff, RD, Yang, Q, Bishop, JM, Contag, CH and Felsher, DW. 2004. MYC inactivation uncovers stem cell properties and induces the state of tumor dormancy in hepatocellular cancer. Nature, 431:1112-1117.
- Contag, PR, Olomu, IN, Stevenson, DK, Contag, CH. 1998. Bioluminescent indicators in living mammals. Nature Med. 4(2):245-247.

Point-of-Care Microscopy: Molecular Imaging with Cellular Resolution

Contag C.H. .

Division of Neonatal and Developmental Medicine, and a member of the BioX faculty at Stanford University.

ccontag@stanford.edu

Micro-optical designs are enabling the development of miniaturized microscopes that can reach inside the body to interrogate disease states microscopically. This is leading to an emerging field of *in vivo* pathology that is changing the diagnostic paradigm from biopsy and conventional histopathology to one of point-of-care histopathology coupled with telepathology. These advances are closing the gap between the patient and the pathologist and have the potential of accelerating diagnosis and guiding therapy. While recent advances in this field have been significant, many issues must be resolved before this clinical transformation may be fully realized. There are technological and translational advances that are driving this field and are leading towards *in vivo* microscopy becoming a standard clinical tool. By removing the spatiotemporal separation between the pathologist and patient, we can accelerate clinical diagnosis and advance clinical care for patients with a wide variety of diseases.

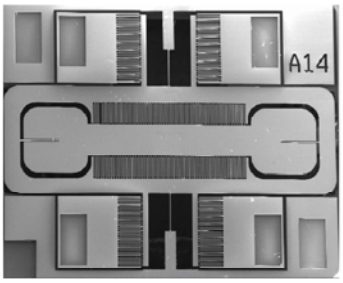

micro–mirror

References

1. Liu, JTC, Mandella, MJ, Loewke, NO, Haeberle, H, Ra, H, Piyawattanametha, W, Solgaard, O, Kino, GS, Contag, CH (2010) Micromirror-scanned dual-axis confocal microscope utilizing a gradient-index relay lens for image guidance during brain surgery. JBO. In Press.
2. Piyawattabanetha, W, Ra, H, Mandella, MJ, Loewke, Wang, TD, Kino, GS, Solgaard, O, Contag, CH (2009) 3-D near-infrared fluorescence imaging using a MEMS-based miniatuire dual axis confocal microscope. IEEE J. Sel. Topics Quantum Electronics. 15(5): 1344-1350.
3. Mackanos, MA, Hargrove, J, Wolters, R, Du, CB, Friedland, S, Soetikno, RM, Contag, CH, Arroyo, MR, Crawford, JM, Wang, TD (2009) Use of an endoscope-compatible probe to detect colonic dysplasia with Fourier transform infrared spectroscopy. J Biomed Optics 14, 044006. PMID: 19725718
4. Liu, JT, Mandella, MJ, Crawford, JM, Contag, CH, Wang, TD, Kino, GS. (2008) Efficient rejection of scattered light enables deep optical sectioning in turbid media with low-numerical-aperture optics in a dual-axis confocal architecture. J Biomed Opt. 13(3):034020.
5. Hsiung, P-L, Hardy, JW, Friedland, S, Soetikno, R, Du, CB, Wu, APW, Sahbaie, P, Crawford, JM, Lowe, AW, Contag, CH, Wang, TD. (2008) Detection of colonic dysplasia *in vivo* using a targeted fluorescent septapeptide and confocal microendoscopy. Nat. Med. 14(4): 454-8.
6. Wang, TD, Triadafilopoulos, G, Crawford, JM, Dixon, LR, Bhandari, T, Sahbaie, P, Friedland, S, Soetikno, R, Contag, CH. (2007) Detection of Endogenous Biomolecules in Barrett's Esophagus by Fourier Transform Infrared Spectroscopy. Proc. Natl. Sci, USA. 104(40): 15864-9.

- **ESMI Plenary Lecture 1: Violaine Sée (Liverpool, UK)**
  Transcription factors dynamics: from discrete pulses to oscillatory pattern to control gene expression
  Chairs: Clemens W.G.M. Löwik (Leiden, The Netherlands) , Leszek Krolicki (Warsaw, Poland)

- **Parallel Session 1: Cancer I – together with ESR**
  Chairs: Markus Schwaiger (Munich, Germany), Peter Brader (Vienna, Austria)

- **Parallel Session 2: Neuroscience I**
  Chairs: Annemie van der Linden (Antwerp, Belgium), David Wyper (Glasgow, UK), Hervé Boutin (Manchester, UK)

- **Parallel Session 3: Technology**
  Chairs: Jorge Ripoll (Heraklion, Greece) , Bernd Pichler (Tuebingen, Germany)

- **Parallel Session 4: Probes I – together with COST**
  Chairs: Eva Jakab-Tóth (Orléans, France) , Silvio Aime (Torino, Italy)

- **ESMI Plenary Lecture 2: Francesca Odoardi (Göttingen, Germany)**
  Immune surveillance and autoimmunity: how encephalitogenic T cells enter their target organ
  Chairs: Renata Mikolajczak (Warsaw, Poland), Chrit Moonen (Bordeaux, France)

- **Plenary Session on Excellent and Late Breaking Abstracts**
  Chairs: Renata Mikolajczak (Warsaw, Poland), Chrit Moonen (Bordeaux, France)

Day 1 - Thursday May 27, 2010

Violaine Sée

Violaine Sée is a BBSRC David Phillips Research Fellow at the University of Liverpool. She graduated in Chemistry and Molecular and Cellular Biology at the University Louis Pasteur in Strasbourg (France). After a Master in Pharmacology, in 2001 she obtained her PhD in Pharmacology and Neurobiology at the University Louis Pasteur. She was then assistant lecturer and subsequently moved to the University of Liverpool as a Post-doctoral Research Fellow. In 2005, she obtained a prestigious David Phillips Fellowship, to develop her work on intracellular signalling dynamics. She is focusing on the imaging of single living cells in order to understand regulation of gene transcription and cell fate. She has recently been interested in using new techniques for single molecule imaging in live cells based on the use of gold nanoparticles.

Selected References

- Nelson, D. E., Ihekwaba, A. E., Elliott, M., Johnson, J. R., Gibney, C. A., Foreman, B. E., Nelson, G., See, V., Horton, C. A., Spiller, D. G., Edwards, S. W., McDowell, H. P., Unitt, J. F., Sullivan, E., Grimley, R., Benson, N., Broomhead, D., Kell, D. B., and White, M. R. (2004) Oscillations in NF-kappaB signaling control the dynamics of gene expression. Science 306, 704-708
- See, V., Rajala, N. K., Spiller, D. G., and White, M. R. (2004) Calcium-dependent regulation of the cell cycle via a novel MAPK--NF-kappaB pathway in Swiss 3T3 cells. The Journal of cell biology 166, 661-672
- Nelson, D. E., See, V., Nelson, G., and White, M. R. (2004) Oscillations in transcription factor dynamics: a new way to control gene expression. Biochemical Society transactions 32, 1090-1092
- Ashall, L., Horton, C. A., Nelson, D. E., Paszek, P., Harper, C. V., Sillitoe, K., Ryan, S., Spiller, D. G., Unitt, J. F., Broomhead, D. S., Kell, D. B., Rand, D. A., See, V., and White, M. R. (2009) Pulsatile stimulation determines timing and specificity of NF-kappaB-dependent transcription. Science 324, 242-246
- See, V., Free, P., Cesbron, Y., Nativo, P., Shaheen, U., Rigden, D. J., Spiller, D. G., Fernig, D. G., White, M. R., Prior, I. A., Brust, M., Lounis, B., and Levy, R. (2009) Cathepsin L digestion of nanobioconjugates upon endocytosis. ACS nano 3, 2461-2468
- Meley, D., Spiller, D.G., White, M.R., McDowell, H., Pizer, B.L., and See, V. (2010) p53-mediated delayed NF-kB activity enhances etoposide-induced cell death in medulloblastoma. Cell Death and Disease 1, In press

Transcription factors dynamics: from discrete pulses to oscillatory pattern to control gene expression

Sée V.

Centre for Cell Imaging, University of Liverpool

violaine@liverpool.ac.uk

At a given time-point, cells in a population are heterogeneous in their functions and fate and it is therefore vital to develop and apply methods that allow the measurement of dynamic molecular processes in single cells. We have shown, using single cell imaging, the critical role of nucleo-cytoplasmic localisation oscillations of the NF-κB transcription factor to control downstream pattern of gene transcription (Nelson et al, Science 2004; Ashall et al, Science 2009). NF-κB regulates cellular stress and immune responses to infection. In most cases, oscillations had previously been masked in population level studies by cellular heterogeneity. We developed a protocol based on cell treatment by repeated short pulses of TNFα at various intervals to mimic pulsatile inflammatory signals. This allowed obtaining synchronous cycles of NF-κB nuclear translocation.

We have also observed cell to cell heterogeneity in other signalling systems such as in cellular response to low oxygen environment (hypoxia). In both inflammatory and hypoxic signalling systems one source of heterogeneity is due to the presence of extrinsic dynamic processes that are functionally coupled and that are occurring over different time scales. We identified the cell cycle as one source of variability as cells must coordinate and prioritise their response to the environment depending on their cell cycle status. We apply mathematical modelling using the quantitative data generated by imaging experiments to predict the role of the negative feedback, to unravel new network motifs and to characterise the cross-talk between the signalling systems.

Multimodal imaging approaches for cell-cell interaction

Massberg S.

Deutsches Herzzentrum München, Technische Universität München

massberg@idi.harvard.edu

Cell-cell interactions play a pivotal role in the control of critical cellular functions, such as cell adhesion, cell migration as well as cell differentiation and proliferation. The scientific focus of our lab is on the mechanisms that regulate cell-cell interactions during scenarios, such as arterial or venous thrombosis, stem cell homing and differentiation, during inflammation as well as in cancer development and progression. To evaluate the interaction between different cell subsets in their physiological (micro-) environment, we have established novel imaging approaches that allow dissecting all the steps involved both in reductionist in vitro assays and *in vivo*. This includes the used of gene-targeted mice, in which distinct cellular lineages are genetically marked in combination with innovative imaging techniques, including intravital multi-photon microscopy. The *in vivo* approaches are complemented by sophisticated in vitro assays allowing investigation of cell-cell interactions on a subcellular and molecular level. The multimodal imaging approaches will contribute to a better understanding of the molecular mechanisms and the kinetic aspects of the dynamic process of cell-cell interactions under physiological conditions and in the disease states.

Molecular imaging for monitoring treatment with protein kinase inhibitors

Weber W.

University Freiburg, Germany

wolfgang.weber@uniklinik-freiburg.de

Targeted drugs that modulate the function of specific molecules in diseased tissues hold great promise for the treatment of many diseases including malignant tumors. However, there are several challenges for the efficient evaluation of these drugs in clinical trials as well as for the use in clinical practice. These include

(i) the selection of patients likely to benefit from treatment with a specific targeted drug,

(ii) finding the right dose and dose schedule,

(iii) monitoring target inhibition, and

(iv) assessing tumor response to therapy.

Standard anatomic imaging continues to play an important role for addressing these challenges, but molecular imaging provides several new opportunities to make the use of targeted drugs more efficient. Using molecular imaging the expression of drug targets can be assessed non-invasively, the concentration of drugs can be measured in the tumor tissue, target inhibition can be monitored and tumor response to therapy can be evaluated earlier than with anatomic imaging techniques.

Therefore it is expected that molecular imaging will play an increasing role for guiding molecularly defined therapeutic interventions.

Potentials of imaging biomarkers in patients

Van Beers B.E.

Department of Radiology and INSERM U 773, Beaujon University Hospital, University Paris Diderot, France.

bernard.van-beers@bjn.aphp.fr

28

Introduction: There is an increasing need for imaging biomarkers to objectively assess the prognosis and response to treatment in cancer.

Methods: Quantitative anatomical, molecular, and functional characteristics can be used as imaging biomarkers.

Results: The RECIST criteria are anatomical imaging biomarkers that are accepted surrogate endpoints in cancer treatment. However, they are not early biomarkers and are limited in the assessment of some tumors and targeted treatments.

The use of molecular imaging biomarkers is restricted by their narrow target specificity and by the complexity of the biology in tumors. In a given tumor type, several different subgroups often exist with overexpression of different proteins and signaling pathways.

Therefore, it is often preferred to assess downstream changes of molecular pathways with functional imaging. The rationale of this approach is that most cancers have acquired the same functional capabilities including upregulated glycolysis, limitless proliferation, extensive angiogenesis, resistance to apoptosis and metastasis formation. These capabilities are assessed with functional biomarkers using PET, dynamic contrast-enhanced CT and MRI, diffusion-weighted MRI, MR elastography and spectroscopy.

Conclusions: Functional biomarkers have an important potential to help in selecting the patients and assessing the response to new treatments, especially in phase 1 and 2 clinical trials.

However, important efforts of validation and standardization remain to be done before the wide use of functional biomarkers and their acceptance as surrogate endpoints that can replace clinical endpoints such as survival or time to progression.

References:

1. Hanahan D, Weinberg RA. The hallmarks of cancer. Cell. 2000;100(1):57-70.
2. Rudin M. Imaging readouts as biomarkers or surrogate parameters for the assessment of therapeutic interventions. Eur Radiol. 2007 (10):2441-57.
3. Padhani AR, Liu G, Koh DM, Chenevert TL, et al. Diffusion-weighted magnetic resonance imaging as a cancer biomarker. Neoplasia. 2009;11(2):102-25.
4. Van Beers BE, Vilgrain V. Biomarkers in abdominal imaging. Abdom Imaging. 2009;34(6):663-7.

Pre-clinical screening of anti - HER2 nanobodies for molecular imaging of breast cancer

Vaneycken I. [(1)], Devoogdt N. [(1)], Peleman C. [(1)], Xavier C. [(1)], Lahoutte T. [(1)], Caveliers V. [(1)].

Vrije Universiteit Brussel, Belgium

ilse.vaneycken@gmail.com

Introduction: Nanobodies are small antigen-binding fragments of camelid heavy-chain antibodies. Besides therapeutic agents, they are also effective as a diagnostic tool for targeted imaging when labeled with a suitable radionuclide[1]. We produced Nanobodies for molecular imaging of Human Epidermal Growth Factor Receptor 2 (HER2) expression in breast cancer patients[2] for a phase I clinical trial. After production, a number of candidate binders are obtained. we designed a standardized selection procedure based on production yield, in vitro and *in vivo* criteria to identify the lead anti-HER2 Nanobody with the highest potential as a tracer for clinical translation.

Methods: A camel was immunized with HER2 recombinant protein and serum IgG2 and IgG3 subclasses with heavy-chain-only antibodies were separated. Eleven different anti-HER2 Nanobodies were produced in E. coli, purified and labeled with 99mTc(I)-tricarbonyl. In vitro saturation binding studies were performed on recombinant HER2 and HER2 positive SKOV3 cells with the native and radiolabeled anti-HER2 Nanobodies. Competition studies allowed assessing whether the anti-HER2 99mTc-Nanobodies competed with the therapeutic anti-HER2 antibodies Trastuzumab and Pertuzumab. *In vivo*, the biodistribution and tumor targeting potential of all 99mTc-Nanobodies was evaluated using pinhole SPECT/micro-CT in nude mice bearing HER2 positive SKOV3 xenografts. The Nanobody showing the most favourable *in vivo* characteristics was additionaly evaluated in nude mice bearing HER2 positive LS174T and HER2 negative MDAMB4357d xenografts.

Results: Nanobodies were labeled with 99mTc and purified to a final radiochemical purity of ≥99%. Saturation binding studies showed that 99mTc labeling was not associated with a significant reduction of immunoreactivity. The Nanobodies appeared to be not or only weakly competitive with the commercial therapeutic antibodies. *In vivo* biodistribution demonstrated that tumor accumulation varied between 0,78 and 4,44 percent injected activity per gram (%IA/g). Of the eleven 99mTc-Nanobodies tested in SKOV3 xenografts, three presented a tumor uptake above 4 %IA/g. One was selected and also showed high tumor uptake (3,76±0,82 %IA/g) in LS174T xenografts, but low uptake in MDAMB435d xenografts (0,71±0,07 %IA/g). In addition, all 99mTc-Nanobodies displayed high renal uptake but low non-specific accumulation in liver, muscle and blood, resulting in high tumor-to-background ratios.

Conclusions: Using a standardized selection procedure for identificiation of high affinity Nanobodies for molecular imaging of cancer, we identified one Nanobody as the lead compound for a phase I clinical trial. This Nanobody meets with all criteria that characterize a good diagnostic tracer.

Acknowledgement: The research at ICMI is funded by the Interuniversity Attraction Poles Program–Belgian State–Belgian Science Policy. Tony Lahoutte is a Senior Clinical Investigator of the Research Foundation–Flanders (Belgium) (FWO).

References:

1. Gainkam LO, Huang L, Caveliers V, et al. Comparison of the biodistribution and tumor targeting of two 99mTc-labeled anti-EGFR nanobodies in mice, using pinhole SPECT/micro-CT. J Nucl Med. 2008;49(5):788-795.
2. Hicks,D.G. et al (2008). HER2+ breast cancer: review of biologic relevance and optimal use of diagnostic tools. American Journal of Clinical Pathology, 129, 263-273.

YIA applicant

30

[18F]-FDG/[18F]-FLT-PET and bioluminescence imaging of therapy response in B-cell lymphoma mice treated with cytotoxic and antiproliferative agents

De Saint-Hubert M. [1], Brepoels L. [1], Devos E. [1], Degroot T. [1], Ibrahimi A. [1], Tousseyn T. [1], Verbruggen A. [1], Mortelmans L. [1], Mottaghy F. [2].

[1] KULeuven, Belgium
[2] RWTH Aachen.

marijke.desainthubert@med.kuleuven.be

Introduction: Early and reliable evaluation of therapy outcome is essential for optimal medical care in oncology. Shortly after treatment the influx of inflammatory cells can interfere with [18F]-FDG uptake while [18F]-FLT is less hampered by this phenomenon. The aim of this study was to image [18F]-FDG and [18F]-FLT response to either cytotoxic or antiproliferative therapy and to correlate the response to the amount of viable cells assessed with Bioluminescence Imaging (BLI).

Methods: Daudi cells (Burkitt lymphoma) were transduced with a lentiviral vector (blasticidin selection marker and firefly luciferase reporter gene) and inoculated in SCID-mice (n=57). When the tumors reached a diameter of 15mm2 animals were treated with either cyclophosphamide (125mg/kg, n=25) or temsirolimus (50mg/kg, n=25). [18F]-FDG and [18F]-FLT small-animal PET was performed on day0 (d0, before treatment) day (d) 2, 4, 7, 9 and 14. On these days we also imaged the tumor cells with BLI. At each time point, 2 mice of each treatment condition were sacrificed and tumors were excised for histopathology (H&E, Ki-67, CD20, TUNEL). Quantitative imaging data were expressed as % signal of the baseline signal measured on d0 and expressed as mean ± standard error of the mean (SEM).

Results: [18F]-FDG uptake decreased immediately (-38% on d2) after cyclophosphamide treatment without a significant reduction in [18F]-FLT uptake which could be due to DNA repair as DNA FACS showed an increased amount of cells in the S-fase early after cyclophosphamide. From d7 [18F]-FLT uptake decreased significanlty corresponding to histology data (ki-67). [18F]-FDG uptake stabilized between d7 and d9 (-57% and -59% respectively) likely due to a high influx of inflammatory cells observed in histology (±40% on d7-d9). Caliper measurements showed tumor shrinkage from d7. Surprisingly the BLI measured an increased signal early after therapy (d2-d4) while only late after therapy a reduction in the signal was observed (d9-d14).

Temsirolimus treatment reduced both the [18F]-FDG and [18F]-FLT uptake immediately (d2) after therapy. [18F]-FDG stabilized between d9 and d14 maybe due to inflammation which was only observed on d14 but this might as well be due to regrowth. The early [18F]-FLT decrease corresponded well to ki-67 stainings and to DNA FACS where an increase of the G0/G1 fase is observed. Tumor size reduced already from d4 after temsirolimus treatment. BLI showed the same signal increase as cyclophosphamide early after therapy and only in a late stage after therapy we observed a reduced amount of viable cells. This early increase might be due to an upregualtion of the promotor after therapy but further evalution of this phenomenon is on the way.

Conclusions: [18F]-FDG reduced early after therapy but stabilized due to a temporary rise in inflammatory cells. [18F]-FLT-PET was able to detect a reduced proliferation after therapy. However, after cytotoxic therapy [18F]-FLT did not change probably due to DNA repair. Therefore caution should be made when imaging [18F]-FLT response immediately after cytotoxic therapy. Bioluminescence imaging showed an early increase which may have important implication for BLI monitoring of therapy.

Acknowledgement: This work was financially supported by the Center of Excellence 'MoSAIC' of the K.U.Leuven.

TF-Pimonidazole: an hypoxia marker suitable for *in vivo* ^{19}F MRS imaging

Heerschap, A. .

Centre for Molecular Life Science, University Nijmegen, The Netherlands

a.heerschap@rad.umcn.nl

Introduction: Hypoxia in tumours is associated with enhanced progression, increased aggressiveness and metastatic potential and poor prognosis. Moreover, hypoxic tumour cells are resistant to radiotherapy and some forms of chemotherapy. Over the years several approaches to assess hypoxia *in vivo* have been explored, ranging from needles measuring local pO_2 invasively to a range of non-invasive (imaging) methods using oxygen sensitive agents. Unfortunately until today none of these methods or agents has entered widespread clinical practice. Here we demonstrate a novel hypoxia marker completely analogous to the commonly used histological hypoxia marker Pimonidazole (PIMO) and labelled with fluorine for *in vivo* ^{19}F MRS imaging.

Methods:1-(2-nitro-1H-imidazol-1-yl)-3-[4-(trifluoromethyl)piperidin-1-yl]propan-2-ol (TF-PIMO) was synthesized in a similar way as described in [1]. C57BL/6 mice carrying a C38 colon carcinoma on the upper leg (size approx. 250 mm^3) were given either 80 or 200 mg / kg TF-PIMO intraperitoneal (IP) at least 3 hours before MR investigations. The mice were anesthetized using a single urethane IP injection. This avoids any spectral interference by fluorinated inhalation anaesthetics. Experiments were performed on a 7 T horizontal bore MR system. A homemade 14 mm solenoid coil was used for transmit/receive of ^{19}F and ^{1}H. After initial localization and basic ^{1}H MR imaging (T2*w GRE) an unlocalized pulse acquire sequence (FID) on ^{19}F was used to detect TF PIMO validating correct injection of the compound. Subsequently a series of 3D ^{19}F chemical shift imaging (CSI) FID experiments using an ultrashort adiabatic half passage pulse was used for TF-PIMO ^{19}F imaging. Further settings of the MRSI sequence: FOV 32 × 32 ×32 mm, matrix 8 × 8 × 8, TR 597 ms, acquisition time 58 m 02 s, 256 averages, weighted phase encoding scheme. After MR, tumours were removed immediately and stored in liquid nitrogen. Frozen tumour sections of 5 µm thickness were cut for staining and further analysis. The tumor sections were subsequently stained and scanned for Hoechst and rabbit anti-pimonidazole.

Results: Figure 1 shows a heat map generated from the 3D ^{19}F MRSI representing the *in vivo* TF-PIMO accumulation in a hypoxic C38 colon carcinoma as was validated by subsequent immunohistochemical analysis of the tumour tissue.

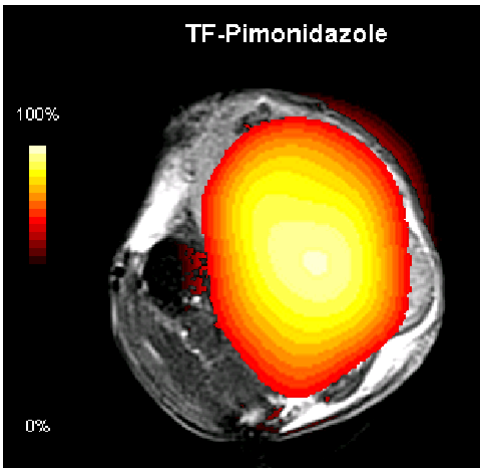

Figure 1: 1H MRI of a C38 murine colon carcinoma on a mouse leg with a heat map generated from a 3D 19F MRSI representing the *in vivo* TF-PIMO accumulation over-layed.

Conclusions: TF-PIMO was synthesized and shown to be a potential non-invasive marker to image tissue hypoxia in tumours by 19F MRSI. Background free functional images are obtained that can be co-registered with conventional MRI. In addition this marker has the advantage that it can be stained with the same anti-body as used to detect the common clinical used marker Pimonidazole and thus allows for easy matching of hypoxia by histology and by MR on the same tumour sample.

Acknowledgement: This work is supported in part by EMIL (LSHC-CT-2004-503569) and NWO (VISTA and INV911-06-021)

References:

1. Raleigh, J. A. et al; *Magn Reson Med* 22:451-466 (1991)

[11C](R)-PK11195- a tricky tracer. Do we really need it to image microglial activation?

Gerhard A. .

Wolfson Molecular Imaging Centre Manchester, UK

alex.gerhard@manchester.ac.uk

Detailed experimental and human post mortem studies have shown that activation of microglia, the brain's resident tissue macrophages, has a particularly close association with active brain pathology. One of the molecules expressed de novo during the 'activation' of microglia is the translocator protein (18kDa), TSPO.PK11195 is a selective ligand for the TSPO.

In vivo and in the absence of invading blood-borne cells the de novo expression of TSPO occurs primarily in activated microglia. Based on this relative cellular selectivity [11C]PK11195 PET has been used to image microglial activation *in vivo* for about 20 years now and it has been possible to demonstrate patterns of increased signal distribution in the brain that correspond well with the localisation of pathological changes in a number of neurological disorders (1).

Recently [11C](R)- PK11195 PET has even successfully been used to show *in vivo* the effect of a pharmacological intervention in a neurodegenerative disorder on microglial activation (2).

Nevertheless there are methodological challenges when using [11C]PK11195 particularly an unfavourable signal to noise ratio. Therefore numerous new ligands for the TSPO have been evaluated at different stages over the last years with some of them having also been assessed in diseases known to be accompanied by microglial activation (3).

The talk will give a brief overview of relevant studies with PK11195, as well as newer TSPO tracers, and will try to highlight their potential advantages and problems.

References:

1. Venneti S, Lopresti BJ, Wiley CA. The peripheral benzodiazepine receptor (Translocator protein 18kDa) in microglia: from pathology to imaging. Prog Neurobiol. 2006;80(6):308-322. Epub 2006 Dec 2006.
2. Dodel R, Spottke A, Gerhard A, et al. Minocycline 1-year therapy in multiple-system-atrophy: Effect on clinical symptoms and [(11)C] (R)-PK11195 PET (MEMSA-trial). Mov Disord. 2010;25(1):11.
3. Chauveau F, Boutin H, Van Camp N, Dolle F, Tavitian B. Nuclear imaging of neuroinflammation: a comprehensive review of [(11)C]PK11195 challengers. Eur J Nucl Med Mol Imaging. 2008;1:1.

Preclinical imaging of the type 1 cannabinoid receptor in neurodegenerative diseases

Casteels C. [1], Van Laere K. [1].

University Leuven, Division of Nuclear Medicine, Belgium

cindy.casteels@med.kuleuven.be

The endocannabinoid system (ECS) is an important modulatory system in the brain. It consists of a family of naturally occurring lipids, the endocannabinoids, of transport and degradation proteins, and of cannabinoid receptors. Type 1 cannabinoid (CB1) receptors are abundantly expressed in all brain areas, especially those involved in the control of motor function. CB1 receptor stimulation modulates GABA, glutamate and dopamine neurotransmitter release in a dynamic activity manner.1

Dysregulation of cannabinoid-mediated control of basal ganglia function have been suggested to play a critical role in the pathogenesis and symptom development of Parkinson's disease (PD) and Huntington's disease (HD), providing rationale for potential ECS-targeted therapy in these diseases.2 However, at present, limited clinical pilot trials have been inconclusive. As only in vitro, ex vivo and post mortem data on the ECS existed until recently, functional *in vivo* imaging may play an important role in the further evaluation of the neurobiological and clinical impact of the ECS in PD and HD. Here, we present the *in vivo* characterization of CB1 receptor alterations in preclinical models of PD and HD using PET and [18F]MK-94703. Both genetic and toxin-based experimental models will be presented. Their relevance to mimic the human condition will be discussed as well.

Acknowledgement: Financial support of the Research Council of the Katholieke Universiteit Leuven (OT/05/58), the Fund for Scientific Research, Flanders, Belgium (FWO/G.0548.06), and the Institute for the Promotion of Innovation by Science and Technology in Flanders (SBO50151) is gratefully acknowledged. This work is performed under European Commission FP6-project DiMI,LSHB-CT-2005-512146

References:

1. Katona et al., Nat. Med. 2008;
2. Maccarrone et al., Prog. Neurobiol. 2007;
3. Burns et al., Proc. Natl. Acad. Sci. U.S.A. 2007.

YIA applicant

34

Longitudinal non-invasive detection of amyloid plaques by combined molecular, functional and morphological imaging in transgenic mouse models of Alzheimers Disease

Maier F. C. [1], Wehrl H. F. [1], Schmid A. [1], Odenthal J. [2], Reischl G. [3], Wiehr S. [1], Mannheim J. [1], Stiller D. [4], Jucker M. [2], Pichler B. [1].

[1] Laboratory for Preclinical Imaging and Imaging Technology of the Werner Siemens-Foundation,
[2] Hertie Institute for Clinical Brain Research,
[3] University Hospital Tuebingen, Radiopharmacy,
[4] Drug Discovery Support, Boehringer Ingelheim Pharma GmbH & Co. KG.

florian.maier@med.uni-tuebingen.de

Introduction: Current small animal imaging instrumentation provides powerful tools to study disease characteristics and progression. However, biomarkers for imaging amyloid plaque deposition and associated physiological changes are not yet fully understood – impeding diagnosis in daily clinics. Thus our aims were to assess the ongoing plaque deposition in an animal model of Alzheimers Disease longitudinally using [11C]PIB, to compare the binding properties in different transgenic mouse models and to monitor perfusion differences with [15O]H2O and Arterial Spin Labeling (ASL) – reflecting disease induced changes in physiology.

Methods: APPPS1 tg mice and Tg2576 mice with respective littermate controls were injected intravenously with 7.6±2.8 MBq [11C]PIB (specific activity > 50GBq/µmol) and with 28.5±3 MBq [15O]H2O for measurement of cerebral perfusion. Dynamic small animal PET scans were performed for 1h p.i. and the mice were anesthetised with 1.5% isofluran in 100% oxygen. In addition, 3D MR images and ASL were acquired for each mouse. The PET images were analysed using cortical regions as target and the cerebellum as internal reference. The obtained time activity curves were processed with the Logan Plot and the simplified reference tissue model (SRTM) by Lammertsma. ASL-MRI data were analyzed with an inhouse programmed Matlab routine using a simplified version of the Bloch equation. Furthermore, the animals were analysed histopathologically.

Results: Both analysis methods revealed significant differences in the binding potential (BP) of [11C]PIB in cortical regions of transgenic APPPS1 mice (Logan 0.28±0.10; SRTM 0.32±0.18) in comparison to littermate controls (Logan 0.13±0.07; SRTM 0.05±0.07, n=8, $p<0.05$, 9.5 months old). In sharp contrast, transgenic Tg2576 mice (Logan 0.05±0.01; SRTM 0.02±0.02) could not be differentiated from age matched controls (Logan 0.06±0.02; SRTM 0.01±0.01, n=4, 18 months old) with [11C]PIB. These results were correlated with the plaque distribution pattern assessed by histological analysis. In 1.5 months old APPPS1 mice the binding potential in cortical regions was comparable to littermate controls (tg 0.00±0.02; co 0.00±0.01), reached 0.17±0.09 in 8.5 months old transgenic animals and 0.26±0.16 in 10 months old animals. Surprisingly, 12-16.5 months old transgenic animals did not show higher binding potentials (0.22±0.06, n=4, p=0.65). Furthermore, transgenic APPPS1 mice showed higher blood perfusion values, while transgenic Tg2576 mice displayed a decreased perfusion when compared to control animals at the age of 18 months.

Conclusions: These results clearly elucidate the potential of [11C]PIB for imaging amyloid plaques in APPPS1 mice in sharp contrast to Tg2576 mice but also show that monitoring of disease progression regarding amyloid plaque-load after 10 months is not possible. If the same issue applies to clinical observations, this could lead to critical misinterpretation of patient data. Thus, other biomarkers and more refined imaging techniques are needed for preclinical therapy evaluation and disease progression monitoring.

Acknowledgement: This work is supported and financed by the BMBF grant 01GI0705

Serotonergic neurotransmission in early Alzheimer's disease

Hasselbalch S. G. [(1)], Marner L. [(1)], Madsen K. [(1)], Lehel S. [(1)], Barré W. [(1)], Knudsen G. M. [(1)].

[(1)]Copenhagen University, Denmark

sgh@nru.dk

Introduction: Post mortem studies suggest involvement of the serotonin system in Alzheimer's disease (AD) and serotonin 2A (5-HT2A) receptors are globally reduced early in the course of the disease (1). However, few studies have investigated other aspects of the serotonergic system, including presynaptic markers (serotonin transporters, SERT) as a measure of serotonergic degeneration (2). Further, recent evidence points to a disease-modifying effect of 5-HT4 agonism through a decrease in beta-amyloid load (3). Therefore, we have investigated SERT and 5-HT4 in early and compared these measures to the reduction in 5-HT2A receptors.

Methods: For the SERT/5-HT2A comparison, we included 12 patients (mean age 73.7 ±7.6 years, 8 males) with AD (average MMSE of 24, range 19-26) and 11 healthy age-matched subjects (mean age 72.5 ±6.8 years, 6 males). Subjects were investigated with a 90 min dynamic [11C]DASB-PET recording to measure SERT (4) and a 40 min steady-state [18F] altanserin-PET recording to measure 5-HT2A receptors (5). In a separate study of 5-HT4 receptors, the novel radioligand [11C]SB207145 was used in twelve healthy individuals (mean age 67.2 y, 6 males) and eleven newly diagnosed AD patients (mean age 70.6 y, 6 males, mean MMSE 24, range 19-27) using the simplified reference tissue model. Volumes of interest (VOIs) were delineated automatically on co-registered 3T MRIs, and partial volume correction was applied to correct for differences in atrophy.

Results: The 5-HT2A receptors were markedly reduced (25-66%) in AD patients in all regions but the striatum. Inc contrast, we found a reduction of SERT binding by 34% (p=0.0003) in the hippocampus, while most other regions were unaffected. Midbrain showed no change in binding (p=0.30). No statistically significant differences in 5-HT4 receptor binding between healthy individuals and AD patients were found in any of the included brain regions: Hippocampus (p = 0.55), posterior cingulate gyrus (p = 0.22), amygdala (p = 0.77), parietal cortex (p = 0.44), temporal cortex (p = 0.74) and prefrontal cortex (p = 0.43).

Conclusions: We showed a marked decrease of 5-HT2A binding in patients with mild AD, consistent with previous findings in MCI (1). The SERT binding was unaffected by the disease in almost all cortical regions and in midbrain, suggesting that the serotonergic innervations and the neuron bodies in dorsal nucleus raphe are intact, at least early in the disease. We interpret the SERT reduction in hippocampus in patients as a decreased serotonergic innervation, which could be secondary to the neuronal degeneration taking place in hippocampus of AD patients. The marked reduction in 5-HT2A may be related to beta-amyloid accumulation. In contrast to the 5-HT2A receptor subtype, the 5-HT4 receptor levels seemed to be unaffected in AD. However, 5-HT4 binding in relation to cognitive function, neuropsychiatric symptoms and beta-amyloid load should be further investigated.

Acknowledgement: Supported by The Lundbeck Foundation, Rigshospitalet, and the Danish Medical Research Council. The John and Birthe Meyer Foundation is gratefully acknowledged for the donation of the Cyclotron and PET-scanner. These studies were funded in part by the EC - FP6-project DiMI, LSHB-CT-2005-512146.

References:

1. S. G. Hasselbalch et al., Neurobiol. Aging. 29, 1830 (2008).
2. K. Nielsen et al., Synapse. 59, 270 (2006).
3. S.J. Robert, et al., Neurodegener Dis 5(3-4):163 (2008).
4. M. Ichise et al., J Cereb. Blood Flow Metab. 23, 1096 (2003). L. H. Pinborg et al., J. Cereb. Blood Flow Metab. 23, 985 (2003).

Qualitative and quantitative assessment of florbetapir F-18 PET (^{18}F-AV45) amyloid deposition PET imaging - validation by pathology. Preliminary report.

Romanowicz G. [1], Saha K. [2], Krautkramer M. [2], Joshi A. [2], Pontecorvo M. [2], Clark C. [2], Carpenter A. [2], Skovronsky D. [2].

[1] Gdański Uniwersytet Medyczny, Poland
[2] Avid Radiopharmaceuticals Inc..

greg@amg.gda.pl

36

Introduction: Various methods for analyzing amyloid brain PET scans have been proposed and tested. The lack of reliable truth standards has complicates the validation and implementation of these methods, and investigators have relied on theoretical modeling and clinical diagnoses as surrogates for true pathology. We applied three methods for assessing florbetapir F18 PET (18F-AV45) amyloid images: a semiquantitative visual read, a mean SUVr quantitation based on VOIs, and a novel automated histogram based quantitative approach. Each method was validated by comparison with amyloid burden measured at post-mortem.

Methods: 6 subjects (3 men; 3 women; mean age at imaging 76y (47-86); diagnosis at enrollment, 1 MCI, 4 AD, 1 PDD) with a life expectancy of < 6 months had a 10 minute PET scan 50 minutes after IV injection of 10 mCi of florbetapir F 18. Images were reconstructed by iterative technique with 4i/16s and 3 mm FWHM post-reconstruction Gaussian filter. For visual assessment (VR) an experienced reader rated florbetapir cortical uptake intensity (VR score) on a 5 point scale ranging from 0, (no difference in uptake between cortex and cerebellum), to 4 (uptake in all cortical brain regions significantly higher vs. both cerebellum and white matter). For the SUVr technique, PET images were spatially normalized by 12 parameter affine registration to Talairach/MNI space and counts extracted from six regional VOIs (frontal, temporal, precuneus, parietal, anterior cingulated and posterior cingulated). Average standardized uptake value ratios (SUVr) were calculated with cerebellum as reference. The values for the six cortical regions were averaged to generate a global SUVr. For the histogram based analysis image data were processed automatically to generate a128 bin count histogram. The first order derivative Gaussian (FWHM= 3mm) convolved histogram curve was searched in the intensity direction to estimate separation of high/low intensity areas. The high/low intensity curve area ratio (CAR) was calculated to estimate specific amyloid binding. After the patient's death (mean interval from imaging 43 days (range 12-158)) their brain was evaluated for of β-amyloid deposition using immunohistochemistry (IHC) and by neuritic plaque rating (modified CERAD method). CAR score, VR score and SUVr were compared with IHC/CERAD using Spearman's (ρ) or Pearson's correlation coefficient (r) as appropriate.

Results: A strong correlation was obtained between each measure of PET amyloid binding and both measures of amyloid deposition at autopsy (VR and IHC (ρ=0.88), VR and CERAD (ρ =0.92); SUVr and IHC (r=0.89), SUVr and CERAD (ρ=0.93); CAR and IHC (r=0.97), CAR and CERAD (ρ =0.64)).

Conclusions: The results confirm that florbetapir F 18 PET imaging provides relevant *in vivo* estimate of brain amyloid pathology irrespectively of the choice of image assessment method. The novel histogram based method is particularly interesting because it is quantitative and does not require fitting images to a template or reorientation of images, kinetic data acquisition, input functions or drawing / applying regions of interest.

Acknowledgement: This work is supported by AVID Radiopharmaceuticals Inc. We would also like to thank A.S. Fleisher, J.A. Schneider, T.G. Beach, B.J. Bedell, S.P. Zehntner and M. Mintun for their contribution to the work.

In-vivo imaging of a mouse traumatic brain injury model using dual-isotope quantitative spect/ct

Máthé D. [1], Szigeti K. [2], Fekete K. [3], Horváth I. [2], Benyó Z. [3].

[1] CROmed Ltd,
[2] Nanobiotechnology and *In Vivo* Imaging Centre Semmelweis University Faculty of Medicine,
[3] Semmelweis University Faculty of Medicine.

domokos.mathe@gmail.com

Introduction: Using a standardized mouse neurotrauma model we aimed at determining the role of high-resolution SPECT/CT in detecting and quantifying the volumetric and functional extent of blood-brain barrier disruption. We chose the freezing trauma model because of its reproducibly standard damage.

Methods: Mice were subjected to a standardized freezing method transcranially using a cooled needle tip. In the presented initial studies, we compared the imaging pattern of the animals at equally 5 hours post the freezing trauma. We used a dedicated, quantitative multiplexed multipinhole SPECT imaging system for laboratory animals. X-ray CT of the structures was also performed together with SPECT data acquisition.

We correlated BBB disruption and blood perfusion with quantitative imaging of the decrease in glial and neuronal potassium uptake. We applied the validated intravenous tracer 99mTc-DTPA to detect the disruption of the BBB. Blood perfusion of the brain was assessed using the also validated tracer 99mTc-HMPAO. A radioactive isotopic potassium analogue, 201Tl was used to track K+ uptake changes quantitatively. 201Tl ions were passed through the BBB by means of diethyl-dithiocarbamate (DDC) complex that redistributes to ionic 201Tl after being taken up in brain tissues.

Uptake volumes (in mm3) and total brain as well as lesion radioactivity values (in kBq) were evaluated on 3D reconstructed brain images of treated mice (n=5 per group) and a non-treated group. Besides imaging of single tracers (3 groups), simultaneous multi-channel imaging was used in two other groups of mice having received 99mTc-DTPA plus 201Tl-DDC or, 99mTc-HMPAO plus 201Tl-DDC.

After imaging, histological control of the brain trauma size and localization was performed in the formaldehyde-fixed brains of all animals.

Results: The uptake of 99mTc-DTPA correlated well with the size and localization of the lesion whereas the cold spot of the lesion at the perfusion image was evident in all animals having received 99mTc-HMPAO. However the cold spot was surrounded by an area of increased perfusion as compared to the same area in control animals. When comparing with 201Tl-DDC images, the penumbra effect became evident, especially in the animals imaged with 99mTc-HMPAO and 201Tl-DDC in the same time. The area of non-active glial and neuronal potassium uptake was significantly larger than the non-perfused area and the hyper-perfused area co-localized with the edge of the disappeared neural potassium uptake volumes in 4 animals out of 5. SPECT/CT identified the dislocation of brain due to increased intracranial pressure in all treated animals.

Conclusions: *In vivo* whole-animal imaging using quantitative SPECT is a very promising method to dissect different activation patterns and regulation of different mechanisms behind the events following neurotrauma (and consequently stroke too). Using a unique dual-isotopic approach to detect multiple events in the same time in the same animals, the size and presence of a penumbral region where perfusion is elevated but neural (both glial and neuronal) K+ utilization is decreased, could be identified.

Acknowledgement: We are grateful for Dr. Jürgen Goldschmidt (Magdeburg) and Roberto Pasqualini (Orsay) for valuable advice and kind hints in 201Tl-DDC application and preparation.

References:

1. Goldschmidt et al. NeuroImage 49 (2010) 303–315

Molecular analysis of adaptive immune function through microscopic and mesoscopic imaging

Stein J. .

University of Bern, Switzerland

jstein@tki.unibe.ch

Introduction: Cell migration is of central importance during development, cancer metastasis and the functioning of the immune system. A powerful approach to dissect molecular mechanisms during cell trafficking on a single cell level requires the adaptation of microscopy techniques to anesthetized animals, usually mice.

Twophoton microscopy (2PM) was developed to examine the molecular mechanisms governing transmigration through endothelium and within tissue. Here, a brief overview is given over the techniques and potential applications of 2PM in the field of lymphocyte trafficking.

The overall internal organization of organ microenvironments, such as B cell follicles and blood microvessels in lymph nodes, has thus far been mainly determined by two-dimensional tissue sectioning, whereby three-dimensional information is lost. Optical Projection Tomography (OPT) and selective plane illumination (SPIM) are recently developed mesoscopic imaging approaches to dissect the overall organization of specimen of 1-15 mm diameter. Their applications in lymphoid structure analysis will be discussed.

Magnetic resonance imaging – from structure to molecular interactions

Rudin M. .

ETH and University of Zürich, Switzerland

rudin@biomed.ee.ethz.ch

Magnetic resonance imaging (MRI) yields images characterized by high spatial resolution and unsurpassed soft-tissue contrast. The latter is the consequence of the fact that the MRI signals depends on multiple parameters such a various relaxation rates, water diffusivity, proton exchange reactions, which are tissue specific. By choice of experimental parameters contrast can be varied to highlight structures of interest. Paramagnetic or superparamagnetic contrast agents can be used to further enhance specific structures. It is therefore not surprising that today MRI has become one of the most important modalities for structural imaging.

Yet MRI provides information beyond mere anatomy. The analysis of dynamic signal changes - e.g. during administration of a contrast agent - yields relevant quantitative information on physiological processes such as blood flow, vascular permeability, or renal function. Probably the most important physiological MRI application is functional MRI (fMRI), which has become an indispensable tool for studying brain function, or more precisely the hemodynamic response to neuronal activity, under normal and pathological conditions. fMRI measures local hemodynamic changes in the CNS that are linked to neural activity through neurovascular coupling.

More recently, MRI has tapped into the field of molecular imaging. By coupling the MRI contrast agent to a targeting moiety, molecular information can be derived at high spatial resolution. Yet the MRI molecular imaging approach suffers from two limitations. MRI is insensitive due to the small quantum energy involved in the process, typically concentrations have to be in the micromolar range to induced chances detectable by MRI. This can be in part be accounted for by increasing the relaxivity of MRI reporters by increase of the payload or by using physiological amplification. The second limitation is that MRI contrast agents are in general bulky, which renders target accessibility difficult. Straightforward molecular targets that can be reached by MRI contrast agents are those expressed on the endovascular side. On the other hand the efficiency of MRI probes, similar to that of fluorescent probes, can be modulated through the molecular interaction with the target. This potentially allows discriminating target-bound from free floating probe, thereby enhancing the contrast-to-background ratio. An attractive application of targeted MRI imaging are studies of cell trafficking. As many cells are rather tolerant to the amount of contrast agent they can carry, sensitivity appears to be less an issue. In fact there are some reports, that under favorable conditions single cells might be detected.

The lecture will discuss the various aspects of MRI with focus on molecular and cellular imaging applications.

Imaging modalities: PET and SPECT

Ziegler S. .

TU Munich, Department of Nuclear Medicine, Germany

sibylle.ziegler@tum.de

Nuclear medical imaging methods, positron emission tomography (PET) and single photon emission computed tomography (SPECT), utilize the detection of gamma rays leaving the body after a radioactive tracer has been administered in vivo. The choice of tracer substance as well as radio-nuclide for labelling depends on the biological process of interest and the organ which is imaged. While electronic collimation is used in PET, mechanical collimators made of high-Z materials need to be employed in SPECT imaging. Depending on the imaging situation, these collimators can be designed for parallel, diverging, or converging projection. Gamma ray detection in either modality is accomplished by scintillation detectors or semiconductor detectors, as in more recent developments. Raw data are projections of the activity distribution, which is reconstructed using analytical or statistical algorithms. Sensitivity of PET allows detecting pico-molar tracer amounts *in vivo* and current technology offers mm (PET) or sub-mm (SPECT) spatial resolution. Quantitative measurement of activity concentration in vivo is the basis for more advanced dynamic studies including biokinetic modelling.

in vivo fluorescence kinetic imaging for improved contrast and studies of temporal and quantitative biodistribution

Mansfield J. [1], Agarwal A. [2], Curtis A. [2], Krucker T. [2].

[1] Cambridge Research & Instrumentation,
[2] Novartis Institutes for BioMedical Research.

jmansfield@cri-inc.com

Introduction: In vivo fluorescence imaging has added an easy and economical modality to the rapidly growing field of molecular imaging. It offers the possibility to perform experiments analogous to bioluminescence imaging through fluorescent proteins, but at longer and more efficient wavelengths. A further distinction is the translational and research aspects enabling the imaging of fluorophore-labelled biologics (e.g., antibodies, peptides, siRNA) and activatable reagents. One unique aspect limiting the sensitivity of *in vivo* fluorescence methodologies is the confounding effect of tissue autofluorescence, which can be addressed through the proper use of spectral imaging [1,2]. However, like other molecular imaging modalities, reagent-based *in vivo* fluorescence imaging also has to contend with sensitivity and contrast problems due to non-specific signals and long wash-out times, both limiting the detection of specifically bound reagent and preventing accurate determination of uptake rates.

Methods: A kinetic imaging modality, Dynamic Contrast Enhancement, or DyCETM, that combines rapid imaging (up to 15 frames/sec monochrome or 10 sec/frame multispectrally) with an advanced data processing methodology was developed. When combined with analysis software, these allow determination of (1) the rates of change of the intensity of the fluorophore in each pixel of the image and (2) the rate of uptake and wash-out in the animal. Mice were injected with a near-infrared fluorescent agent (IgG antibody) that was taken up in the liver and imaged for 80 minutes following injection at a rate of 1 multispectral dataset per minute. Each timepoint's data were unmixed and kinetic data and "movies" assembled from these.

Results: By utilizing the uptake and wash-out rate information, a much higher contrast image of the accumulating fluorophore was obtained in a much shorter period of time (minutes and hours vs. days). In addition, body compartment data determined from the kinetic data can provide information on the temporal distributions of a fluorescent agent during the experiment and can act as inputs for rate-of-change or body compartment models.

Conclusions: This broadly applicable temporal-biodistribution methodology can be used, for example, to differentiate between the rate of liver uptake vs. the rate of tumor uptake and quantitate each signal relative to general body and/or bladder distribution. This information can then be combined with multispectral imaging and used to quantitate the biodistribution of multiple fluorophores simultaneously, each without interference from autofluorescence. When combined with models of peripheral, tumor, blood and wash-out (bladder) distributions, this kinetic imaging data can be transformed into a physiologically based pharmacokinetic model of agent distribution that provides an estimate of the pK values between the various compartments. Potentially such a method can also be used to establish optimal drug treatment schedules aiding drug discovery and development.

References:

1. Levenson, Mansfield, Cytometry A. 2006 Aug; 69(8):748-58.
2. Tam et al., Mol Imaging. 2007 Oct-Dec;6(4):269-76.

Cerenkov radiation imaging of a xenograft murine model of mammary carcinoma

Boschi F. [1], Calderan L. [1], D'ambrosio D. [2], Marengo M. [2], Fenzi A. [1], Calandrino R. [3], Sbarbati A. [1], Spinelli A. E. [3].

[1] University of Verona,
[2] S. Orsola – Malpighi University Hospital,
[3] S. Raffaele Scientific Institute.

federico@anatomy.univr.it

Introduction: 2-[18F]fluoro-2-deoxy-D-glucose (^{18}F-FDG) is a well known radiotracer for the *in vivo* studies of several diseases. In a previous paper [1] we showed that the positrons emitted by ^{18}F-FDG, travelling into tissues faster than the speed of light in the same medium, are responsible of Cerenkov Radiation (CR) emission which is prevalently in the visible range. The purpose of this work was to show that Cerenkov radiation escaping from tumour tissues of small living animals injected with ^{18}F-FDG can be detected with optical imaging (OI) techniques using a commercial optical instrument equipped with charged coupled detectors.

Methods: In order to demonstrate as a proof of principle the possibility of imaging tumours using CR we studied an experimental model of mammary carcinoma named BB1. BB1 tumours were obtained by subcutaneous injection of BB1 cells, which are epithelial cells, from spontaneous mammary carcinomas of FVB transgenic mice for HER-2/neuT oncogene. The BB1 carcinomas exhibit histopatological and vascular features very similar to those of the parent spontaneous tumours. The BB1 mouse tumour model was well explained by Galiè and coworkers [2] and will not be described here.

Mice injected with ^{18}F-FDG or saline solution underwent dynamic OI acquisition and a comparison between images were performed. Multispectral analysis of the radiation was used to estimate the deepness of the source of Cerenkov light. Small animal PET images were also acquired in order to compare the ^{18}F-FDG bio-distribution measured using OI and PET scanner.

Results: The first Cerenkov *in vivo* whole body images of tumour bearing mouse and the measurements of the emission spectrum (560-660 nm range) were presented. Brain, kidneys and tumour were identified as a source of visible light in the animal body: the tissue time activity curves reflected the physiological accumulation of ^{18}F-FDG in these organs. The identification is confirmed by the comparison between CR and ^{18}F-FDG images.

Conclusions: These results will allow the use of conventional optical imaging devices for the *in vivo* study of the cancer glucose metabolism and the assessment, for example, of anti-cancer drugs. Moreover this demonstrates that ^{18}F-FDG can be employed as it is as bimodal tracer for PET and OI techniques.

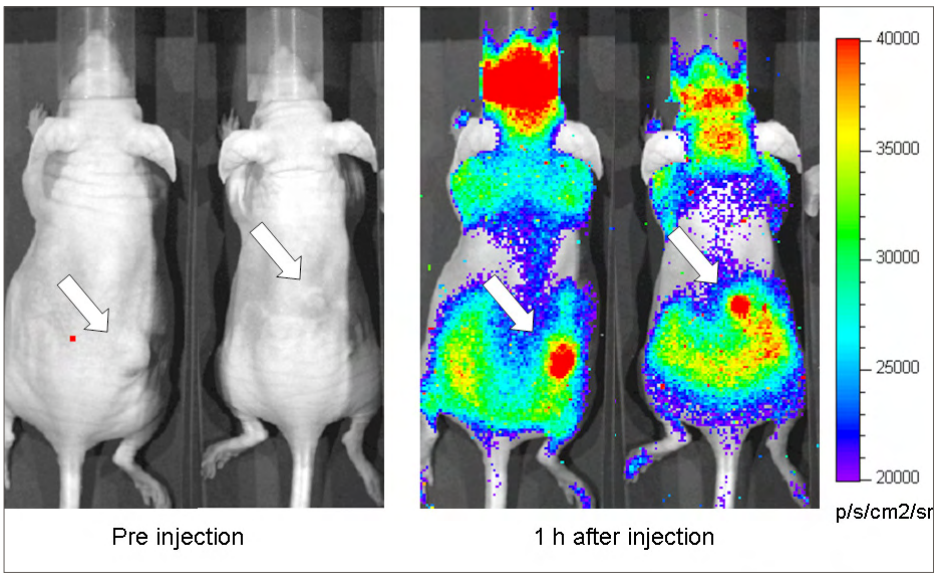

The images show a comparison between images acquired pre injection (left image) and 1 hour after 18F-FDG injection for two mice. White arrows indicate the position of the tumour masses.

References:

1. Spinelli A E et al; Phys. Med. Biol. 55(2):483-495 (2010)
2. Galiè M et al; Carcinogenesis. 26:1868-1878 (2005)

A system for 4D (3D+Kinetics) molecular imaging in bioluminescence and fluorescence

Maitrejean S. [1], Kyrgyzov I. [1], Bonzom S. [1], Levrey O. [1], Le Masne Q. [1], Hernandez L. [1], Raphael B. [2].

[1] Biospace Lab,
[2] CEA/DSV/ I2BM / SHFJ / LIME.

smaitrejean@biospacelab.com

Introduction: Several technologies and systems are now capable of delivering tri-dimensional data in Bioluminescence and Fluorescence imaging. However, all are based on sequential acquisitions, and therefore any of them allow the production of real kinetic data in 3D. In this work we demonstrate a new device which is able to acquire Bioluminescence and Fluorescence data from several views simultaneously, allowing the reconstruction of tri-dimensional images while keeping all kinetic properties of the acquisition.

Methods: Multiple views of Bioluminescence and Fluorescence data are acquired simultaneously using a photon counting device (Photon ImagerTM) in which a specific add-on with four mirrors is installed. This device (named 4Views) allows the concurrent acquisition of the ventral, dorsal, right, and left views of the animal in a single image. The size and intensity of the four sub-images (i.e. the four views) are corrected by taking the true optical path into account. The corrected photon counting data are recorded in a list mode file with time information (43 frame/s) as can be seen in Fig1.

In a second step a micro video projector is used to project a moving spot on the animal. For each position of the spot, the height of the animal is calculated by triangulation and a map of the surface of the animal is produced. As the chosen reconstruction method is based on the finite elements method, the volume of the animal is represented by a tetrahedral mesh (about 30 000 tetrahedrons) using the Delaunay algorithm, while the surface is approximated by triangles, using a marching cube method. Then, the forward problem is solved for given light sources that are placed at the nodes of tetrahedrons and the light intensities on the surface of the triangles are computed. The forward problem is based in this first version on a diffusion model with average constant absorption and diffusion parameters. In a next version, a registration of the surface of the animal with an anatomical atlas will allow to use optical parameters associated with each organ. In the following step measured data is extracted from the list mode file and mapped on the triangulated surface. Since the detected events are stored separately, any time interval from 22 ms (one frame) up to the total scan duration can be used to create the data. In the last step of the process, the inner light sources are estimated as the result of the inverse problem using a least square criterion with a Tikhonoff regularization term. This regularisation term is chosen as an entropic term in order to favour connected solution. The two last steps can be performed using any time interval of the list mode file and therefore 3D kinetic data can be computed for times scales larger than 22 ms.

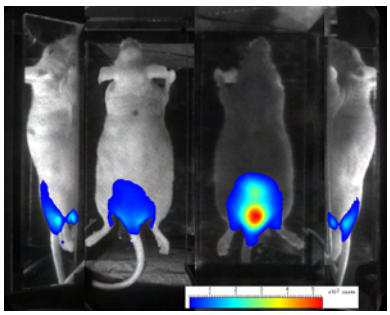

Fig1: simultaneous acquisition of four views in bioluminescence imaging.

Results: The validity of the method has been first tested using light beads (Microtek) inside a half cylinder of a scattering material (delrin). It has been demonstrated that two light beads as close as three millimetres could be separated, at a depth of one centimetre. A second set of tests has been realised on an animal (nude mice) by placing the light beads in the rectum of the animal. On the second image (Fig 2) , two beads 9 mm far from each other were placed in the rectum. It was possible to reconstruct the two positions of the light sources. The distance between the two reconstructed sources is 9.77 mm in good agreement.

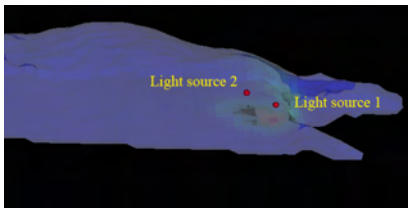

Fig2: Reconstruction of two light sources based on the four views data of fig1.

Conclusions: 3D optical reconstruction is known to be approximate, but can give useful and satisfactory results in a large number of applications. We have demonstrated that this four view approach is able to provide 3D kinetic molecular imaging data with a spatial accuracy similar to other methods.

Acknowledgement: This work was supported in part by the DIMI and ENCITE networks.

The alignment of target-specific lipoCEST MRI contrast agents

Langereis S. [1], Burdinski D. [1], Pikkemaat J. [1], Gruell H. [1], Huskens J. [2].

[1] Philips Research Europe,
[2] University of Twente.

sander.langereis@philips.com

Magnetic resonance imaging (MRI) offers a unique combination of advantages such as the recording of contrast enhanced and anatomical images with a high spatial resolution, while avoiding the use of ionizing radiation. MRI for imaging sparse molecular epitopes on diseased cells is hampered by its low sensitivity, which can potentially be overcome with liposomal chemical exchange saturation transfer (lipoCEST) contrast agents (CAs).1-3 In this case, MR detection is based on the saturation of the intraliposomal water signal with a selective radiofrequency pulse. Water exchange across the liposomal membrane causes partial saturation of the bulk water signal and, as a consequence, negative contrast enhancement in the MR image. For *in vivo* applications, it is crucial to achieve large intraliposomal chemical shifts of the water protons, as larger shifts allow for better lipoCEST contrast enhancement, reduce the interference with background magnetization transfer effects, and allow for frequency-based multiplexing. Large chemical shift differences have been obtained upon aspherical deformation of liposomes encapsulating a chemical shift agent in response to osmotic shrinkage, and the additional incorporation of amphiphilic, paramagnetic lanthanide complexes within the liposomal bilayer.

The direction of the chemical shift is governed by the alignment of the aspherical liposomes in the external magnetic field, which in turn is dictated by the sign of the magnetic anisotropy of the incorporated amphiphilic lanthanide complex. The use of lipoCEST CAs as targeted probes for molecular MRI applications entails their specific binding and immobilization at the target site, for example, the surface of a biological structure or a cell. To maximize the attractive interactions, such aspherical liposomes will tend to align with the target structure (Scheme 1).4 This enforced orientation may, however, be different from the magnetic alignment. As a consequence, the chemical shift of the intraliposomal water of the bound lipoCEST CA may differ from that of the unbound CA. It is therefore essential to understand the interplay between the preferred magnetic and the enforced mechanical alignment of such aspherical lipoCEST CAs. Herein, we address the alignment change of such aspherical liposomes upon multivalent binding to a target surface, which was studied by using routine CEST MR methods.4

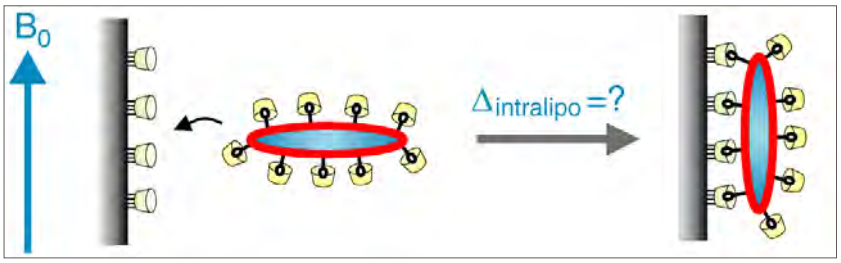

Fig1.: Reorientation of aspherical lipoCEST contrast agents upon binding to a target surface with respect to an external magnetic field (B0).4

References:

1. Aime, S.; Delli Castelli, D.; Terreno, E. Angew. Chem. Int. Ed. 2005, 44, 5513-5515.
2. Terreno, E.; Cabella, C.; Carrera, C.; Delli Castelli, D.; Mazzon, R.; Rollet, S.; Stancanello, J.; Visigalli, M.; Aime, S. Angew. Chem. Int. Ed. 2007, 46, 966-968.
3. Langereis, S.; Keupp, J.; van Velthoven, J. L. J.; de Roos, I. H. C.; Burdinski, D.; Pikkemaat, J. A.; Grüll, H. J. Am. Chem. Soc. 2009, 131, 1380-1381.
4. Burdinski, D.; Pikkemaat, J. A.; Emrullahoglu, M.; Costantini, F.; Verboom, W.; Langereis, S.; Grüll, H.; Huskens, J. Angew. Chem. Int. Ed. 2010, 49, 2227-2229.

Lanthanide-based *in vivo* luminescence imaging

Petoud S. .

CNRS, France

spetoud@pitt.edu

Introduction: Fluorescence and luminescence are detection techniques that possess important advantages for bioanalytical applications and biologic imaging: high sensitivity, versatility and low costs of instrumentation. A common characteristic of biologic analytes is their presence in small quantities among complex matrices such as blood, cells, tissue and organs. These matrices emit significant background fluorescence (autofluorescence), limiting detection sensitivity.

The luminescence of lanthanide cations has several complementary advantages over the fluorescence of organic fluorophores and semiconductor nanocrystals, such as sharp emission bands for spectral discrimination from background emission, long luminescence lifetimes for temporal discrimination and strong resistance to photobleaching. In addition, several lanthanides emit near-infrared (NIR) photons that can cross deeply into tissues for non-invasive investigations and that result in improved detection sensitivity due to the absence of native NIR luminescence from tissues and cells. The main requirement to obtain lanthanide emission is to sensitize them with an appropriate chromophore.

Methods: An innovative concept for such sensitization of lanthanide cations is proposed herein; the current limitation of low quantum yields experienced by most mononuclear lanthanide complexes is compensated for by using larger numbers of lanthanide cations and by maximizing the absorption of each discrete molecule, thereby increasing the number of emitted photons per unit of volume and the overall sensitivity of the measurement. To apply this concept, we are developing a family of dendrimer-naphthalimide ligands that are able to incorporate several lanthanide cations. Polyamidoamine (PAMAM) dendrimers have been chosen as a basis for these complexes because the oxygen atoms of the amido groups located along their branches can bind and protect the lanthanide cations inside the dendrimer core.1,2 Derivatives of naphthalimide groups, required for the sensitization of the lanthanide cations, are located at the branch termini. Our synthetic approach allows facile modification of the dendrimer complex for control over photophysical properties and solubility. It also provides for the attachment of different types of targeting agents such as peptides, oligonucleotides or proteins, as well as other sensing agents, to provide functionality to these compounds in a broad range of applications.

Results: In this paper, we will describe several examples of luminescent polymetallic lanthanide complexes based on dendrimers. We will also present examples of their applications as reporters and sensors for biologic imaging in living cells and small animals.

References:

1. J. P. Cross, M. Lauz, P. D. Badger, S. Petoud, Journal of the American Chemical Society, 2004, 126, 16278.
2. D. R. Kauffman, C. M. Shade, H. Uh, A. Star and S. Petoud, Nature Chemistry 2009, 1, 500.

New perspectives for imaging molecules and metabolism *in vivo*

Gruetter R. .

University of Lausanne and Geneva, Switzerland

rolf.gruetter@epfl.ch

46

Magnetic resonance imaging is subjected to continuous advances and discoveries, much of which are lead by either improved data acquisition techniques and/or higher magnetic fields or the detection of novel principles/contrast mechanisms altogether. This presentation will highlight on one hand the possibility to detect contrast agents at very low concentrations using a new approach to MR, based on hyperpolarized media using dissolution DNP. The potential will be demonstrated especially for long-lived nuclei with long T1, such as Lithium-6, Yttrium-89 and N-15, but also C-13 will be illustrated. The ability to detect low-concentration nuclei or rare spin nuclei opens new possibilities for molecular imaging. On the other side, for imaging molecules (metabolism) recent advances have allowed to attain in rodent brain a spatial resolution of below 1umol at 14.1 Tesla that matches or even exceeds that possible by nuclear imaging modalities, in particular PET. The quantitative nature of the MR spectroscopic imaging approach allows insights into cellular biochemistry and metabolism that complements the capabilities of PET and SPECT and opens new windows on characterizing disease evolution and treatment opportunities, as will be illustrated with the example of ischemia and cancer, among others.

In vivo biodistribution of radiolabeled matrix metalloproteinase-2 activatable cell penetrating peptides

Van Duijnhoven S. [(1)], Robillard M. [(2)], Nicolaij K. [(1)], Gruell H. [(1)].

[(1)] University of Technology Eindhoven, The Netherlands
[(2)] Philips Research Laboratories. The Netherlands

s.m.j.v.duijnhoven@tue.nl

Introduction: Activatable cell penetrating peptides (ACPPs) are a new class of promising molecular imaging probes for the visualization of proteolytic activity *in vivo*[1-3]. The cell penetrating function of a polycationic peptide is efficiently blocked by intramolecular electrostatic interactions with a polyanionic peptide. Proteolysis of a cleavable linker present between the polycationic cell penetrating peptide and the polyanionic peptide affords dissociation of both domains and enables the activated cell penetrating peptide to enter cells. Fluorescently labeled ACPPs cleavable by matrix metalloproteinase-2 (MMP-2) have been reported as specific probes for MMP-2 expressing tumors in mice[1-3]. Here, we developed MMP-2 activatable dual isotope radiolabeled ACPPs and assessed their *in vivo* biodistribution in HT-1080 tumor-bearing mice. These probes enabled us to discriminate activated from intact ACPP.

Methods: MMP-2 activatable and non-activatable cell penetrating peptides (ACPP and non-ACPP, respectively) containing an n-terminal tyrosine were prepared by Fmoc solid-phase peptide synthesis, site specifically conjugated with DOTA chelate succinimidyl ester at the c-terminus, purified by HPLC, and characterized by LC-MS. Furthermore, a DOTA-conjugated cell penetrating peptide (CPP) was synthesized as positive control. Nude mice were injected subcutaneously with approximately 3.0 x 10^6 MMP-2 positive HT-1080 fibrosarcoma cells. When the tumors reached a size of 8-50 mm^3, the mice (n=6 per probe) were used for *in vivo* studies. Therefore, the cell penetrating peptide and polyanionic peptide of ACPP or non-ACPP (60 nmol) were labeled with ^{177}Lu and ^{125}I, respectively, analyzed by iTLC and HPLC, injected into the tail vein, and *in vivo* biodistribution was determined 24h post-injection.

Results: Radiolabeled ACPP (>98% radiochemical purity for both ^{177}Lu and ^{125}I) showed a significant ~3-fold increase in tumor uptake relative to a negative control peptide with a scrambled linker (t-test, $p<0.01$). Furthermore, the uptake of ACPP in tumor was significantly higher (~5-fold) than in muscle ($p<0.01$), suggesting tumor associated activation of ACPP by MMP-2. Interestingly, our data showed a higher significant ACPP uptake compared to the negative control in near to all tissues, including MMP-2 negative tissues such as muscle and heart ($p<0.01$). Furthermore, the *in vivo* biodistribution studies demonstrated that the higher tissue uptake of ACPP results from uptake of its activated form. Next, the biodistribution of ^{177}Lu radiolabeled CPP showed no significantly different tumor-to-tissue ratios compared to ACPP ($p>0.05$).

Conclusions: These data show that the MMP-2 sensitive ACPP is activated tissue non-specifically, but most likely in the blood, resulting in an a-specific biodistribution of the activated ACPP. Therefore, the observed positive tumor-to-muscle ratio of ACPP is not a result of tumor-associated ACPP activation as suggested earlier[1-3].

Acknowledgement: This research was supported by the Center for Translational Molecular Medicine and the Netherlands Heart Foundation (TRIUMPH).

References:

1. Jiang T et al.; PNAS. 51:17867-17872 (2004)
2. Aguilera TA et al.; Integr Biol (Camb). 1:371-381 (2009)
3. Olson ES et al.; Integr Biol (Camb). 1:382-393 (2009)

YIA applicant

48

Bioresponsive MRI contrast agents based on self-assembling β-cyclodextrin nanocapsules

Martinelli J. [(1)], Fekete M. [(1)], Tei L. [(1)], Botta M. [(1)].

Università del Piemonte Orientale "A. Avogadro", Italy

jonathan.martinelli@unipmn.it

Introduction: One of the most exciting research area in the development of MRI contrast agents is the design of responsive or "smart" probes, whose performance is modulated by changes in physiological environment such as pH, partial oxygen pressure, metal ion concentration, enzyme activity etc. We have designed and synthesized a new type of nanosized Gd-based MRI probe containing disulfide bonds, that can be activated (i.e. switched on or off) under reducing conditions like those where specific enzymes or high radical concentrations are associated with a disease state (e.g. tumors, strokes etc.). The activation of the agent is signaled by a large change in the relaxation properties.

Methods: The macromolecular architecture of the agent is based on nanocapsules prepared from perthiolated β-cyclodextrins via oxidation of the thiol groups to form S-S bridges.1 The assembly was carried out in the presence of either an equimolar amount or an excess of Gd-benzyl-AAZTA2 as the MRI-active paramagnetic complex, able to form inclusion adducts with the cyclodextrin building-blocks and thus being "trapped" inside the capsules during their formation. After purification of the nanomaterials and removal of the external Gd-complexes by prolonged dialysis, the macromolecular systems were characterized by analytical and NMR relaxometric techniques. Reduction kinetic experiments were carried on by monitoring the variation in the longitudinal relaxation rate vs. time upon addition of tris(2-carboxyethyl)phosphine (TCEP)3 as a reducing agent able to cleave the disulfide bonds between the CD units.

Results: High relaxivity nanoparticles made up of several β-CD units were formed which include in the inner core a relatively large number of Gd-chelates. The ICP analyses and NMRD profiles confirmed that a significant amount of complex was caged within the macromolecular structures. The relaxivity is as high as 22 mM-1 s-1 at 20 MHz and 25 °C for the system prepared with a 5:1 complex/CD ratio. Dynamic light scattering measurements also showed that the size of the nanocapsules prepared in the presence of the Gd-complex is sensibly bigger than in its absence (120-200 nm vs. 30 nm). Following addition of TCEP and cleavage of the S-S bridges, a significant decrease (ca. 30%) in the water proton relaxation rate was observed.

Conclusions: The high relaxivity values measured for the Gd-loaded nanocapsules imply a high permeability of water through the cyclodextrin units of the surface shell. Upon disruption of the nanoparticles following the cleavage of the disulfide bonds between the CD units by the reducing agent TCEP, the complexes are released and originate an equilibrium between the free form and their adduct with the monomeric CDs. This is signaled by a remarkable decrease in the relaxivity as a consequence of the shortening of the reorientational correlation time τR.

According to these data, our β-cyclodextrin nanocapsules containing Gd-complexes appear to be promising as MRI contrast agents responsive to reducing biological environments.

Acknowledgement: This work is supported by the Regione Piemonte (Italy) as part of the NanoIGT project.

References:

1. Jones, L. C.; Lackowski, W. M.; Vasilyeva, Y.; Wilson, K.; Chechik, V. Chem. Commun. 2009, 1377-1379.
2. Aime, S.; Calabi, L.; Cavallotti, C.; Gianolio, E.; Giovenzana, G. B.; Losi, P.; Maiocchi, A.; Palmisano, G.; Sisti, M. Inorg. Chem. 2004, 43, 7588-7590.
3. Burns, J. A.; Butler, J. C.; Moran, J.; Whitesides, G. M. J. Org. Chem. 1991, 56, 2648-2650.

Photochemical activation of endosomal escape of MRI-Gd-agents in tumor cells

Gianolio E. [1], Arena F. [1], Hogset A. [2], Aime S. [3].

[1] Centro di Imaging Molecolare,
[2] PCI Biotech AS Laboratories,
[3] Molecular Imaging Center, Torino Italy.

eliana.gianolio@unito.it

Introduction: The cellular uptake of xenobiotics often procedes through the entrapment into endosomes. As recently reported1,2, in the case of cellular labeling with Gd-based complexes, the confinment into endosomal vesicles negatively affects the attainable relaxation enhancement of water protons. In fact it has been shown that, upon increasing the number of Gd(III) per cell, a quenching effect on the observed relaxivity takes place. It is the consequence of the fact that the term |R1end – R1cyt| is > than the water exhange rate between the vesicular and cytosolic compartments. In this communication we report an efficient method for endosomal escape of paramagnetic Gd(III) chelates that yields to a marked improvement of the efficiency in cellular labeling.

Methods: The Photosensitizer TPPS2a (LumiTrans®) and the Lumisource® lamp were provided by PCI Biotech AS laboratories (Oslo, Norway). For cellular labeling, ca. 3-4×106 HTC,K562, NEURO2A and C6 cells were incubated for 18 hours at 37°C with different concentrations (5-100mM) of Gd-HPDO3A in the absence and in the presence of the Photosentisizer (2µl/ml). After this incubation time cells were washed three times and incubated for additional 4 hours at 37°C. Then the cells containing the Photosentisizer were exposed to LumiSource light for 5 minutes. Then cells were detached, washed and transferred into glass capillaries for registraion of MR-images on a Bruker Avance300 spectrometer operating at 7.1T.

Results: The cellular labeling has been pursued by pynocitosis (18h at 37°C) at different concentration of Gd-HPDO3A in the presence and in the absence of PCI treatment. As shown in the figure 1A, a marked enhancement in the labeling efficiency has been observed upon application of photochemical stimulus to cells entrapping Gd-HPDO3A and TPPS2a. This considerable gain in signal intensity achieved when cells are processed with PCI tehnology is due to the release of Gd-units from endosomes to cytosol. As shown in Fig. 1B, the "quenching" effect on the relaxivity of cells processed with PCI technology is reached when the number of Gd-HPDO3A per cell is ca. One order of magnitude higher than the number causing the same effect when the paramagnetic complexes are confined into endosomes. Thus, on going from the endosome-entrapped to cytoplasm-entrapped Gd(III), the paramagnetic loading can be several times higher thus allowing a marked improvement in the MRI detection of labelled cells.

Conclusions: The PCI methodology appears an excellent route to pursue the endosomal escape of Gd-HPDO3A molecules entrapped by pynocitosis in different types of cells. It as been shown that it allows to exploit high payload of Gd-HPDO3A before the quenching effect becomes detectable.

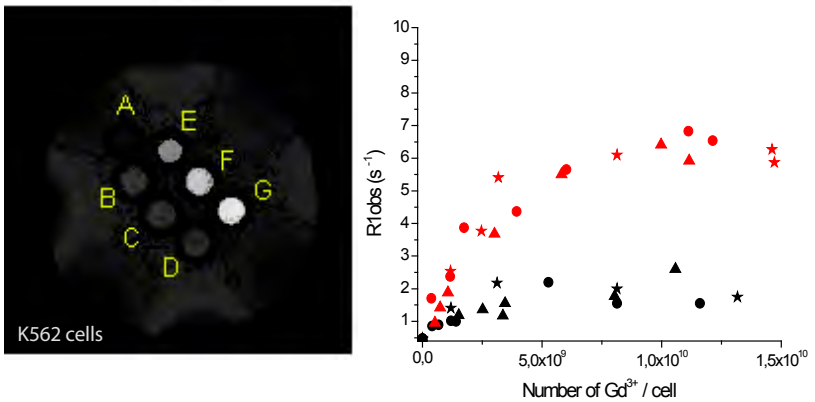

Fig.1: A) T_1-weighted spin echo images of K562 cells labeled with Gd-HPDO3A. Phantoms E, F and G contain cells treated with the PCI technology while phantoms B, C, and D contain cells simply labeled by pynocitotic uptake. B) Observed relaxation rates of cells (HTC stars; NEURO-2a circles; C6 triangles) labelled with Gd-HPDO3A with endosomic (black symbols) distribution as a function of the number of Gd(III) found in each cell.

References:

1. Terreno, E et al., Magnetic Resonance in Medicine, 2006, 55, 491-497.
2. Strijkers G.J. et al. 2009, 61, 1049-58.

Francesca Odoardi

Education and Research Experience:

Degree in Medicine and Surgery at the Catholic University of Rome (Italy).

Membership of the College of Physicians and Surgeons of Rome (Italy).

Specialization in Neurology at the Catholic University of Rome (UCSC).

Post-graduate research at the laboratory of muscular disease of the neurological department at the Catholic University of Rome (UCSC).

PhD in Neuroscience at the Neuroscience Department of the Catholic University of Rome (UCSC) within a joint collaboration with the department of Neuroimmunology of the Max Planck Institute for Neurobiology (Martinsried, Germany).

Post doctoral position at the Max Planck Institute of Neurobiology, department of Neuroimmunology (Martinsried, Germany).

Group leader position at the Institute for Multiple Slerosis Research (IMSF) of the Georg-August Universität of Göttingen.

Dissertation: Visualization of antigen presentation and T cell activation after treatment with high doses of soluble antigen.

Selected references:

- I. Bartholomäus, N. Kawakami, F. Odoardi, C. Schläger, D. Miljkovic, J.W. Ellwart., W.E.F Klinkert., C. Flügel-Koch, T.B. Issekutz, H. Wekerle, A. Flügel. Effector T cell interactions with meningeal vascular structures in nascent autoimmune lesions, Nature. 2009 Nov 5; 462 (7269):94-8.
- W. Dammermann+, B. Zhang+, M. Nebel+, C. Cordiglieri+, F. Odoardi, T. Kirchberger, N. Kawakami, J. Dowden, F. Schmid, K. Dornmair, M. Hohenegger, A. Flügel*, A.H. Guse*, B.V.L. Potter* (2009) NAADP mediated Ca2+ signaling via type 1 ryanodine receptor in T cells revealed by a synthetic NAADP antagonist, PNAS, 2009 Jun 30; 106 (26): 10678-83. +,* equal contribution.
- Odoardi F, Kawakami N, Klinkert WE, Wekerle H, Flügel A. Blood-borne soluble protein antigen intensifies T cell activation in autoimmune CNS lesions and exacerbates clinical disease. Proc Natl Acad Sci U S A. 2007 Nov 20;104(47):18625-30.
- Flügel A, Odoardi F, Nosov M, Kawakami N. Autoaggressive effector T cells in the course of experimental autoimmune encephalomyelitis visualized in the light of two-photon microscopy. J Neuroimmunol. 2007 Nov;191(1-2):86-97.
- Odoardi F, Kawakami N, Li Z, Cordiglieri C, Streyl K, Nosov M, Klinkert WE, Ellwart JW, Bauer J, Lassmann H, Wekerle H, Flügel A. Instant effect of soluble antigen on effector T cells in peripheral immune organs during immunotherapy of autoimmune encephalomyelitis. Proc Natl Acad Sci U S A. 2007 Jan 16;104(3):920-5.
- Kawakami N, Nägerl UV, Odoardi F, Bonhoeffer T, Wekerle H, Flügel A. Live imaging of effector cell trafficking and autoantigen recognition within the unfolding autoimmune encephalomyelitis lesion. J Exp Med. 2005 Jun 6;201(11):1805-14.

Immune surveillance and autoimmunity: how encephalitogenic T cells enther their target organ

Odoardi F. .

Max Planck Institute of Neurobiology, Germany

odoardi@neuro.mpg.de

Introduced in the immunological field in 2002 two-photon microscopy is the method of choice for visualizing living cells in their anatomical compartment because it allows to image deep in the tissue with negligible phototoxicity and photobleaching. We applied this technique in order to visualize in living Lewis rat the fate of genetically labeled MBP specific effector T cells in the menigeal vessels during the initial phase of experimental autoimmune encephalomyelitis, a classical model of multiple sclerosis. We observed that the incoming cells remained in close association with pial blood vessels, crawling on surfaces within the outline of the vessels. This behavior was specific to the CNS: in peripheral organs, for example in peripheral nerves, muscle or subcutaneous tissue, MBP T cells mainly rolled along the inner surface of the vessels. The crawling was completely abolished by the treatment with anti VLA-4 and LFA-1 antibodies. After diapedesis, the cells continued their scan on the abluminal vascular surface and the underlying leptomeningeal (pial) membrane. Here they established contact with local meningeal phagocytes and these interactions were crucial to induce the production of proinflammatory and to trigger tissue invasion.

Exendin-4 derivatives labeled with radiometals for the detection of insulinoma: a "from bench to bed approach"

Wild D. [1], Wicki A. [1], Mansi R. [1], Béhé M. [1], Keil B. [1], Bernhardt P. [1], Christofori G. [1], Ell P. J. [1], Reubi J. C. [1], Maecke H. [1].

[1] University of Freiburg, Department of Nuclear Medicine

damian.wild@uniklinik-freiburg.de

Introduction: Strong overexpression of glucagon-like peptide-1 (GLP-1) receptors in human insulinoma provides an attractive target for imaging. We have shown that GLP-1 receptor SPECT/CT using a Lys(Ahx-DOTA)NH2 C-terminal extended Exendin-4 derivative labeled with 111In shows high sensitivity in the detection of hardly detectable insulinoma [1]. For obvious reasons 111In is not an ideal nuclear imaging probe label. We therefore aimed at the development of 99mTc-(SPECT/CT) and 68Ga-, 64Cu-(PET/CT) labeled peptides. In addition we extended our clinical studies with a DTPA-modified peptide for higher specific activity labeling with 111In.

Methods: Internalisation, biodistribution and imaging studies were performed in the Rip1Tag2 mouse model and the corresponding cell line. The Results were compared with the "gold standard" Lys40(Ahx-DOTA-111In)NH2-Exendin-4. Kidney blocking was studied with poly-glutamic acid and Gelofusine. Clinical data were obtained with the 111In-labeled DTPA-analog.

Results: The tumor uptake of Lys40(Ahx-DOTA-68Ga)NH2-Exendin-4 was very high, at 205±59 %IA/g (1h pi) and was very similar to Lys40(Ahx-DOTA-111In) NH2-Exendin-4. > 90% of this uptake could be blocked by the preinjection of cold peptide. Normal organs showed much lower uptake resulting in a high lesion-to-background ratio. Kidney uptake was high and comparable to the tumor uptake. Lys40(Ahx-HYNIC-99mTc/EDDA)NH2-Exendin-4 shows distinctly lower tumor but also normal tissue uptake. Tumors with 1-3.2 mm in size could be visualised easily by SPECT and PET.

The kidney uptake could be reduced by 49-78% using poly-glutamic acid, Gelofusine or a combination of both.

Clinical studies using SPECT/CT with Lys40(Ahx-DTPA-111In)NH2-Exendin-4showed 100% sensitivity in the localisation of benign insulinoma of the first consecutive 13 patients. Some of the localisations such as an ectopic insulinoma could only be localised with SPECT/CT. Due to the long residence time in the tumor intraoperative localisation with an endoscopic gamma probe was possible even 2 weeks i.p..

Conclusions: These very promising pharmacokinetic data show that the two new imaging probes are good candidates for clinical translation: Especially the 99mTc-labeled peptide may increase the availability and distribution of the method whereas the 68Ga derivative may even allow to image and localise very small lesions

Acknowledgement: Oncosuisse grant No OSC-01778-08-2005 and grants from the Novartis Foundation and Swiss National Science Foundation are gratefully achnowledged.

References:

1. Wild D, Macke H, Christ E, Gloor B, Reubi JC. Glucagon-like peptide 1-receptor scans to localize occult insulinomas. N Engl J Med. 2008;359(7):766-768.

Assessment of HIF transcriptional activity in a mouse tumor model using GPI anchored avidin– a novel protein reporter for *in vivo* imaging

Lehmann S. [1], Garcia E. [2], Blanc A. [2], Schibli R. [2], Keist R. [1], Rudin M. [1].

[1] Animal imaging center,
[2] Paul Scherrer Institute, Villigen, Switzerland.

lehmann@biomed.ee.ethz.ch

Introduction: With the emergence of multimodal imaging approaches genetic reporters, which can be flexibly combined with multiple imaging methods, are highly attractive. Here we present the feasibility of using glycosylphosphatidylinositol anchored avidin (av-GPI) (1) as a novel reporter for multimodal *in vivo* imaging. Expressed on the extracelluar side of cell membranes, av-GPI can be targeted with biotinylated imaging probes. In this study, we employed av-GPI to read out on the activity of hypoxia inducible factors (HIFs) in tumors. Induced by tumor hypoxia to mediate the adaptation of cells to low oxygen tensions these transcription factors play an important role in cancer progression. Typically, the expression of HIF in human cancer patients is associated with more aggressive tumor phenotypes and poor patient prognosis. Imaging HIF activity in live tumors hence provides an important tool to study the mechanisms leading to its activation in cancer.

Methods: Mouse C51 cells were stably transfected with pH3SVG, a reporter construct driving the expression of avidin-GPI from a minimal SV40 promoter and 3 hypoxia response element (HRE), bound by HIF, from the human transferrin gene (2). To monitor HIF activity *in vivo*, pH3SVG transfected C51 cells were subcutanouesly implanted into Balb/C nude mice. 10 days after tumor inoculation, mice received an i.v. injection of alexa-594-biocytin and were imaged using fluorescence reflectance imaging.

Results: Fluorescence stainings of av-GPI expressing cells demonstrated that this protein is specifically expressed on the extracellular side of cell membranes. Moreover, upon pharmacological activation of HIF, we observed a shift in fluorescence indicative of an increased expression of av-GPI in fluorescent activated cell sorting (FACS) experiments involving pH3SVG transfected cells. *In vivo* fluorescence imaging showed a specific uptake of a biotinylated dye (alexa-594-biocytin) in the tumor from 60 minutes after contrast injection, whilst there was no accumulation of an unbiotinylated control probe (alexa-594-cadaverine). On ex vivo tissue sections alexa-594 biocytin was found to co-localize with zones positive for pimonidazole, a commonly used hypoxia marker (3) but also showed staining in regions devoid of pimonidazole uptake. In additional experiments, biotinylated 67Ga-DOTA was shown to specifically label avidin expressing cells in vitro.

Conclusions: Overall, we demonstrate the utility of av-GPI as a reporter for *in vivo* imaging of HIF transcriptional activity in an optical, fluorescence reflectance approach. In vitro binding studies with 67Ga-DOTA showed a high specificity of the probe in targeting av-GPI in cells, which implies that this reporter can indeed be combined with different imaging modalities. Its application in SPECT is currently being tested.

References:

1. Pinaud, F., King, D., Moore, H.-P. & Weiss, S. (2004) Bioactivation and Cell Targeting of Semiconductor CdSe/ZnS Nanocrystals with Phytochelatin-Related Peptides. Journal of the American Chemical Society 126: 6115-6123
2. Wanner, R. M., et al. (2000) Epolones induce erythropoietin expression via hypoxia-inducible factor-1 alpha activation. Blood 96: 1558-65
3. Raleigh, J. A., et al. (1998) Hypoxia and vascular endothelial growth factor expression in human squamous cell carcinomas using pimonidazole as a hypoxia marker. Cancer Res 58: 3765-8

YIA applicant

54

A leukocyte ligand of vascular adhesion protein-1 as an imaging tool in PET

Autio A. [1], Saanijoki T. [1], Sipilä H. [1], Jalkanen S. [2], Roivainen A. [3].

[1] Turku PET Centre,
[2] MediCity Research Laboratory, National Public Health Institute,
[3] Turku PET Centre, Turku Centre for Disease Modeling.

akauti@utu.fi

Introduction: Vascular adhesion protein-1 (VAP-1) is both an endothelial glycoprotein and a semicarbazide-sensitive amine oxidase (SSAO) enzyme playing a critical role in leukocyte trafficking to the sites of inflammation. Although VAP-1 was identified more than 15 years ago, the leukocyte ligand has remained unknown until very recently. Last year it was shown that Siglec-10 (sialic acid-binding immunoglobulin-like lectin) expressed on a subpopulation of lymphocytes can bind to VAP-1 and serve as its substrate [1]. According to phage display screening and structural modeling also Siglec-9 expressed on granulocytes and monocytes interacts with VAP-1. In this study, we investigated a Siglec-9 peptide as a potential imaging tool in positron emission tomography (PET).

Methods: A cyclic peptide binding to recombinant human VAP-1 was conjugated with DOTA-chelator through PEG-linker and 68Ga-labeled for PET studies as previously described [2]. The interaction between VAP-1 and 68Ga-Siglec-9 peptide was evaluated in vitro in human plasma samples possessing different SSAO levels. The VAP-1 specificity was further tested with competition assay in mice bearing melanoma xenografts by PET imaging and autoradiography. *In vivo* imaging of inflammation was examined in a rat model. All *in vivo* studies were confirmed by ex vivo measurements.

Results: The Siglec-9 peptide binding to the enzymatic groove of VAP-1 could specifically detect inflammation in rat and tumor in mouse. Competition experiments with excess of unlabeled Siglec-9 peptide revealed 3-fold lower tumor uptake in mice. According to autoradiography of the tumor cryosections, the radioactivity co-localized notably with VAP-1 as demonstrated by immunohistochemistry ($P<0.0001$). In a rat model, the Inflammation-to-muscle ratio of 68Ga-Siglec-9 peptide was 5.9±2.3. Moreover, in radio-HPLC analyses, the amount of intact 68Ga-Siglec-9 peptide in human plasma was significantly different between low and high levels of SSAO activity ($P=0.0007$).

Conclusions: Our results show that the Siglec-9 peptide detects VAP-1 in inflammation and tumor vasculature in animal models and it may also have potential in imaging of these diseases in patients.

Acknowledgement: The study was conducted within the Finnish CoE in Molecular Imaging in Cardiovascular and Metabolic Research supported by the Academy of Finland, University of Turku, Turku University Hospital and Åbo Akademi University. Anu Autio is a PhD student supported by the Drug Discovery Graduate School.

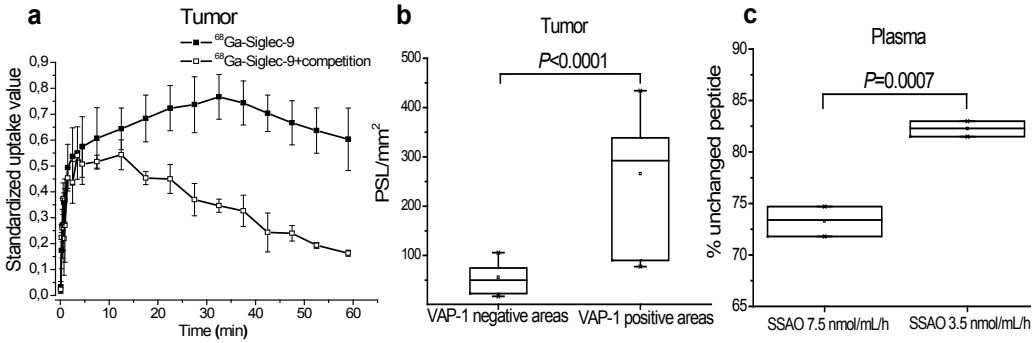

Fig1: Uptake of 68Ga-Siglec-9 peptide in melanoma xenografts in mice is specific and correlates with VAP-1 expression. (a) PET study (b) Autoradiography study (c) HPLC study.

References:

1. Kivi E et al; Blood. 114:5385–5392 (2009)
2. Ujula T et al; Nucl Med Biol. 36:631-641 (2009)

Clinical translation of *ex vivo* sentinel lymph node mapping for colorectal cancer using invisible near-infrared fluorescence light

Hutteman M. [1], Choi H. S. [2], Mieog S. [1], Van Der Vorst J. [1], Ashitate Y. [2], Kuppen P. [1], Löwik C.W.G.M. [1], Van De Velde C. [1], Frangioni J. [2], Vahrmeijer A. [1].

[1] Leiden University Medical Center,
[2] BIDMC / Harvard Medical School.

m.hutteman@lumc.nl

Introduction: Sentinel lymph node (SLN) mapping in colorectal cancer may have prognostic and therapeutic significance, however, currently available techniques are not optimal. We hypothesized that the combination of invisible near-infrared (NIR) fluorescent light and ex vivo injection could solve remaining problems in the field.

Methods: The FLARE™ imaging system was used for real-time identification of SLNs after injection of the lymphatic tracer HSA800 in the colon and rectum of (n = 4) pigs. A total of 32 SLN mappings were performed in pigs, *in vivo* and ex vivo after oncologic resection, using an identical injection technique. Guided by these results, SLN mappings were performed in ex vivo tissue specimens of 6 colorectal cancer patients undergoing resection (Figure 1).

Results: Using NIR fluorescent imaging, lymph flow could be followed in real-time from the injection site to the SLN. Pre-clinically, in pigs, the SLN was identified in 32/32 (100%) SLN mappings in both colon and rectum, under both *in vivo* and ex vivo conditions. Clinically, SLNs were identified in all patients (n = 6) using the ex vivo strategy (Figure 1). No false negatives were found. SLNs were identified within 5 minutes after injection of the fluorescent dye.

Conclusions: The current study shows proof of principle that ex vivo NIR fluorescence-guided SLN mapping can provide high-sensitivity, rapid, and accurate identification of SLNs in colon and rectum. This will permit optimized, non-FDA-approved NIR fluorescent lymphatic tracers to be translated immediately to the clinic.

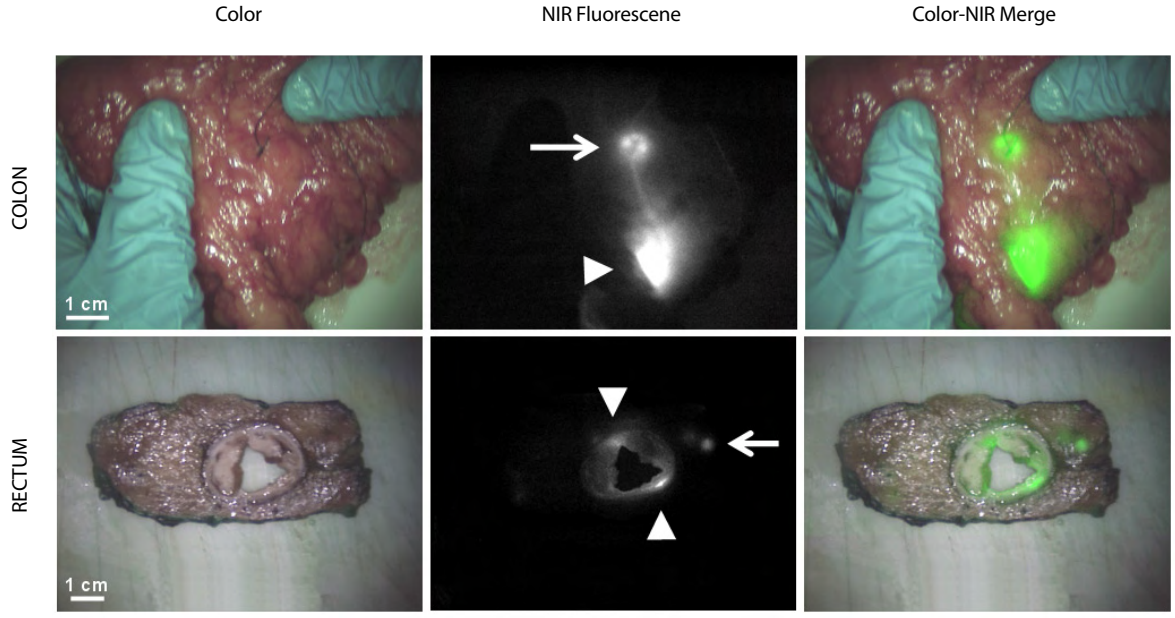

Fig1.: NIR Fluorescence-Guided SLN Mapping in Patients with Colorectal Cancer

YIA applicant

56

Development of strategies for *in vivo* MRI and Optical Imaging of neural stem cells distribution for the treatment of traumatic spinal cord injury

Lui R. [(1)], Merli D. [(1)], Libani I. V. [(1)], Madaschi L. [(1)], Marra F. [(1)], Marfia G. [(1)], Carelli S. [(1)], Clerici M. S. [(2)], Gorio A. [(3)], Lucignani G. [(1)], Ottobrini L. [(1)].

[(1)] University of Milan,
[(2)] University of Milan and Don Gnocchi Foundation IRCCS,
[(3)] University of Milan and Humanitas IRCCS, Rozzano, Milan.

ramona.lui@unimi.it

Introduction: The use of adult stem cells in cell-mediated therapies is an area of considerable interest within tissue regeneration research. However, important parameters such as the distribution of the injected cells, cell survival, target organ localisation, cell proliferation and differentiation cannot be evaluated *in vivo*. Here we propose multiple labelling protocols for *in vivo* visualisation by MRI, and Optical fluorescence imaging of murine neural stem cells (mNSC) originating from the subventricular zone of the adult murine brain in spinal cord injury animal models.

Methods: mNSC were isolated and cultured as described[1]. Cells were directly labelled for 24 hours with 200 µg Fe/ml of SPIOs (Endorem®) in presence of different amount of Protamine Sulphate (PS) (ratio Fe/PS 1:0,025; 1:0,05) and immediately analysed for viability, iron content (Perl's Staining and spectrophotometer analysis), morphology, staminality and differentiation capability. Labelled cells were injected into the tail vein of a spinal cord injury murine model and followed by MRI for a month to visualize their distribution. Initial cell distribution was also followed with scintigraphy after cell labelling with 111Indium-oxine (60 µCi/106 cells). Cells localization, distribution e viability, over time, were analysed *in vivo* with CCD camera after injection of mNCS infected with a viral vector expressing Luciferase under a PGK promoter (PLW vector).

Results: mNSC incubated for 24 with 200 µg Fe/ml Endorem® did not show significant differences in terms of viability and proliferation rate between labelled/non-labelled cells in presence or absence of different amount of PS[2]. The percentage of viable cells was 85% for Fe/PS 1:0.025 ratio, and 77% for Fe/PS 1:0.05 ratio compared to the 95% of the control. On the contrary, the percentage of iron-positive cells increased in proportion to the PS content in the medium. In particular we obtained 94,5% of iron-positive cells in the samples incubated with Fe/PS 1:0.025 ratio and 99% iron-positive cells in the samples incubated with Fe/PS 1:0.05 ratio. The iron content increased from 110 pg Fe/cell to 210 pg Fe/cell increasing PS concentration. In both cases, labelled cells were able to give rise to floating neurospheres as observed by optical microscopy after further 5 days of culture, demonstrating their maintenance of the self-renewal capability. Immune fluorescence analysis for Nestin confirmed these data. Differentiation capability was also maintained as confirmed by β-TubulinIII and GFAP expression. Scintigraphic techniques confirmed initial distribution to lung, spleen and liver while MRI showed iron signal due to stem cell localization into the lesion site at 21 and 28 days after injection. Neural stem cells, infected with the viral vector PLW, were detected up to one week after i.v. injection within the lesion of injured mice. Infected cells intramedullary injected as control were detected at the same timepoint as well.

Conclusions: These results showed that adult neural stem cells can be efficiently labelled with different molecules without significantly perturbing physiological stem cell features and self-renewal capability. This labelling protocols can be applied for the *in vivo* visualisation by MRI, scintigraphy, and Luminescence imaging of the distribution of stem cells after their transplantation into murine model of disease.

Acknowledgement: this work is supported by CARIPLO Foundation grant. Dr Lui R is supported by a fellowship from the Doctorate School of Molecular Medicine, University of Milan.

References:

1. Bottai D et al. Mol Med (2008) 14:634-644
2. Politi LS et al. Neuroradiology (2007) 49:523–534

Validation of bone marrow-derived stromal cell graft position by colocalisation of histology, bioluminescence and magnetic resonance imaging.

De Vocht N., Van Der Linden A. .

Universiteit Antwerpen – Bio Imaging Lab

nathalie.devocht@ua.ac.be

Introduction: The use of stem cell transplantation as a therapeutic tool to treat neurodegenerative disorders (e.g. traumatic brain injury, stroke, multiple sclerosis) has gained increasing interest over the last decade. However, a profound knowledge of cell implant migration, differentiation and survival will be necessary to understand the physiological mechanisms involved in regeneration of injured brain tissue. For this, the development of multimodal cell imaging techniques, both *in vivo* and post-mortem, is currently of highest importance.

Methods: We optimised a multimodal labelling strategy for bone marrow-derived stromal cells (BMSC), based on (i) genetic modification with both the eGFP and Luciferase reporter genes, and (ii) endocytic uptake of blue fluorescent magnetite-containing micron-sized particles (MPIO). This combined labelling strategy allows unambiguous identification of cell localisation, survival and differentiation using pre-mortem bioluminescence / magnetic resonance imaging (BLI/MRI) and post-mortem histological analysis.

Results: For this study, we labelled Luciferase/eGFP-expressing BMSC (BMSC-Luc/eGFP, Bergwerf et al. 2009) with 1.63 µm fluorescent (Glacial Blue) MPIOs from Bangs Laboratories. MPIO labelling of BMSC-Luc/eGFP did not influence their phenotypic properties and self-renewal capacity. In order to evaluate the suitability of these MPIO particles for *in vivo* multimodal imaging, we implanted 4 x 105 MPIO labelled (n = 15) or unlabelled (n = 15) cells by stereotactic injection in the right hemisphere (DV: 2mm beneath the dura; ML: 2mm; AP: -2mm) of syngeneic male FVB mice (10-12 weeks old). Survival of unlabelled and MPIO-labelled MSC-Luc/eGFP implants was monitored during 2 weeks by BLI, which demonstrated equal survival of both cell populations. Moreover, T2- and T2*-weighted MR images clearly demonstrated the presence of iron oxide particles in mouse brain. Additionally, combined immunohistochemistry and fluorescence microscopy was able to confirm cell identity and the presence of MPIO particles within BMSC-Luc/eGFP grafts.

Conclusions: We here demonstrate that combining three labelling strategies allows unambiguous identification of MSC following implantation in mouse brain. The MPIO-labelling allows for pre-mortem MRI detection of cell implant localisation. In addition, BMSC survival was followed up using BLI up to two weeks post-injection. Finally, the combination of eGFP expression and MPIO-labelling allows for discrimination of cell implants (eGFP+/MPIO+) from inflammatory cells (green background fluorescence/MPIO-) and free particles (eGFP-/MPIO+), enabling an improved qualitative histological analysis of cell implantation.

Acknowledgement: This work was supported in part by: (i) the EC-FP6-NoE funded DiMI (ii) the Flemish government-funded IWT-SBO BRAINSTIM Project and (iii) the FWO Flanders.

References:

1. Bergwerf I, De Vocht N, et al., BMC Biotechnology 2009; 9:1

- **ESMI Plenary Lecture 3: Theodorus W.J. Gadella Jr. (Amsterdam, The Netherlands)**
  New probe-based strategies for quantitative microscopy of signaling dynamics in single cells
  Chairs: Vasilis Nziachristos (Munich, Germany) , Bengt Långström (Uppsala, Sweden)

- **Parallel Session 5: Neuroscience II**
  Chairs: Markus Rudin (Zürich, Switzerland), Veerle Baekelandt (Leuven, Belgium), Mathias Hoehn (Cologne, Germany)

- **Parallel Session 6: Cardiovascular I – together with ESR**
  Chairs: Tony Lahoutte (Mons, Belgium), Nicolas Grenier (Bordeaux, France)

- **Parallel Session 7: Probes II – together with EANM**
  Chairs: Frédéric Dollé (Orsay, France), Denis Guilloteau (Tours, France)

- **Parallel Session 8: Gene and Cell Based Therapies – together with CliniGene**
  Chairs: Ludwig Aigner (Salzburg, Austria), Cornel Fraefel (Zürich, Switzerland)

- **ESMI Plenary Lecture 4: Hans-Jürgen Wester (Munich, Germany)**
  Molecular imaging of CXCR4 receptors
  Chairs: Adriana Maggi (Milano, Italy), Adriaan Lammertsma (Amsterdam, The Netherlands)

- **Plenary Session on Current Contribution of Imaging Technologies to Drug Development**
  Chairs: Adriana Maggi (Milano, Italy), Adriaan Lammertsma (Amsterdam, The Netherlands)

Day 2 - Friday May 28, 2010

Theodorus W.J. Gadella Jr.

Chairman of section of Molecular Cytology, Director Centre for Advanced Microscopy
Swammerdam Institute for Life Sciences, University of Amsterdam, The Netherlands
www.mc.bio.uva.nl

Dr. Gadella is founder/director of the Centre for Advanced Microscopy (CAM) at the University of Amsterdam and full professor in Molecular Cytology chairing a group of 25-30 scientists including 4 assistant professors. The CAM and chairgroup are positioned within the Swammerdam Institute for Life Science at the Science Faculty of the University of Amsterdam and fully integrated within the Netherlands Institute for Systems Biology founded in 2007. Dr Gadella personally supervises a research team on spatiotemporal cell signaling. His team wants to understand how cells can achieve and maintain a local signal in order to drive morphogenesis, to define new cytoskeletal anchorage or vesicle-docking sites. The focus is on signal flow across and in the plane of the membrane of living mammalian cells. To this end genetic encoded fluorescent biosensors are employed and the in situ molecular interactions between signaling molecules including phospholipid-second messengers, receptors, G-proteins and downstream targets are analyzed. By multiparameter imaging approaches several signaling events are visualized and quantified simultaneously in individual living cells with sub-second temporal and submicron spatial resolution. The in situ cellular imaging research heavily depends on advanced bioimaging. To this end advanced automated microscopy approaches such as fluorescence resonance energy transfer (FRET) microscopy (including bleaching-, spectral-, ratio- and fluorescence lifetime-imaging approaches), fast live cell microscopy (including spinning disk, line-scanning and controlled light exposure confocal microscopy, and total internal reflection microscopy (TIRF)), and photochemical microscopy approaches such as photoactivation, uncaging, fluorescence recovery after photobleaching (FRAP), fluorescence loss in photobleaching microscopy (FLIP), fluorescence correlation spectroscopy (FCS), cross-correlation (FCCS), lifetime-correlation (FCLS) have been implemented developed and applied to quantifying cell signalling phenomena. Currently, the palette of advanced imaging instrumentation is expanded with superresolution localization microscopy approaches such as PALM and STORM.

The research group is funded from university resources (roughly 40%), national grant agencies (NWO-ALW, CW, FOM and STW) and several international grants (ESF and EU-FP6/7 projects including integrated projects, STREPs and TMR programs).

The Gadella lab has numerous (inter)national collaborations in the field of signal transduction (Dr. C. Hoffman, Univ. Würzburg; M. Wymann, Univ. Basle; K. Jalink, NKI Amsterdam) and collaborations on probe development (dr. C. Schultz, EMBL Heidelberg; dr. K. Lukyanov & D. Chudakov, Moscow) and collaborations on advanced light microscopy (prof. van Noorden (AMC); dr. A. Houtsmuller, Erasmus MC; dr. H. Gerritsen, Utrecht; dr. Dobrucki, Univ. Krakow; prof. M. Carmo Fonseca, Lisbon). In 2007 prof Gadella was elected president of the Netherlands Society for Advanced Microscopy. Recently he was appointed as national coordinator of the advanced light microscopy activities of the Netherlands for the new large EU infrastructure (ESFRI) programme EuroBioimaging that recently entered the startup phase.

New probe-based strategies for quantitative microscopy of signaling dynamics in single cells

Gadella T.W.J. jr, Goedhart J., Van Weeren L., Crosby, K., Hink M.A.

Section of Molecular Cytology and Centre for Advanced Microscopy, Swammerdam Institute for Life Sciences & Netherlands Institute for Systems Biology, University of Amsterdam, Science Park 904, NL-1098 XH Amsterdam.

Th.W.J.Gadella@uva.nl

Since the cloning of the green fluorescent protein from Aequoria victoria, numerous fluorescence microscopy applications have been described in the literature. By exploiting the spectroscopic axis in microscopy (excitation/emission wavelength, fluorescence lifetime) utilizing spectral variants of GFP colocalization and FRET applications were enabled. In the other direction, the spectroscopical axis in microscopes can also be used to obtain novel GFP variants with optimized properties. Here we report a screening method that, in addition to fluorescence intensity, quantifies the excited state lifetime of a fluorescent protein, providing a direct measure for the quantum yield of the fluorescent protein. The novel approach was used to screen a library of cyan fluorescent protein (CFP) variants yielding the brightest cyan fluorescent protein variant described thus far which we dubbed mTurquoise. mTurquoise has a marked increased quantum yield of 0.84, and a seriously increased lifetime of 3.7 ns. Because of its monoexponential decay and high R0 for FRET to SYFP2 (5.7 nm), it is the preferred donor in FRET studies. In addition, the lifetime screening method also yielded several other CFP lifetime variants with identical spectra. It is demonstrated that three spectrally identical CFP variants can be separated in single FLIM experiment in living cells and their distribution & molecular stoichiometry can be quantified. The triple unmixing technique using the new lifetime variants can be combined with spectral separation of other GFP color variants with a great potential for multiparameter/multiplexed imaging.

We apply the different probes for the study of GPCR-triggered signaling in single mammalian cells. The design of a Gq FRET sensor reporting on activation by endogenous expressed receptors, multiparametric imaging of lipid-derived second messengers, PtdInsP2-dependent PLC translocation, and RhoGEF activation using a variety of FRET-, ratio imaging- and TIRF-microscopic applications will be presented.

Potential to use transgenic animals for imaging of neurological diseases

Aigner L. .

Institute of Molecular Regenerative Medicine, Paracelsus Medical University, Austria

ludwig.aigner@pmu.ac.at

Transgenic animal models represent an elegant and innovative tool to image the multitude of events including degenerative, inflammatory and regenerative responses in the brain. However, there are currently no transgenic animal models that would image specifically one or another neurological disease. Typically, a transgenic reporter animal highlights the activity of a gene promoter that is specifically active in one or another cell type during a certain physiological process, upon response to injury, along the course of neurodegeneration or during a regenerative response. Thus, transgenic animal models allow the imaging of physiological and pathophysiological responses that are associated with neurological / neurodegenerative diseases, but not the disease itself. For example, currently available models allow the elucidation of several aspects of neurodegeneration: 1) Inflammatory events can be visualized using transgenic animals with the TLR2 promoter controlling the expression of reporter genes; herein, these reporters are up-regulated in response to the onset of an inflammatory response hand in hand with endogenous TLR2 and microglial activation (Lalancette-Hebert, Gowing et al. 2007). 2) Reactive gliosis may be pictured using GFAP-reporter mice as a result of stroke in living animals (Cordeau, Lalancette-Hebert et al. 2008). 3) Hypoxia might be imaged due to the application of models like the HRE-GFP transgenic animals where cells that suffer from oxygen deprivation express reporter proteins induced by low-oxygen-responsive transcription factors (Berchner-Pfannschmidt, Frede et al. 2008). 4) Neuroplasticity after brain ischemia comprises the recovery of dendritic structure, and this event may be imaged using transgenic models with fluorescent proteins expressed throughout a distinct cell population and including the cellular protrusions (Li and Murphy 2008). 5) Neurogenesis and the migration of young neurons can be visualized using DCX-promo luciferase mice. This presentation will provide a summary and an overview on the current state of transgenic models in the field of neurological diseases.

Specific cell labeling with imaging reporters *in vivo* by viral vectors: the challenges

Reumers V. [1], Ibrahimi A. [2], Toelen J. [2], Aelvoet S. A. [1], Van Den Haute C. [1], Debyser Z. [2], Baekelandt V. [1].

[1] Neurobiology and Gene Therapy, Katholieke Universiteit Leuven,

[2] Molecular Virology and Gene Therapy, Katholieke Universiteit Leuven. From MoSAIC, the Molecular Small Animal Imaging Center, K.U.Leuven, Belgium

Veerle.Baekelandt@med.kuleuven.be

Viral vectors are extremely efficient tools for gene transfer into living cells. We are using lentiviral vectors and adeno-associated viral (AAV) vectors for stable overexpression and suppression of gene expression in rodent brain. Stereotactic injection of these viral vectors into different brain regions of mouse and rat brain induces overexpression or inhibition of disease-related genes, which can be used for target validation, functional genomics and generation of disease models. We have invested over the last years into reporter gene technology and non-invasive imaging in rodent brain. We have optimized bioluminescence imaging to monitor gene expression in mouse brain and to track neuronal stem cell migration and differentiation. In order to specifically target certain neuronal cell populations we have recently developed conditional lentiviral and AAV viral vectors based on Cre-mediated recombination. Application of these viral vectors in specific cre-transgenic mouse strains allows to specifically label endogenous neural stem cells in the subventricular zone or dopaminergic cells in the substantia nigra. This approach holds promise to non-invasively follow up endogenous neurogenesis and neurodegeneration over time.

YIA applicant

Optimization of an MRI method to measure microvessel density: application to monitor angiogenesis after stroke

Boehm-Sturm P. [(1)], Adamczak J. [(1)], Farr T. D. [(1)], Jikeli J. [(2)], Kallur T. [(1)], Hoehn M. [(1)].

[(1)] MPI for Neurological Research in Cologne, Germany
[(2)] Center of Advanced European Studies and Research in Bonn.

philipp.boehm-sturm@nf.mpg.de

Introduction: Angiogenesis is the growth of new vessels from an existing vascular network and is highly upregulated following ischemia. Increases in microvessel density (MVD) have been reported to occur in the peri-infarct zone of stroke patients, which was correlated with increased survival time [1]. Steady-state-contrast-enhanced (SSCE) MRI provides the ability to monitor MVD *in vivo*. To do so, the changes in relaxivities $\Delta R2/\Delta R2^*$ due to an i.v. injection of a paramagnetic blood pool contrast agent are evaluated by spin-echo (SE) and gradient-echo (GE) imaging, and the MVD index $Q=\Delta R2/(\Delta R2)2/3$ is mapped [2,3]. However, noise in the MR images can significantly distort the results of the method. Therefore, the goal of this study is to optimize the SSCE MRI parameters in simulations in order to find a noise-resistant protocol. We aim to apply the method to monitor angiogenesis after stroke in rats and to validate this by immunohistochemistry.

Results: The simulations revealed that the error in Q is minimal for a TESE of 30-40 ms and a TEGE of 10-15 ms. Areas with increased Q could be detected close to the infarct in a few of the rats as early as 7 days and in most of the rats at 14 days post MCAO. BrdU/RECA double staining was established to identify newly formed endothelial cells and laminin staining confirmed the presence of an intact basement membrane in the vessels.

Conclusions: Our results show that scanner noise can severely limit the capabilities of SSCE MRI but a set of optimal scan parameters can minimize this problem. The method has been shown to monitor potential changes of the microvasculature longitudinally and non-invasively in the ischemic rat brain. It will in the future allow to study neo-angiogenesis in the course of (stem)cell-based therapies after cerebral lesions.

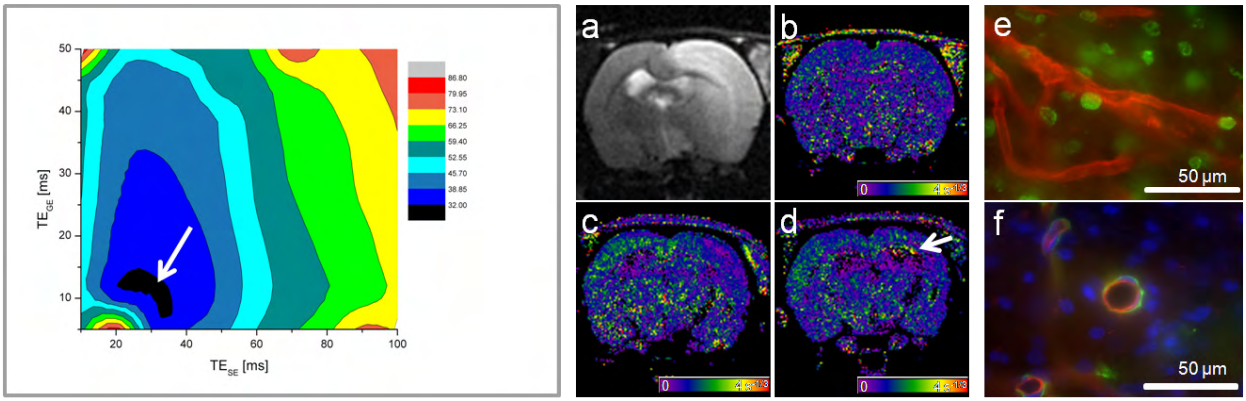

Left: simulated relative error in Q (in %) over TESE and TEGE at a fixed noise level; the arrow indicates the optimal set of TEs. Right: lesion in SE image 48 h after MCAO (a) and Q at 7 days prior (b), and 7 (c), and 14 days (d) post MCAO of the same animal. Arrow indicates an area with high Q value. Typical RECA (red)/BrdU (green) (e) and Hoechst(blue)/RECA(red)/laminin (green) (f) fluorescence microscopy images close to the infarct.

Methods: Q-maps were simulated for different levels of noise and echo times TESE/TEGE of the SE/GE images. Male Wistar rats (n=7) were scanned with SSCE MRI 7 days prior, and 7 and 14 days post 60 min transient MCAO. An SE image was acquired 48 h post MCAO to depict the lesion extent. Rats received Bromodeoxyuridine (BrdU) injections between 3-7 days post MCAO in order to label proliferating cells. Following the final SSCE MRI scan at 14 days, animals were perfused and brain sections stained for BrdU, rat endothelial cell antigen (RECA), and laminin.

Acknowledgements: Generous supply of ENDOREM by Drs. C. Corot and P. Robert is gratefully acknowledged. This work was supported in part by grants from the European Union under FP6 program (StemStroke, LSHB-CT-2006-037526), and under FP7 program (ENCITE, 201842), and an Alexander von Humboldt Research Fellowship to TDF.

References:

1. Krupinski et al, Stroke (1994) 25:1794-1798;
2. Jensen et al., MRM (2000) 44:224–230;
3. Wu et al., NMR Biomed (2004) 17:507–512

MRI study of intra-arterial bone marrow-derived macrophage administration after acute focal ischemic stroke in rats

Riou A. [1], Chauveau F. [1], Cho T.H. [1], Nataf S. [2], Berthezene Y. [1], Nighoghossian N. [1], Wiart M. [1].

[1] CREATIS-LRMN : CNRS UMR5220, INSERM U630, Univ. Lyon1, INSA-Lyon, France
[2] CNRS UMR5220, INSERM U630.

adrien.riou@live.fr

Introduction: In the past few years numerous studies have been published to assess if cell-based therapy after stroke can enhance long-term recovery. It is well established that cerebral ischemia results in a complex inflammatory cascade that mainly involves cells from the mononuclear phagocyte system1, although the beneficial or deleterious effect of this activation following stroke is still a matter of controversy. Furthermore, therapeutic benefits gained from cell-based therapy depend on migration and localization of grafted cells within the target tissue that is closely related to the cell delivery route2 and therapeutic time window3 chosen for the therapy. The aim of this study was to assess the feasibility of *in vivo* early intra-arterial (IA) bone marrow-derived macrophage (BMDM) administration for acute focal ischemic stroke treatment, using multiparametric magnetic resonance imaging (MRI).

Methods: BMDM were obtained from a sacrificed littermate of recipient rats by flushing out one hindlimb. Bone marrow cells were then seeded on uncoated flasks at 5 x 105 cells/ml in medium supplemented with murine macrophage-colony stimulating factor and flt3 ligand (mM-CSF and flt3L at 10ng/ml) for one week. At day 6, cells were labeled with anionic superparamagnetic nanoparticles overnight (AMNP, CNRS UMR 7612, Paris, France, [Fe]=1mM). Male Sprague Dawley rats (250 to 350g, n=17) were subjected to 1-h intraluminal transient middle cerebral artery occlusion (tMCAO) (n=12) or sham procedure (n=5). IA administration of AMNP-labeled cells was performed at the time of reperfusion in all tMCAO animals and in 3 shams animals (4 million in 1-ml except for one sham: 1 million in 1-ml). Ischemia / reperfusion and cell injection were monitored by transcranial laser doppler flowmetry. MRI was performed on a Bruker Biospec 7T/12cm magnet at D0 just after cells administration and from D1 to D9. The MR exam included T2-, T2*-, diffusion- and perfusion-weighted imaging and multi-echo 3D imaging. Animals were sacrificed after completion of the MRI exams and brains were prepared for immunohistological analysis with Prussian blue for iron detection and Ox-42 for macrophage detection.

Results: IA administration in tMCAO group lead to heterogeneous results: 3 rats died following injection, 2 had cells detectable only in the temporalis muscle and 7 had cells detectable in the ipsilateral parenchyma but with heterogeneous patterns: 3 had a widespread persistent hypointense signal distribution, while 4 had only few local spots of signal loss on follow-up scans. Furthermore, IA administration in the sham group caused lesion formation on follow-up scans in all injected animals (n=3), even when cell number was decreased, as opposed to the non-injected sham rats that did not have any lesions. Immunohistological analysis is in progress to ascertain iron-labeled macrophage localization.

Conclusions: Our results were consistent with that of previous studies2, 4 showing that IA delivery route efficiently brought a large number of cells to the brain soon after transplantation, but severely increased mortality. More importantly, lesions observed in the sham group (undemonstrated to date to our knowledge) suggested that this high mortality rate resulted from cell embolisation in cerebral vessels leading to formation or worsening of the ischemic lesion. This result points out a serious limitation for the translation of this cell delivery route into the clinics.

References:

1. Huang J, et al. Surg Neurol.;66:232-45 (2006).
2. Li L, et al. J Cereb Blood Flow Metab (2009).
3. de Vasconcelos Dos Santos A, et al. Brain Res.1306:149-58 (2010).
4. Walczak P, et al. Stroke. 2008;39:1569-74 (2008).

YIA applicant

Inactivated paramagnetic tissue plasminogen activator predicts thrombolysis outcome following stroke

Gauberti M. [(1)], Montagne A. [(1)], Vivien D. [(1)], Orset C. [(1)].

INSERM U919 SP2U Serine protease and pathophysiology of the neurovascular unit, France

gauberti@cyceron.fr

Introduction: Ischemic stroke is the third leading cause of death in developed countries. Despite numerous clinical trials, tissue plasminogen activator (tPA) induced thrombolysis remains the only treatment of the acute phase. However there is growing body of evidences that parenchymal tPA has deleterious effects including increased risk of intra cranial hemorrhages and neurotoxicity. To limit these side effects, only rigorously selected patients (onset of symptoms < 4.5 hrs, age < 85 hrs, etc.) benefit from thrombolysis, with more than 90% of patients being untreated. In previous in vitro studies we showed that vascular tPA can cross the intact blood brain barrier (BBB) by Low Density Lipoprotein Receptor Protein (LRP) mediated transcytosis [1]. Accordingly, increasing data of the literature suggest that BBB specific permeability to tPA could be critical for brain outcome following thrombolysis [2] [3].

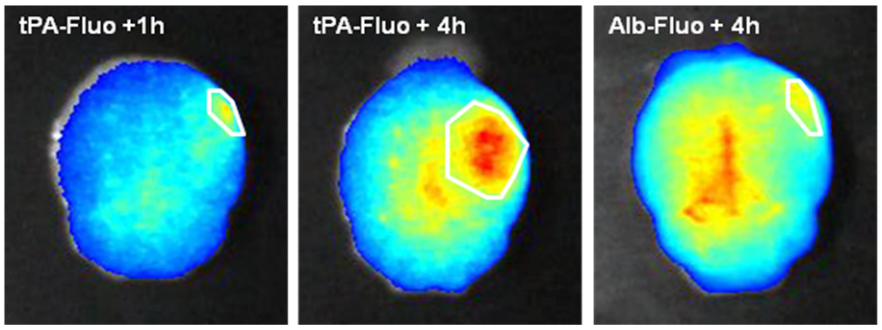

Figure 1. Ex-vivo NIRF brain imaging of fluorescent tPA and albumin administered at 1 or 4 hours after permanent middle cerebral artery occlusion in mice. Unlike albumin which has the same molecular weight, tPA can cross the BBB at 4 hours post ischemia.

Results: Here in a model of permanent middle cerebral artery occlusion in mice, we show that intravenous tPA aggravates ischemic lesion size and BBB permeability if administrated at 4 hours but not at 1 hour after ischemia. In parallel, although BBB remains impermeable to albumin, we provide evidences both by microscopic epifluorescence and near infrared fluorescence (NIRF) brain imaging of a passage of tPA across the BBB only when administrated at 4 hours post ischemia. Using MRI and inactivated paramagnetic tPA as molecular probe, we are tempting to demonstrate that such type of brain imaging could allow us to pre-select stroke patients who would not be susceptible to haemorrhagic transformations following rtPA-induced thrombolysis.

Conclusions: Non invasive imaging of inactivated paramagnetic tPA could allow clinicians to include stroke patients for thrombolysis with objective brain imaging data independently of the time post-stroke onset. As long as the BBB remains impermeable to tPA, thrombolysis seems safe.

References:

1. Benchenane et al.; Circulation 111:2241-2249 (2005).
2. Benchenane et al.; Stroke 38:1036 (2005).
3. Roussel et al.; Thromb Haemost. 102:602-608 (2009).

Matrix metalloproteinase-9 – a possible therapeutic target in intractable epilepsy

Wilczynski G. .

Nencki Institute, Poland

g.wilczynski@nencki.gov.pl

Introduction: Temporal lobe epilepsy (TLE) is a chronic, devastating, pharmacologically intractable disease in which aberrant synaptic plasticity plays a major role. Recently, MMP-9, a matrix metalloproteinase, has been implicated in synaptic plasticity, long-term potentiation and learning and memory formation. We asked, whether MMP-9 might play a pathogenic role in epileptogenesis.

Methods: High resolution light- and electron-microscopic immunocytochemistry, in situ hybridization, in situ zymography; use of transgenic animals; antibody microarrays

Results: Our study revealed MMP-9 as a novel synaptic enzyme, and a key pathogenic factor in two distinct animal models of TLE: kainate-evoked-epilepsy and pentylenetetrazole (PTZ) kindling-induced epilepsy. In particular, sensitivity to PTZ-induced epileptogenesis is decreased in MMP-9 knockout (KO) mice, whereas it is increased in MMP-9-overexpressing rats. Moreover, confocal- and immunoelectron-microscopic analyses demonstrated that MMP-9 associated with hippocampal dendritic spines bearing asymmetric (excitatory) synapses. In addition, both MMP-9 protein levels as well as its enzymatic activity became strongly increased upon seizures. Furthermore, MMP-9-deficiency diminished seizure-evoked pruning of dendritic spines, and it decreased aberrant synapse formation following mossy-fibers sprouting.

We then asked whether MMP-9 could play an important role also in human intractable epilepsy. Accordingly, we have studied the expression and localization of MMP-9 in samples of human epileptic brain tissue, obtained upon surgical treatment of childhood intractable epilepsy. By antibody microarrays, we found MMP-9, but none of the other seven MMPs studied, to be consistently upregulated in epileptic lesions, as compared to autopsy brain tissue. By immunohistochemistry of epileptic tissue, increased MMP-9 localized specifically to affected neurons.

Conclusions: Taken together, the aforementioned results suggest that the synaptic pool of MMP-9 is critically involved in the sequence of events that underlie epileptogenesis, both in rodents and humans. Therefore, the enzyme should be considered as a candidate target for therapeutic pharmacological intervention.

Acknowledgement: The work was supported by Polish-Norwegian Research Grant

References:

1. Wilczynski et al., Important role of matrix metalloproteinase 9 (MMP-9) in epileptogenesis. J Cell Biol 180: 1021-1035, 2008.
2. Konopacki et al., Synaptic localization of seizure-induced matrix metalloproteinase-9 mRNA. Neuroscience; 150:31-39, 2007

Potentials of new contrast agents for vascular molecular imaging in patients

Douek P., Boussel L., Sigovan M., Cannet E. .

Creatis, Hopital Louis Pradel, Lyon University, France

philippe.douek@creatis.univ-lyon1.fr

Introduction: Atherosclerosis is a diffuse and multisystem, chronic inflammatory disorder involving vascular, metabolic, and immune systems leading to plaque instability and / or vascular trombosis. The traditional risk assessment relies on clinical, biological and conventional imaging tools. However, they fall short in predicting near future events particularly in patients with unstable carotid artery disease or coronary artery disease. The plaque instability is dictated in part by plaque morphology, which in turn is influenced by pathophysiologic mechanisms at the cellular and molecular level. In current clinical practice, anatomic imaging modalities such as intravascular ultrasound, high-resolution magnetic resonance imaging can identify several morphologic features supporting the unstable plaque, but give little or no information regarding molecular and cellular mechanisms. optical imaging, PET, Molecular MR imaging, or more recently spectral CT may identify some of these molecular and cellular processes.

Methods: We aimed to review

1) the role of relevant biological, factors and advances in atherosclerosis biology, that illuminate key biological aspects of atherosclerosis, including macrophage activity, protease activity, lipoprotein presence, apoptosis, and angiogenesis

2) imaging agent chemistry (nanotechnology, chemical biology screens)

3) recent advances in the field of molecular imaging that have led to the development of novel paramagnetic and superparamagnetic targeted contrast agents that bind exclusively to cells such as macrophages, or molecules such as albumin, fibrin, angiogenesis markers... with either PET, MR, US or CT .and

Results: 4) a few clinically promising applications of molecular imaging for high-risk atherosclerosis and its potential for current and emerging treatments in clinical trials.

Conclusions: A multimodal assessment of plaque instability involving the combination of systemic markers, high resolution imaging and molecular imaging targeting inflammatory and thrombotic components and the potential of new drugs targeting plaque stabilization may lead to a new stratification of the atherothrombotic risk and to a better prevention of atherothrombotic stroke or myocardial infarction.

Protease specific nanosensors in atherosclerosis

Schellenberger E. .

Charité Berlin, Germany

eyk.schellenberger@charite.de

Introduction: Atherosclerosis and especially the consequences of rupture of atherosclerotic plaques are the foremost cause of death in industrialized societies. Up to date the identification of vulnerable atherosclerotic plaques prone to rupture has not been solved for the clinics. The pathological processes leading to destabilization of such plaques are highly complex and involve inflammatory action and pathological tissue remodeling of the extracellular matrix performed by proteases. Therefor the imaging of specific protease activity by high resolution MR imaging could be an important tool to find dangerous plaques that need urgent treatment.

Results: Optical imaging with activatable fluorescent smart probes has become the modality of choice for experimental *in vivo* detection of protease activity. Recently we introduced a novel high-relaxivity nanosensors that are suitable for *in vivo* imaging of protease activity by MRI. Upon specific protease cleavage, the nanoparticles rapidly switch from a stable low-relaxivity stealth state to become adhesive, aggregating high-relaxivity particles. To demonstrate the principle, we chose a cleavage motif of matrix metalloproteinase 9/2 (MMP-9 and MMP-2), proteases that important during the destabilization of the extracellular matrix of plaques. Based on clinically tested very small iron oxide particles (VSOP), the MMP-9-activatable protease-specific iron oxide particles (PSOP) have a hydrodynamic diameter of only 25 nm. PSOP are rapidly activated, resulting in aggregation and increased T2*-relaxivity of the particles.

Conclusions: PSOP could be useful sensors for the *in vivo* identification of vulnerable plaques in the future.

YIA applicant

Imaging of inflamed carotid artery atherosclerotic plaques with the use of 99mTc-HYNIC-IL-2 scintigraphy in the end-stage renal disease patients

Opalinska M. [1], Hubalewska-Dydejczyk A. [2], Stompor T. [3], Krzanowski M. [4], Mikołajczak R. [5], Garnuszek P. [5], Karczmarczyk U. [6], Maurin M. [5], Rakowski T. [7], Sowa-Staszczak A. [2], Glowa B. [2].

[1] Nuclear Medicine Unit, Chair and Department of Endocrinology, Jagiellonian University Medical School, [2] Nuclear Medicine Unit, Chair and Department of Endocrinology, Jagiellonian University Medical School, [3] Chair and Department of Nephrology, Hypertesiology and Internal Medicine, University of Warmia and Mazury, [4] Chair and Department of Nephrology, Jagiellonian University Medical School, [5] Radioisotope Center POLATOM, [6] Departament of Radiopharmaceuticals, National Medicines Institute, [7] 2nd Cardiology Clinic, Institute of Cardiology, Jagiellonian University Medical School.

mkal@vp.pl

Introduction: Cardiovascular diseases are the main cause of death in developed countries. In some patients' populations, including those with end-stage renal disease (ESRD), cardiovascular related mortality is 30 times higher compared to the general population.

Such a high cardiovascular mortality is associated with significantly accelerated atherosclerosis in ESRD mainly due to intense inflammatory state.

Therefore serum concentrations of inflammatory agents that promote atherosclerosis are often used to evaluate the cardiovascular risk.

The histological studies of the atherosclerotic plaque revealed that at least 20% of inflammatory cells within unstable plaque comprise lymphocytes T, which contain receptors for interleukin 2 (IL-2); those receptors can be identified by scintigraphy with radiolabeled IL-2.

Methods: 28 patients (13 men, 15 women, aged 55,2 ± 9,6, 17 on peritoneal dialysis, 11 on hemodialysis) underwent scintigraphy with the use of 99mTc-HYNIC-IL-2. In all cases ultrasound examination of the carotid arteries was performed to obtain information about localization and morphology of atherosclerosis plaques and intima-media thickness (IMT) measurement. Furthermore, levels of selected proinflammatory factors, atherogenic markers and calcium-phosphate balance parameters were measured. Finally, target/non-target (T/nT) ratio of IL-2 uptake in atherosclerotic plaques confirmed by carotid USG with IMT, presence of calcifications in atherosclerotic plaques and concentration of the measured agents were compared.

Results: Increased 99mTc-IL-2 uptake in atherosclerotic plaques previously visualized by neck ultrasound in 38/41 (91%) cases was detected. Median T/nT ratio of focal 99mTcIL-2 uptake in atherosclerotic plaque was 2,35 (range 1,23– 3,63, average 2,35 ± 0,70). Mean IMT value on the side of plaque assessed in scintigraphy was 0,79 ± 0,18 mm (median 0,8, range 0,5 – 1,275).

No statistically significant association was found between 99mTc-IL-2 T/nT ratio and mean value of either IMT or classical cardiovascular risk factors. Inversely, proportional dependence between scintigraphy results and hemoglobin concentration ($R = - 0,21$, $p = 0,02$) was found. Furthermore, relationships between T/nT ratio and homocysteine ($R = 0,22$, $p = 0,037$), ApoB ($R = 0,31$, $p = 0,008$), ApoB/ApoA-I ratio ($R= 0,29$, $p= 0,012$) and triglycerides concentration ($R = 0,26$, $p = 0,021$) were detected. Lower T/nT ratio in patients with better parameters of nutrition state (hemoglobin, albumin, adiponectin) in comparison with patients with worse nutritional parameters (3,20 ± 0,5 vs 2,16 ± 0,68, $p = 0,025$) was revealed as well as the difference between values of T/nT ratio in groups of patients with values of ApoB, sCD40L and ADMA above and below median (3,18 ± 0,52 vs 2,16 ± 0,68 $p = 0,031$). An interesting relationship between T/nT ratio in atherosclerotic plaques with and without calcifications (2,35 ± 0,68 vs 1,924 ± 0,55 $p = 0,088$) was observed.

Conclusions: Scintigraphy with the use of labeled IL-2 can be a tool for inflamed atherosclerotic (vulnerable) plaque visualization within common carotid arteries in ESRD patients. Quantitative results of the carotid arteries scintigraphy with labeled IL-2 correlate with serum concentration of selected cardiovascular risk markers

Acknowledgement: This work is supported by the Polish Committee for Scientific Research (KBN) within Research Project 2 P05B 003 28

References:

1. Annovazzi A et al; 99mTc-interleukin-2 scintgraphy for the *in vivo* imaging of vulnerable atherosclerotic plaque. Eur J Nucl Med Mol Imaging 2006; 33: 117 – 126.

Uptake of ^{68}Ga-Chloride in Atherosclerotic Plaques of LDLR$^{-/-}$ApoB$^{100/100}$ Mice

Silvola J. [1], Laitinen I. [2], Sipilä H. [1], Laine J. [3], Leppänen P. [4], Ylä-Herttuala S. [4], Knuuti J. [1], Roivainen A. [5].

(1) Turku PET Centre, University of Turku,
(2) Nuklearmedizinische Klinik der TU Muenchen, Technische Universitaet Muenchen,
(3) Department of Pathology, Turku University Hospital,
(4) A.I. Virtanen Institute, University of Kuopio,
(5) Turku Centre for Disease Modelling, University of Turku.

jmuhau@utu.fi

Introduction: Atherosclerosis is an inflammatory disease in which monocytes/macrophages have essential role in the development of plaques. Radiogallium has been used for decades for *in vivo* imaging of inflammation. 68Ga is a positron emitter with a half-life of 68 min and it is suitable for PET imaging. Purpose of this study was to explore the uptake of 68Ga-chloride in atherosclerotic plaques in mice.

Methods: Uptake of intravenously administered 68Ga-chloride (17 ± 2 MBq) was investigated in 9 atherosclerotic LDL-/-ApoB100/100 mice and 6 control mice at 3 hours after injection. LDL-/-ApoB100/100 mice were kept in on a high fat, Western-type diet for 3-4 months, starting at 7 months of age. Control mice were fed with regular chow. The biodistribution of the tracer was evaluated, and aortic cryosections were further analysed by digital autoradiography. Subsequently, the autoradiographs were combined with histological and immunohistological analysis of sections [1].

Results: According to the autoradiography analysis, the radioactivity uptake in atherosclerotic plaques was higher compared to healthy vessel wall (ratio 1.8 ± 0.2, P = 0.0002) and adventitia (ratio 1.3 ± 0.2, P = 0.0011). Some 68Ga-radioactivity was also detected in calcified regions of plaques. Autoradiography signal co-localized with macrophages as demonstrated by Mac-3 immunohistochemistry. In both mice strains, the highest level of radioactivity was found in the urine and blood.

Conclusions: We observed a moderate but significantly higher 68Ga-chloride uptake in the aortic plaques of atherosclerotic mice. While the uptake of 68Ga-chloride was promising in this animal model, the slow blood clearance may limit the usability of 68Ga-chloride in clinical imaging of atherosclerotic plaques.

Acknowledgement: The study was conducted within the Finnish Centre of Excellence in Molecular Imaging in Cardiovascular and Metabolic Research, supported by the Academy of Finland, University of Turku, Turku University Hospital and Åbo Akademi University. This work was further funded by the Finnish Foundation for Cardiovascular Research, Instrumentarium Foundation and the Drug Discovery Graduate School.

References:

1. Haukkala J et al; Eur J Nucl Med Mol Imaging. 36:2058–2067 (2009)

YIA applicant

Hybrid imaging using dual energy µCT and FMT for characterization of atherosclerotic plaques in ApoE -/- mice

Gremse F. [1], Rix A. [2], Bzyl J. [1], Lederle W. [1], Schulz R.[2], Perkuhn M.[3] Schober A. [3], Weber C. [3], Kiessling F. [1].

[1] Department of Experimental Molecular Imaging, Medical Faculty, RWTH Aachen University,
[2] Chair for Biological Imaging, Technical University Munich, Germany,
[3] Department of Diagnostic Radiology, Medical Faculty, RWTH Aachen University,
[4] Institute of Molecular Cardiovascular Research RWTH Aachen University, Germany.

fgremse@ukaachen.de

Introduction: To evaluate the ability of combined µCT and fluorescence mediated tomography (FMT) to characterize early and late stages in atherosclerotic plaque formation.

Methods: Three groups of ApoE -/- mice were scanned by dual energy µCT and FMT. Iodine based blood pool CT contrast agent and a fluorescent probe for active cathepsins were used. CT and FMT datasets were fused using automated marker detection and registration. Group 1 consisted of 5 mice with an age of more than 40 weeks fed with normal chow. Group 2 included 6 mice (age < 20 weeks) with 12 weeks of cholesterol diet and group 3 consisted of 5 mice (age <20 weeks) fed with normal chow. Blood vessels were visualized by µCT using dual energy functionality. For statistical testing the Kruskal Wallis test was used.

Results: All mice of group 1 had calcified plaques at the aortic arch and the brachiocephalic trunk. One calcified plaque was found at the bifurcation of the left common carotid artery. No calcified plaques were found in the other two groups. The inner vessel diameter of the brachiocephalic trunk was measured and normalized by body weight. Mice of group 1 and 2 had smaller normalized diameters than group 3 ($p<0.05$). Cathepsin activity in the region of the ascending aorta, aortic arch and the carotids was higher for old and cholesterol mice than for young mice ($p<0.05$). In all groups high activity was also found in axillary lymph nodes and some activity was found in lymph nodes along the jugular veins.

Conclusions: The combination of dual energy µCT and FMT is favourably suited to characterize atherosclerotic mouse models. Inflammation and remodelling of the vessel wall in the large arteries is reflected by a decrease in relative vessel diameter, which holds true for young mice fed with cholesterol diet and old mice fed with normal chow. Plaque calcification only occurs in ApoE -/- mice of advanced age and may be interpreted as the long term consequence of arterial inflammation. In contrast, cathepsin activity as a measure of macrophage infiltration is capable of indicating the inflammatory stage at early and late stages. However, due to cathepsin activity in activated lymph nodes along the jugular vein it is mandatory to accurately fuse the FMT and µCT data to prevent the misinterpretation of lymph nodes as plaques.

Acknowledgement: CT-Imaging GmbH enabled rapid development of a multi-modality mouse bed.

References:

1. Nahrendorf M, Waterman P, Thurber G, Groves K, Rajopadhye M, Panizzi P, Marinelli B, Aikawa E, Pittet MJ, Swirski FK, Weissleder R (2009) Hybrid *in vivo* FMT-CT imaging of protease activity in atherosclerosis with customized nanosensors, Arterioscler Thromb Vasc Biol. 2009 Oct;29(10):1444-51.

Long circulating emulsion based ct contrast agents

De Vries A. [1], Custers E. [2], Lub J. [2], Nicolay K. [1], Gruell H. [1].

[1] Eindhoven University of Technology, The Netherlands
[2] Philips Research, Eindhoven, The Netherlands

A.d.Vries@tue.nl

Introduction: With X-ray and CT moving forward into the interventional care, such as stent placement, balloon dilatation, vascular surgery, and electrophysiological procedures, there is a need for contrast agents that have long circulation times [1]. Previously, we prepared iodinated emulsion-based CT contrast agents that remain in the blood pool for several hours [2]. The primary blood clearance occurs *via* uptake in the reticuloendothelial system (RES), which is known to be dose dependant. Here, we tested if circulation times of these iodinated emulsions can possibly be extended by a co-injection with liposomes to slow down RES uptake of the contrast agents. We co-injected the iodinated emulsion (radiolabeled with ^{111}Indium) together with liposomes (radiolabeled with ^{177}Lutetium) and investigated the biodistribution of iodinated nanoparticles and liposomes by *in vivo* CT and γ-counting.

Methods: Liposomes were prepared using DPPC, cholesterol and DOTA-DSPE (mol ratio 65.7/33.3/1) and were radiolabeled with ^{177}Lutetium. Iodinated nanoparticles were prepared using 2% *w/w* PBD-PEO (with 1 mol% PBD-PEO-DOTA) and 20% *w/v* 3,7-dimethyloctyl 2,3,5-triiodobenzoate and were radiolabeled with ^{111}Indium. Swiss mice were used in the study, in which 2 mL/kg body weight of iodinated contrast agent (113 mgI/mL) together with 2 mL/kg body weight of a) physiological salt (n=5) (control) or b) liposomes (n=5) was injected, leading to an injected dose of 225 mg I/kg body weight. Helical CT scans were acquired pre-injection (reference) and up to 3 hours post-injection using a dedicated small animal SPECT/CT system (nanoSPECT/CT®, Bioscan). The uptake of ^{177}Lutetium and ^{111}Indium in dissected organs was measured using a γ-counting wizard.

Results: Fig. 1 shows the Hounsfield Unit (HU) increase of blood after the injection of emulsion and emulsion together with liposomes as a function of time. The blood half life increased by 40 minutes to $t_{½}$=116 min when liposomes were co-injected ($t_{½}$=77 min for pure emulsion; blood half time was derived from a single-exponential fit). The CT and biodistribution data (γ-counting) showed that when co-injecting liposomes, the emulsion particles are taken up in a lower degree by the spleen as compared to the control group.

Conclusions: Circulation times of the iodinated emulsions as CT contrast agents can be further extended when co-injecting liposomes. The liposomes are likely taken up by the RES system, thereby slowing down the clearance of the iodinated emulsion in a dose dependant manner. As liposomes are well tolerated with little toxicity at high doses, the above strategy can be exploited to formulate well tolerated long circulating iodinated contrast agents without increasing the administered iodine dose.

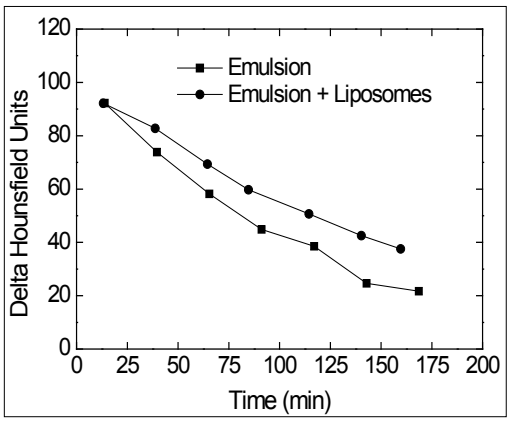

References:

1. Vera DR, Mattrey RF; Acad Rad. 9(7):784-792 (2002)
2. de Vries, A. et al. Biomaterials, submitted (2010)

Application of microfluidics to the ultra-rapid preparation of fluorine-18 and carbon-11 labelled compounds

Miller P. .

Imperial College London, UK

philip.miller@imperial.ac.uk

Introduction: The advantages associated with the miniaturisation of chemical reactions have been recognised for well over a decade now. Such benefits include controlled and predicable mixing regimes, efficient heat transfer, reduced reagent consumption, small reaction volumes (nL-μL), improved safety and enhanced processing capabilities. Microfluidic reactors, the devices used to perform and process small scale chemical reactions, contain enclosed microchannels typically 10-500 μm in diameter and can be fabricated from a wide range of materials including various polymers, silicon and glass (figure 1). The use of microfluidic reactors for rapid synthesis with the short-lived isotopes 11C (t1/2 = 20.4 min) and 18F (t1/2 = 109 min), commonly used in positron emission tomography, has been recognised since 2003. Interest in the application of microfluidics to PET radiosynthesis has come about primarily because miniaturised reaction systems have the potential to address several key challenges in PET radiochemistry, including increasing the speed, reducing the scale and improving the processing of radiolabelling procedures.[1,2] This talk will provide a succinct and critical overview, to the non-specialist, of the emerging and developing field of using microfluidics for the rapid preparation of 11C and 18F labelling compounds.

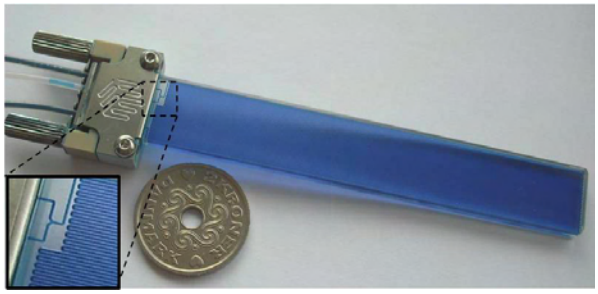

Figure 1

Acknowledgement: PWM is grateful to the EPSRC for the award of a Life Sciences Interface fellowship (EP/E039278/1).

References:

1. P. W. Miller, J. Chem. Technol. Biotechnol. 2009, 84, 309. [2] P. W. Miller, A. J. deMello and A. D. Gee, Curr. Radiopharmaceuticals.accepted for publication.

Radioligand for *in vivo* measuring neurotransmitters release

Halldin C. [(1)], Finnema S. [(1)], Varrone A. [(1)], Farde L. [(1)].

Karolinska Institutet, Sweden

christer.halldin@ki.se

Introduction: This report deals with an overview of radioligands useful for *in vivo* measuring neurotransmitter release. In particular this will be exemplified by a PET-study evaluating the effect of (±)-fenfluramine- induced serotonin release on the binding of the selective serotonin 5-HT1B receptor radioligand [11C]AZ10419369 in cynomolgus monkeys. In a classical displacement paradigm after bolus administration of radioligand fenfluramine caused a dose-dependent reduction in specific binding ratios. The aim of this study was to confirm our previous findings by using a bolus plus continuous infusion approach in monkey.

Materials and Methods: A total of 18 PET measurements were conducted using a bolus plus infusion paradigm of [11C]AZ10419369 in three cynomolgus monkeys. On six of the nine experimental days a baseline measurement was followed by a displacement measurement in which fenfluramine (1.0 or 5.0 mg/kg) was infused i.v. between 80 and 85 minutes after the bolus radioligand injection. On three of the nine experimental days a baseline measurement was followed by a pretreatment measurement in which fenfluramine (5.0 mg/kg) was infused i.v. between 30 and 25 minutes before the bolus radioligand injection. Emission data were acquired for 125 or 155 minutes using the HRRT PET-system. For determination of the fenfluramine effect the binding potential (BPND) was calculated for different time frames with the cerebellum as reference region.

Results: Administration of fenfluramine had no evident effect on radioactivity in the cerebellum. After administration of fenfluramine (1.0 and 5.0 mg/kg), the respective binding potentials decreased in the occipital cortex by 19% (7-34%) and 47% (40-57%) in the displacement paradigm, and by 39% (32-45%) in the pretreatment paradigm (5.0 mg/kg).

Conclusions: This study confirms that the 5-HT1B-ligand [11C]AZ10419369 is sensitive to endogenous serotonin levels *in vivo*.

18f-tracers for amyloid plaques

Guilloteau D. .

CHRU Tours, INSERM Imaging and Brain, France

denis.guilloteau@univ-tours.fr

As documented by the increasing literature, PET imaging using probes binding to amyloid plaques represents a major opportunity to investigate early symptoms and prodromal phase of AD, and in other hand to follow up the efficiency of new treatment.

The most well-known tracer used for this molecular imaging is the [11C]-PIB. Numerous studies with PIB have demonstrated that the properties of this tracer permit the visualization and the quantification of amyloid deposits, but its [11C] labelling limits considerably its potential use due to its short half-life.

A strong effort have been performed by different groups in order to develop a tracer labelled with [18F] for amyloid plaques. Several 18F amyloid binding compounds belonging to different families have been described. Of these 18F-AV-45 (Florbetapir) is most advanced in clinical development (end of Phase III) but Phase I / II clinical results have also been reported on 18F-FDDNP, 18F-Flumetametamol, 18F-BAY94-9172 (AV-1). We will present these results and discuss the similarities and differences regarding the specificity and the sensitivity of the brain uptake.

Some results obtained with [18F]-FDDNP and ([18F]-AV45 in our University Hospital will be presented.

Chelators for radiocopper: biological/pharmacokinetic differences of [Tyr³,Thr⁸]octreotide conjugates

Abiraj K. [1], Fani M. [2], Tamma M. L. [1], Reubi J. C. [3], Barnard P. [4], Schibli R. [5], Dilworth J. [6], Maecke H. [2].

[1] University Hospital of Basel, Switzerland
[2] University Hospital of Freiburg, Germany
[3] University of Bern, Switzerland
[4] University of Melbourne,
[5] ETH Zurich,
[6] University of Oxford.

keelaraa@uhbs.ch

Introduction: Copper-64 has attracted great deal of attention as radioisotope for targeted positron emission tomography (PET) and radionuclide therapy due to its dual decay characteristics (β+: 17.4%; E β+max= 653 keV; β-: 39%; E β-max= 579 keV), favorable half life (t1/2=12.7 h) and increased availability.1 Owing to the instability of copper complexes under '*in vivo*' condition, continuous efforts are being made to develop bifunctional chelators (BFC's) which can form stable copper complexes for labeling of biomolecules.1-3 In the present study, we conjugated [Tyr3,Thr8]octreotide (TATE), to four different chelating systems, radiolabeled with 64Cu and evaluated the biological/pharmacokinetic differences of these radioconjugates.

Methods: The BFC's DOTA(tBu)3 and NODAGA(tBu)3 are commercially available whereas CB-TE2A(tBu) and PHENDAM were synthesized using suitable synthetic methodologies. TATE was synthesized on solid phase using standard Fmoc strategy and coupled to each BFC. The conjugates were labeled with 64Cu using 0.1 M ammonium acetate buffer (pH 8.0) under different labeling conditions. Receptor affinity measurements were performed using radioligand assays and autoradiographic methods. The radiolabeled conjugates were evaluated in vitro and *in vivo* in tumor-bearing nude mice, using the HEK-sst2 cell line. Imaging studies were performed using a clinical PET/CT camera.

Results: Synthesis of orthogonally protected cross-bridged cyclam-based BFC (CB-TE2A(tBu)) allows facile conjugation to targeting biomolecules such as peptide on solid phase. Synthesis of PHENDAM provides a new N4-macrocyclic ligand for conjugation to biomolecule and subsequent labeling with 64Cu. All the conjugates (DOTA-TATE, NODAGA-TATE, PHENDAM-TATE and CB-TE2A-TATE) showed high binding affinity to somatostatin receptor subtype-2 (sst2) with IC50 values ranging from 0.6 nM to 2.5 nM. The labeling of NODAGA-TATE could be performed at room temperature (radiolabeling yield >97% at specific activity of >20 GBq/μmol) whereas other conjugates required elevated temperature. All the radioconjugates showed substantially high and receptor mediated uptake by HEK-sst2 cells. Biodistribution studies with nude mice showed high uptake of the radioconjugates in HEK-sst2 xenografts at 1h p.i. (64Cu-DOTA-TATE: 20.29±2.74%, 64Cu-NODAGA-TATE: 29.39±4.13%, 64Cu-PHENDAM-TATE: 16.97±1.46%, and 64Cu-CB-TE2A-TATE: 19.34±2.55% ID/g). The radioactivity in tumor persisted at 4h p.i., but 24h p.i. data showed fast washout in case of all the conjugates. Compared to 64Cu-DOTA-TATE, the other three radioconjugates showed improved pharmacokinetics. High *in vivo* stability of radiometal complex in case of 64Cu-NODAGA-TATE and 64Cu-CB-TE2A-TATE was apparent from their low uptake in liver and blood at all time points. Interestingly, 64Cu-PHENDAM-TATE showed fast washout from the kidneys resulting in high tumor-to-kidney ratio at early time points. The PET/CT images acquired at 8 h p.i. clearly delineated the tumor and showed images in accordance with the biodistribution data.

Conclusions: Among four different chelating systems evaluated, 64Cu-NODAGA-TATE and 64Cu-CB-TE2A-TATE showed superior *in vivo* stability of the radiocopper complex. The study infers that triazacyclononane and cross-bridged cyclam based chelating systems might be ideal for 64Cu labeling of biomolecules intended to be used in targeted PET imaging and radionuclide therapy but PHENDAM may be a new 64Cu chelating system of interest for protein labeling.

Acknowledgement: Swiss National Science Foundation, European Molecular Imaging Laboratories (EMIL), COST BM0607.

References:

1. Shokeen W et al; J. Acc. Chem. Res. 42: 832-841 (2009)
2. Boswell C A et al; J. Med. Chem. 47: 1465-1474 (2004)
3. Prasanphanich A F et al; PNAS 104: 12462-12467 (2007)

[11C]SOMADAM: potential sert ligand for pet studies and comparison with [11C]MADAM

Gourand F. (1), Emond P. (2), Bergström J. P. (3), Takano A. (3), Gulyas B. (3), Guilloteau D. (2), Barré L. (1), Halldin C. (3).

(1) CEA/DSV CI-NAPS, France
(2) INSERM U930-Université François Rabelais de Tours CHRU Bretonneau, France
(3) Karolinska Institutet, Sweden

gourand@cyceron.fr

Introduction: Although [11C]MADAM is an appropriate PET radioligand for the visualization and quantification of SERT *in vivo*, metabolite analysis in human and non-human plasma samples using HPLC separation have shown that [11C] MADAM was rapidly metabolized.[1,2]

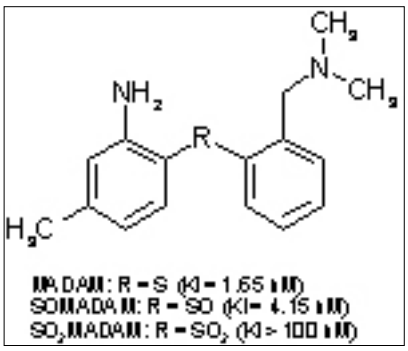

A possible metabolic pathway is the S-oxidation which could lead to SOMADAM and SO_2MADAM. In vitro evaluation of these two potential metabolites have shown that SOMADAM exhibited a good affinity for SERT and a good selectivity for SERT over NET and DAT.[3] In view of its in vitro biological properties, SOMADAM has been labelled with carbon-11 and evaluated as a potential radioligand for *in vivo* quantification of SERT in the monkey brain using PET.

Methods: The labeling of [11C]SOMADAM is based on the N-alkylation reaction of the N-desmethyl precursor using [11C]methyl triflate in acetone. Comparative PET imaging studies in cynomolgus monkey with [11C]MADAM and [11C]SOMADAM were carried out and plasma samples were analyzed using reverse phase HPLC.

Results: The incorporation of [11C]methyl triflate to [11C]SOMADAM was in the range of 50% and after purification by reverse phase HPLC, [11C]SOMADAM was obtained with a radiochemical purity higher than 99%. PET imaging studies in monkey using [11C]SOMADAM showed 1) a rapid and high brain uptake and 2) an homogenous distribution of the radioactivity. A rapid washout in all regions was observed, indicating a high non-specific binding. As it has already been shown in previous PET studies, the radioactivity accumulation of [11C]MADAM is consistent with the known densities of SERT sites. HPLC analysis of plasma samples obtained after either [11C]MADAM or [11C]SOMADAM injection gave radiochromatograms with a similar profile where all the radioactive metabolites detected were more hydrophilic than the parent compound. After [11C]MADAM injection, one radioactive species has been identified as [11C]SOMADAM and the fraction was approximatively 5% at 4 min and 1% at 15 min.

Conclusions: From PET imaging studies in monkey, it appears that [11C]SOMADAM does not present any advantages over [11C]MADAM, either in terms of brain kinetics and specific binding. Nevertheless, [11C]SOMADAM has been identified in plasma sample as a minor labeled metabolite of [11C]MADAM.

References:

1. Halldin C et al; Synapse. 58:173-183 (2005)
2. Lundberg J et al; J Nucl Med. 46:1505-1515 (2005)
3. Vercouillie J et al; Bioorg Med Chem Lett. 16:1297-1300 (2006)

MR imaging of extracellular redox by a thiolsensitive Gd(III)-DO3A derivative

Menchise V. [1], Gianolio E. [2], Digilio G. [3], Cittadino E. [2], Napolitano R. [2], Fedeli F. [2], Catanzaro V. [2], Aime S. [2].

[1] Institute for Biostructures and Bioimages (CNR) c/o Molecular Biotechnology Center University of Turin, Italy
[2] Department of Chemisty IFM & Center for Molecular Imaging, University of Turin, Italy
[3] Department of Environmental and Life Sciences, University of Eastern Piedmont "A. Avogadro", Alessandria, Italy

valeria.menchise@unito.it

Introduction: The characterization of the microenvironment around and within tumors is of great importance to evaluate the invasiveness of cancers and to predict resistance to radio- and chemotherapy. Severe hypoxia and acidosis has been related to aggressive cell phenotype, poor clinical outcome and low likelihood of patient survival.[1] More reducing microenvironment conditions are related to increased cancer cell proliferation and increased resistance to chemotherapies. Any method for the imaging of the parameters characterizing the tumor microenvironment would be therefore of immense value for the characterization/grading of the tumor and for the choice and calibration of therapies. We have recently described a series of Gd-DO3A based compounds that exploit exofacial protein thiols (EPTs) to be taken up by cells. The most effective

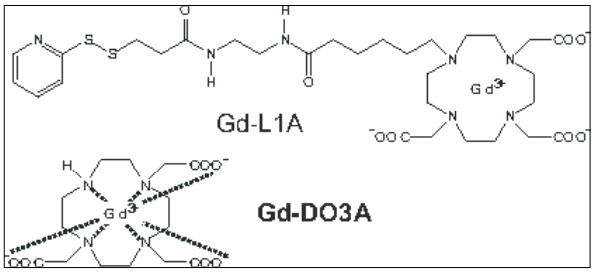

of these compounds, named Gd-L1A, can reach an intracellular concentration as high as $1.2x10^{10}$ Gd atom per single cell.[2] The fact that the uptake of Gd-L1A by cells is proportional to the amount of EPTs makes it an interesting candidate as a probe for the MR molecular imaging of the extracellular redox microenvironment.

Methods: In labeling experiments, cells grown to a confluence of 80% were subjected to a 4 hours incubation with Gd-L1A (0.5 to 3mM) at 37 °C, washed three times, mechanically harvested and finally subjected to mineralization and quantitative analysis of Gd(III) by a relaxometric assay. MR images were acquired on mice grafted with B16 tumor before and after intratumor/intramuscle injection of Gd-L1A using a T1-weighted multislice multiecho protocol (TR/TE 250/7.7) on an ASPECT spectrometer operating at 1T.

Results: Uptake experiments of GdL1A carried out on B16 melanoma cells treated with chemicals known to block EPTs have shown that the extent of Gd uptake increases with the concentration of free EPTs on the cell membrane. Imaging of EPTs has been performed in an animal tumor model obtained by inoculating about 1 million of B16 melanoma cells subcutaneously in B57Bl/6 mice. Gd-L1A has been delivered to tumor areas in these mice models and signal enhancement monitored over time and compared to that found in non-tumor bearing tissue. Gd-DO3A has been used as a control.

A significant signal enhancement has been found in the tumor area of mice treated with Gd-L1A, with wash-out kinetics of the contrast agent consistent with its internalisation by tumor cells.

Conclusions: These results show that Gd-L1A is suitable to image EPTs, that are in turn sensitive and responsive to the extracellular redox.

Acknowledgement: This work is supported by FP6 Project NMP4-CT-2006-026668 (MediTrans) and by Regione Piemonte (PIIMDMT)

References:

1. Tatum et al. Int J Radiat Biol., 82: 699-757 (2006)
2. Digilio G. et al., Chem. Commun. 893–895 (2009)

Everything but not cell replacement with somatic neural stem cell transplantation

Pluchino S. .

San Raffaele Scientific Institute Milano, Italy

pluchino.stefano@hsr.it

Introduction: Since the first transplant of stem cells into the spinal cord of rodents in which an acute demyelinating lesion was induced, we have witnessed a spur of experimental cell-based transplantation approaches aimed at fostering biological and molecular mechanisms underlying CNS repair. Theories assuming that very little renewing potential is identified within the adult CNS have been contravened, new promising sources of myelinogenic cells for transplantation purposes have been characterized, and new cell-replacement strategies have been proposed and established. A better understanding of the dynamics of endogenous remyelination has been achieved, and insights concerning the process of remyelination driven by site-specific myelin-forming cell transplantation have been discovered.

Methods: Some major limitations have – however – not been overcome yet:

(i) the limited amount of highly myelinating cells that can be grown in vitro and

(ii) the limited migratory capacity of myelinating cells once transplanted. Somatic stem cells might represent therefore an alternative and promising area of investigation with some potential in its essence.

Results: New hopes have been recently raised by the encouraging preliminary results obtained by transplanting CNS-derived NPCs and bone marrow mesenchymal/stromal stem cells in rodents with experimental MS. However, most of the results with stem cells as therapeutic weapons for MS have consistently challenged the sole and limited view that stem cells therapeutically work exclusively throughout cell replacement. Indeed, the transplantation of somatic (non-hematopoietic) stem cells promotes substantial CNS repair via a number of bystander mechanisms, mainly exerted by undifferentiated stem cells releasing *in vivo* a milieu of tissue-trophic and immune modulatory molecules, whose release is likely to be temporally and spatially orchestrated by specific (micro)environmental cues. These molecules are indeed are pleiotropic and redundant in nature as well as 'constitutively' secreted by stem cells. In this view, the therapeutic plasticity of stem cell can be viewed as the capacity of stem cells to adapt their fate and function(s) to specific environmental needs occurring as a result of different pathological conditions.

Conclusions: While further studies are certainly required to assess the overall safety, efficacy and *in vivo* therapeutic plasticity of NPCs, the great challenge for any future human application of NPC-based protocols in MS will be to develop more reliable and reproducible approaches optimizing both (tissue) trophic as well as immune regulatory capacities of stem cells for functional and anatomical rescuing of myelin architecture in MS patients.

Detailed review of the most recent data on the highly peculiar immune regulatory stem cell signature will be here provided.

Mesenchymal stem cell transplantation: an option to promote remyelination?

Aigner L. .

Institute of Molecular Regenerative Medicine, Paracelsus Medical University Salzburg, Austria

ludwig.aigner@pmu.ac.at

Mesenchymal stem cells (MSCs) have been used previously in a number of animal models for neurological / neurodegenerative diseases. Moreover, clinical studies that are using MSCs for therapy of CNS diseases are currently ongoing. In animal models, systemic or local transplantation of MSCs provided functional improvement. The therapeutic effects of MSCs are derived from their immuno-modulatory activity and from the fact that MSCs secrete a number of neuroprotective cytokines. Moreover, there is evidence that MSCs might be able to influence the pool of endogenous stem or progenitor cells. Along this line, we have recently demonstrated that MSCs secrete activities that promote oligodendroglial fate and differentiation of neural progenitors (Rivera et al., 2006). Here, we will present data on the effects of MSC transplantation on endogenous spinal cord progenitors after spinal cord injury. Like in the in vitro situation, the presence of MSCs in the lesioned spinal cord promoted oligodendroglial and inhibited astroglial differentiation of endogenous progenitors. This supports the possibility of use MSC transplantation for strategies to remyelinate axons in the diseased CNS.

Viral vector-mediated transcriptional targeting of dendritic cells for antigen-specific tolerance induction in EAE/MS.

Dresch C. .

Univesity of Zürich, Switzerland

cdresch@vetvir.uzh.ch

Introduction: The cause of multiple sclerosis (MS) is unknown and the pathogenic processes leading to disease development is incompletely understood. Current knowledge supports a T cell mediated autoimmune pathogenesis targeting myelin components or myelin-producing cells. Immunization of susceptible animals with myelin antigens or transfer of myelin antigen-reactive T cells induces experimental autoimmune encephalomyelitis (EAE), an inflammatory disorder of the CNS which closely resembles MS. Because the ethiology of MS is not yet completely understood, there is no curative treatment available at present.

Methods: The aim of this project was to induce permanent, antigen-specific tolerance in EAE/MS. The strategy includes the ex vivo modification of autologous hematopoietic stem cells (HSC) with lentiviral vectors that express antigens involved in EAE/MS from a dendritic cell-specific promoter. After reinfusion, the modified HSC will give rise to all cells of the immune system including antigen expressing dendritic cells. As lentivirus vectors mediate the genomic integration of transgenes in HSC, there is a constant supply of antigen expressing "steady-state" dendritic cells. We hypothesized that the stable antigen presentation by these cells in thymus and periphery in a non-inflammatory condition would tolerize self-reactive T cells and, therefore, prevent/revert disease development.

Results: We demonstrated the effectiveness of this strategy for inducing myelin oligodendrocyte glycoprotein (MOG)-specific tolerance in an EAE model in mice. We show the efficient deletion of MOG specific T cells in chimeras that received HSC transduced with a MOG-expressing lentivirus vector. Also, 0% of mice which received HSC transduced with the MOG-expressing lentivirus vector developed EAE upon induction (clinical score 0), while 100% of mice that received BM cells transduced with a GFP-expressing control lentivirus vector developed EAE.

Conclusions: We confirmed the potential of lentivirus vectors that transcriptionally target transgene expression to dendritic cells for antigen-specific tolerance induction in autoimmune diseases. This strategy completely prevented MOG induced EAE in mice. We will further investigate the mechanisms of vector mediated tolerance induction, in particular the involvement of regulatory T cells and cytokines. The strategy presented here is particularly promising for clinical applications. Moreover, these tools will also prove useful for studying disease mechanisms and for addressing fundamental questions in immunity and tolerance.

Acknowledgement: Swiss-MS Society.

Delivery of a bioluminescent transgene to a tumor via bone marrow engraftment and local control of gene expression by non invasive local hyperthermia

Fortin P. Y. [(1)], Lepetit-Coiffe M. [(1)], Genevois C. [(1)], Debeissat C. [(1)], Quesson B. [(1)], Moonen C. [(1)], Couillaud F. [(1)].

[(1)] University of Bordeaux/CNRS, France

py.fortin@imf.u-bordeaux2.fr

Introduction: The success of a gene therapy strategy depends on several parameters including the right choice of therapeutic gene, efficient delivery method and reliable control of gene expression. In the present study, we investigate an *in vivo* strategy to deliver a transgene around a tumor and to control the expression of the transgene. This strategy includes bone marrow engraftment of genetically engineered cells into a wild type mouse to create a chimera with nucleated circulating blood cells (CBC) expressing the firefly luciferase (lucF) reporter gene under the transcriptional control of a thermosensitive promoter. Later on, a subcutaneous tumor is induced and as part of the physiological inflammatory process, CBC accumulate into and around the tumor. Finally, lucF expression detected by bioluminescence imaging (BLI) is induced "on demand" by local hyperthermia using MR guided high-intensity focused ultrasound (MRgHIFU).

Methods: Bone marrow cells (BMCs) were obtained from homozygote C57/BL6 (CD45.2) transgenic mice (NLF-1) containing the lucF transgene under transcriptional control of the heat shock protein 70 (Hspa1b) promoter. BMCs were transplanted into a congenic mouse (CD45.1) pre-treated with Busilvex®, an injectable form of busulfan (2 busulfan IP injections, 25 mg/Kg) to induce medullar aplasia. The level of engraftment was measured 2 months later by measuring CD45.1/CD45.2 ratio using Fluorescence Activated Cell Sorting (FACS). Carcinoma Mouse Tumor 93 (CMT-93, ATCC) were implanted subcutaneously (2 millions cells) to generate a tumor on the left leg. Tumors were heated (44°C, 8 min) for local gene activation using either a water bath or MRgHIFU. LucF expression was evaluated *in vivo* 6 hours post heating by BLI.

Results: After 2 months, about 80% of engrafted mice exhibited more than 65% of CBC from the donor mouse as demonstrated by FACS. CMT-93 cells implanted into engrafted mice formed tumors ranging from 5 and 10 mm in one month. Tumors heated (44°C, 8 min) by dipping the tumor-bearing leg into a water bath, in mice exhibiting more than 65% of engraftment, induced lucF activation and transient light emission 6 hours later. Light emission was found in and around the tumor, for about 50% of the mice. The remaining mice did not exhibit any light emission. A week later light-emitting mice did not produce light anymore. They were heated again (44°C, 8 min) but using the MRgHIFU device. Six hours later, light emission was found around the heated focal region corresponding to both tumors and the surrounding region (n = 15). Light emission was also detected in an additional location (n = 6) corresponding to head and apical region of bone both on ipsi and contralateral legs.

Conclusions: The bioluminescent chimera mice express the lucF reporter under transcriptional control of a thermosensitive promoter in hematopoietic cells. This model allows for studying gene delivery to tumor using circulating blood cells. Local gene expression was induced "on demand" by local hyperthermia. MRgHIFU heating reveals both expected (inside and around the tumor) and unexpected (contralateral leg) activation patterns further to be explored.

Acknowledgement: This work was supported in part by Diagnostic Molecular Imaging and the Conseil Régional d'Aquitaine.

YIA applicant

Dendritic cell labelling with paramagnetic nanoparticles and ^{111}In-oxine for *in vivo* magnetic resonance imaging and scintigraphic imaging

Martelli C. [(1)], Borelli M. [(1)], Rainone V. [(1)], Ottobrini L. [(1)], Degrassi A. [(2)], Russo M. [(2)], Texido G. [(3)], Pesenti E. [(2)], Fiorini C. [(4)], Clerici M. [(5)], Trabattoni D. [(1)], Lucignani G. [(1)].

[(1)] University of Milan ,
[(2)] Nerviano Medical Sciences,
[(3)] Pharmacology Department, BU Oncology, Nerviano Medical Sciences, Nerviano, MI,
[(4)] Politecnico of Milan,
[(5)] University of Milan and on Gnocchi Foundation.

cristina.martelli@unimi.it

Introduction: Better understanding of the biology and the role of dendritic cells (DCs) in regulating immune responses is driving the development of innovative anti-neoplastic DC based immunotherapies both at clinical and pre-clinical levels[1]. The aim of this study is the development and the evaluation of a tumour-specific DC vaccine, tested on a transgenic murine model of breast cancer (MMTV-v-Ha-Ras). MRI and SPET methodologies were tested for their feasibility in showing the migration to local draining lymph nodes (DLNs) of DC, properly labelled with paramagnetic nanoparticles (MNPs, Endorem®) or ^{111}In-oxine [2].

Methods: Total bone marrow cells were extracted from wt mice. DC differentiation was studied by flow cytometry; at the 6th day of culture DCs were labelled with commercial MNPs (200 ugFe/ml, for 16h). Labelling efficiency was checked by optical microscopy after Perl's staining and relaxometric analysis. Tumour lysates from breast cancer lesions of transgenic mice were used to load immature DCs (iDCs), and maturation was monitored by flow cytometry. Stimulatory activity of Ag-loaded DCs and migratory ability were evaluated in vitro. MNP labelled and Ag loaded DCs were then injected into the footpad of a transgenic tumour bearing mice. The same cells were labelled after antigen loading with ^{111}In-Oxine (30 uCi/10^6 cells). MRI and SPET imaging were performed at 4, 24 and 48h after cells injection. MRI was performed on a 7T Bruker Pharmascan instrument, and MSME and FLASH sequences were used. SPET imaging was carried out with a new prototype of gamma camera developed within an European Project by Politecnico of Milano. Ex vivo Perl's staining and gamma counting of explanted DLNs was performed to validate imaging data and DC migration.

Results: Perl's staining showed constant iron content of DCs in all the experiments. Mean Iron content was 240 pg/cell. DCs labelling with ^{111}In-oxine showed a very high efficiency (83%). Vitality was not significantly affected by both labelling strategies. Labelling with MNPs did not affect DC immune-phenotype or functionality, as demonstrated by CD86 and CD83 expression levels, T-cell proliferation and INF-γ production. Migration assays showed that Ag-loaded DCs were able to migrate in the presence of stimulatory chemokines (6Ckine and MIP3β). MRI evidenced the presence of an hypointense signal in both axillary and popliteal LN, in relation to the injection site, 4h after cell injection. Signal was visible up to 24 h after DC injection. Perl's staining of LN sections after *in vivo* injection of labelled DCs loaded with the antigens, showed the presence of iron within the node, indicating that mature and labelled DCs migrate *in vivo* from the site of injection to the DLN. SPET imaging demonstrated as well DCs migration from the injection site to the DLN. Ex vivo analysis of different organs showed a statistically significant higher signal within the LN omolateral to the injection site in comparison with the controlateral one.

Conclusions: Labelling protocols do not perturb DC physiology and functionality. Dynamic *in vivo* MRI and SPET imaging monitoring of DCs distribution will shed light on the fundamental parameters responsible for anti-neoplasic efficacy[3], while the use of clinically approved MNPs and tracers will speed up the transfer from pre-clinical studies to clinical trials.

Acknowledgement: this work is supported by the FP6 funded Hi-CAM project (LSHC-CT-2006-037737), PRIN (20082NHWH9) and AIRC (IG2009-9311) and by fellowships from the Doctorate School of Molecular Medicine, University of Milan.

References:

1. de Vries IJ et al. Nature Biotech, 2005,23(11):1407-1413
2. Baumjohann D et al. Eur. J. Immunobiology 2006; 36: 2544-2555
3. Lucignani G et al. TRENDS in Biotechnology 2006; 24(9): 410-418

The type 2 cannabinoid receptor as a new PET reporter gene for the brain

Vandeputte C. [1], Evens N. [1], Toelen J. [1], Deroose C. [1], Ibrahimi A. [1], Verbruggen A. [1], Debyser Z. [1], Bormans G. [1], Baekelandt V. [1], Van Laere K. [1].

[1] K.U. Leuven, Belgium

caroline.vandeputte@med.kuleuven.be

Introduction: Reporter genes play an important role in the understanding of gene expression and function in living subjects. However, for the brain no successful PET reporter systems are available with low endogenous background gene expression and good blood-brain-barrier (BBB) penetration of the PET probe. The aim of this study was to develop a new PET reporter gene system which can be applied to the brain. The type 2 cannabinoid receptor (CB_2) has a very low brain expression in physiological conditions and CB_2 PET radioligands crossing the BBB were recently developed.

Methods: We constructed lentiviral (LV) and adeno-associated viral vector (AAV) transfer plasmids encoding human CB_2, harboring a point mutation at position 80 (D80N) referred to as CB_2(D80N), as such or in combination with enhanced green fluorescent protein (eGFP) or firefly luciferase (FLuc). Rats were stereotactically injected with either 5 µl of AAV-eGFP-T2A-CB_2(D80N) in the right striatum and 5 µl of AAV control vector in the left striatum or 5 µl of AAV-fLuc-T2A-CB_2(D80N) in the right striatum. At different time points (6, 13, 18, 73, 96 and 252 days) after stereotactic injection of the AAV, a CB_2 selective carbon-11 labeled radioligand [^{11}C]GW405833 was injected intravenously and dynamic µPET images (Focus 220, Siemens) were acquired. BLI scans were performed at 16, 58 and 281 days after surgery. Time-activity curves (TAC) and parametric binding potential maps were determined. The animals were sacrificed and perfused and double immunohistochemical staining against CB_2 and eGFP of the brain slices was performed.

Results: The observed CB_2 binding potential increased over time and reached a maximum in right striatum between 18 and 58 days after vector injection in the brain. The time-activity curves persistently expressed an increased uptake in right striatum compared to control left striatum and cerebellum. Immunohistochemical analysis showed colocalization of both CB_2 and eGFP in right striatum. In contrast, only eGFP expression was seen in the contralateral hemisphere.

Conclusions: We have successfully developed a new PET reporter gene system consisting of a lentiviral or an adeno-associated viral vector expressing the CB_2 receptor as the reporter gene which can be quantified for several months.

Acknowledgement: We gratefully acknowledge the financial support by the European Commission for EC-FP6-STREP-STROKEMAP, BRAINSTIM SBO-IWT-060838, DIMI LSHB-CT-2005-512146 and the K.U. Leuven Center of Excellence 'MoSAIC' (Molecular Small Animal Imaging Center).

Hans-Jürgen Wester

Department of Nuclear Medicine , Klinikum rechts der Isar
Technische Universität München, Ismaninger Straße 22
D-81675 München, Germany
Phone: +49-(0)89-4140-4586, Fax: +49-(0)89-4140-4841

Graduation:

1981-1985	Study of Chemistry, University of Cologne
1992-1996	Diploma and PhD, Radiochemistry, Res. Center Juelich, Germany
1995-1997	Scientific Assistant, Department of Nuclear Medicine, Technische Universität München (TUM)
1997-2004	Research Associate, Department of Nuclear Medicine (TUM)

Academic Appointments

since 2003 five national and international offers (W3 Radiopharm. Chem. , C4 Bioinorg. and Radiopharm. Chem., C3 Radiopharm. Chem., Assoc. Prof. for Radiology, Assoc. Prof. for Radiat. Oncol.). Since 2004 Professor for Radiopharmaceutical Chemistry at the TU München, Faculty of Medicine)

Scientific Focus

Development of specific molecular probes for the non-invasive imaging of diseases, new strategies for production of radiopharmaceuticals, radionuclide therapy, tissue selective targeting of imaging probes and therapeutic compounds, transfer of genomic and proteomic information into new imaging methods.

Molecular imaging of CXCR4 receptors

Wester H.J.[1], Demmer O.[2], Dijkgraaf I.[1], D´Alessandria C.[1], Kessler H.[2] .

[1]Department of Nuclear Medicine, Klinikum rechts der Isar, Technische Universität München, 81675 Munich, Germany
[2]Institute for Advanced Study, Technische Universität München, Lichtenbergstrasse 4, 85747 Garching, Germany

H.J.Wester@lrz.tu-muenchen.de

Chemokines play a key role in tumor metastasis and are also involved in tumor growth. The receptor subtype CXCR4 has been found to be highly expressed in >30 different types of cancer. Similar to the homing of hematopoietic progenitor and stem cells, the chemokine receptor subtype CXCR4 and its endogenous ligand, the stromal cell derived factor 1-alpha (SDF1-alpha or CXCL12), have been found to be responsible for "hijacking" circulating tumor cells in organs and tissues expressing CXCL12. In primary tumors, expression and binding of CXCL12 to CXCR4 promotes tumor proliferation and activates cell migration. In addition, CXCL12 induces recruitment of progenitor cells, which allows for tumor angiogenesis. It has been demonstrated that CXCR4 gene expression in mammary cancer cells is coregulated by Her2/neu, and also activated by HIF-1-alpha, implicating hypoxia-induced metastasis. A high CXCR4 density has also been reported for *cancer stem cells*. Consequently, CXCR4 directed therapies are currently under development aiming to inhibit tumor growth and metastasis by blocking CXCL12 binding to CXCR4 using antibodies, large and small peptides as well as small molecules. CXCR4-directed PET probes should be useful tracers for monitoring those CXCR4-directed therapies in the future, i.e. for patient selection, therapy planning and monitoring response and may also independently allow for imaging the ´metastatic potential` of primary tumors.

Antibodies, radiolabeled SDF, medium sized peptides and newly developed cyclic CXCR4 peptides antagonists are currently assessed as probes for monitoring CXCR4 expression or CXCR4 targeted therapies using metastasizing tumor models in rodents.

With the aim to develop suitable radiolabeled probes to image CXCR4 receptor expression, we initially started with the evaluation of 4-[^{18}F]Fluorobenzoyl-TE14011-Me. Initial experiments showed unfavourable in vitro characteristics and low labelling yields. Using a similar approach by Hanoka et al (2006), Ac-TZ14011 (Acetyl-Arg^{1}-Cit^{6}-Arg^{7}-Lys^{8}(In-DTPA)-T140-amide), labelled with In-111, showed high uptake in liver and kidney of tumor bearing mice reached, whereas tumor uptake was only negligible.

Exploiting our experience in the development of small peptides, i.e. on cyclic RGD- pentapeptides as high affinity ligand for the alpha(v)beta(3) integrin, we focussed our research on small CXCR4-binding pentapeptides. We have synthesized approximately 150 monomeric and dimeric peptides and evaluated their binding characteristics on Jurkat cells and transfected CMS5 cells stably expressing the hCXCR4 receptor. Selected candidates were labelled with ^{123,125}I-iodine, ^{18}F-fluorine and ^{68}Ga-gallium and investigated in nude mice bearing CMS5/CXCR4+ fibrosacoma and metastasizing OH-1 SCLC tumors. Based on c(Gly-D-Tyr-Orn-Arg-NaI), 4-fluorobenzoylated and 2-fluoropropionylated versions showed IC_{50} of 11±2 nM and 35±1 nM (^{125}I-CXCL12 as competitor), and radioiodinated c(Gly-D-Tyr-Arg-Arg-NaI) exhibited an IC_{50} of 4nM. We could demonstrate that N-methylated peptides showed an improved IC_{50} when compared to the non-methylated analogues. A variety of linkers were investigated allowing for conjugation of chelators without affecting the affinity of the entire molecule. The DOTA-Ahx-Asp (Ahx= aminohexanoic acid) conjugate of a cxclic D-Orn-peptide version showed an IC_{50} of 38nM (with free chelator) and 13.7nM after complexation with indium. A variety of dimers were synthesized, the linkers and linker length optimized and the generated constructs assessed. C4-C16 dicarbonic acid spacers showed a continuously increasing affinity in the series C4 (6.6nM) – C10 (2.3nM), whereas longer spacers were unsuitable. The first of a series of promising ^{68}Ga-labeled peptides is renally excreted leading to high tumor-to-background contrast and high contrasting small animal PET-imaging approx. 1h post injection.

Compared to the other CXCR4-probes described, the small cyclic peptides developed offer significant advantages and will allow for broadening state-of-the-art high contrast peptide receptor imaging to another important class of GPCRs.

Evaluation of the temporal window for drug delivery following ultrasound mediated membrane permeability enhancement

Yudina A. [1], Lepetit-Coiffé M. [1], Moonen C. [1].

Laboratoire IMF CNRS UMR 5231 / Université Bordeaux 2, France

anna@imf.u-bordeaux2.fr

Introduction: Ultrasound (US)-mediated delivery is a new therapeutic option to locally facilitate the passage of drugs through cell plasma membrane by reversibly altering its permeability[1] possibly via the formation of pores that are known to spontaneously reseal within a short time – seconds to minutes[2]. However under certain conditions the effects of US for drug delivery last for hours after the exposure[3]. The present work is the first in vitro attempt to confirm and quantitatively assess the temporal window for the US-mediated intracellular drug delivery by live-cell imaging.

Methods: Cell-impermeable optical chromophores with fluorescence intensity increasing 100-1000 fold upon intercalation with nucleic acids served as smart agents for reporting cellular uptake. Opticell chambers with a monolayer of C6 cells were subjected to ultrasound in the presence of microbubbles followed by varying delays between 0 and 24 hours before addition of Sytox Green optical contrast agent. Micro- and macroscopic fluorescence imaging was used for qualitative and quantitative analysis.

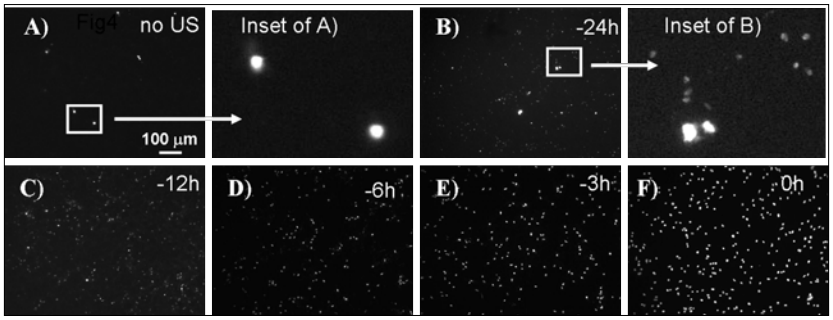

Figure 1. In the absence of US only occasional cells with the compromised membrane show the uptake of cell-impermeable Sytox green (A). However the effects of the US on membrane permeability can last up to 24h (B), with the fluorescence intensity increasing as the time between US application and fluorophore administration shortens (C-F).

Results: Strong enhancement of the fluorescence signal upon binding to nucleic acids allowed efficient visualization of the local effect of US on internalization of cell-impermeable intercalating dyes. Up to 25% of viable cells showed uptake of contrast agent with a half time of 8 hours, with cellular uptake persisting even at 24 hours (Figure 1). Only cells exposed to ultrasound showed the effect.

Conclusions: Optical imaging showed that temporal window of increased membrane permeability is much longer than previously suggested. This may have important repercussions for *in vivo* studies in which membrane permeability may be temporally separated from drug administration to better adapt to pharmacokinetic / pharmacodynamic properties of the drug or drug carrier.

Acknowledgement: This work is supported by the EC-project FP7-ICT-2007-1-213706 SonoDrugs and Foundation InNaBioSanté-project ULTRAFITT. Microscopy was performed in the Bordeaux Imaging Center of the Neurosciences Institute of the University of Bordeaux II.

References:

1. Hernot S, Klibanov AL; Adv Drug Deliv Rev. 60(10):1153-66 (2008)
2. van Wamel A et al.; J Control Release. 112(2):149-55 (2006)
3. Hancock HA et al. Ultrasound Med Biol. 35(10):1722-36 (2009)

Integrisense: a novel near-infrared fluorescent probe for $\alpha_v\beta_3$ integrin and its applications in drug discovery

Sur C. [1], Lin S.A. [1], Gleason A. [1], Kossodo S. [1], Pickarski M. [1], Coleman P. [1], Rajopadhye M. [2], Duong L. T. [1], Yared W. [2], Peterson J. [2], Bednar B. [1].

[1] Merck Research Laboratories, Westpoint US
[2] ViSen Medical.

cyrille_sur@merck.com

Introduction: The $\alpha_v\beta_3$ integrin belongs to the superfamilly of dimeric transmembrane cell adhesion receptors involved in critical biological processes such as cell-to-cell, and cell-to-extracellular matrix binding. As these activities are central to pathological conditions such as inflammation and tumor progression, the RGD-binding $\alpha_v\beta_3$ integrin has been considered as clinically-relevant biomarkers of these disease states. Although, RDG peptides have been developed for PET and SPECT imaging, the operating cost of these modalities limits their widespread deployment in drug discovery teams. In contrast optical molecular imaging allows the non-invasive monitoring and quantification of fluorescent probes *in vivo* with less expensive equipment that can be installed at multiple research sites. In order to take full advantage of the rich biology of integrins, a partnership has been established between Merck Research Laboratories and VisEn Medical to develop a novel near-infrared (NIR) fluorescent integrin probe, IntegriSense™. The pharmacological and biological characterization of IntegriSense™, a peptidomimetic antagonist-based molecule with improved specificity and binding affinity will be presented together with research applications in the oncology and atherosclerosis research fields.

Methods: The in vitro cell biology and pharmacological profiling of IntegriSense™ were conducted with recombinant HEK-293 cells expressing $\alpha_v\beta_3$ and included confocal microscopy for cellular localization and flow cytometry for binding and kinetic constant determination. *In vivo* pharmacodynamics and tumor localization studies were performed in female NU/NU mice bearing different human tumor xenografts. IntegriSense™ NIR fluorescent signal was acquired with a Fluorescent Molecular Tomography imaging system (FMT2500). The potential application of IntegriSense™ in atherosclerosis was evaluated in apolipoprotein E-deficient (ApoE-/-) and human cholesteryl ester transfer protein (CETP) knockin/LDL receptor-deficient (C57BL/6-Tg(CETP)-Ldlrtm1) mice. Transgenic as well as control C57Bl/6 mice were fed a cholesterol enriched diet (9% fat, 0.15% cholesterol) to induce atherosclerosis. IntegriSense™ NIR signal was measured *in vivo* 24 and 48 hours after probe injection and its localization in inflamed aortas was further evaluated by ex-vivo imaging and histology.

Results: Integrisense-680 has absorption/emission spectra centered at 674nm/692nm and an extinction coefficient of $2.02x10^5 M^{-1}cm^{-1}$. Binding of IntegriSense™ to HEK-293 stably expressing recombinant human $\alpha_v\beta_3$ yielded a Kd of 4.2±0.6 nM and a dissociation constant koff of $1.08x10^{-4}s^{-1}$. Plasma pharmacokinetic analysis revealed a two compartmental profile with t1/2 of 6 min and 210 min corresponding to clearance of free and bound IntegriSense™, respectively. Biodistribution studies in mice with xenograft tumors showed a specific uptake of IntegriSense™ by tumor cells and supported using IntegriSense™ to monitor tumor growth in animal models.

In vivo measurements with FMT2500 in mice atherosclerosis models detected a longitudinal increase in IntegriSense™ fluorescence in the thorax area that was three to five fold higher when compared with control animals. This NIR signal originated from atherosclerotic lesions in the aortic arch, carotid, and subclavian arteries as confirmed by ex vivo imaging of the dissected vessels and histopathology.

Conclusions: This report demonstrated that the $\alpha_v\beta_3$ integrin optical reporter, IntegriSense™ developed by Merck and VisEn partnership can be used as a molecular imaging biomarker for *in vivo* imaging studies. For instance, IntegriSense™ can be used to monitor tumor growth as well as to detect inflammation in atherosclerosis plaques. The ability of this biomarker to report on several important cellular and physiological functions makes it a tool of choice to evaluate preclinically the therapeutic potential of novel anticancer and atherosclerosis drugs.

Harnessing the power of bioluminescence to cross the *in vitro–in vivo* divide

Watson J. [1], Klaubert D. [1], Biserni A. [2], Ciana P. [2], Maggi A. [2], Allard S. [1].

[1] Promega
[2] TOP (Transgenic Operative Products)srl

John.watson@promega.com

Introduction: Bioluminescence imaging is accomplished by sensitive detection of light emitted following chemical reaction of the luciferase enzyme with substrate. The imaging process in animal models requires a reporter construct that leads to production of luciferase enzyme. The most commonly used reporter for this purpose is a construct that can express firefly luciferase (1). Data will be presented that shows how a number of biomarkers can be measured using bioluminescence in vitro, including caspase-3/7, ATP and transcriptional activation. We will also describe the in vivo characterization of VivoGlo Caspase-3/7 Substrate, a modified firefly luciferase substrate that in apoptotic cells is cleaved by caspase-3 to liberate aminoluciferin, which can be consumed by luciferase to generate a luminescent signal. Evidence will be shown illustrating the possibility to merge a line of reporter mice (repTOP) engineered for the ubiquitous expression of the luciferase reporter gene (2-4) and the modified luciferase substrate, VivoGlo Caspase-3/7 Substrate, to measure molecular apoptotic events in whole living animals. We will also demonstrate that this substrate can be used to non-invasively observe the apoptotic affects of chemotherapy several days before they are able to be detected by traditional methods (5).

Methods: In this study, liver apoptosis was induced in luciferase reporter mice by a single i.p. injection of D-galactosamine (D-GalN; 800mg/kg) and Lipopolysaccharide (LPS; 100mg/kg) (6). Six hours after LPS/D-GalN or vehicle administration, mice were treated i.p. with increasing doses (17-150mg/kg) of the VivoGlo™ Caspase-3/7 substrate (Z-DEVD-Aminoluciferin, Sodium Salt) and subjected to the bioluminescence in vivo imaging procedure.

Results: The in vivo imaging data obtained clearly showed a dose-dependent increase of photon emission in the hepatic area of mice treated with D-GalN/LPS. No photon emission was observed in organs not affected by the apoptotic treatment. A complete analysis of pro-apoptotic effects induced by the treatment was carried out by ex vivo imaging acquisition of photon emission in several dissected tissues. This investigation confirmed that light emission observed in vivo was produced selectively by liver and adipose tissues. Western blot analysis and the measure of Caspase-3/7 enzymatic activity fully supported in vivo imaging data.

Conclusions: The work here shows the power of a modified luciferin substrate such as VivoGlo Caspase-3/7 Substrate to detect apoptotic cells in living animals, providing an important advancement over current imaging methodologies based on fluorescence, nuclear or magnetic resonance including: virtually no background, high sensitivity and simple instrumentation needed for the in vivo imaging measurement of the Caspase-3/7 activity. The present application carried out in reporter mice genetically engineered to develop specific cancers will open the way to novel, more predictive approaches for the study of anti-cancer treatments that will enable researchers to measure drug efficacy in space and time, providing relevant information to be rapidly translated to human therapy.

References:

1. Zinn, KR et al; ILAR Journal. 49:103-115 (2008)
2. Ciana, P et al; Nat. Med. 9:82-86 (2003)
3. Maggi, A and Ciana, P; Nat. Rev. Drug Discov. 4:249-255 (2005)
4. Maggi, A et al; Trends Pharmacol. Sci. 25:337-342 (2004)
5. Hickson, J et al; Cell Death Differ. doi:10.1038/cdd.2009.205 (2010)
6. Nakama, T et al; Hepatology. 33:1441-1450 (2001)

In vivo imaging in drug discovery: the example of application in the development of novel estrogenic compounds.

Biserni A. [1], Rando G. [2], Ciana P. [2], Komm B. [3], Maggi A. [2].

[1] TOP (Transgenic Operative Products)srl,
[2] University of Milan,
[3] Wyeth Research .

andrea.biserni@top-mice.com

Introduction: Intracellular Receptor (IR) signalling is temporally organized at different levels: at the cellular level, post-translational modification and proteolysis were shown to be responsible for IR-dependent recruitment of co-regulators and proteins of the transcriptional apparatus necessary to modulate IR activity in time. At the whole organism level, circadian rhythms and pulsatility of hormone release may be responsible for maintaining a state of activity of IR that is critical for hormone action. With hormone therapy, the reinstatement of the receptor oscillatory activity may be a key element for achieving the desired beneficial effect. To date, the lack of appropriate models to study the response to pharmacological treatments in time has been a limiting factor in the study of spatio-temporal activity of drugs. The availability of the ERE-Luc reporter mouse model where the application of BLI-based imaging methodologies allows one to study estrogen receptor activity in living animals, opens the way to a more in-depth analysis of the effect of estrogen therapy (ET). The aim of this study was to set up a protocol for the study of ET and SERM (Selective Estrogen Receptor Modulator) therapies to verify their ability to efficaciously restore the effects of the natural endocrine state in reproductive and non reproductive organs.

Methods: The study was carried out in the ERE-Luc reporter mouse model where the luciferase reporter gene is expressed under the transcriptional control of an ER responsive promoter. In this model, MARs (Matrix Attachment Regions) insulator sequences flanking the transgene guarantee a ubiquitous and tightly regulated expression of the biosensor making it suitable for pharmacological studies. In the present study, we treated ovariectomized, female mice with CE (3 mg/kg/day), raloxifene (RAL; 10 mg/kg/day) and bazedoxifene (BZA, 10 mg/kg/day) for 21 days. To measure ER state of activity, mice were subjected to in vivo imaging. Photon emission was measured by the use of a segmentation algorithm enabling the automatic quantification of photon emission in different body regions of mouse images. At the end of the study a further analysis was carried out on tissue extracts by luciferase enzymatic assay.

Results: In the initial analysis, we evaluated the effect of each treatment in the genital, hepatic, abdominal area and limbs at 0, 3, 7, 14 and 21d. CE had a major effect in the genital and hepatic areas shown by a significant increase of ER activity. As expected the effect of SERMs was significant in the skeletal (limbs) where ER activity started to be significantly increased only after day 14. In the body areas affected by treatments, we observed time-dependent changes: i.e. in the liver CE activity decreased with time, while in the limbs ER activity was shown to increase with the time of exposure to SERMs. This observation prompted us to perform a more in-depth analysis of ER activity by measuring photon emission daily. This second analysis demonstrated that ER activity oscillates in time with a period and amplitude that is tissue specific and is differentially affected by the hormonal treatments. Furthermore, the analysis of ER oscillation revealed that ovariectomy does not fully disrupt the fluctuation observed in intact, cycling mice indicating the existence of mechanisms other than circulating hormone responsible for ER transcriptional activity. The treatments evaluated partially restored the physiological oscillatory behavior of the receptor.

Conclusions: Our study: Provides evidence for a novel, long paced, oscillatory activity of ERs that is independent of ovarian function. This oscillatory ER activity may be relevant for the whole body homeostatic control and may be of relevance for the identification of safer and more efficacious therapies. Points to the importance of whole animal imaging for drug development and for the study spatio-temporally drug activity on targets.

Novel protocols for a wider application of BLI to the study of molecular events in vivo should be developed.

Acknowledgement: Grants from: NoE DIMI LSHB-CT-2005-512146; IP CRESCENDO LSHM-CT-2005-018652), National Institutes of Health (RO1AG027713), and Wyeth Pharmaceutical Co.

- **ESMI Plenary Lecture 5: Jagat Narula (Irvine, USA)**
  Molecular Imaging of unstable coronary plaques
  Chairs: Uwe Haberkorn (Heidelberg, Germany), Helmut Maecke (Freiburg, Germany)

- **Parallel Session 9: Cardiovascular II**
  Chairs: Klaas Nicolay (Eindhoven, The Netherlands), Michael Schäfers (Münster, Germany)

- **Parallel Session 10: Cancer II – together with COST action BM0607**
  Chairs: Marion de Jong (Rotterdam, The Netherlands), Fabian Kiessling (Aachen, Germany)

- **Plenary Session and Closing Ceremony**
  Chairs: John Clark (Edinburgh, UK), Bertrand Tavitian (Orsay, France)

Day 3 - Friday May 29, 2010

Jagat Narula

Jagat Narula MD, PhD, FACC, FRCP [Edin, Hon]

Professor of Medicine and Chief, Division of Cardiology
Director, Memorial Heart & Vascular Institute
Medical Director, Edwards Lifesciences Center for Advanced Cardiovascular Technology
University of California, Irvine School of Medicine

Jagat Narula completed his cardiology training in India at the All India Institute of Medical Sciences, Delhi, and relocated to Massachusetts General Hospital and Harvard Medical School in 1989. After fellowships in heart failure, transplantation, and cardiovascular imaging, he joined the Massachusetts General cardiology faculty. In 1997, he moved to Hahnemann University School of Medicine in Philadelphia. At Hahnemann, he was the Thomas J. Vischer Professor of Medicine, Chief of Division of Cardiology, and Vice-Chairman of Medicine. He joined University of California, Irvine in 2003 as Professor of Medicine Chief, Division of Cardiology, and Associate Dean for Research. Dr. Narula is involved in clinical and basic research in the fields of heart failure and atherosclerosis, with major emphasis on development of novel noninvasive imaging techniques. He has made vital contributions to the imaging of apoptotic cell death in heart muscle, and to the imaging of atherosclerotic plaques that are vulnerable to rupture. His research is not limited by any one imaging modality; and uses integrated imaging approaches for better identification of cardiovascular pathology. His research is funded, in part, by grants from the National Institutes of Health. Dr. Narula has authored more than 700 research publications or presentations and edited 25 books and journal supplements. He has been awarded “Best Young Investigator” on several occasions by the Cardiovascular Council, the Society of Nuclear Medicine, and the American Society of Nuclear Cardiology. He serves on various committees of the American Heart Association. He is the editor-in-chief of the Journal of the American College of Cardiology- Imaging. He has also been an Associate Editor of the *Journal of the American College of Cardiology* and the Founder Editor of *Heart Failure Clinics of North America*.

Molecular imaging of unstable coronary plaques

Narula J. .

University of California, USA

narula@uci.edu

Sudden cardiac death and acute myocardial infarction often occur as the first manifestation of coronary artery disease. Otherwise asymptomatic individuals with subclinical atherosclerosis almost always have a classic risk-factor profile and it is essential that they are identified before the occurrence of an acute coronary event. The ability to recognize such individuals requires the development of noninvasive strategies that can localize unstable atherosclerotic lesions. Plaques that are vulnerable to rupture demonstrate distinct histological characteristics, including large plaque and necrotic core volumes covered by attenuated fibrous caps and extensive remodeling of the vessel at the lesion site. The morphologic features can be characterized by CT angiography and magnetic resonance imaging.

In addition to characteristic morphological profile, monocyte-macrophage infiltration of the fibrous cap is one of the strongest determinants of plaque instability, and amenable to molecular inaging. After crossing the intimal border, infiltrating monocytes express receptors for chemoattractants (such as MCP-1 or adhesion molecules), and subsequently develop scavenger receptors in the subintimal layers for ingestion of oxidized LDL. Although multiple cellular processes can be targeted for the identification of plaque inflammation only a few molecular imaging strategies have been successfully employed for clinical imaging. The inflammatory cells in plaques have high metabolic activity. In contrast to granulocytes, which carry a supply of glycogen to provide energy for their phagocytic activities, the macrophages in an atheroma require exogenous glucose for their metabolism. Incidental uptake of a glucose analog, [18F]-FDG, commonly used to characterize malignant tumors, has been demonstrated in the aorta, carotid arteries and, rarely, the coronary vessels of patients with tumors. Carotid endarterectomy specimens have demonstrated that uptake correlates with macrophage content, and is reduced in patients treated with statins. A prospective study has demonstrated that FDG uptake can be seen in the coronary arteries if background FDG uptake in the myocardium is adequately suppressed. Following coronary interventions, intense FDG uptake has been seen at the sites of stent implantations in patients with acute coronary events; no uptake was observeat the stent sites in patients with stable disease. Concurrent CT angiography was performed in these patients for precise anatomical localization of FDG uptake on PET imaging. Another clinical approach with molecular imaging has utilized radiolabeled annexin A5 to target apoptotic macrophages in the atherosclerotic lesions. A large proportion of macrophages in the attenuated fibrous caps of vulnerable and ruptured plaques undergo apoptosis. The annexin uptake in the carotid vessels has been predominantly seen in symptomatic carotid disease. Annexin imaging of coronary vessels has not been attempted. Various other molecules targeting evolution of receptors such as MCP-1 and scavenger receptors, as well as those targeting the products of inflammation such as metalloproteinases are being successfully employed for the imaging of atherosclerosis in experimental models.

Advances in contrast-enhanced MRI of the mouse heart

Strijkers G. .

Biomedical NMR Eindhoven, The Netherlands

g.j.strijkers@tue.nl

Introduction: In preclinical cardiovascular research using mouse models, MRI has proven to be the imaging modality of choice for studying cardiac pathology. This is mainly thanks to its high temporal and spatial resolution, enabling accurate determination of cardiac functional parameters.

MRI contrast agents are used to differentiate between viable and infarct myocardium. Recently, it has become possible to use MR contrast agents for the evaluation of the mouse myocardial perfusion status. Molecular MR imaging techniques are being developed, allowing contrast agents to specifically target disease markers, providing additional information about the infarction. The use of contrast agents in the mouse myocardium requires innovative mouse cardiac MRI techniques to quantify contrast agent kinetics and concentration in the myocardium.

Results: In this presentation I will present recent advances in the contrast-enhanced MR imaging of the mouse heart.

First, I will discuss new MR technology, which enables the assessment of mouse myocardial perfusion. This methodology involves intravenous injection of an MRI contrast agent, after which the first pass of the contrast agent through the heart is monitored in a time-series of images. The combination of the high heart rate (400-600 bpm), small heart size (5-6 mm left ventricle (LV) diameter) and fast systemic blood circulation time (4-5 s) require a very fast imaging protocol while preserving adequate spatial resolution to visualize the regional myocardial inflow of the contrast agent.

Secondly, I will discuss recent advances in the T1 quantification of the mouse myocardium, which enables quantification of contrast agent concentration. The T1 quantification method uses a combination of 3D IntraGate FLASH steady-state imaging together with DESPOT1 analysis. The 3D IntraGate FLASH makes use of a navigator echo that retrospectively triggers the acquisition to the heartbeat and respiration cycle.

Acknowledgement: Grant sponsor: Dutch Technology Foundation STW, applied science division of NWO and the Technology Program of the Ministry of Economic Affairs; Grant numbers: 07952 and 10191. Grant sponsor: European Union Network of Excellence Diagnostic Molecular Imaging; Grant number: 512146 (LSHB-CT-2005-512146).

Molecular imaging of $\alpha_v\beta_3$ integrin expression with ^{18}F-galacto-RGD after experimental myocardial infarction: comparison with left ventricular remodeling and function.

Saraste A. [(1)], Sherif H. [(1)], Nekolla S. [(1)], Weidl E. [(1)], Higuchi T. [(1)], Reder S. [(1)], Tapfer A. [(1)], Botnar R. [(1)], Wester H. J. [(1)], Schwaiger M. [(1)].

Technische Universität München, Germany

antti.saraste@utu.fi

Introduction: Myocardial infarction (MI) and subsequent left ventricular (LV) remodeling are the most frequent cause for development of chronic heart failure. Expression of $\alpha_v\beta_3$ integrin receptors is increased early after MI as part of the healing process. Poor infarct healing can contribute to progressive LV remodeling. ^{18}F-galacto-RGD (RGD) is a PET tracer that binds to $\alpha_v\beta_3$ integrin receptors. We studied whether molecular imaging of myocardial RGD uptake early after MI can predict long-term LV remodeling in rat.

Methods: Wistar rats underwent permanent left coronary artery (LCA) ligation to induce myocardial infarction (MI) or sham operation. One week post-MI, rats were imaged with a small animal PET scanner after injection of 13N ammonia to define perfusion defect area, and 90 minutes post injection of RGD in order to measure $\alpha_v\beta_3$ integrin expression. Myocardial RGD uptake (%ID/cc) in the infarcted (defect area) and remote myocardium were measured in co-registered polar maps. Cardiac magnetic resonance imaging (MRI) with 1.5T scanner, small animal coil and ECG triggering was used to measure LV remodeling and function repeatedly 1 week and 12 weeks post-MI.

Results: One week after LCA ligation, RGD uptake was significantly higher in the defect area than in the remote myocardium of MI rats and in controls (0.2±0.05 vs. 0.06±0.03 and 0.07±0.04 %ID/cc, respectively, $p<0.001$). Compared with 1 week post-MI, LV end-diastolic volume (EDV) and end-systolic volume (ESV) were larger, and ejection fraction (EF) was lower at 12 weeks post-MI by MRI. In those rats with the most severe LV remodeling, i.e. >20% increase in EDV, early RGD uptake in the defect area was 29% lower than in rats with less than <20% increase in EDV ($p < 0.05$). RGD uptake in the defect area at 1 week also showed an inverse correlation with change in EDV ($r=-0.61$, $p<0.001$) and direct correlation with change in EF ($r=0.51$, $p<0.05$) from 1 week to 12 weeks.

Conclusions: High level of RGD uptake in the perfusion defect area early after MI predicted the absence of significant LV remodeling after 12 weeks follow-up. These results suggest that increased $\alpha_v\beta_3$ integrin expression is associated with myocardial healing after MI and enables monitoring by molecular imaging with possible prognostic information.

Acknowledgement: This work is supported in part by the FP6 European NoE DiMI (LSHB-CT-2005-512146).

Existing and emerging animal models mimicking cardiovascular disease and their relevance for molecular imaging

Schäfers M. .

European Institute for Molecular Imaging – EIMI, University of Münster

schafmi@uni-muenster.de

Appropriate animal models, mimicking the pathology of cardiovascular human diseases is essential for progress in the field of cardiovascular research and for the transfer of preclinical results into the clinical setting. In principle, a variety of animal species can be used in cardiovascular research. Although larger animal such as pigs (a classical model for myocardial infarction) are used in cardiovascular research, the focus has been shifted to small animal models such rats and mice recent years. Animal models of cardiovascular diseases can rely both on genetic manipulations or surgical interventions and do nowadays cover the wide spectrum of cardiovascular human diseases. In this talk, examples for relevant human cardiovascular diseases, myocardial infarction and atherosclerosis, already being studied by small animal imaging is given.

Imaging of Matrix Metalloproteinase Activity in Vulnerable Human Carotid Plaques with Multispectral Optoacoustic Tomography

Razansky D. [1], Harlaar N. J. [1], Hillebrands J. L. [2], Taruttis A. [1], Herzog E. [1], Zeebregts C.J. [2], Van Dam G. M. [2], Ntziachristos V. [1].

[1] Technical University of Munich and Helmholtz Center Munich, Germany
[2] University Medical Center Groningen, The Netherlands.

tdr@tum.de

Introduction: The indication for a carotid endarterectomy is nowadays mainly based on symptomatology or, alternatively, on the degree of stenosis in carotid arteries (>80%). Those indications however do not provide an accurate assessment of plaque vulnerability and therefore only a small percentage of patients do actually benefit from the surgical intervention by preventing a major cerebro-vascular event especially in the asymptomatic group [1]. High activity levels of tissue biomarkers, such as cathepsins, integrins, and matrix metalloproteinases (MMPs), have been associated with atherosclerotic plaque instability, thus can potentially be used for highly specific diagnosis [2]. While fluorescent tagging of such molecules has been amply demonstrated, no imaging method has so far been shown capable of resolving inflammation-associated tags with high fidelity.

Methods: We showcase herein the ability to resolve activation of common probes sensitive to matrix metallo-proteinases with unprecedented image quality and resolution utilizing multi-spectral optoacoustic tomography (MSOT) [3], thus revealing atherosclerotic activity. Human carotid plaque specimens from patients were incubated ex vivo with an MMP-sensitive activatable fluorescent probe (MMPsense 680TM) directly after endarterectomy. The specimen were subsequently imaged using an MSOT scanner capable of simultaneous high resolution visualization of morphology and molecular activity with better than 200 micron resolution.

Results: MSOT analyses identified heterogeneous MMP activity throughout the plaques, revealing hot and cold spot regions indicative of relatively high and low MMP activity respectively. The results from intact specimen corresponded well with epi-fluorescence images made on thin cryosections. Elevated MMP activity in the hot spot regions resolved was further confirmed by in situ zymography, accompanied by increased macrophage influx. Results from both MSOT investigations and histological sections confirmed that most of the plaque formation activity occurs, as expected, close to the bifurcation area of the carotid artery.

Conclusions: We show, for the first time to our knowledge, the ability of multispectral optoacoustic tomography to deliver volumetric images of activatable molecular probe distribution deep from optically opaque tissues. High resolution mapping of MMP activity in the vulnerable plaque of human carotid specimen was demonstrated. This ability directly relates to clinical potential as it can allow highly specific visualization and staging of plaque vulnerability in atherosclerosis during surgical intervention or by intravascular or potentially non-invasive imaging; thus impacting therapeutic clinical decision.

Acknowledgement: This research was partially supported by the German Research Foundation (DFG) Research Grant (RA 1848/1), ERC Senior Investigator Award, and the Medizin Technik BMBF award for excellence in medical innovation.

References:

1. Chambers BR et al; Cochrane Database Syst Rev. 2:CD001923 (2000).
2. Libby P.; Inflammation in atherosclerosis. Nature. 420:868-874 (2002).
3. Razansky D et al.; Nature Phot. 3:3525-3529 (2009).

c-Jun N-terminal kinase promotes inflammation at atherosclerosis-prone sites by enhancing expression and activity of NF-κB transcription factors

Evans P. [1], Cuhlmann S. [1], Van Der Heiden K. [1], Haskard D. [1], Krams R. [1], Gsell W. [1], Carlsen H. [2], Jones H. [1].

[1] Imperial College London,
[2] University of Oslo, Norway.

paul.evans@imperial.ac.uk

Introduction: Atherosclerosis is a chronic inflammatory disease of arteries that causes heart attack or stroke. Early lesions contain monocytes and T lymphocytes which are recruited from the circulation to activated vascular endothelial cells (ECs). This process relies on NF-κB transcription factors which induce pro-inflammatory molecules (e.g. VCAM-1) in ECs. Atherosclerosis develops predominantly at branches and bends of arteries that are exposed to low, oscillatory shear stress (frictional force exerted by flowing blood on ECs). We previously demonstrated that c-Jun N-terminal kinase (JNK), a MAP kinase, is activated in ECs at atherosusceptible but not atheroprotected sites (Chaudhury et al 2010). Here we combined in vitro studies with molecular imaging techniques in murine models to study the function of JNK in arterial EC.

Methods: We studied the function of JNK by performing microarray analysis of cultured ECs treated with a pharmacological JNK inhibitor. En face immunostaining was used to determine the expression of particular proteins in ECs at atheroprotected and atherosusceptible sites of murine arteries. In addition, we assessed NF-κB transcriptional activity in murine arteries of transgenic NF-κB-luciferase reporter mice by measuring luminescence using an ultrasensitive camera (Xenogen). Inflammation was also assessed by F18-FDG PET/CT imaging of murine arteries and identification of CD68-positive macrophages by immunostaining.

Results: Transcriptome profiling of cultured ECs treated with a pharmacological inhibitor revealed that JNK functions as a positive regulator of NF-κB transcription factors. This observation was confirmed by silencing of JNK1 and ATF2 (a downstream transcription factor) which led to reduced NF-κB expression in cultured ECs. We validated our findings by studying ECs in the aorta of wild-type and JNK1-/- mice. En face immunostaining revealed that EC expression of NF-κB and VCAM-1 and accumulation of CD68-positive macrophages was enhanced at atherosusceptible compared to atheroprotected sites in wild-type mice. Genetic deletion of JNK1 suppressed NF-κB and VCAM-1 expression at the atherosusceptible site, indicating that JNK1 positively regulates NF-κB expression and inflammation. Similarly, studies of transgenic NF-κB-luciferase mice revealed that NF-κB activity in ECs was enhanced at atherosusceptible compared to atheroprotected sites. To determine whether a causal relationship exists between shear stress and vascular inflammation we altered blood flow in the murine carotid artery by placing a flow altering cuff. We observed that low, oscillatory shear stress enhanced JNK activity, increased the expression of NF-κB and VCAM-1, promoted the accumulation of macrophages and enhanced arterial uptake of F18-FDG.

Conclusions: We conclude that JNK1-ATF2 signalling promotes EC activation and inflammation at atherosusceptible sites exposed to low, oscillatory shear stress by enhancing NF-κB expression. Our findings illuminate a novel level of cross-talk between the NF-κB and JNK signalling pathways that may influence the spatial distribution of atherosclerotic lesions.

Acknowledgement: Funded by the European Union FP6 NoE DiMI (LSHB-CT-2005-512146) and British Heart Foundation.

References:

1. Chaudhury et al. 2010 Arterioscler. Thromb. Vasc. Biol. 30(3):546-53.

Absolute Quantification in Small Animal Pinhole Gated Myocardial Perfusion SPECT

Goethals L. [(1)], Devos H. [(1)], Vanhove C. [(1)], De Geeter F. [(1)], Lahoutte T. [(1)].

[(1)] VUB Brussels, Belgium

lode.goethals@vub.ac.be

Introduction: Previously, our group has demonstrated the feasibility of absolute quantification using SPECT [1] imaging by incorporating a CT derived non-uniform attenuation correction (AC) map and a triple energy scatter window correction in the reconstruction algorithm of SPECT images. In this study we apply these techniques to the rat myocardium, which has a size below the resolution of our imaging system, thus suffering from a partial volume effect, which results in an underestimation of the activity concentration in the target tissues. To compensate for this underestimation we performed ultrasound imaging prior to SPECT imaging to determine myocardial wall thickness. We then derived a recovery coefficient (RC) from phantom studies to correct for the partial volume effect.

Methods: SPECT/CT scans were performed in 9 healthy Wistar rats 30 min after injection of 99mTc-Tetrofosmin. Prior to SPECT/CT imaging, 2D cardiac ultrasound images were acquired in the midventricular segments to determine diastolic and systolic myocardial wall thickness. After SPECT/CT imaging, animals were sacrificed and 6 midventricular segments (anterior-anterolateral-inferolateral-inferior-inferoseptal-anteroseptal) of the left ventricle were excised and counted in a gamma well counter. Using 6 midventricular ROI's in AMIDE, the effect of scatter correction (SC) and attenuation correction (AC) was determined in every midventricular segment.

The activity in every ROI was expressed in Curie per gram (taking into account the density of myocardial tissue of 1,055 Kg/L). These image-derived activities were compared to the ex vivo activity concentrations counted in the gamma counter. To correct for the partial volume effect, a RC was determined from a phantom study. All values obtained after AC and SC were corrected by this RC and compared to the ex vivo counting data.

Results: AC leads to a significant increase in counts in every midventricular segment, whilst SC results in a decrease in counts in every midventricular segment. The combination of both S and AC leads to a significant increase in counts in the inferior midventricular segment (paired Student's T test, $p < 0,05$).

After combined AC and SC, there remains a vast underestimation of activity in the myocardium, compared to the ex vivo data. Incorparation of a recovery coefficient derived from the phantom study, alleviates this problem: in the sub 5mm region, a RC of $Y = 17,252 . X$ (with X = myocardial size in mm, Y = RC in %) was derived from the phantom studies. Dividing the combined AC and SC values by a RC derived from the average wall thickness (diastolic + systolic / 2) leads to an adequate estimation of activity, correlating well with the ex vivo data. Use of the diastolic thickness as source of the RC leads to an overestimation of activity, use of the systolic thickness as a source of the RC leads to an underestimation of activity on the non-gated images. Use of the appropriate RC on the corresponding gated images also leads to an adequate estimation of activity on images.

Conclusions: Combining attenuation, scatter and partial volume effect corrections in small animal myocardial perfusion SPECT allows for non invasive absolute quantification of myocardial perfusion.

Acknowledgement: Researh at ICMI is funded by the Interuniversity Attraction Poles Program - Belgian State - Belgian Science Policy. Tony Lahoutte is a Senior Clinical Investigator of the Research Foundation - Flanders (Belgium) FWO. Lode Goethals is a PhD fellow of the research foundation – Flanders (Belgium) -FWO.

References:

1. Improved quantification in single-pinhole and multiple-pinhole SPECT using micro-CT information. Vanhove C, Defrise M, Bossuyt A, Lahoutte T. Eur J Nucl Med Mol Imaging. 2009 Jul;36(7):1049-63.

Cancer imaging

Haberkorn U. .

University Heidelberg, Germany

Uwe.Haberkorn@med.uni-heidelberg.de

Increased metabolism has been found to be one of the most prominent features of malignant tumors. This property led to the development of tracers for the assessment of glucose metabolism and amino acid transport and their application for tumor diagnosis and staging. Prominent examples are fluorodeoxyglucose, methionine and tyrosine analogs which have found broad clinical application. Since quantitative procedures are available these techniques can also be used for therapy monitoring. Another approach may be based on the non-invasive detection of apoptosis with tracers for phosphytidyl-serine presentation and/or caspase activation as surrogate marker for therapeutic efficacy. Finally, the use and development of specific ligands to target structures overexpressed in tumor tissue may be a valuable tool for diagnosis and novel therapeutic interventions.

Controlled drug delivery under image guidance

Gruell H. [1], Langereis S. [1], De Smet M. [2], Sanches P. [2], Hijnen N. [2], Rossin R. [1], Bohmer M. [1], Keupp J. [1], Tiemann K. [3], Heijman E. [1].

[1] Philips Research,
[2] Eindhoven University of Technology,
[3] University Hospital Münster.

holger.gruell@philips.com

Introduction: Focused ultrasound (FU) is an excellent method for local triggered drug delivery using either pressure or temperature sensitive delivery systems. Temperature sensitive liposomes (TSLs) as drug carriers are promising to maximize delivery of drugs to tumors that are heated slightly above body temperature using FU. Besides heating, the pressure pulses of ultrasound waves can be exploited to disrupt microbubbles, which can lead to formation of transient pores in the endothelial wall. The latter is termed sonoporation and was shown to mediate cellular uptake of therapeutic agents. Either way, imaging based method to visualize, follow, and control drug delivery in-vivo are of importance to establish more quantitative treatment protocols.

Methods: TSLs of different lipid compositions and a release temperature slightly above body temperature were loaded with T1, CEST or fluorinated MRI contrast agents and the drug doxorubicin. MRI was used to assess the signal change upon heating the TSLs from T=310 K to T=315 K using FU. For pressure induced drug delivery, microbubbles were injected into tumor bearing mice. Tumor and muscle tissues were treated with FU. Subsequently, radiolabeled albumin was injected and the extravasation in tumor and muscle tissue was followed and quantified using single photon computed tomography (SPECT).

Results: Focused ultrasound is used to locally heat tissue, while MRI provides spatial and temperature control of the process. Co-encapsulation of drugs and MRI contrast agents allows to image the drug carrier system as well as to quantify release of drugs under hyperthermia conditions with MRI, making this modality the perfect choice for temperature induced drug delivery under image guidance. The temperature of drug release but also contrast properties can be tuned by nature and composition of the phospholipid bilayer. The rapid release of drugs and contrast agents can be explained by the formation of transient pores in the lipid membrane upon heating. For pressure induced drug delivery, the cavitation of microbubbles by ultrasound creates transient pores in the endothelial layer allowing macromolecules to efficiently extravasate. This effect is found to be more pronounced in muscle tissue than in tumors. In healthy muscle tissue the intact endothelial layer prevents extravasation of macromolecules while the leaky and premature vasculature in tumors is more permeable for macroscopic compounds.

Conclusions: Focused Ultrasound allows to non-invasively trigger drug delivery in vivo, either using a local heating or focused pressure pulses in combination with suited drug delivery vehicles. The drug delivery process can be planned, controlled and followed using diagnostic imaging modalities such as MRI or ultrasound in combination with smart drug delivery vehicles. Above approach allows local non-invasive image guided treatment of a tissue that potentially leads to an improvement of the therapeutic window or even enables delivery of completely different classes of drugs such as siRNA or plasmid DNA.

Acknowledgement: This project was funded in part by the EU Project Sonodrugs (NMP4-LA-2008-213706)

References:

1. Langereis et al., J. Am. Chem. Soc. 131, 1380 (2009).
2. De Smet et al. J. Contr. Release 143, 120 (2010).

Comparative biodistribution of twelve gastrin/CCK2 receptor targeting peptides

De Jong M. .

Erasmus MC Rotterdam, The Netherlands

m.hendriks-dejong@erasmusmc.nl

Introduction: Molecular targeted radionuclide cancer therapy is becoming of increasing importance, especially for disseminated diseases. Systemic chemotherapies often lack selectivity; targeted radionuclide therapy has important advantages as the radioactive cytotoxic unit of the targeting vector is specifically directed to the cancer, sparing normal tissues. The basis of COST Action BM0607 is the great potential of targeted radionuclide therapy using a variety of vectors and radionuclides. This Action brings together the different disciplines involved and provides a reliable and rapid means for developing new (fundamental) knowledge, method standardization and products.

Minigastrin and CCK analogs have been developed for radionuclide imaging and therapy of CCK2R expressing tumors. One project in COST Action BM0607 aims to select the optimal gastrin/CCK analogs for targeting MTC and SCLC expressing the CCK2R. In the present study, twelve DOTA-conjugated analogues were labeled with In-111 and their in vitro and in vivo CCK2R targeting properties were studied in nude mice with CCK2R expressing A431 tumors.

Methods: All peptides were labeled with In-111 at high specific activity. Receptor affinity and internalization were tested in vitro using CCK2R-transfected A431 tumor cells. Mice with CCK2R-transfected A431 tumors in the left flank and with mock-transfected A431 tumors in the right flank received radiolabeled peptide intravenously for imaging and biodistribution studies.

Results: All peptides demonstrated high receptor affinity and receptor-specific internalization in vitro and tumor targeting in the CCK2R expressing tumor in vivo. Tumor uptake at 1 h p.i. ranged from 2.53 ± 0.47 %ID/g for CP07 to 13.3 ± 4.9 %ID/g for CP10, whereas uptake at 4 h p.i. ranged from 1.88 ± 1.12 %ID/g to 9.90 ± 2.0 %ID/g, respectively. Uptake in non-target tissues was low for all peptides, except for high kidney uptake for CP10 and CP11. Highest tumor-to-kidney ratios (3-5) were obtained with the gastrin analogues CP01, CP02, CP03 and CP09.

Conclusions: All peptides showed good CCK2R-mediated tumor-targeting in vitro and in vivo, with low uptake in non-target organs except for the kidneys in some cases. CP01, CP04 and CP05 displayed favorable in vivo characteristics, combing high tumor uptake with low kidney retention.

Acknowledgement: This study is part of COST Action BM0607

Targeting cancer stem cells using radiolabeled Sonic Hedgehog

Tworowska I. [(1)], Delpassand E. S. [(1)], Sims-Mourtada J. [(1)].

[(1)] RadioMedix Housten, USA

itworowska@radiomedix.com

Introduction: Sonic Hedgehog (SHH) is an extracellular signalling protein involved in embryo development and morphogenesis [1]. Constitutive activation of the hedgehog pathway is observed in several types of cancers [2], especially in the most aggressive cancer stem cells and it is associated with their chemo/radiation resistance [3]. This work reports results on characterization of the SHH conjugates and their application to the cancer imaging using positron emission tomography (PET).

Methods: 6xHis-tagged recombinant SHH (19.5kDa) with terminal NH2 group was conjugated to the DOTA (1,4,7,10-Tetraazacyclododecane-N,N',N'',N'''-tetraacetic acid) in phosphate buffer and purified by dialysis. Alternatively SHH ligand was coupled to the maleimido-monoamide-DOTA chelator through thiol group of cysteine. Protein conjugates were further characterized using MALDI-MS and HPLC. Radiolabeling of the DOTA-SHH was performed in 0.1M NH4OAc (pH=4.4) using 68GaCl3 eluted from 68Ge/68Ga generator (iThemba). In vitro bioactivity was evaluated by cellular uptake studies of the radiolabeled ligand in the several cancer cell lines and enriched stem cancer-cells population (mammospheres).

Results: DOTA-SHH was obtained with total yield of 74%-89%. Reaction proceeded with radiochemical purity of >98% and specific activity of 3.38E+05 MBq/g, (theoretical specific activity = 3.64E+11 MBq/gram) as assessed by radio-TLC and radio-HPLC. 68Ga-DOTA-SHH have shown high affinity to Patched receptors (PTCH) in cancer cells (BT-474, MDA-MB-231, MCF-7) and its cellular uptake correlates with PTCH receptor expression levels. Cellular uptake of the SHH conjugates in the presence of the hedgehog pathway inhibitor, cyclopamine, was reduced by more than 50%. Competitive uptake studies in the presence of the cold SHH, have also shown reduced cellular uptake by approximately 90%. In vitro uptake of 68Ga-DOTA-SHH was approximately 12-fold higher in cancer stem-cells (MCF-7 cultures) compared to the total cell population.

Conclusions: Our studies have shown that 68Ga DOTA-SHH conjugates have potential application to non-invasive imaging of cancer, especially the most aggressive cancers. This is the first report on application of radiolabeled SHH conjugates for identification of the cancer stem-cell from the total tumor population. SHH conjugates may be also useful to evaluate new therapies targeting cancer stem-cells.

References:

1. Hammerschmidt M., Brook A., McMahon A.P., Trends Genet., (1997), 13, 14-2.
2. Beachy P.A., Karhadkar S.S., Berman D.M., Nature (2004), 432, 324-331; Mullor JL, Sánchez P, Altaba A.R., Trends Cell Biol.,(2003), 12 (12): 562–9.
3. Al-Hajj M., Becker M.W., Wicha M., Weissmann I., Clarke M.F., Curr. Opin. Genet. Dev., (2004), 14(1), 43-47

YIA applicant

Evaluation of the photosensitizer Bremachlorin for photodynamic treatment of breast cancer bone metastasis.

Van Driel P. [(1)], Que I. [(1)], Snoeks T. [(1)], Mol I. [(1)], Xie B. [(1)], Keereweer S. [(1)], Kaijzel E. [(1)], Löwik C.W.G.M. [(1)].

Leiden University Medical Center

tpieter_v_driel@hotmail.com

106

Introduction: Photodynamic therapy (PDT) is a promising treatment for tumors in which harmless light is used for the irradiation of nontoxic photosensitizers to create highly toxic reactive oxygen species for the destruction of certain tumors. In this study, the photosensitizer Bremachlorin™ (Brema Pharma Int.), derived from the seaweed spirulina, consisting of the compounds Chlorin e6, Purpurin 5 and Chlorin p6, was evaluated for PDT of breast cancer derived bone metastasis.

Methods: The uptake of Bremachlorin in the human breast cancer cell line MDA-MB231 luc D3H2LN was quantitatively measured with flow cytometry and visualized with confocal laser scan microscopy. Cell viability after photodynamic treatment was measured with a luciferase assay and colorimetric MTS cell proliferation assay to identify the cytotoxic potential of Bremachlorin on these cells.The tumor cells were injected in the bone marrow cavity in femurs of immunodeficient mice to form osteolytic tumors. In vivo effects of PDT with Bremachlorin were followed by whole body bioluminescent imaging (BLI).

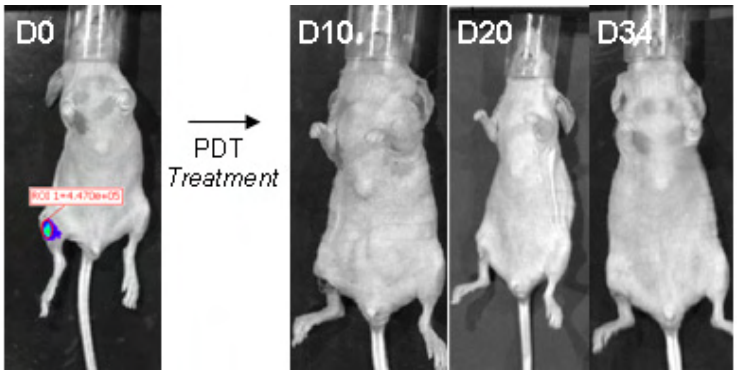

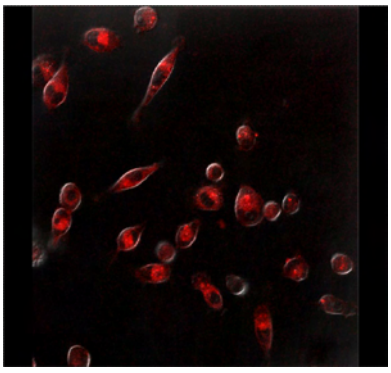

Results: Flow cytometry analysis showed Bremachlorin uptake by the tumor cells was (close to) 100%. Also, fluorescent signal increased with an increasing dose of Bremachlorin. Complete cell death in vitro was already achieved after an incubation time of 5 hours with a concentration of 2 mg/l Bremachlorin. In vivo BLI experiments showed the partial or total eradication of the osteolytic tumors after a single pulse treatment of Bremachlorin-treated animals. In case of partial cure, the tumors were successfully eradicated by a second PDT treatment

Conclusions: Our in vitro results show the tumor selective uptake of the photosensitizer Bremachlorin and its cytotoxic effects on the human breast cancer cells. Furthermore, with whole body BLI we show that PDT treatment of Bremachlorin-treated animals is an interesting therapy to eradicate aggressive tumors deep down in bone marrow. These results are very promising and interesting for future clinical use of photodynamic treatment of tumors with the photosensitizer Bremachlorin.

Acknowledgement: Dhr. H. Vink and Andrei Reshetnickov from Brema Pharma

In vivo targeting of HEK-hsst$_{2/3/5}$ Xenografts by ^{111}in-labeled [(DOTA)Ser^{1},Leu^{8},trp^{22},Tyr^{25}]-SS-28 in SCID mice

Maina T. [1], Tatsi A. [1], Marsouvanidis I. P. [1], Krenning E. P. [2], De Jong M. [2], Nock B.A. [1].

[1] IRRP, NCSR "Demokritos",
[2] Dept. of Nuclear Medicine, EMC Rotterdam.

maina_thea@hotmail.com

Introduction: Radiolabeled pansomatostatin-like analogs are expected to enhance the diagnostic sensitivity and to expand the clinical indications of currently applied sst$_2$-specific radioligands (like OctreoScan®) [1,2]. We have previously reported on [(DOTA)Ser^{1},Leu^{8},trp^{22},Tyr^{25}]SS-28 displaying a high affinity for all five hsst$_{1-5}$. In mice, the ^{111}In-radioligand showed specific uptake in AR4-2J tumors which express the rat sst$_2$ [3]. We were further interested to investigate the ability of [(^{111}In-DOTA)Ser^{1},Leu^{8},trp^{22},Tyr^{25}]SS-28 to target human sst$_x$ expressing tumors *in vivo*.

Methods: HEK-293 cells stably transfected with one of the hsst$_{2A}$, the hsst$_3$ or the hsst$_5$ were cultured in a humidified-5% CO_2 atmosphere at 37^{0}C in DMEM GLUTAMAX-I supplemented with 10%FBS, 100 U/mL penicillin / 100 µg/ml µg/mL streptomycin and 400 µg/mL G418. Cells were cropped, suspended in PBS and cell-suspension was equally divided in Eppendorf tubes (1 – 2 x 10^7 cells, 150 mL). Inoculation was performed by subcutaneous injection of a cell suspension bolus in the left flank of young SCID mice. After 10-18 days well-palpable tumor masses developed at the inoculation site and biodistribution experiments were performed. On the day of the experiment the radioligand was injected as a bolus (100 µL, 2 µCi) in the tail vein, alone or together with a high excess sst$_x$-binding peptide (blocker). Animals were sacrificed in groups of four at 4 h postinjection (pi) and tissues were excised, weighed and counted in a gamma-counter. Values were calculated as percent injected dose per gram (%ID/g) tissue and are expressed as mean ± SD.

Results: [(^{111}In-DOTA)Ser^{1},Leu^{8},trp^{22},Tyr^{25}]SS-28 showed significant and specific uptake in the hsst$_{2A}$-positive HEK implants of 4.43 ± 1.5%ID/g vs. 0.49 ± 0.0%ID/g block (50 µg Tate) at 4 h pi (the previously reported values in the rsst$_2^+$-AR4-2J tumor, were 9.35 ± 1.31%ID/g and 0.35 ± 0.0%ID/g, respectively [3]). Equally high and specific uptake was displayed in the hsst$_3^+$-HEK xenografts with a 4.88 ± 1.1%ID/g vs. 0.52 ± 0.05%ID/g block at 4 h pi (100 µg Demo-Pan 2 [2]). Preliminary values in the hsst$_5^+$-HEK xenografts were slightly inferior (<3%ID/g) and could be only marginally reduced by co-injection of 35 nmol [(DOTA)Ala^{1},trp^{8}]SS-14. Experiments with the use of other sst$_5$-affine peptides as blockers are currently in progress. In all cases, renal uptake was found extremely high (200-300%ID/g at 4 h pi) and could be hardly reduced by co-injection of lysine or gelofusine.

Conclusions: The pansomatostatin radioligand [(^{111}In-DOTA)Ser^{1},Leu^{8},trp^{22},Tyr^{25}]SS-28 specifically localizes in HEK-hsst$_{2/3/5}$-positive xenografts in SCID mice. Differences in tumor uptake may be attributed to different levels of sst$_x$-expression across the cell lines used for tumor induction. The very high renal uptake remains a serious handicap of the radioligand and a variety of kidney protection regimens are currently evaluated to circumvent this problem.

Acknowledgement: This study has been performed within the framework of COST Action BM0607:Targeted Radionuclide Therapy.

References:

1. Reubi JC et al; Eur J Pharmacol. 456:45-49 (2002)
2. Charalambidis D et al; Eur J Nucl Med Mol Imaging. 35 (Suppl. 2): 491, S209 (2008)
3. Maina et al; Eur J Nucl Med Mol Imaging. 36 (Suppl. 2): OP521, S260 (2009)

poster

Poster Session

Guided Poster Sessions – Poster Walks 1 to 7

Guided Poster Session 1, Day 1: Thursday May 27, 2010 from 14:30 to 16:00

Poster Walk 1: Imaging Cancer Biology – P001 to P012 & P105 to P106
Co-Chairs: Fabian Kiessling (Aachen, Germany), Markus Rudin (Zürich, Switzerland)

Poster Walk 2: Technology & Data Analysis Methods – P070 to P078 & P097 to P104
Co-Chairs: Serge Maitrejean (Paris, France), Adriaan Lammertsma (Amsterdam, The Netherlands)

Poster Walk 3: Molecular Neuroimaging – P034 to P047 & P107
Co-Chairs: Sabina Pappata (Naples, Italy), Andreas Jacobs (Muenster, Germany)

Poster Walk 4: Probe Design – P058 to P069
Co-Chairs: Frédéric Dollé (Orsay, France), Helmut Maecke (Freiburg, Germany)

Guided Poster Session 2, Day 2: Friday May 28, 2010 from 14:30 to 16:00

Poster Walk 5: Imaging in Cancer & Drug Development – P013 to P022 & P023 to P030
Co-Chairs: Peter Brader (Graz, Austria), NN

Poster Walk 6: Imaging in Other Diseases – P031 to P033 & P079 to P083 & P084 to P091
Co-Chairs: Bertrand Tavitian (Orsay, France), Nicolas Grenier (Bordeaux, France)

Poster Walk 7: Imaging-guided Gene and Cell based and Targeted Therapies – P048 to P057 & P092 to P096
Co-Chairs: Ludwig Aigner (Salzburg, Austria), NN

overview poster presentations – per title

MI in CANCER BIOLGY

IMAGING in DRUG DEVELOPMENT

CANCER from BENCH to BEDSIDE

MI in CARDIOVASCULAR DISEASE

NEUROIMAGING from BENCH to BEDSIDE

GENE and CELL based THERAPIES

PROBE DESIGN

TECHNOLOGY

ENDOCRINE DISEASES

INFECTION and INFLAMMATION

TARGETED THERAPY

MI DATA ANALYSIS METHODS

Late Breaking

P-001

In vivo MRI multicontrast kinetic analysis of intracellular trafficking of liposomes

Aime S. , Delli Castelli D. , Dastrù W. , Terreno E. , Cittadino E. , Torres E. , Mainini F. , Spadaro M. .

University of Torino, Italy

silvio.aime@unito.it

Introduction: Liposomes are mainly used in the pharmaceutical field as drug delivery systems. Despite their large use, there is still a lack of information about the interaction between the nanovesicles and the cells in tumor environments and their intracellular fate after the cellular uptake. Most of the information on this topic comes out from in vitro cellular studies that are not always reliable models for mimicking the in vivo system. The aim of this work is the visualisation of the metabolic pathway of these vesicles directly in vivo by means of MRI. Since MRI does not provide enough spatial resolution to directly observe events at subcellular level, we have developed a multicontrast analysis that provides indirect evidence about the uptake and the intracellular trafficking of the nanovesicles. The method relies on the peculiarity of nanovesicles encapsulating paramagnetic Ln(III)-based complexes that may act as T1, T2, and CEST agents. In order to account for the observed MRI data, a kinetic model able to describe the underlying biological processes has been developed. The fit of the data provides a rough estimate of the kinetic constants for each process considered in the model.

Methods: Non targeted, stealth or pH-sensitive, liposomes encapsulating paramagnetic lanthanide(III) complexes were prepared and in vitro characterized. The liposomes were locally injected in B16 melanoma tumor xenografted on C57 mice. The temporal evolution of T1, T2 and CEST MR contrast was followed at 7 T until 48 h post-injection.

Results. The evolution over time is different among the three contrast modes (T1,T2, CEST). The process taking place (cellular uptake, intracellular release, esocytosis, and wash out) have been modeled and rough estimates for the kinetic constants have been determined upon the simultaneous interpolation of all the data. Moreover, the intracellular trafficking of stealth vs pH sensitive liposomes has been compared.

The comparison among the evolution of the three contrast modalities for the two different liposomes is quite different. In particular, the maximum T1 contrast was observed at 5hrs post injection while for the stealth one it occurs at 24hrs post injection.

Conclusions: The MRI multicontrast analysis developed in this work represents an innovative way to get deeper insight into the in vivo detection of sub-cellular process. In particular, the intracellular trafficking of two liposomal formulations (pH-sensitive and conventional stealth) of great relevance in the field of drug delivery have been compared. The kinetic analysis revealed that both liposomes are taken up quite fast from Tumor Associated Macrophages but the intracellular release of the imaging reporters is much faster for the pH sensitive one.

Diffusion-weighted MRI for differentiation of breast lesions at 3.0 Tesla: a new biomarker for breast imaging

P-002

Bogner W. , Gruber S. , Pinker K. , Grabner G. , Moser E. , Trattnig S. , Stadelbauer A. , Helbich T. .

Department of Radiology, Vienna, Austria

thomas.helbich@akhwien.at

Introduction: To compare the diagnostic quality of different diffusion weighting schemes with regard to apparent diffusion coefficient (ADC) accuracy, ADC precision, and diffusion-weighted image (DWI) contrast-to-noise ratio (CNR) for different types of lesions and breast tissue. Based on these assessments a new biomarker for breast imaging will be defined.

Materials and Methods: Institutional Review Board approval and written, informed consent were obtained. Fifty-one patients with histopathologic correlation or follow-up were included in this study on a 3.0 Tesla MR scanner. There were 112 regions of interest (ROIs) drawn in 24 malignant, 17 benign, 20 cystic, and 51 normal tissue regions. ADC maps were calculated for combinations of ten different diffusion-weightings (b-values), ranging from 0 to 1250 s/mm². Differences in ADC among tissue types were evaluated. The CNR of lesions on DWI was compared for all b-values. A repeated measure ANOVA was used to assess lesion differentiation.

Results: ADC (mean±SD x10-3mm²/s) values calculated from b=50 and 850 s/mm² were 0.99±0.18, 1.47±0.21, 1.85±0.22, and 2.64±0.30 for malignant, benign, normal, and cystic tissue, respectively. An ADC threshold of 1.25 x10-3mm²/s allowed discrimination of malignant from benign lesions with a diagnostic accuracy of 95% (p<.001). ADC calculations using multiple b-values were not significantly more precise than calculations using two b-values. We found an overestimation of ADC for maximum b-values of up to 1000 s/mm². The best CNR for tumors was identified at 850 s/mm².

Conclusion: Optimum ADC determination and DWI quality at 3.0 Tesla was found for a combination of two b-values: 50 and 850 s/mm². The assessed value provides a high accuracy for differentiation of benign and malignant breast tumors and represents a new biomarker for imaging.

POSTER

MI in CANCER BIOLGY

P-003

Imaging tumour apoptosis with 68Ga-labelled AnnexinA5 derivatives early after cancer therapy

De Saint-Hubert M. [1], Bauwens M. [1], Devos E. [1], Deckers N. [2], Reutelingsperger C. [2], Verbruggen A. [1], Mortelmans L. [1], Mottaghy F. [3].

[1] KULeuven, Heverlee, Belgium
[2] University Maastricht, The Netherlands
[3] RWTH Aachen, Germany

marijke.desainthubert@med.kuleuven.be

Introduction: Molecular imaging of apoptosis offers a direct and early measurement of response to cancer therapy which allows a fast decision making in cancer treatment. One of the early characteristics of apoptosis is externalization of phosphatidylserine (PS) on cell membranes. Annexin V (AnxA5) binds with a high affinity to membrane-bound PS. Due to suboptimal imaging quality of ^{99m}Tc labelled AnxA5 we aimed to specifically label AnxA5 with an emerging radioisotope, ^{68}Ga, allowing Positron Emission Tomography (PET).

Methods: We radiolabelled AnxA5 with ^{68}Ga using two mutated forms of AnxA5 with a single cysteine residue at position 2 or 165, respectively Cys2-AnxA5 and Cys165-AnxA5, allowing site-specific coupling of ^{68}Ga-Dota-maleimide. In vitro cell binding of both radiotracers was studied in healthy and anti-Fas treated Jurkat cells. Biodistribution and pharmacokinetics were studied with µPET in healthy mice and in a hepatic apoptosis model (anti-Fas Ab treated) up to 60 min p.i.. Daudi (Burkitt lymphoma) tumour bearing mice were scanned before and after treatment with combined chemotherapy (125 mg/g Endoxan) and radiotherapy (10 Gy/tumour) using µPET and µMRI. Tracer uptake was measured and imaged ex vivo using autoradiography and correlated to histological evidence of apoptosis (TUNEL).

Results: ^{68}Ga-Dota-maleimide labelling yield was at least 98% and coupling yield of ^{68}Ga-Dota-maleimide to Cys2-AnxA5 and Cys165-AnxA5 was ~70%. Labelling and purification took about 60 min, with a final radiochemical purity of at least 98%. In vitro binding of ^{68}Ga-Cys2-AnxA5 and ^{68}Ga-Cys165-AnxA5 to anti-Fas treated tumour cells was 5 times higher compared to normal cells.

Dynamic PET images in normal mice revealed that both tracers showed a fast clearance from the blood towards the kidneys, with no significant change in biodistribution from 30 min p.i. on. Dissection data confirmed clearance was mainly via the urinary tract.

Dynamic PET images of anti-Fas treated animals revealed a major shift of radioactivity from the kidneys to the (apoptotic) liver for both ^{68}Ga-Cys2-AnxA5 and ^{68}Ga-Cys165-AnxA5. Compared to normal mice anti-Fas treated animals showed a 7 to 9 times higher liver uptake (for respectively ^{68}Ga-Cys2-AnxA5 and ^{68}Ga-Cys165-AnxA5) as compared to healthy animals. Autoradiography images confirm the higher uptake in anti-Fas treated livers, corresponding to TUNEL positive cells.

MRI-PET fusion images allowed clear delineation of each tumor. Using this technique, we noted that the post-therapy SUV values significantly exceeded those prior to therapy. The absolute tumour uptake of ^{68}Ga-Cys2-AnxA5 and ^{68}Ga-Cys165-AnxA5 was respectively only 0.5 ± 0.1 % ID/g and 1.0 ± 0.3 % ID/g and significantly increased to 1.5 ± 0.2 % ID/g and 1.6 ± 0.1 % ID/g after therapy. Autoradiography confirms an increased activity in treated tumors with several regions showing 10-20 times higher uptake compared to the tumor uptake prior to treatment while other regions were found relatively unaffected. The same heterogeneous distribution of apoptosis was observed with TUNEL stainings.

Conclusions: ^{68}Ga-Cys2-AnxA5 and ^{68}Ga-Cys165-AnxA5 can be prepared with a high yield and within a reasonable time period. Apoptosis targeting capacity was clearly demonstrated in a model of hepatic apoptosis. PET-MRI fusion images demonstrated a higher tumor uptake after cancer therapy, indicating that ^{68}Ga-AnxA5 may be useful for the early evaluation of tumor therapy.

Acknowledgement: This work was financially supported by the European Union through the grant Euregional PACT II by the Interreg IV program of Grensregio Vlaanderen-Nederland (IVA-VLANED-1.20).

^{68}Ga-RGD-based PET tracers for imaging $\alpha_v\beta_3$ expression: a comparative study

P-004

Dumont R. [1], Maecke H. [1], Haubner R. [2], Behe M. [1], Weber W. [1], Fani M. [1].

[1] University Clinic Freiburg, Germany
[2] Medical University Innsbruck, Austria

rebecca.dumont@uniklinik-freiburg.de

Introduction: The integrin $\alpha_v\beta_3$ is a cellular adhesion molecule that is frequently expressed on malignant tumors and acts as an important receptor affecting tumor angiogenesis, local invasiveness, and metastatic potential. For imaging of the $\alpha_v\beta_3$ integrin, cyclic pentapeptides containing the tripeptide sequence arginine-glycine-aspartate (RGD) have been developed. These peptides specifically bind to $\alpha_v\beta_3$ in its activated state and recent clinical trials have shown that PET imaging with radiolabelled RGD peptides allows quantitative determination of activated $\alpha_v\beta_3$ integrin in patients with various malignant tumors [1,2]. Development of a ^{68}Ga-RGD-based tracer would be of great clinical utility given the increasing clinical importance of oncologic PET imaging and the excellent imaging properties and availabilty of ^{68}Ga. Thus, we developed [^{68}Ga]-DOTA-c(RGDfK) [3] and most recently [^{68}Ga]-NODAGA-c(RGDfK) [4]. The aim of this study was to compare the tracer properties in a U87MG human glioblastoma xenograft model.

Methods: The conjugate DOTA-c(RGDfK) was synthesised according to the literature [3]. An alternative head-to-tail cyclization protocol of the linear RGDfK was followed for the conjugate NODAGA-c(RGDfK) using a 50% solution of 1-propanephosphonic acid cyclic anhydride (T3P), triethylamine, and 4-di(methylamino)pyridine (DMAP). The two conjugates NODAGA-c(RGDfK) and DOTA-c(RGDfK) were labelled with ^{68}Ga in sodium acetate buffer 0.2 N, pH 4.0 using the Modular-Lab PharmaTracer *module by Eckert & Ziegler.* Biodistribution studies were performed in balb-c nude mice bearing subcutaneous U87MG human glioblastoma xenografts 1 h post-injection of the radiotracers (600 pmol / 4 MBq / mouse). To evaluate specificity of the compounds, blocking studies were done with an excess of the commercially available c(RGDfV). Static images were concurrently accquired with a microPET Focus small animal scanner and all results were evaluated comparatively.

Results: Both conjugates were labelled with ^{68}Ga with radiochemical purity > 97% and specific activity of 8-10 MBq/nmol at room temperature (NODAGA-c(RGDfK)) or elevated temperatures (DOTA-c(RGDfK)). The biodistribution profile of the two radio-conjugates was similar. However, [^{68}Ga]-NODAGA-c(RGDfK) showed faster blood clearance and higher tumor uptake compared to [^{68}Ga]-DOTA-c(RGDfK) (5.2 ± 1.4 %IA/g *vs* 3.5 ± 0.8 %IA/g) and improved tumor-to-blood and tumor-to-kidney ratios (27.7 ± 7.0 *vs* 9.2 ± 1.1 and 2.6 ± 0.3 *vs* 1.6 ± 0.1, respectively). Specificity of both tracers was demonstrated by successful blocking of tumor uptake in the presence of excess c(RGDfV), present on both biodistribtion and imaging studies. PET imaging quantitatively confirmed tumor targeting and biodistribution results of both conjugates.

Conclusions: Compared to [^{68}Ga]-DOTA-c(RGDfK), the superior labelling conditions and *in vivo* profile of [^{68}Ga]-NODAGA-c(RGDfK) make this compound a compelling radiotracer candidate for use in PET imaging of $\alpha_v\beta_3$-expressing tumors.

References:

1. Haubner R et al., PLoS Med. 2:e70 (2005)
2. Beer AJ et al., Clin Cancer Res. 12:3942-9 (2006)
3. Decristoforo C et al., Eur J Nucl Med Mol Imaging. 35:1507-1515 (2008)
4. Knetsch P et al., J Label Compd Radiopharm. 52: S413 (2009)

POSTER

MI in CANCER BIOLGY

P-005

Influence of anaesthetics on tumor tracer uptake in radiopeptide receptor imaging (PRI) and radionuclide therapy (PRRT)

Haeck J. , De Poel M. , Bijster-Marchand M. , Verwijnen S. , De Swart J. , Bernsen M. , De Jong M. .

Erasmus Medical Centre, Oegstgeest, The Netherlands

j.haeck@erasmusmc.nl

Introduction: Neuro-endocrine tumors originating from various organs are known to over express somatostatin receptors (SSR) on the cell membrane (1). PRI and PRRT enable selective imaging and treatment of tumor cells over expressing SSR using radiolabelled somatostatin analogues, e.g. the SPECT tracer ^{111}In-DTPA-octreotide. In experimental studies, in vivo imaging and measurement of tracer uptake in tumors and in normal organs is generally performed in anaesthetised laboratory animals. Different methods of anaesthesia are used according to the possibilities, experience and common practice in a laboratory. However, in many in vivo experiments the influence of changes in physiology due to anaesthetics is not taken into account. The aim of the current study was to determine the influence of different anaesthetics on bio-distribution of radioactive ^{111}In-DTPA-octreotide, a somatostatin analogue, in rats bearing SSR positive tumors.

118

Methods: Lewis rats (n=8) were inoculated with 0.5 million CA20948 (SSR-positive) pancreatic tumor cells in the flank. The tumors were grown to approximately 1.5 cm^2 before imaging. Prior to i.v. injection of the radiolabelled peptide (50 MBq in 0.4 µg) the animals were anaesthetized with either inhalant-anaesthetic isoflurane (n=4) or a mixture of injectable anaesthetics consisting of sufentanil (300µg/kg) and medetomidine (300µg/kg) injected intra-peritoneally (n=4). The rats were kept under anaesthesia during 1h tracer circulation and subsequent SPECT/CT imaging. After imaging the rats were euthanized and tumor and organs were removed to study the peptide biodistribution ex-vivo. Biodistribution was performed at 3h p.i.

Results: A significantly higher tumor uptake of ^{111}In-DTPA-octreoscan was found when the rats were anaesthetized with isoflurane in comparison to medetomidine/sufentanil (figure 1), $p<0,05$. This was shown in tumors on either flank, and the mean uptake of both tumors, over all rats. There was no significant difference between left and right tumor under the same anaesthetic. In several other organs, such as SSR-positive pancreas and stomach, the extent of tracer uptake was also dependent on the type of anaesthesia used

Conclusions: There is a significant influence of anaesthetics on the binding of radiolabelled somatostatin analogue to SSR on tumor cells. This influence is not subtle and therefore has an effect on the experimental outcome. When conducting a study on PRI or PRRT in tumors the effects of anaesthetics on the behaviour of the tracer binding has to be taken into account.

Acknowledgement: Funding was provided by the Dutch Cancer Society grant no. 2008-4037 (KWF kankerbestrijding) and Erasmus MC – University Medical Center Rotterdam, The Netherlands

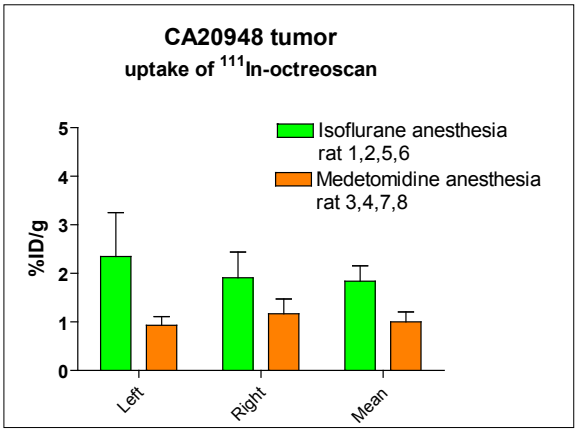

References:

1. Endocrine Reviews 24 (4): 389-427, 2003

P-006

Optical imaging of oral squamous cell carcinoma and cervical lymph node metastasis using near-infrared fluorescent probes in a mouse model – a pilot study

Keereweer S. [1], Mol I. [2], Snoeks T. [2], Kerrebijn J. [1], Van Driel P. [2], Xie B. [2], Kaijzel E. [2], Baatenburg De Jong R. J. [1], Löwik C.W.G.M. [2].

[1] Erasmus Medical Center, Rotterdam, The Netherlands
[2] Leiden University Medical Center, The Netherlands

s.keereweer@erasmusmc.nl

Introduction: In head and neck cancer surgery, intra-operative assessment of the tumor-free margin is critical to completely remove the tumor, thereby improving the prognosis of the patient. Currently, this mostly relies on visual appearance and palpation of the tumor. However, optical imaging techniques provide real-time visualization of the tumor, warranting intra-operative, image-guided surgery. The use of the near-infrared (NIR) light spectrum offers two additional advantages: increased tissue penetration of light and an increased signal-to-background-ratio of contrast agents. We performed a pilot study to assess the possibilities of optical imaging of oral squamous cell carcinoma and cervical lymph node metastasis using near-infrared fluorescent probes in a mouse model.

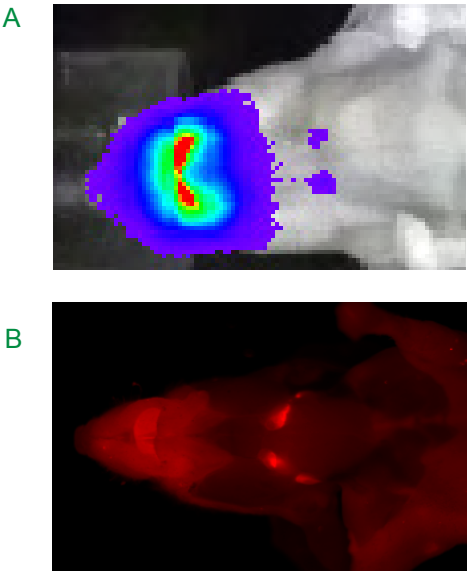

Fig1. A. Bioluminescence image of oral carcinoma and cervical lymph node metastasis. B. Fluorescence image showing increased signal of Prosense680TM in the tongue and cervical lymph nodes.

Methods: An oral tumor model was developed using luciferase-bearing OSC19 (human oral squamous cell carcinoma) cells that were injected directly into the tongue of 8 Balb/C nu/nu female mice. Tumor progression was followed by bioluminescence imaging (BLI) using the IVIS-100™ (Caliper LS) and by inspection of the tongue. At day 21, different NIR fluorescent probes were systemically injected, targeting cathepsins (Prosense680TM, VisEn Medical), matrix metalloproteinases (MMPsense 680TM, VisEn Medical), increased glucose uptake (800CW 2-DG™, LI-COR) and increased epidermal growth factor expression (800CW EGF™, LI-COR) of the tumor. Fluorescence imaging of the mouse and organs (after surgical removal) was performed using the Maestro™ (CRi) and Odyssey™ (LI-COR). A control group of 8 Balb/C nu/nu mice without tumor was used to compare light intensity between healthy and cancer tissue.

Results: After 7 days, oral squamous cell carcinoma was established in all 8 mice. After 11 days, all mice had developed cervical lymph node metastasis, which was confirmed by a BLI signal (figure 1,A). The primary tumor and cervical lymph node metastases were successfully detected by the use of all NIR fluorescent probes, with increased tumor-to-control ratios that varied per probe (figure 1,B).

Conclusions: This preliminary study shows the establishment of an oral squamous cell carcinoma mouse model, which progress could be followed by bioluminescence. Moreover, real-time visualization of the primary tumor and cervical lymph node metastases was achieved by fluorescence imaging using various NIR fluorescent probes. This technique can be used for intra-operative, image-guided surgery, which could improve complete removal of oral squamous cell carcinoma.

POSTER

MI in CANCER BIOLGY

P-007

Spectral unmixing of red and green luciferases for *in vivo* bioluminescence imaging

Mezzanotte L. [1], Kaijzel E. [2], Michelini E. [1], Que I. [2], Calotti F. [2], Hoeben R. [2], Roda A. [1], Löwik C. W.G.M. [2].

[1] University of Bologna, Bologna, Italy
[2] Leiden University Medical Center, Leiden, The Netherlands

laura.mezzanotte@libero.it

Introduction: Amongst the numerous luciferase reporter genes cloned from different animal species and mutated to achieve different emission properties only a few have been employed for in vivo bioluminescence imaging (BLI). Good thermostability, high and stable photon emission and codon optimization of the luciferase gene are required (1,2). Moreover, spectral overlap prevents them from being measured simultaneously. Recently, spectral unmixing methodologies have been employed to unmix and quantify signals from images obtained from the collection of light emitted from proteins with different emission spectra (3,4). Here we investigated the combined use of green click beetle luciferase (CBG99, max. emission 537nm) and a red codon-optimized mutant of P.pyralis (Ppy-RE8, max emission 618nm) for in vivo BLI purposes.

Methods: Both in vitro and in vivo studies were carried out to analyse the different luciferases. Lentiviruses expressing Red Ppy-RE8 and Green CBG99 luciferase reportergenes were generated and human embryonic kidney (Hek293) cells were subsequently transduced to express the different variants of luciferase. Cell population of red and green emitting were mixed in different proportions and BLI measurements were carried out in a plate luminometer with appropriate filters.

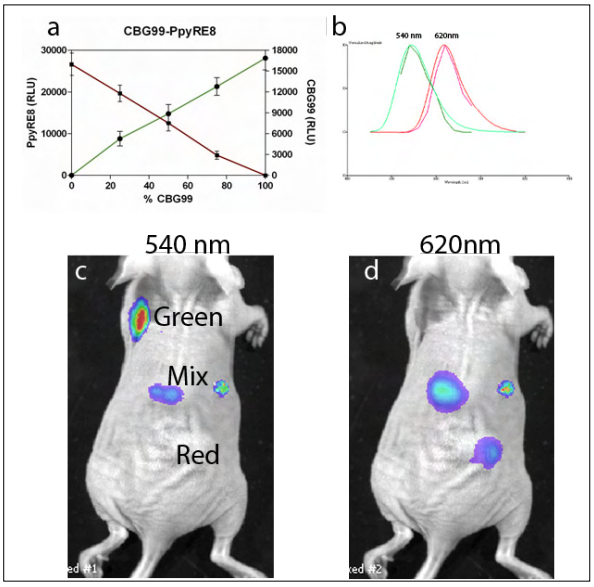

Fig1.: CBG99 and PpyRE8 expressing cells were mixed in different ratios and measured in vitro (a) and in vivo at 540nm (c) and 620nm (d).The graph (b) shows the max. emission peaks of the different luciferases.

In addition, Hek293 cells co-expressing the mentioned luciferases were imaged using the IVIS Spectrum system (Caliper LS) by collecting BLI signals at different wavelengths. Finally, the cells expressing Ppy-RE8 or Green CBG99 were injected subcutaneously into immunodeficient mice and BLI imaging was performed in vivo using the same system. Signals from the two luciferases were unmixed using Living Image 3.2 software.

Results: Both in vitro as in vivo results demonstrated the feasibility to use Red Ppy-RE8 and Green CBG99 luciferase reporter genes, simultaneously. These luciferase variants demonstrated to be a good couple for dual luciferase applications employing the same substrate luciferin. Using a pair of band pass filter (535nm and 628nm) contributions of red- and green-emitting luciferases can be calculated using a luminometer. Confirmative results were obtained using the Living image software to spectrally unmix the images composed by the signals of the two different luciferases and obtained from both in vitro and in vivo experiments.

Conclusions: The possibilities of a combined use of the selected red and green luciferases have been demonstrated. Preliminary in vivo data envisage the future application of these couple of luciferases for monitoring of multiple events simultaneously by means of bioluminescence imaging.

References:

Branchini BR et al. Anal Biochem. 2010 Jan 15;396(2):290-7.
Mezzanotte L, et al. Mol Imaging Biol. 2009,Nov 25.
Gammon ST, et al. Anal Chem. 2006 Mar 1;78(5):1520-7.
Michelini E, et al. Anal Chem. 2008 Jan 1;80(1):260-7.

High resolution redox imaging of intact cells by rxYFP, a ratiometric oxidation- sensitive fluorescent protein

P-008

Pani G. , Maulucci G. , Mele M. , Labate V. , Panieri E. , De Spirito M. .

Catholic University Medical School, Rome, Italy

gpani@rm.unicatt.it

Introduction: Plasmid encoded redox sensitive fluorescent probes promise to pave new avenues for realt time imaging of oxidative signaling in live cells. We have recently shown that rxYFP, a redox-sensitive variant of the Yellow Fluorescent Protein, can be used ratiometrically to construct high resolution redox maps of live cells. Confocal analysis of cell fluorescence at two excitation wavelenghts allows in fact to monitor, voxel by voxel, the distribution of the probe between its reduced and oxidised states, while normalizing fror probe concentration and photobleaching.

Methods: rxYFP was transiently transfected in 293T human kidney carcinoma and B16F10 murine melanoma cells plated on glass bottom dishes (IbiDi). Cell fluorescence was analysed by confocal microscopy at two different excitation wavelengths (450 and 488nm) and fluorescence ratios calculated by a dedicated software and converted into pseudocolors to construct redox-based cell maps.

Results: By imaging cells based on rxYFP distribution between reduced and oxidised states, we were able to confirm that, in human and murine malignant cells, the nucleus is significantly more reduced than the cytosol; additionally, simple deconvolution of redox images constructed with untargeted rxYFPallows to identify hypereduced perinuclear spots that correspond to mitochondria, as further confirmed by the use of a mitochondrially targeted form of the probe. In 2D scans, the cell border of adherent cells consistently appears to be significantly more oxidised than the inner cytosol, while 3D cell reconstruction oxidation is polarized towards the bottom of the cells; finally, in a spontaneously migrating cell the leading edge appears to me more oxidised than the trailing one.

Conclusions: This set of obserbations suggests, in keeping with our previous biochemical studies, that integrin signaling and cuytoskeleton rearrangement are associated with increased prooxidant activity, with relevant implications for cell invasion and metastasis.

Acknowledgement: Work partially supported by DiMI FP6 European NoE DiMI (LSHB-CT-2005-512146)

References:

1. Maulucci G, Labate V, Mele M, Panieri E, Arcovito G, Galeotti T, Østergaard H, Winther JR, De Spirito M and Pani G High resolution imaging of redox signaling in live cells through an oxidation-sensitive yellow fluorescent protein Sci. Signal. 1, pl3 (2008).
2. Maulucci G, Pani G, Labate V, Mele M, Panieri E, Papi M, Arcovito G, Galeotti T, De Spirito M. 2009 Investigation of the spatial distribution of glutathione redox-balance in live cells by using Fluorescence Ratio Imaging Microscopy. Biosens Bioelectron. 25:682-687.
3. Maulucci G, Pani G, Fusco S, Papi M, Arcovito G, Galeotti T, Fraziano M, De Spirito M. 2009 Compartmentalization of the redox environment in PC-12 neuronal cells. Eur Biophys J. in press
4. P. Chiarugi, G. Pani , E. Giannoni, L. Taddei, R. Colavitti, G. Raugei, M. Symons, S. Borrello, T. Galeotti, and G. Ramponi 2003 Reactive oxygen species as essential mediators of cell adhesion:The oxidative inhibition of a FAK tyrosine phosphatase is required for cell adhesion J. Cell. Biol. 161, 933-944

POSTER

MI in CANCER BIOLGY

P-009

Assessment of antiangiogenic therapy effects in preclinical tumour models: Implementation of a novel contrast - enhanced 3 D scanning technique and comparison to established ultrasound imaging protocols

Rix A. , Lederle W. , Bzyl J. , Gaetjens J. , Fokong S. , Grouls C. , Kiessling F. , Palmowski M. .

Helmholtz Institute for biomedical engineering , Aachen, Germany

arix@ukaachen.de

Introduction: Assessment of antiangiogenic therapy effects in rodent tumours plays an important role in drug development. Different ultrasound imaging protocols are described, predominantly using 2 D contrast-enhanced techniques. However, a limitation of 2 D scans is the reduced reproducibility of the data. Even if the acquired slice might be representative for the entire tumour, it will be impossible to find the identical slice position in longitudinal studies. In our study, we implemented a novel contrast-enhanced 3 D scanning technique, evaluated its sensitivity and compared it to established 2 D and 3 D ultrasound imaging protocols.

Methods: S.c epidermoid carcinoma xenografts in nude mice were scanned using a small animal ultrasound system (40 MHz). B-mode images with a low mechanical index and a slice thickness of 300 µm were acquired and merged into a 3 D dataset. Prior to administration of the contrast agent, only one image was acquired per slice. During stable blood levels of polybutylcyanoacrylate-microbubbles, 5 frames per slice were acquired (frame rate: 8 Hz). The maximum intensity of each voxel per slice was recorded and compared to the pre-contrast dataset. To compare the potential role of this technique, a non contrast-enhanced 3 D Power Doppler scan (HF-VPDU: High frequency - volumetric power Doppler ultrasound [1]) and a 2 D dynamic contrast-enhanced scan (analyzed using the MIOT post-processing technique [2]) were performed. The sensitivity of all methods for assessing the antiangiogenic effects of SU11248 were examined at day 0, 1, 2 and 4 after treatment start. Tumour vascularisation was validated by determining the vessel density on corresponding histological sections. Mann-Whitney test was used for statistical analysis.

Results: The novel 3 D contrast-enhanced imaging protocol could be applied to all animals successfully. The vascularisation of untreated control tumours slowly increased during the study, whereas a reduction was observed in tumours of treated animals. Differences in vascularisation between both groups were significant at day 1 ($p<0.05$) and highly significant at day 2 and 4 ($p<0.01$).Similar significant (day1) and highly significant (day2 and 4) differences in vascularisation between control and treated tumours were measured using the 2D MIOT technique, indicating its high accuracy. The sensitivity of the HF-VPDU was not high enough for assessing very early changes in vascularisation in response to the antiangiogenic therapy. Immunohistochemistry confirmed the findings of the 2 D and 3 D contrast-enhanced scans, showing a significantly reduced area of CD31 positive blood vessels in treated tumours ($p<0.01$).

Conclusions: The newly implemented 3 D scanning protocol allows a sensitive assessment of early antiangiogenic therapy effects. Surprisingly, a comparable sensitivity can be obtained using the 2 D MIOT technique. This may be explained by a homogenous vascularisation in the A431 tumours. The accuracy of a 2 D imaging technique might be lower in tumors with a more heterogenous vascularisation.

Acknowledgement: This work is supported by the German Federal Ministry of Education and Research (BMBF-0315017).

References:

1. Jugold M, et al. Volumetric high-frequency Doppler ultrasound enables the assessment of early antiangiogenic therapy effects on tumor xenografts in nude mice. European Radiology (2008) 18: 753-758
2. Palmowski M, et al. Comparison of conventional time-intensity curves versus maximum intensity over time for post processing of dynamic contrast-enhanced ultrasound. European Journal of Radiology (2009) Epub ahead of print

Influence of the BMP pathway on cell cycle regulation and its differentiation inducing potential on brain tumor initiating cells

P-010

Rudan D. [(1)], Monfared P. [(1)], Viel T. [(1)], Hadamitzky M. [(1)], Euskirchen P. [(1)], Knödgen E. [(1)],tSchneider G. [(1)], Jacobs A.H. [(1,2)].

[(1)] Max Planck Institute for Neurological Research, Cologne, Germany
[(2)] European Institute for Molecular Imaging, , Germany

daniel.rudan@nf.mpg.de

Introduction: Glioblastoma multiforme is the most common type of brain tumor, and several alterations of the cell cycle and DNA repair mechanisms have led to increasing resistance against chemotherapy. Latest findings suggest that a subset of tumor cells, the brain tumor initiating cells (BTIC) with stem cell like properties, are responsible for initiation and maintenance of the disease. Approximately 1-1000 out of 1.000.000 cells within a glioma is a BTIC. These cells are thought to bring about relapse and metastasis through their tumorigenic potential and chemotherapeutic resistance1,2. Design of a specific therapeutic strategy against BTICs may improve overall survival and quality of life for patients with gliomas. The aim is to examine a novel, experimental therapy against malignant gliomas by differentiating their BTIC population. Building on our previous work3, where we demonstrated that BMP-7 treatment decreases the proliferation of Gli36ΔEGFR-LITG glioma cells up to 50% via a cell cycle arrest in G1 phase, we will further characterize and compare the effect of the BMP-pathway on cell cycle regulation of different glioma cell lines and "glioma stem cells".

Methods: We want to determine (i) whether BMP treatment, alone or in combination with state-of-the-art chemotherapeutic agents, could be applied in a disease-tailored therapy against gliomas by depleting their BTIC pool and (ii) whether our reporter construct (LITG) can quantify the responses to such a treatment in culture and in vivo. Glioma cell lines, primary glioma cell cultures and BTICs with different genetic profiles are being utilized to analyze the influence of BMP-7 and BMP pathway inhibitors on cell cycle regulating protein expression, cell viability and caspase activation as well as its differentiation-induction potential in culture. BTIC will be transduced with lentiviral reporter vectors to image changes in cell cycle regulation, differentiation status and BMP pathway activity non-invasively in vivo upon treatment.

Results: Western blot data indicates that BMP-7 treatment causes an arrest in cell cycle progression in the established glioma cell line A172 by influencing the expression of the key cell cycle regulators (p53 , p21 E2F-1). Furthermore we have shown the differentiation-induction potential of BMP-7 on BTICs in culture optically and on the protein level. Upon BMP-7 treatment and respective growth-factor withdrawal the expression of the neural stem cell marker Mshi1 is clearly downregulated. Currently we focus on the design of a lentiviral reporter vector for imaging the observed BMP-Pathway reponses.

Conclusions: Antagonizing the proliferative potential of BTICs by targeting the BMP pathway, thereby triggering cellular differentiation of malignant stem cells, could provide a promising means of improving the prognosis for patients with gliomas.

Acknowledgement: This work is supported in part by the FP6 European NoE DiMI (LSHB-CT-2005-512146).

References:

1. Singh SK, Hawkins C,Clarke ID, Squire JA, Bayani J, Hide T, Henkelman RM, Cusimano MD, Dirks PB, Nature 432, 396 (2004)
2. Piccirillo SG, Reynolds BA, Zanetti N, Lamorte G, Binda E, Broggi G, Brem H, Olivi A, Dimeco F, Vescovi AL, Bone morphogenetic proteins inhibit the tumorigenic potential of human brain tumour-initiating cells, Nature 444, 761 (2006)
3. Klose A, Waerzeggers Y, Klein M, Monfared P, Vukicevic S, Kaijzel EL, Winkeler A, Löwik CW, Jacobs AH, Imaging bone morphogenetic protein induced cell cycle arrest in experimental gliomas, In Submission

POSTER

MI in CANCER BIOLGY

P-011

A near infrared fluorescent-based method for imaging breast cancer induced osteolysis

Snoeks T. , Que I. , Mol I. , Kaijzel E. , Löwik C.W.G.M. .

Leiden University Medical Center, The Netherlands

t.j.a.snoeks@lumc.nl

Introduction. In vivo bioluminescence imaging (BLI) of luciferase (Luc) expressing tumor cell lines has become a well accepted method to quantitatively follow tumor growth over time. Fluorescence imaging (FLI) can be used to visualize and quantify specific structures, molecules and even enzymatic activity using targeted dyes and enzyme activated smart probes. Two of such targeted fluorescent dyes are OsteoSense-680TM (VisEn Medical) and BoneTag-680TM (LI-COR Biosciences) both of which are directed specifically to bone.

Traditionally, osteolytic lesions and subsequent bone loss are quantified using x-ray radiographs and µ-CT scans. These procedures are often time consuming and both methods possibly irradiate the animal limiting the number of repeated measurements.

The aim of this study was to assess the possibility to quantify osteolysis by a loss of fluorescent signal after pre-labelling the skeleton with a bone-specific fluorescent probe. In this setup, we compared the performance of the two aforementioned commercially available bone specific fluorescent probes; OsteoSense-680TM and BoneTag-680TM.

Methods. Immunodeficient mice received an intra venous injection with either OsteoSense-680 (2 nmol, n=5) or BoneTag-680 (8 nmol, n=5). Three days after injection of the fluorescent probes the human breast cancer cell line MDA-BO2-Luc was inoculated in the femur bone marrow cavity of the right leg to form an osteolytic tumor. Tumor growth was followed by weekly BLI measurements using the IVIS Spectrum (Caliper LifeSciences) over a period of 6 weeks. Fluorescent data was obtained weekly using the IVIS Spectrum and at day 2, 8, 19 and 42 using the Pearl Imager (LI-COR Biosciences). In addition, µCT scans of each animal were made at day 21 and 42 using the SkyScan-1076 µCT (SKYSCAN).

Results. All inoculated mice developed a tumor in the right leg confirmed with BLI. Both bone specific probes remained detectable throughout the experiment, 45 days after injection, in the healthy leg. The fluorescence signal decreased faster in the tumor bearing legs than in the healthy legs, this loss of signal could be quantified (Fig 1). The analysis of the x-ray and µCT data and the subsequent correlation between oslteolytic lesion size and the loss of fluorescence signal is still ongoing.

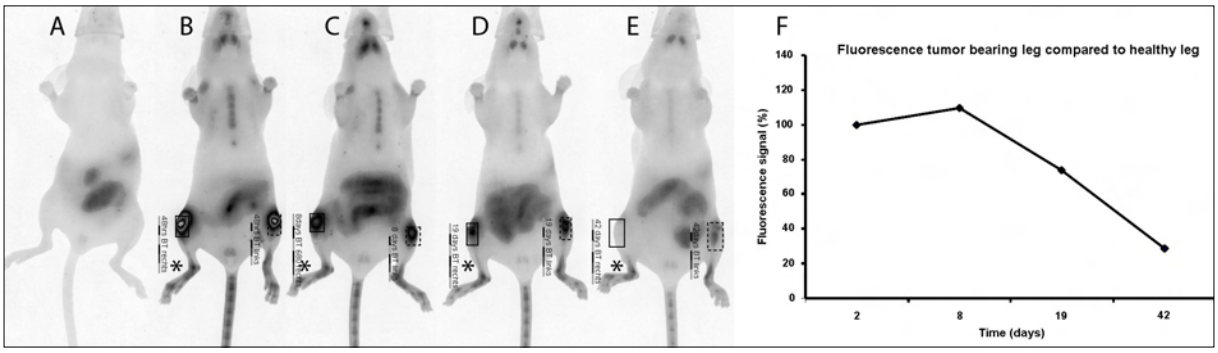

Fig1.: Decrease of fluorescence signal on osteolysis. Representative mouse labelled with BoneTag-680, imaged with the Pearl imager. A) Background FLI image before labelling with BoneTag-680. B-E) FLI images at day 2, 8, 19 and 42 after tumor cell inoculation in the right leg (*). F) Quantification of the fluorescent signal of the tumor bearing leg compared to the healthy leg.

Conclusions. Preliminary results show the possibility to follow osteolysis over time using an animal pre-labelled with a bone specific probe.

Acknowledgement: Supported by the Dutch Cancer Society (Grant UL2007-3801)

Near infrared fluorescent probes for whole body optical imaging of 4T1-luc2 mouse breast cancer development and metastasis

P-012

Xie B. , Snoeks T. , Mol I. , Van Driel P. , Keereweer S. , Kaijzel E. , Löwik C.W.G.M. .

Leiden University Medical Center , The Netherlands

b.xie@lumc.nl

Introduction: The rapid development of molecular imaging has improved early diagnosis and treatments for various diseases including cancer. The imaging modalities vary broadly in their sensitivitie, and the high sensitivity of optical imaging, especially near infrared fluorescent (NIRF) imaging, makes it an excellent experimental tool for imaging small animals like mice. NIRF light has advantages such as considerably low tissue absorption coefficient in the NIR region (700-900 nm) and low tissue autofluorescence so that deeper light penetration can be achieved. These advantages make NIR light ideal for whole body optical imaging. Furthermore, NIRF probes are becoming available for clinical applications, e.g. imaging-guided surgery. In the current work, we have implanted mouse mammary gland cancer cell line 4T1-luc2 in nude mice, and then assessed 2 commercially available NIRF probes in their ability and specificity of detecting tumor progression and metastasis by whole body FLI in comparison with BLI.

Methods: The following NIRF probes were tested and validated on detecting the mouse mammary gland cancer cell line 4T1-luc2 both *in vitro* and *in vivo*: Prosense680™(VisEn Medical) and 800CW 2-DG™(LI-COR Biosciences). *In vitro*, studies included cell-based fluorescent assay by Odyssey measurements, flow cytometry analysis, and visualization of probe uptake by confocal laser scan microscopy analysis. *In vivo,* 20.000 4T1-luc2 cells were implanted into the upper mammary fat pad (MFP) of immunodeficient mice. BLI was used as an internal control to evaluate the luciferase expression level in tumor areas, and also for co-locolization of the NIRF probes. After time-dependent BLI and FLI measurements, thoracic cavities of mice bearing tumors were surgically opened and reimaged to reveal the metastasis of surrounding tissues and axial lymph nodes (LNs). Organs were quickly removed, and *ex vivo* BLI and FLI were performed. Tissues with positive signals were further analyzed by histochemistry.

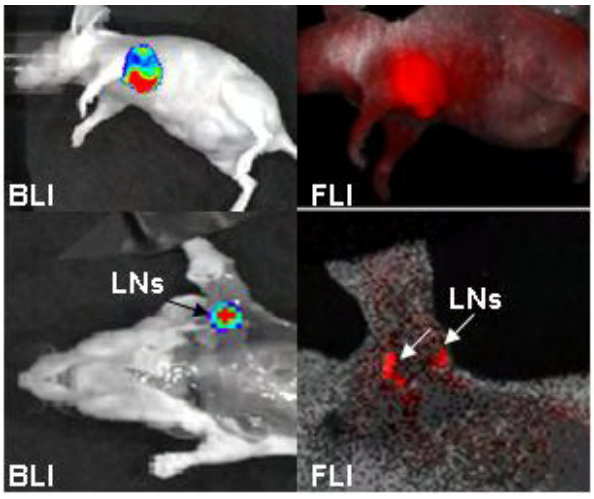

Figure: Upper panel shows BLI and FLI Prosense680TM imaging. Lower panel shows BLI and FLI Prosense680TM imaging of LNs.

Results: Both tested probes could successfully visualize 4T1-luc2 mouse breast cancer cells, both *in vitro* and *in vivo*. Our *in vivo* data showed that there was already a nice increase in the BLI signal 3 days after implanting 4T1-luc2 cells in the MFP of nude mice. We could also detect the tumor progression using the NIRF probes in intact animals. At the end of the experiment (18 days) the animals were surgically opened up, and we could clearly detect lung and axial LNs metastases, both by BLI and FLI. This was confirmed by *ex vivo* imaging and histochemistry.

Conclusions: This preliminary study of 4T1-luc2 mouse breast cancer indicates that the development and metastasis of cancer can not only be detected by BLI but also by FLI, using commercially available NIRF probes, especially after surgically opening up the animals. This should pave the way for real-time visualization of tumor tissues during operation, making radically removal of all tumor tissues and local metastases possible.

Acknowledgement: This study is supported by the Dutch CTMM Project MUSIS

P-013

Improved animal models to study tumor growth and spontaneous metastases: bioluminescence imaging characterization of the HT-29 human colorectal cancer cell line

Fernández Y. , Miranda S. , López M.E. , Suárez L. , Céspedes M.V. , Mangues R. , Herance J. R. , Rojas S. , Abasolo I. , Schwartz Jr S. .

CIBBIM-Nanomedicina. Edifici Hospital General. Bioquímica, Barcelona, Spain

yofernan@ir.vhebron.net

Introduction: The main problem in the treatment of colorectal cancer (CRC) is not so much the eradication of the primary tumor, but rather the formation of incurable metastases. To improve survival of these patients, there is an urgent need for new treatment strategies. For this purpose, the development of reliable, reproducible, clinically-relevant and inexpensive mouse models that fulfill tumor progression, invasion and metastasis of human CRC is needed. A new era of modeling cancer metastasis involves the use of optical imaging technologies to monitor tumor growth and colonization after introduction of cancer cells into the animals. The purpose of this study was to characterize the behavior of the human colon cancer cell line HT-29 in a subcutaneous, experimental metastases and orthotopic mouse models using non-invasive bioluminescence imaging (BLI) technologies, thereby providing an additional method to study CRC disease.

Methods: Luciferase expressing HT-29 cells were injected subcutaneously, into the left ventricle and orthotopically into the cecal wall of immunodeficient nude mice. The tumor growth and metastatic dissemination patterns were quantitatively and continuously followed up via BLI. Non-invasive monitoring of tumorigenicity and metastasis was also compared to the traditional assays of tumor volume, weight or histology. Ex vivo BLI and histological analyses were performed to further identify the exact nature and location of lesions. BLI results were also validated using the positron emission tomography (PET) imaging.

Results: We show that BLI has been successfully used to monitor colorectal tumor growth and metastases in vivo, and even helps to identify new metastatic sites. In the subcutaneous mouse model, BLI production and traditional tumor volume measurements show a strong correlation, demonstrating that BLI is an appropriate method to non-invasively quantify tumor burden. The left cardiac ventricle injection resulted in colonic tumor colonies in most organs, including the skeletal system of mice. In orthotopic implants, locoregional tumor growth and distant metastases occur spontaneously and rapidly, closely resembling clinical human disease progression that includes lymphatic, hematogenous and celomic dissemination. Ex vivo BLI confirmed the localization of metastases and dictated which tissues were going to be analyzed by histopathology reducing the number of histology rounds required to eventually detect all the small micrometastases identified by BLI.

Conclusions: Our findings show that BLI improves upon and refines traditional animal cancer models by using fewer animals, offering a rapid, sensitive and less invasive monitoring of early neoplastic growth and metastases. Moreover, it provides an accurate and temporal assessment in the same animal over time increasing the statistical power of the model. In conclusion, BLI is a powerful tool for high-throughput longitudinal monitoring of tumor load in small animals and allows the implementation of more advanced orthotopic tumor models in therapy intervention studies with almost the same simplicity as when measuring traditional ectopic models. The availability of these bioluminescent models are powerful and reliable tools with which to investigate metastatic human CRC and novel therapeutic strategies directed against it.

Acknowledgement: We are grateful to the Spanish Ministry of Science and Innovation for supporting laboratory technician and pre-doctoral personal, and CIBER-BBN for funding the project.

References:

1. Taketo, M. M. & Edelmann, W.; Gastroenterology 136, 780-98 (2009)
2. Cespedes, M. V.; et al. Am J Pathol 170, 1077-85 (2007)
3. Weissleder, R. & Pittet, M.; J. Nature 452, 580-9 (2008)
4. O'Neill, et al.; J Pathol 220, 317-327 (2009)

Development of dorsal skin-fold window chamber for the analysis of blood vessel modifications induced by electropermeabilization

P-014

Golzio M. [1], Bellard E. [1], Markelc B. [2], Cemazar M. [2], Sersa G. [2], Teissie J. [1].

[1] IPBS-CNRS, Toulouse, France
[2] Institute of Oncology, Slovenia

muriel.golzio@ipbs.fr

Introduction: Recent developments in intravital microscopy (IVM) enable studies of tumour angiogenesis and microenvironment at the cellular level after different therapies. Preparation of skin fold chamber enables to follow fluorescent events on live animal.

Electroporation/electropermeabilization, i.e. application of electric pulses to tissues, is a physical method for delivery of exogenous molecules. It is already used in clinical therapies of cancer, for electrochemotherapy of tumors (ECT). Its use was recently developed in electrogene therapy (EGT). *In vivo*, "electroporation" is associated with a blood -flow modifying effect resulting in decreased blood flow.

The aim of our study was to observe directly on the living animal the effects of "electropermeabilization" on subcutaneous normal blood vessels by monitoring changes in morphology (diameter) and dynamics (vasomotricity, permeability and recovery).

Methods: These parameters were measured using fluorescently labelled dextrans injected in the blood vessels observed via a dorsal skin fold window chamber, intravital digitized stereomicroscope, in vivo intravital biphoton microscopy and custom image analysis. A mathematical modelling gave access to the changes in permeability from the time lapse observation. Delivery of electric pulses was operated on the microscope stage directly on the animal under anaesthesia.

Results: It resulted in immediate constriction of blood vessels that was more pronounced for arterioles (up to ~65%) compared to venules (up to ~20%). A rapid increase in vascular permeability was present that gradually decreased to basal (control) levels at 1 h post-treatment. The decay of the high increase in vascular permeability was biphasic with an initial fast decrease, but was still present at 1h post-treatment. Furthermore, vasoconstriction of arterioles after "electropermeabilization" resulted in a "vascular lock" that remained for at least 6 minutes. This correlated approximately with the duration of decreased diameters of arterioles that lasted for 8 minutes.

Conclusions: the results of our study provided direct in vivo monitoring of a vascular effect of electric pulses on normal vessels. The observed increase in permeability of vessels associated with delayed perfusion induced by electric pulses explains the improved delivery of molecules into tissues induced by this method after systemic delivery.

Acknowledgement: CNRS, Region Midi Pyrenees, ARC, canceropole GSO, ANR "Cemirbio", Slovenian French Proteus

References:

1. Cemažar M, Golzio M, et al. Current Pharmaceutical Design 12: 3817-3825. (2006).
2. Marty M, et al. EJC 4(11): 3-13. (2006).
3. Sersa G, et al. Br J Cancer; 98: 388-398 (2008).
4. Golzio M., et al. Gene Therapy 11, S85-S91 (2004).

P-015

Characterization and evaluation of a tumor specific RGD optical probe for time-domain near-infrared fluorescence imaging

Mathejczyk J.E. [1], Resch-Genger U. [2], Pauli J. [2], Dullin C. [3], Napp J. [1], Tietze L. F. [4], Kessler H. [5], Alves F. [1].

[1] Max-Planck Institute for Experimental Medicine, Göttingen, Germany
[2] BAM Federal Institute for Materials Research and Testing, , Germany
[3] University Medical Center Göttingen, Germany
[4] University of Göttingen, Germany
[5] Technical University of Munich, Germany

jmathej@gwdg.de

Introduction: RGD peptides provide useful tools for specific targeting of tumors overexpressing $\alpha_v\beta_3$ integrins. We used a cyclic RGDfK peptide, coupled to the near-infrared fluorophore, Cy5.5, via an aminohexaonic spacer (RGD-Cy5.5) for functional imaging of $\alpha_v\beta_3$ integrins on tumors *in vivo*. To assess the suitability and the achievable sensitivity of RGD-Cy5.5 for tumor imaging we characterized the spectroscopic properties of the optical probe and applied time-domain near-infrared fluorescence (NIRF) imaging for noninvasive and specific tumor targeting *in vivo*.

Methods: Application-relevant properties like the fluorescence quantum yield, lifetime and the thermal stability of the cyclic RGDfK peptide coupled to Cy5.5 via an aminohexanoic acid spacer and its parent fluorophore, Cy5.5 were analyzed spectroscopically. For *in vivo* imaging, human $\alpha_v\beta_3$ integrin-expressing glioblastoma cells, U87MG, were subcutaneously implanted into nude mice. Imaging was performed using the time-domain fluorescence imager, Optix MX2 (ART, Montreal, Canada).

Results: RGD-Cy5.5 shows excellent spectroscopic properties making it a useful tool for *in vivo* NIRF imaging. Remarkable is the enhancement in fluorescence quantum yield of Cy5.5 in RGD-Cy5.5 increasing from 0.29 to 0.34. *In vivo*, the specificity of the RGD-Cy5.5-derived signals was confirmed by fluorescence lifetime measurements which were used to distinguish the probe signals from unspecific fluorescence. RGD-Cy5.5 binds selectively to glioblastoma with a maximum fluorescence intensity resulting 5 h after probe injection. The binding specificity was further confirmed by reduction of this fluorescence after application of an excess of unlabeled RGD peptides.

Conclusions: Knowledge of the spectroscopic properties of fluorescent conjugates represents an important prerequisite for the successful application and sensitive detection of fluorescent probes in vivo. With RGD-Cy5.5, we developed a strongly emissive and stable optical probe for targeting $\alpha_v\beta_3$ integrin receptors. Fluorescence lifetime measurements contributed to a further enhancement in detection sensitivity as compared to conventional steady state NIRF imaging in the intensity domain. Since the RGD probe contains an aminohexanoic acid spacer, that allows an easy and effective coupling with anti-cancer agents, this probe might be applied in oncology for therapeutic and diagnostic purposes.

^{18}F labeling of insulin via click chemistry

P-016

Paris J. , Mercier F. , Thonon D. , Kaisin G. , Lemaire C. , Goblet D. , Luxen A. .

University of Liege, Belgium

J.Paris@ulg.ac.be

Introduction: As a positron emission tomography probe, a new ^{18}F-bearing insulin derivative was prepared by an original labeling method. This tracer was required as a radiolabelled active principle model compound to perform biodistribution imaging studies of new pulmonary administrable formulations.

Methods: A 1,3-dipolar azide/alkyne cycloaddition (click chemistry) approach was developed for the mild and efficient linking of the radioactive probe onto insulin (Fig1).

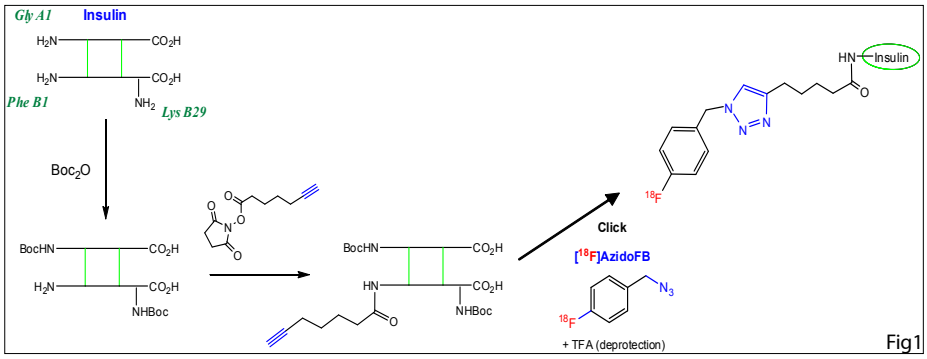

Fig1

As an initial step, native insulin had to be derivatized in order to present an accessible alkyne group at an appropriate position. For this, two of the three amino functions available on the molecule (Glycine A1 and Lysine B29) were first protected as N-Boc derivatives. An alkyne bearing prosthetic group could then be selectively grafted on the phenylanine B1 residue which does not interfere in the insulin-receptor binding process [1]. The final [^{18}F] fluorine insertion step was carried out by reacting this insulin derivative with the radioactive azide synthon 1-(azidomethyl)-4-[^{18}F]-fluorobenzene[2]under Cu(I) catalysis conditions.

Results: The clickable ^{18}F azide 1-(azidomethyl)-4--[^{18}F]-fluorobenzene was obtained in 65 minutes with good radiochemical yield (40-45% decay-corrected) and radiochemical purity (>90%) thanks to a fully automated preparation method developped on remote-controlled commercial radiosynthesis unit. Subsequent copper catalyzed click reaction on the alkyne bearing insulin derivative was performed at room temperature in less than 20 minutes with current radiochemical yields of 70-80% (decay-corrected).

Conclusions: A mild and efficient radiolabelling strategy of insulin was succesfully developped using click chemistry. This radiotracer can now be incorporated in new inhalable pharmaceutical formulations for biodistribution imaging studies.

Acknowledgement: NeoFor and Keymarker research platforms from the BioWin projects of the Walloon Region are acknowledged for their financial support.

References:

1. Guenther K.J. ; Yoganathan, S.; Garofalo, R.; Kawabata, T.; Strack, T.; Labiris, R.; Dolovich, M.; Chirakal, R. and Valliant, J.F., J.Med.Chem., 49: 1466-1474 (2006)
2. Thonon, D. ; Kech, C. ; Paris, J. ; Lemaire, C. and Luxen, A.; Bioconjugate Chem., 20(4):817-823, (2009)

POSTER

IMAGING in DRUG DEVELOPMENT

P-017

Whole-body distribution, pharmacokinetics and dosimetry of radioiodinated fully humanized anti-VAP-1 antibody – a PET imaging study of rabbits

Roivainen A. [1], Autio A. [2], Suilamo S. [2], Mali A. [2], Vainio J. [2], Saanijoki T. [2], Oikonen V. [2], Luoto P. [2], Teräs M. [2], Karhi T. [2], Vainio P. [2].

[1] Academy of Finland/University of Turku, Finland
[2] Turku PET Centre, Finland

anne.roivainen@utu.fi

Introduction: Vascular adhesion protein-1 (VAP-1) is an inflammation inducible endothelial glycoprotein [1]. It plays a key role in leukocyte trafficking and is a potential target for anti-inflammatory therapy. The antibody BTT-1023 is first-in-class, fully human monoclonal antibody to VAP-1. BTT-1023 is potentially useful for the treatment of inflammatory diseases and in vivo imaging of inflammation. Positron emission tomography (PET) is powerful, non-invasive method particularly suitable for drug development because of its high sensitivity and ability to provide quantitative and kinetic data without sacrificing the animal. We assessed the usefulness of PET in evaluation of iodine-124 labeled antibody pharmacokinetics and distribution in rabbits.

Methods: BTT-1023 was labeled with [^{124}I] using Chloramine-T method. Immunoreactivity of [^{124}I] BTT-1023 was verified in human VAP-1 transfected Chinese Hamster Ovary cells and by time-resolved immunofluorometric assay using human recombinant VAP-1. Ten rabbits were intravenously injected with [^{124}I]BTT-1023. PET/CT was obtained over the first 2 h after dosing and at 24, 48 and 72 h post-injection. Blood samples were collected during PET study to clarify in vivo stability and pharmacokinetics. As a final point, the human radiation dose estimates were extrapolated from rabbit information.

Results: Binding of [^{124}I]BTT-1023 to hVAP-1 transfected cells was app. 600-fold higher than in mock transfected controls. In rabbits, the radioactivity was distributed especially to liver and thyroid. Also heart and lungs showed some uptake whereas brain uptake was very low. Liver uptake is likely mediated, at least in a large part, by VAP-1, since the antigen is found on sinusoidal endothelia in the liver. Thyroid gland radioactivity is due to the de-iodination of [^{124}I] from the antibody. The plasma half-life of [^{124}I]BTT-1023 was 58.3 h and clearance 7.8 mL/h/kg. [^{124}I]BTT-1023 showed good *in vivo* stability (80% of signal from intact antibody at 72 h after injection). The estimated human radiation dose resulting from [^{124}I]BTT-1023 was 3.66 mSv/MBq. Provided that thyroid gland uptake is blocked, the effective dose in a human adult of about 70 kg would decrease to 0.55 mSv/MBq, which is equivalent to 21 mSv from 35 MBq and 30 mSv from 50 MBq of [^{124}I]BTT-1023 PET.

Conclusions: [^{124}I]BTT-1023 retained its biological activity to bind hVAP-1 also after radioiodination. This PET study of [^{124}I]-labeled VAP-1 targeting BTT-1023 antibody further elucidated whole-body distribution and pharmacokinetics of the therapeutical antibody, and supports clinical trials with [^{124}I] BTT-1023 at doses of 50 MBq or less.

Acknowledgement: The study was conducted within the Finnish CoE in Molecular Imaging in Cardiovascular and Metabolic Research supported by the Academy of Finland, University of Turku, Turku University Hospital and Åbo Akademi University. Anu Autio is a PhD student supported by Drug Discovery Graduate School.

References:

1. Salmi M, Jalkanen S. Science. 257:1407-1409 (1992)

Pharmacological characterization of iodine labeled adenosine kinase inhibitors

P-018

Sihver W. [1], Schulze A. [1], Kaufholz P. [1], Meyer A. [1], Grote M. [2].

[1] Research Center Jülich, Germany
[2] Hannover Medical School, Germany

w.sihver@fz-juelich.de

Introduction: The intracellular enzyme adenosine kinase (AK) catalyzes the phosphorylation of adenosine to adenosine monophosphate thus controlling the adenosine concentration. The inhibition of AK enhances the amount of adenosine, which is suggested to have neuroprotective, anticonvulsant, and antinociceptive effects [1,2]. Years ago, the non-nucleoside AK inhibitor ABT-702 has been investigated in vivo and in vitro [3,4]. In the present study the distribution of the radioiodine labeled adenosine kinase inhibitors [^{131}I]iodotubercidine ([^{131}I]IT) and [^{131}I] ABT-702 as well as the pharmacological behaviour of other known AK inhibitors (e.g. A134974) versus [^{131}I]IT was compared in rat brain. Furthermore the AK inhibiting strength of other halogenated ABT-702 derivatives was determined.

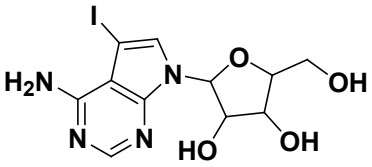

5-Iodotubercidine (IT)

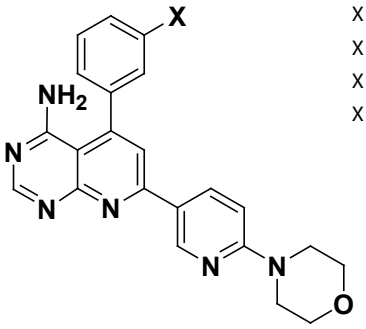

X = Br: ABT-702
X = I: I-ABT-701
X = Cl: Cl-ABT-702
X = F: F-ABT-702

Methods: The syntheses of [^{131}I]IT and [^{131}I]ABT-702, as well as the different halogenated ABT-702 derivatives were performed in house. Autoradiography was conducted using frozen rat brain sections. Binding competition was done with IT and ABT-702 vs. [^{131}I] IT. AK inhibition assays were performed with [^{3}H] adenosine and ATP using pig hippocampus cytosol.

Results: Autoradiography showed generally high binding all over the brain, but more distinct in the hippocampus, outer layers of the cortex, and gray matter of cerebellum using [^{131}I]IT (10nM) compared to [^{131}I]ABT-702 (7 nM). [^{131}I]IT Binding could be blocked more than 90% with 5-IT and A134974, about 70% with tubercidine and 60% with ABT-702. [^{131}I]ABT-702 Binding could be blocked not even 50 % with ABT-702, and even less with the other AK inhibitors. K_is of IT and ABT-702 were 20 nM and 850 nM, respectively, in rat hippocampus vs. [^{131}I]IT.

In the AK assays, A134974 and IT had the highest AK inhibition strength in hippocampal cytosol, followed by ABT-702 > I- ABT-702 > Cl- ABT-702 > F- ABT-702 with 78%, 62%, 42%, 30% and 21% inhibition, respectively.

Conclusions: As a result of this study it is suggested that [^{131}I]IT and [^{131}I]ABT-702 binding represent AK distribution in rat brain. [^{131}I]IT appears to be the preferred ligand for in vitro binding compared to [^{131}I]ABT-702. ABT-702 Has recently shown beneficial therapeutic potential [3, 5], but radioiodo-ABT-702 seems to be unsuited as radiotracer.

The AK inhibition strength was high both for IT and ABT-702, but low for the halogenated ABT-702 derivatives. Since IT shows good in vitro behaviour as a radioligand as well as AK inhibitor, further experiments with [^{131}I]IT in vivo might be interesting.

References:

1. Kowaluk EA et al.; Expert Opin Investig Drugs.9:551-64 (2000)
2. Boison D; Drug News Perspect. 20:607-11 (2007)
3. Jarvis MF et al.; J Pharmacol Exp Ther. 295:1156-64 (2000)
4. Kowaluk EA et al.; J Pharmacol Exp Ther. 295:1165-74 (2000)
5. McGaraughty S et al.; Curr Top Med Chem. 5:43-58 (2005)

POSTER

IMAGING in DRUG DEVELOPMENT

P-019

Determining the nasal residence time of protein-polymer conjugates for nasal vaccination using a novel imaging technique

Slütter B. [1], Que I. [2], Soema P. [1], Hennink W. [3], Kaijzel E. [2], Löwik C.W.G.M. [2], Jiskoot W. [1].

[1] Amsterdam Center for Drug Research (LACDR), The Netherlands
[2] Leiden University Medical Center, The Netherlands
[3] Utrecht Institute for Pharmaceutical Sciences (UIPS), The Netherlands

bslutter@lacdr.leidenuniv.nl

Introduction: Nasal administration of vaccines holds great promise as a painless alternative for the use of needles. Nonetheless, only one nasal vaccine is currently on the market (Flumist®). A major hurdle for successful nasal vaccination is the relatively short residence time of the vaccine in the nasal cavity, which hampers efficient uptake of the antigen through the nasal epithelium. Increasing the nasal residence time of the antigen is therefore an interesting approach to improve the efficacy of nasal vaccines. Here we investigated the possibility of extending the nasal residence time of a small antigen (ovalbumin, OVA) with a mucoadhesive polymer, trimethyl chitosan (TMC), using a novel live imaging technique1.

Methods: A near-IR fluorescent probe (IR dye CW800) was covalently linked to OVA. TMC was either mixed with or conjugated to OVA using the SPDP method2. After nasal administration of the antigen to hairless mice, the fluorescence intensity in the nasal cavity was assessed using an IVIS Spectrum® and followed in time (Fig1).

Results: We observed an exponential decay of fluorescence intensity after administration of OVA alone, whereas after co-administration of OVA with TMC or TMC-OVA conjugate fluorescence decay was delayed substantially.

Conclusions: Using a live imaging technique we successfully studied the nasal residence time of a model subunit antigen. TMC prolongs the nasal residence time of OVA, either by mixing it with or conjugating it to the antigen.

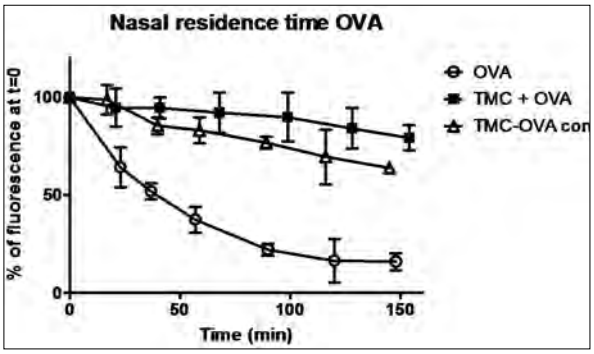

Fig1: Nasal residence time of OVA determined using fluorescent detection of OVA-IRdye CW 800. Intensity of fluorescence signal from the nasal cavity was measured in time and normalized for time point 0. n=3+/- SEM.

References:

1. Hagenaars et al. Role of trimethylated chitosan (TMC) in nasal residence time, local distribution and toxicity of an intranasal influenza vaccine. J Control Release. 2010, in press.
2. Slütter et al. Conjugation of ovalbumin to trimethyl chitosan improves immunogenicity of the antigen. J Control Release. 2010, in press.

Nanotubes as mutli-modality vehicles for imaging and therapy of cancer

P-020

Tworowska I. [1], Mackeyev Y. [2], Sims-Mourtada J. [1], Wilson L. J. [2].

[1] RadioMedix, Houston, USA
[2] Rice University, Houston, USA

itworowska@radiomedix.com

Introduction: There is a growing interest in development of new radiolabeled nanocarriers for targeted delivery of isotopes. Nanotubes have been actively explored as new systems for delivery of anticancer drugs [1], fluorescent probes [2], genes [3], and peptides [4] to the target tissues. Previously reported synthesis of Gd-loaded US-tubes [5] and I_2-modified US-tubes [6] have opened new possibilities in designing of contracts agents for MRI and CT. Here, we report on the synthesis of radiolabeled SWNT that can serve as vehicles for PET/SPECT imaging and cancer therapy.

Methods: HiPco single-wall nanotubes (SWNTs) were chemically cut into US-tubes, using the established procedure [7], sonicated at RT in 0.5M HNO_3 for 30min-2h. US-tubes were loaded with radioisotopes: $^{177}LuCl_3$, $^{99m}TcCl_3$, $^{68}GaCl_3$, and cold Re compounds ($ReCl_5$, NH_4ReO_4, $[NBu_4]^+ReClO_4^-$) manually or using automated module for labelling, SmarTrace™. The radiochemical yield was determined by radio-TLC and ICP-OES (Inductively coupled plasma optical emission spectrometry). Stability tests of labelled US-tubes were performed at RT for 1- 24h using 1M PBS, 0.1% FBS and transchelator (0.1M EDTA) to determine the desorption half-life of the labelled US-tubes.

Results: Loading of US-tubes with ^{68}Ga was performed in 0.5M NH_4OAc buffer at 90°C for 10 min using $^{68}GaCl_3$ eluted from $^{68}Ge/^{68}Ga$ generator (iThemba). Yield of the synthesis was found to be pH dependent with over 70% loading at pH=3.6- 4.1 and to decrease drastically to 1% at pH<1.7.

Optimum ^{99m}Tc labelling of US-tubes proceeded in the presence of $SnCl_2$ (reducing agent) in 0.5M NH_4OAc buffer with final yield >51%. Yield of the reaction decreased to 1% in the absence of $SnCl_2$, or when reduction proceeded after completion of labelling.

Best ^{177}Lu loading of US-tubes was performed in 0.1 M NH_4OAc at pH=5.1 at 90°C for 20 min. The final yield of this synthesis was found to be >55% after repeated dialysis with 0.1M EDTA, pH=4.7.

Loading of US-tubes with cold $ReCl_5$ proceeded in 0.6M NaOH at 90°C for 1h with final yield > 20%. Application of other Re compounds ($[NBu_4]^+ReClO_4^-$ and NH_4ReO_4) for modification of nanotubes gave products with yield higher than 17% and approximately 0.4%, respectively.

Conclusions: Our preliminary studies have shown that loading of US-tubes with imaging and therapeutic isotopes is feasible. Application of nanotubes in nuclear medicine may expand possibilities for development of new multi-modality agents for early detection and therapy of cancer.

References:

1. Tripisciano C., Kraemer K., Taylor A., Borowiak-Palen E., Chem. Phys. Lett., 2009, 478, 200-205
2. Wong Shi Kam N., Liu Z., Dai H., Angew. Chem. Int. Ed., 2006,45, 577-581
3. Ramathan T, Fisher F.T., Ruoff R.S., Brinson L.C., Chem. Mater., 2005, 17, 1290-1295
4. Kam N.W., Dai H., J. Am. Chem. Soc., 2005, 102, 6021-6026
5. Mackeyev Y., Hartman K.B, Ananta J.S., Lee A.V., Wilson L.J., J. Am. Chem. Soc., 2009; 131(24): 8342–8343
6. Ashcroft J.M, Hartman K.B., Kissel K.R., Mackeyev Y., Pheasant S., Young S., Van der Heide P.A., Mikos A., Wilson L.J., Advanced Materials, 2007, 19, 573-576
7. Mickelson E.T., Huffman C.B., Rinzler A.G., Smalley R.E., Hauge R.E., Margrave J.L., Chem Phys Lett, 1998, 296, 188-194.

POSTER

IMAGING in DRUG DEVELOPMENT

P-021

Early assessment of temozolomide treatment efficacy in glioblastoma using [^{18}F]FLT PET imaging

Viel T. [(1)], Backes H. [(1)], Hadamitzky M. [(1)], Monfared P. [(1)], Rapic S. [(1)], Rudan D. [(1)], Schneider G. [(1)], Neumaier B. [(1)], Jacobs A.H. [(1,2)].

[(1)] MPI for Neurological Research, Köln, Germany
[(1,2)] European Institute for Molecular Imaging – EIMI, University Muenster, Germany

thomas.viel@nf.mpg.de

Introduction: Temozolomide chemotherapy to radiation therapy is now the standard therapy for glioblastomas[1]. However there is considerable uncertainty with regard to the indication for and the chances of success of chemotherapy in affected patients. Standard Temozolomide treatment in clinic consists of 5 days treatment with 150-200 mg/m2 per day, repeated every 28 days. Treatment efficacy assessment is performed using MRI Imaging before treatment and after 3 cycles of treatment (meaning after 3 months). Due to the rapid evolution of the disease (median survival of patient bearing glioblastoma is around 15 months), methods to assess TMZ efficacy early during treatment is needed. In several clinical studies [^{18}F]FLT PET imaging has been validated to assess proliferation of different types of tumors in vivo[2], and could therefore be of interest for evaluation of TMZ during treatment of glioblastoma.

The purpose of this study was to monitor the metabolic effects of temozolomide (TMZ) chemotherapy in malignant gliomas by means of repeated Positron Emission Tomography (PET) with [^{18}F]FLT.

Methods: A glioma cell line, displaying a low resistance to TMZ (Gli36) was treated with two low doses of TMZ (25 and 50 µM). Two stable cell lines were obtained and characterized regarding their resistance to TMZ by growth and clonogenic assay. Resistant and sensitive cells were xenografted into nude mice. Mice were treated during five days with daily intra-peritoneal injection of 50 mg/kg of TMZ. Efficacy of TMZ treatment is followed using FLT imaging, before treatment as well as two and seven days after beginning of treatment.

Results: Two stable cell lines resistant to TMZ were established (Gli36-25TMZ and Gli36-50TMZ). The EC50 for the induction of cytotoxicity cell death (as determined by growth assay) were 10 µM (Gli36), 110 µM (Gli36-25TMZ) and 460 µM (Gli36-50TMZ). The EC50 for the prevention of clonogenic growth (as determined by clonogenic assay) were 10 µM (Gli36), 50 µM (Gli36-25TMZ) and 325 µM (Gli36-50TMZ). *In vivo*, the TMZ treatment induced a strong reduction of Gli36 tumor volume, while Gli36-50TMZ continued to grow. Correlation between diminution of SUV in the tumor after two days of treatment (with regards to SUV before treatment) and diminution of tumor size seems to be observed so far (n=3 for each tumor type).

Conclusions: Our results so far indicate that [^{18}F]FLT PET scan could be appropriate for an early evaluation of the response of Glioblastoma to TMZ chemotherapy.

Acknowledgement: This work is supported in part by DiMI (LSHB-CT-2005-512146).

References:

1. Norden AD, Drappatz J, et al; Lancet Neurol. 7(12):1152-60 (2008).
2. Ullrich RT, Zander T, et al; PLoS One. 3(12):e3908 (2008).

Sensitive time-gated FRET microscopy of G-Protein coupled receptors using suicide enzymes, lanthanide cryptates and fluorescent ligands

P-022

Zwier J. [1], Laget M. [1], Cottet M. [2], Durroux T. [2], Mathis G. [1], Trinquet E. [1].

[1] Cisbio Bioassays, Bagnols sur Cèze, France
[2] Insitut de Génomique fonctionelle, France

jzwier@cisbio.com

Introduction: Donor crosstalk and non-specific fluorescence in classical biological FRET experiments using fluorescent proteins remains a major concern in high content screening. Using a time-gated microscope equipped with an intensified CCD camera [1], lanthanide cryptates and fluorescent-ligands it is possible to visualize G-protein coupled receptors (GPCR) labeled with the SNAP-tag® suicide enzyme at the cell membrane. Oligomerization of GPCR's can be studied using time gated FRET without significant background. Using fluorescent ligands, binding and receptor trafficking can be imaged without ratiometric treatment of data.

Methods: A bright terbium-cryptate (lumi4®-Tb) coupled to 0^6-Benzylguanine is used to covalently label GPCR's tagged with the SNAP-tag suicide enzyme developed by the laboratory of Kai Johnsson [2]. The luminescence of this lanthanide compound, which has a lifetime of about 2 ms, can be time-gated in such a way that all background fluorescence from the cells has decayed and only specific lanthanide or sensitized acceptor emission to either red or green emitting dyes can be detected. An in-house developed microscope equipped with an intensified CCD camera can monitor this luminescence. HEK/COS/CHO cells were either stably or transiently transfected with plasmids containing the SNAP-tagged GPCR under study and labeled with the benzylguanines of choice after which they are fixed.

Results: Due to the significant Förster radius of 58 A of the lumi4-Tb/red donor-acceptor couple, homodimerization of a GPCR can be monitored using a mix of the Tag-lite® reagent SNAP-Lumi4-Tb and SNAP-red wich results in a bright time gated sensitized emission image at 665 nm. These results confim the results obtained by dimerization assays [3] in standard plate readers.

Due to the advantages of this technique it is also possible to visualize specific labeling of fluorescent ligands on the GPCR of interest. Using fluorescent ligands without the use of time gating gives significant contributions of non-specific binding. Since sensitized emission only occurs when donor and acceptor are in close proximity ligand receptor interactions were monitored for several GPCR's-ligand couples including chemokine receptors.

Conclusions: Time gated microscopy with terbium-cryptate is a convenient and novel way to avoid non-specific emission signals and to monitor FRET intensities showing genuine interactions between proteins and their ligands. This might become a powerful method to develop high content assays for drug evaluation.

Acknowledgement: Tag-lite is a registered trademark of Cisbio bioassays. Lumi4 is a registered trademark of Lumiphore Inc. SNAP-tag is a registered trademark of New England Biolabs.

References:

1. Ghose S et al, J. Alloys and cmpds 451:35-37 (2008)
2. Keppler A et al, Nature Biotechnology 21:86-89 (2003)
3. Maurel D, Comps-Agrar L et al, Nature Methods 5:561-567 (2008)

POSTER

IMAGING in DRUG DEVELOPMENT

P-023

Selection of a nanobody scaffold with low renal retention

D'huyvetter M. , Vaneycken I. , Tchouate Gainkam O. , Hernot S. , Caveliers V. , Xavier C. , Devoogdt N. , Lahoutte T. .

Vrije Universiteit Brussel, Jette, Belgium

mdhuyvet@vub.ac.be

Introduction: Nanobodies are small (15kDa) antibody fragments, derived from heavy chain-only antibodies present in Camelidae. The structure consists of a scaffold and three CDR loops. The CDR loops determine the specificity of the nanobody. Nanobodies, labelled with a therapeutic radionuclide, could be used for the treatment of cancer. Unfortunately, the in vivo biodistribution shows high renal retention of radio-labeled nanobodies in the kidney cortex and this could result in an important kidney toxicity. However, during the in vivo screening of a large set of nanobodies we noticed that there is a wide variety in this kidney retention. This variability could be partially related to the amino acid sequence of the nanobody scaffold. In this study we aim to identify the nanobody scaffold with the lowest renal retention.

Methods: The renal retention of 8 Nanobodies was evaluated in healthy Wistar rats. 99mTc labeling was performed using 99mTc-tricarbonyl (Isolink, Covedien). Dynamic planar imaging with a gamma camera was performed immediately after injection (100 frames of 30s). Three hours post injection an additional static image was acquired. Time activity curves of the kidney were generated using AMIDE.

Results: We measured two distinct kinetic profiles: one showing a steadily increase in function of time and the other showing an initial peak (5 min p.i.) followed by a decrease. The highest renal activity measured at 1h p.i. was 46.8 % IA (range 41.6-53.3 %IA), while the lowest was 11.3 % IA (range 10.1-13.2 %IA). At 3h p.i. we measured upto 69.3 %IA in the kidney for the group with a steadily increasing profile, while for the other group it remained low at 14.8 %IA.

Conclusions: We identified a scaffold with low renal retention. The use of this scaffold for nanobody based targeted radionuclide therapy could significantly reduce kidney toxicity.

Acknowledgement: The research at ICMI is funded by the Interuniversity Attraction Poles Program – Belgian State – Belgian Science Policy. Matthias D'huyvetter is funded by SCK-CEN/VUB.

In vitro assessment of androgen mediated uptake of ^{18}F-FDG, ^{11}C-choline and ^{11}C-acetate in prostate cancer

P-024

Emonds K. [1], Swinnen J. [1], Van Weerden W. [2], Nuyts J. [1], Mortelmans L. [1], Mottaghy F. [3].

[1] KULeuven, Belgium
[2] Josephine Nefkens Institute, The Netherlands
[3] University Hospital Aachen, Germany

Kimy.Emonds@med.kuleuven.be

Introduction: Androgen deprivation is one of the first line palliative treatment approaches in recurrent prostate cancer. Although ^{18}F-FDG is mostly applied in oncological PET imaging, a low diagnostic performance has been shown for prostate cancer detection. Otherwise, both ^{11}C-choline and ^{11}C-acetate offer a higher diagnostic efficiency for PET detection of relapsing patients. With this study we aimed to evaluate the androgen dependency of the uptake of metabolic PET tracers (^{18}F-FDG, ^{11}C-choline and ^{11}C-acetate) in five different human prostate cancer cell lines, distinctive considering their androgen responsiveness, in order to define the most reliable tracer for treatment response assessment.

Methods: Cell uptake experiments were performed with the prostate cancer cell lines LNCaP, PC346C, 22Rv1, PC346DCC and PC3, and the benign prostatic hyperplasia cell line BPH-1. Prior to the uptake experiments, cells were cultured in the presence of charcoal treated serum (native). In parallel cell cultures 10^{-8}M R1881, 10^{-10}M R1881, 10^{-6}M bicalutamide or the combination of 10^{-10}M R1881 and 10^{-6}M bicalutamide was added to the medium. The significant influence of androgens on the uptake of ^{18}F-FDG, ^{11}C-choline and ^{11}C-acetate in each prostate cancer cell line was evaluated using ANOVA and Tukey-HSD post-hoc analysis. The relative tracer uptake was evaluated in all prostate cancer cell lines with respect to the tracer uptake in BPH-1.

Results: A significant increased ^{11}C-choline uptake is observed in the androgen responsive and unresponsive cell line, respectively PC346C and 22Rv1, grown in the presence of androgens (10^{-8}M R1881). The same androgen concentration also caused a significant increase in ^{18}F-FDG uptake in LNCaP (androgen dependent) and 22Rv1. In both androgen unresponsive cell lines (PC3, PC346DCC) androgens did not significantly affect the uptake of these metabolic PET tracers. Unlike ^{11}C-choline and ^{18}F-FDG, ^{11}C-acetate uptake was not influenced by androgen supplementation in any prostate cancer cell line.

Compared to the tracer uptake in BPH-1, all prostate cancer cell lines showed a significant higher ^{11}C-acetate and ^{11}C-choline uptake. In contrast, a relative increased ^{18}F-FDG uptake was only observed in PC346C and -DCC.

Conclusions: ^{11}C-acetate uptake is androgen independent in every prostate cancer cell line, whereas a significant higher ^{11}C-choline and ^{18}F-FDG uptake was established by androgens in respectively two (PC346C, 22Rv1) and three (LNCaP, PC346C, 22Rv1) human prostate cancer cell lines. Also, ^{11}C-acetate has the most clearly elevated uptake in all prostate cancer cell lines with respect to the benign prostatic hyperplasia cell line.

The absent influence of androgens on ^{11}C-acetate uptake and the better differentiation of cancer from benign prostatic hyperplasia with this PET tracer compared to ^{11}C-choline and ^{18}F-FDG, suggests a higher efficiency of ^{11}C-acetate PET for evaluation of treatment response.

POSTER

CANCER from BENCH to BEDSIDE

P-025

Comparison of two ^{68}Gallium-labeled octreotide analogues for molecular PET(CT) imaging of neuroendocrine tumours

Garcia C. , Woff E. , Muylle K. , Ghanem G. , Van der Linden B. , Vandormael S. , Rutten E. , Flamen P. .

Institut Jules Bordet. Université Libre de Bruxelles, Brussels, Belgium

camilo.garcia@bordet.be

Introduction: PET(CT) using ^{68}Ga-labeled octreotide analogues is able to show the expression of somatostatin receptors (SSR) on gastroenteropancreatic neuro-endocrine tumours (GEP NET). The study aim was to compare the biodistribution and the tumour uptake intensity of two radiolabeled octreotide analogues, ^{68}Ga-DOTA-TOC ([DOTA-DPhe1,Tyr3]-octreotide) and ^{68}Ga-DOTA-TATE ([DOTA-DPhe1,Tyr3]-octreotate).

Methods: Octreo-PET(CT) was performed on 58 patients: 29 patients using 68Ga-DOTA-TOC and 29 patients using ^{68}Ga-DOTA-TATE. Standard Uptake Values (SUV) was measured in normal organs and in the lesions (SUVmax). Patient preparation, acquisition and image processing was standardized and identical in both subgroups. None of the patients had received any peptide therapy or radiolabeled peptide therapy before the study. The time delay between tracer injection and PET(CT) acquisition for respectively DOTA-TOC vs. DOTA-TATE patients was 95 min ± 0.01 vs. 100 min ± 0.01 (p=NS); the mean injected tracer activity was 90.28 MBq ± 46.62 vs. 88.8 MBq ± 21.09 (2.44 mCi ± 1.26 vs. 2.40 mCi ± 0.57) (p=NS), and BMI 25.7 ± 3.71 vs. 25.2 ± 3.6 (p=NS).

Results: PET(CT) identified 107 tumor lesions: 52 (49%) in the DOTA-TOC, and 55 lesions (51%) in the DOTA-TATE group. No significant differences of SUV(max) values were found in GEP NET lesions between DOTA-TATE and DOTA-TOC groups. Physiologic uptake in organs did not significantly differ between the 2 radiopharmaceuticals, except for the uptake of ^{68}Ga DOTA-TOC which was significantly lower in the head of pancreas than the uptake of ^{68}Ga DOTA-TATE (3.4 ± 1.5 vs. 4.6 ± 1.6) (P<0,05). On the other hand, ^{68}Ga DOTA-TOC was significantly higher in prostate (4.6 ± 1.7 vs. 3.4 ± 1.0) and in blood pool (1.7 ± 0.6 vs. 1.5 ± 0.3) (P<0,05).

Conclusions: ^{68}Ga-DOTA-TOC and ^{68}Ga-DOTA-TATE show similar tumour uptake intensities in GEP NET lesions. ^{68}Ga-DOTA-TOC seems to have lower physiologic uptake in the head of the pancreas and higher in the prostate.

References:

1. Kumar U et al. Diabetes. 1999 Jan;48(1):77-85.
2. Reubi JC et al. Ann N Y Acad Sci 1994;733:122–37.
3. Reubi JC et al. Metabolism. 1990;30(suppl 2):78–81.
4. Reubi, JC.et al J. Clin. Endocrinol. & Metab. 65:1127-1134.
5. Reubi JC, et al Eur J Nucl Med 30:781–793
6. Hofmann M et al Eur J Nucl Med 2001; 28:1751–1757.
7. Maecke H et al J Nucl Med 2005;46:172S–8S.

Real time per operative optical imaging for the improvement of tumour surgery in an *in vivo* micro-metastases model

P-026

Keramidas M. , Josserand V. , Righini C. , Coll J. L.

INSERM U823, Grenoble, France

michelle.keramidas@ujf-grenoble.fr

Introduction: In a wide range of cancer cases, surgery is the first therapeutic indication before radiotherapy and chemotherapy. In that way the prognostic strongly depends on the tumour removal exhaustiveness and in particular on metastases elimination.

We developed a couple near-infrared fluorescent tracer / per operative detection system in order to improve tumour surgery efficacy.

RAFT-c(RGD)4-Alexa 700 (Angiostamp®, Fluoptics) specifically bind to integrin αvß3, a receptor strongly expressed in angiogenesis and in many tumour types. The per-operative detection system (Fluobeam 700, Fluoptics) is a portative 2D fluorescent imager that can be used in white light environment and so, could be used directly during surgery to help the surgeon for tumour and metastases excision.

We already demonstrated in animal models the very significant improvement in primary tumours resection: higher number of tumour nodules removed, sane margins on the removed fragments and surgery time divided by 2 (Keramidas M., British Journal of Surgery 2010).

In the clinical situation, recurrence of cancer by metastases invasion after primary tumour surgery is a critical point. The aim of the present study is to evaluate the metastases resection impact on the survey. In order to proceed we first need to establish a suitable animal model of micro-metastases following primary tumour surgery. After calibration of the metastatic in vivo model, we will evaluate the survey of the twice-operated animals (metastases resection after primary tumour removal) versus the once-operated animals (only primary tumour removal).

Methods: Luciferase positive tumour cells (TS/Apc-luc) are injected in the kidney capsule of nude mice and the primary tumour growth is followed by in vivo bioluminescence imaging. 7 days after tumour cells implantation, the tumoral kidney is removed and the metastases development is followed by in vivo bioluminescence imaging. Then RAFT-c(RGD)4-Alexa 700 is injected intravenously and twenty-four hours later the portative fluorescence detection system is used to assist the metastases excision. The possible recurrence of cancer is followed by in vivo bioluminescence imaging. Mice are sacrificed when they loose 10% of their weight. The mice survey is compared with the one of two control groups: in one group the mice don't undergo the second surgery for metastases resection, and in a second group the mice don't undergo any surgery and keep the primary kidney tumour.

Results: Micro-metastases appear about 7 days after the primary tumour removal and soar up to 20 days after the first surgery. The metastases removal assisted by the RAFT-c(RGD)4-Alexa 700 and the per operative fluorescence detection system significantly improved the mice survey (36 days).

Conclusions: We developed an in vivo model of micro-metastases invasion following primary tumour surgery which is very relevant regarding to the clinical situation of head and neck or prostate cancer. The use of RAFT-c(RGD)4-Alexa 700 coupled with the portative device allows micro-metastases detection, significantly improve their resection and increase the mice survey.

References:

1. Intraoperative near-infrared image guided surgery for peritoneal carcinomatosis in a preclinical experimental model. M. KERAMDAS, V. JOSSERAND, RIGHINI C.A., WENK C., FAURE C. And COLL J.L. British Journal of Surgery,2010.

P-027

Fluorescence imaging modalities for imaging gastrointestinal tumor models

Schulz P. , Cordula D. , Rexin A. , Wiedenmann B. , Groetzinger C. .

Charite, Universitätsmedizin Berlin, Germany

petra.schulz@charite.de

Introduction: A number of peptide receptors have been found to be overexpressed in tumors of the GI tract. The overexpression of somatostatin receptors in neuroendocrine gastroenteropancreatic tumors has long been utilized for molecular imaging using radiolabelled somatostatin analogs in scintigrafic procedures. Other peptide GPCRs may therefore represent attractive new targets. The ongoing project is occupied in particular with the design of GPCR peptide ligands, which bind with high specificity to surface receptors of tumor cells. Pharmacologically optimized peptides could be used as vehicles for transport of contrast agents as well as therapeutics.

Methods: The ongoing project follows four main goals: (1) The validation of GPCR peptides as tumor targets for the gastrointestinal tract (2) The identification of new peptide binding targets (3) The Optimization of peptide structures for imaging and targeted therapy and (4) the development of NIRF-probes and –techniques for a better diagnosis of tumors. NIRF probes are validated in established in vivo tumor models, including subcutaneous tumor models and in a number of orthotopic tumor models using planar and tomografic fluorescent imaging, micro CT and endoscopy for small animals. For monitoring and characterization of tumor growth of human cancer cells in nu/nu mice the bioluminescence imaging approach is utilized. For this purpose several stable cancer lines (colorectal, pancreatic, neuroendocrine), expressing the luciferase gene were established. Results: Currently, a number of peptide, antibody and small-molecule contrast agents are validated. Each tracer is characterized for its potency as a contrast agent by imaging with a 2-D fluorescence imaging system, which reveals target-to background ratios of the contrast agents, characteristic for target tissue specificity. Limitations of planar imaging systems are still the lack of depth resolution and difficult quantification. Currently we are therefore evaluating a fluorescence tomographic system with regard to deep tissue imaging and signal quantification. Tomograpic images also allow fusion with other imaging mmodalities such as CT to confirm the anatomical localization of the fluorescent signal.

Conclusions: Although near-infrared radiation has a higher penetration depth than the visual light, scattering and absorption still prevent whole-body imaging. One potential application for the use of near-infrared optical agents in humans is therefore fluorescence-guided endoscopy. We are currently establishing a protocol for endoscopic imaging in mice with colorectal cancer with a rigid endoscopic device in combination with fluorescence-guided detection using a fiber endoscope.

Acknowledgement: This work was supported by grant 03IP614 from German ministry of research (BMBF)

Assessment of effectiveness and toxicity of the therapy with somatostatin analogue labelled 90Y-DOTATATE in patients with non-functional pancreatic neuroendocrine tumours (PNT)

P-028

Sowa-Staszczak A. .

Nuclear Medicin Unit, Krakow, Poland

sowiana@gmail.com

Introduction: Therapy with labelled somatostatin analogues is the modern approach to the patients with disseminated or unresectable NETs expressing somatostatin receptors (SSTR). Octreotate is the somatostatin analogue with very high affinity to the SSTR type 2, most commonly present in neuroendocrine tumours. In non-functional PNT, grading and systemic metastases have a significant impact on survival. Overall, the 5-year survival rate is about 33%. The chemotherapy is the most common treatment approach. The aim of the study was to assess the efficacy and toxicity of peptide receptor radionuclide therapy (PRRT) with the use of the high affinity somatostatin receptor subtype 2 analogue, 90Y labelled Tyr3-octreotate, (90Y-DOTATATE) in non-functional pancreatic neuroendocrine tumours.

Methods: 19 patients with metastatic NET were diagnosed in the Department of Endocrinology UJCM. 5 patients with high proliferation index (Ki >20%, 4-negative SRS, tumour size 3-7cm) were directed to chemotherapy. 14 patients with positive SRS scan due to disseminated and/or unoperable PNTs (2 patients) were qualified to PRRT (6 men, 8 women, mean age 54,7 years old, Karnofsky's index > 70-100%). The size of the tumour was 2,3-12cm, Ki-67 was <15%, the most frequent localization was in the tail of the pancreas. Each patient received 7,4 GBq/m2 of PRRT divided in 4-5 cycles (most often 100mCi per cycle), every 6 to 9 weeks. For nephroprotection amino-acids formula Vamin 18, before and after each cycle of PRRT, was administered.

Results: Among all patients partial remission was observed in 14% of cases, stabilization in 64% and progression of the disease in 22% of patients. 2 patients due to progression of the disease received additional cycles of PRRT. The mean observation time was 17,2 months. The mean time to progression was 14,5 months. 4 patients died. After the treatment the creatinine level was 96,37 umol/l. Mean platelets level was 231 000/ul. Mean hemoglobin level was 10,9 g/l. In one patient the value of Hb was assessed as toxicity grade 3. Mean leukocytes level was 5530/ul.

Conclusions: After PRRT, stabilization of the disease was observed in the majority of patients. PRRT did not cause mielotoxicity and nephrotoxicity.

POSTER

P-029

Intra operative near-infrared fluorescent imaging of colorectal liver metastases using clinically available Indocyanine Green in a syngene rat model

Van Der Vorst J. , Hutteman M. , Mieog J. , De Rooij K. , Kuppen P. , Kaijzel E. , Löwik C.W.G.M. , Van De Velde C. , Vahrmeijer A. .

Leiden University Medical Centre, The Netherlands

j.r.van_der_vorst@lumc.nl

Introduction: The survival of patients with colorectal carcinoma is mostly determined by the occurrence of distance metastases. When liver metastases occur, surgical resection can offer a 5-year survival of 35-40%. However, during resection, an adequate assessment of the extent of disease is limited, resulting in a high percentage of recurrence (40-50%). Ishizawa et al. reported that liver cancer could be identified using near-infrared (NIR) fluorescence and the clinically available indocyanine green (ICG) (1). However, the optimal dose of ICG and the interval between the administration of ICG and surgery is unclear.

Methods: In the current study, the NIR probe ICG and the Mini-FLARE (Dr. J.V. Frangioni, Boston, USA) camera system were used. In 6 rats, 125,000 CC531 cells were inoculated subcapsularly in three different lobes of the liver. After four weeks, tumors of approximately 3-5 mm diameter were present. In each rat, fluorescence was measured at 24 and 48 hours post-injection of 0.04 mg (n = 3) or 0.08 mg (n = 3) ICG.

Results: In 6 rats, all colorectal liver metastases (n = 10) were intraoperatively identified using ICG and the Mini-FLARE camera system (Figure 1). The fluorescent signal of the colorectal liver metastases was significantly higher than the signal of surrounding normal liver tissue ($P < 0.001$). No significant difference in mean signal to background ratio was found between imaging at 24 and 48 hours post-injection. Furthermore, no significant difference in mean signal to background ratio was found between injection of 0.04 and 0.08 mg of ICG.

Conclusions: This study demonstrated that colorectal liver metastases can be clearly identified during surgery using the clinically available NIRF probe ICG and the Mini-FLARE camera system. When the current intraoperative identification can be improved using this technique, resections can be performed more accurately and preoperatively missed metastases can be involved in surgical decision making during surgery.

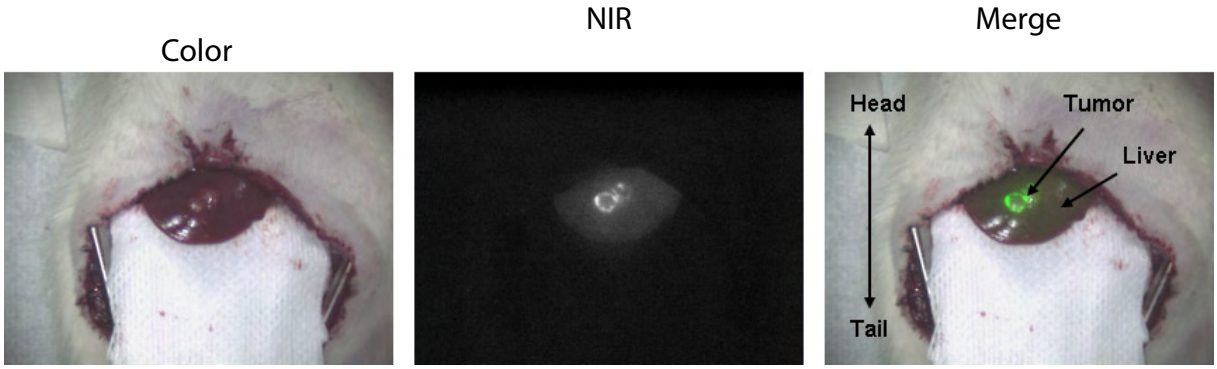

Fig1: Intraoperative NIRF identification of colorectal liver metastases

References:

1. Ishizawa et al.; Cancer. 1;115(11):2491-504. (2009)

Molecular imaging of resistance to EGFR tyrosine kinase inhibitors by 18F-FLT PET/CT and its reversal in non small cell lung cancer

P-030

Zannetti A. [1], Iommelli F. [1], Lettieri A. [1], Pirozzi G. [2], Salvatore M. [3], Del Vecchio S. [3].

[1] Institute of Biostructures and Bioimages, National Research Council, Naples, Italy
[2] Department of Experimental Oncology, National Cancer Institute, Naples, Italy
[3] Institute of Biostructures and Bioimages, National Research Council; Department of Biomorphological and Functional Sciences, University of Naples "Federico II", Naples, Italy

antonella.zannetti@ibb.cnr.it

Introduction: Multiple molecular mechanisms may underlie the resistance to EGFR tyrosine kinase inhibitors (TKIs), including the occurrence of secondary mutations such as T790M in the kinase domain of EGFR, redundant lateral signalling or alterations of apoptotic program mainly due to dysregulation of Bcl-2 family members. The aim of our study was to test whether 18F-Fluorothymidine (18F-FLT) could detect EGFR TKI refractory tumors and identify the mechanisms underlying such resistance so that specific therapeutic strategies can be adopted in patients with non-small cell lung cancer (NSCLC).

Methods: EGFR TKI sensitive and resistant NSCLC cells were evaluated for drug-induced apoptosis and growth arrest. Cells were also tested for inhibition of downstream signalling and expression or drug-induced upregulation of Bcl-2 family members. Nude mice bearing sensitive and resistant NSCLC were i.v. injected with 7.4 MBq of 18F-FLT and then subjected to microPET/CT (eXplore Vista Pre-Clinical PET Scanner GE Healthcare) before and after treatment with reversible or irreversible EGFR TKIs.

Results: We found that NSCLC bearing T790M mutations showed a persistent high uptake of 18 F-FLT after treatment with reversible inhibitors and lack of growth arrest. Treatment of the same animals with irreversible inhibitors caused a reduction of 18F-FLT uptake in tumors indicating the reversal of T790M mutation-dependent resistance. Conversely, NSCLC cells that were resistant due to dysregulation of Bcl-2 family members became sensitive to EGFR TKIs when treatment included Bcl-2 inhibitors.

Conclusions: Resistance to EGFR TKI may be caused by multiple mechanisms. Molecular imaging with 18F-FLT may contribute to the selection of patients that may benefit from treatment with irreversible EGFR TKI inhibitors.

POSTER

CANCER from BENCH to BEDSIDE

P-031

Synchronised Cardiac and Lung CT in Rodents Using the Mobile CT Scanner LaTheta™

Glowalla A. .

Zinsser Analytic GmbH, Frankfurt, Germany

a.glowalla@zinsser-analytic.com

Introduction: Historically, in vivo CT images of the chest region of small animals were blurred and streaked due to movement artefacts caused by the heartbeat and breathing during scanning. However, synchronised Cardiac and Lung CT in rodents has the enormous potential to contribute greatly to research in heart and lung diseases. Using the mobile CT Scanner LaTheta™, scanning artefacts are greatly reduced. Here we present scanning results of the chest region of mice and discuss their relevance in pre-clinical research.

Methods: Manufacturers standard protocols for synchronised CT scanning were used to scan the chest region of anaesthetised mice with respiratory rates below 75bpm, as below:

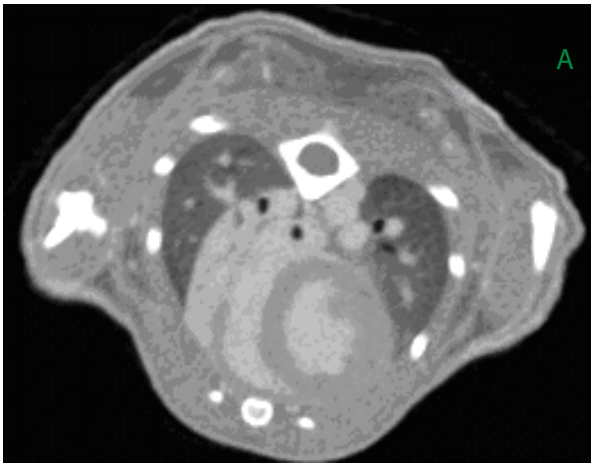

Synchronised CT scanning results for A) heart in systole phase and B) lung in mouse

A) Cardiac Sync. Scan (systole + diastole)
- scan range axial: heart, 15mm length
- scan time: 13.1min

B) Respiratory Sync. Scan
- scan range axial: heart, 10mm length
- scan time: 4.5min

X-ray tube voltage: 50kV at 0.5mA; Pixel resolution: 48um; Slice thickness: 192um; Contrast media: Iopamiron 300, 1.5ml/h in 30g mouse given 10min. before scanning.

CT images were constructed using methods for reduction of motion artefacts and with focus on soft tissues.

Results: CT images of heart (diastole and systole phases) and lung were acquired and reconstructed without common blurring and streaking effects.

Conclusions: Synchronised scanning modes with LaTheta™ LCT-200 produce high-resolution CT cross-sections of heart and lung in living mice within a short time period. Similar methods are applicable also for rats. Since no additional sensor hardware is necessary, handling of the animal is as simple as for standard CT.

The potential for the detection of lung diseases such as pulmonary fibrosis, pulmonary emphysema and also lung tumours has already been validated by manufacturer. With this technology LaTheta™ LCT -200 can also contribute to the studies of cardiovascular diseases in rodents.

Acknowledgement:

1. Manufacturer of LaTheta(TM): Aloka Co., Ltd., 6-22-1 Mure, Mitaka-shi, Tokyo, 181-8622, Japan
2. Distributor: Zinsser Analytic GmbH, Eschborner Landstr. 135, 60489 Frankfurt am Main, Germany

Molecular imaging of neurovascular inflammation in a mouse model of focal cerebral ischemia using Ultra small Superparamagnetic Particles of Iron Oxide (USPIOs) targeted to vascular cell adhesion molecule-1 (VCAM-1)

P-032

Montagne A. [1], Gauberti M. [1], Orset C. [1], Macrez R. [1], Rubio M. [1], Raynaud J. S. [2], Vivien D. [1], Maubert E. [1].

[1] Inserm U919 UMR 6232 CNRS Ci-Naps, Caen, France
[2] Experimental Imaging, MRI unit. Research Division. GUERBET, Roissy CdG, France

amontagne@cyceron.fr

Introduction: Among several mechanisms, brain inflammation is thought to have critical functions in lesion progression during acute and subacute stages of ischemic stroke. Accordingly, anti-inflammatory strategies are neuroprotective in preclinical studies [1]. However, to date, all clinical trials with anti-inflammatory agents have failed to improve clinical outcome in acute ischemic stroke patients. New tools for non-invasive monitoring of inflammation following stroke are needed to select patients who are more susceptible to benefit from anti-inflammatory treatment. Vascular cell adhesion molecule 1 (VCAM-1), an endothelial adhesion molecule, is overexpressed in the injured brain and is therefore thought to be a good target for the molecular imaging of inflammatory processes [2]. The aim of this study was to investigate the use of targeted USPIOs against VCAM-1 to follow neurovascular inflammation in a mouse model of in situ thromboembolic stroke with recombinant tissue-type plasminogen activator (rt-PA) induced reperfusion [3].

Results: Our present data confirm an increase of vascular cell adhesion molecule-1 (VCAM-1) immunoreactivity (-ir) in the ischemic brain with a peak at 24 hours post-ischemia. Interestingly, V-CAM-1-ir was significantly increased in late rt-PA-thrombolyzed animals (4 hours after clot formation) compared to early (20 minutes) or unthrombolyzed mice. These data suggest that inflammation could be involved in the deleterious clinical outcome reported with late rt-PA mediated thrombolysis. Targeted USPIOs against VCAM-1 showed numerous signal voids in the ipsilateral side by 7T magnetic resonance imaging (MRI) at 24 hours post-ischemia and the use of an antibody directed against polyethylene-glycol (USPIOs coating) confirmed histologically our MRI analysis.

Conclusions: Our data indicate that non invasive imaging of VCAM-1 with targeted USPIOs allows reliable imaging of brain inflammation after stroke. Such molecular MRI approaches could be used to evaluate inflammatory processes in stroke patients and thus to adapt therapy on an individual basis. Furthermore, molecular imaging of VCAM-1 could also provide valuable clinical information in other diseases involving inflammatory processes (atherosclerosis, multiple sclerosis …).

References:

1. Machado L et al; Stroke. 40;3028-3033 (2009).
2. Hoyte L et al; J Cereb Blood Flow Metab.1-10 (2010).
3. Orset C et al; Stroke. 38;2771-2778 (2007).

P-033

Scintigraphy with the use of ^{123}I-IL-2: a new promising tool for cardiovascular risk assessment in patients with high cardiovascular risk

Opalinska M. [1], Hubalewska-Dydejczyk A. [1], Stompor T. [2], Krzanowski M. [3], Mikołajczak R. [4], Sowa-Staszczak A. [1], Karczmarczyk U. [5], Glowa B. [1], Kuśnierz-Cabala B. [6], Pach D. [1], Sułowicz W. [3].

[1] Nuclear Medicine Unit, Department of Endocrinology, Jagiellonian University Medical School, Krakow, Poland [2] Chair and Department of Nephrology, Hypertesiology and Internal Medicine, University of Warmia and Mazury , Olsztyn, Poland [3] Chair and Department of Nephrology, Jagiellonian University Medical School, Krakow, Poland [4] Radioisotope Center POLATOM, Otwock-Swierk, Poland [5] Departament of Radiopharmaceuticals, National Medicines Institute, Warsaw, Poland [6] Chair of Clinical Biochemistry, Jagiellonian University Medical School, Krakow, Poland

mkal@vp.pl

Introduction: Cardiovascular diseases are the main cause of deaths in general population (0,28%/year) whereas in selected population like in end-stage renal disease patients, mortality reaches even 20%. More than half of the cardiovascular events occur among the patients without any previous symptoms of cardiovascular disease, when atherosclerotic plaques obliterate less than 50% of arterial lumen.

The majority of widely available methods of cardiovascular risk estimation are based on arterial lumen assessment, estimation of atherosclerotic plaque size or on intima-media complex measurements. It means that those methods may by imprecise in the identification of plaques of the highest risk of rupture. For that reason, the methods which enable the visualization and estimation of the intensity of inflammatory process within atherosclerotic lesions, seem to play the most promising diagnostic role.

The histopathological studies of the atherosclerotic plaque have revealed that activated lymphocytes T, which contain IL-2 receptors on their surfaces, comprise at least 20 % of inflammatory cells in unstable plaques. Those receptors can be identified with the use of scintigraphy with labeled IL-2.

Methods: 10 patients (5 women, 5 men, aged 62,4 ± 10,4), with the highest cardiovascular risk, were chosen from 67 peritoneal dialysis cohort patients. All of them underwent ^{123}I-IL2 scintigraphy, coronary calcium scoring by CT and common carotid artery intima-media thickness assessment by USG. The levels of some atherogenic, inflammatory and calcium-phosphate indicators were measured. Target/non-target ratio of ^{123}I-IL-2 uptake in atherosclerotic plaque confirmed by carotid artery USG with IMT, calcium score result and concentration measured agents were compared.

Results: In the performed scintigraphies increased focal ^{123}I-IL-2 uptake in 16/16 (100%) atherosclerotic plaques previously visualized by neck ultrasound was detected. Mean T/nT ratio of focal ^{123}I-IL-2 uptake within atherosclerotic plaques was 3,15 ± 0,54 (median 3,22, range 2,0 – 3,6). The levels of the inflammatory and atherogenic factors and IMT (mean 0,975 ± 0,337 mm) were increased in the majority of patients. High positive correlation between 123I-IL-2 uptake within atherosclerotic plaques and IMT in corresponding artery was observed (R = 0,92, p = 0,01). Significantly higher ^{123}I-IL-2 uptake on scintigraphy in patients who developed cardiovascular event during observation period (average 36 months), compared to patients without cardiovascular event, was revealed (3,45 ± 0,22 vs 2,91 ± 0,54, p = 0,046). No statistically significant association was found between ^{123}I-IL-2 uptake and the levels of measured agents, calcium score or classical cardiovascular risk factors.

Conclusions: Scintigraphy with the use of labeled ^{123}I-IL-2 enables the visualization of inflamed atherosclerotic (vulnerable) plaque within common carotid arteries in end-stage renal disease patients.

Quantitative results of the carotid arteries scintigraphy with ^{123}I-IL-2 correlate with the results of IMT and the risk of cardiovascular event during 3 years of follow-up.

Acknowledgement: This work is supported by the Polish Committee for Scientific Research (KBN) within Research Project 2 P05B 003 28

References:

1. Annovazzi A et al; 99mTc-interleukin-2 scintgraphy for the in vivo imaging of vulnerable atheroslerotic plaque. Eur J Nucl Med Mol Imaging 2006; 33: 117 – 126.
2. Buyukhatipoglu H et al; Inflammation as a risk factor for carotid intimal-medial thickening, a measure of subclinical atherosclerosis in haemodialysis patients: the role of chlamydia and cytomegalovirus infection. Nephrology 2007; 12: 25 – 32.

MEMRI-DTI study of focal transient ischemia in immature rat brain

P-034

Dupont D. , Bogaert-Buchmann A. , Sebrie C. , Gillet B. .

IR4M , UMR 8081 CNRS-Univ. Paris-Sud, ORSAY, France

damien.dupont1@u-psud.fr

Introduction: The aim of the study was to investigate anatomo-functional changes in immature rat brain after focal transient cerebral ischemia occurred when they were 7-day-old. The MRI study was carried out 14 days after ischemia by serial MEMRI combined with DTI.

Methods: Focal ischemia was induced in P7 rats as previously described [1], and the size of the lesion was pointed out by DWI 3h after ischemia. MRI studies were carried out at 7T on P21 rats (n=5), 14 days after focal transient ischemia and compared to normal P21 rats (n=5). DTI sequence used was DTI-EPI (2 b-values=500/1000s/mm2; 30 directions; resolution=0.156*0.156*1 mm3). For the MEMRI experiments, 160nl of a 50mM isotonic manganese chloride aqueous solution (pH=7.3) was injected in S1 at 1.5mm below the dura, at a rate of 20nl/min. T1-weighted experiments were achieved at 3, 5, 7 and 24h post-injection, using 3D MP-RAGE sequence (resolution=0.156*0.156*0.5mm3; TR/TE=15/4.5ms, α=20°; Ti=1s). The manganese containing voxels were defined as hyper intense voxels and selected as those with a significant higher signal ($p<0.05$) than in the contralateral cortex, and the high-lighted images obtained overlaid the corresponding anatomical T2-weighted images acquired with TurboRARE sequence (TR/TE= 3500/40 ms; rare factor 8, same resolution).

Results: ADC maps registered 3h after ischemia permit to check that the lesion was limited to the ipsilateral cortex. MEMRI: In stroke rat, 3 hours post injection (3h PI), the overlaid images showed that the manganese enhanced signal was only located at injection site. At 5h PI, signal intensity from caudate putamen and thalamic nuclei appeared enhanced, revealing manganese transport in those structures. At 7h PI, same areas are involved and had evolved. In healthy rats, hypersignal zones appeared from 3h PI in ipsilateral cortex and in sub-cortical areas, like caudate putamen and thalamus nuclei. At 5h PI signal intensity and volume had increased in sub-cortical enhanced areas and remained quite similar at 7h PI (Fig.1A). DTI: We used FA maps in order to investigate structural changes induced by ischemia. Those maps revealed that, as expected, the ispilateral cortex has been disrupted and that FA values were inferior in the sub cortical area (particularly in the caudate putamen) compared to that ones measured in controlateral hemisphere and in healthy rats (Fig.1B). That showed a loss of architecture in area that was not included in primary ischemic zone.

Conclusion: A cortical lesion seems to change the anatomic architecture development of ipsi- sub-cortical areas. Results showed that a cortical transient ischemia on a new born rat causes a functional deficiency of the cortico-thalamic pathway (MEMRI), and affect the FA in the same zone. We have revealed that a cortical injury induced remote anatomo-functional changes in the sub-cortical area.

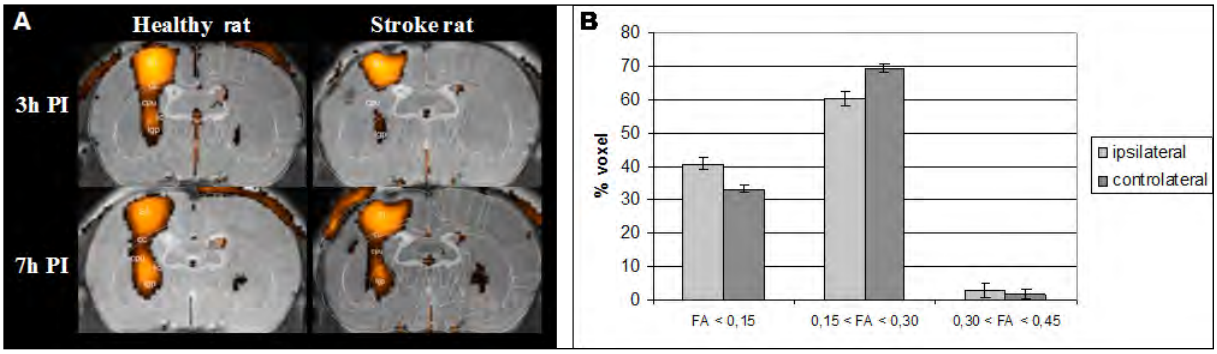

References:

1. Fau S and al. *Exp. Neurol*. 208, 297-304 (2007).

POSTER

NEUROIMAGING from BENCH to BEDSIDE

P-035

A clinically relevant model of in situ embolic stroke in the anesthetized monkey (macaca mulatta): long-term electrophysiological and mri analyses

Gauberti M. [1], Guedin P. [1], Etard O. [2], Diependaele A.S. [2], Chazalviel L. [3], Lamberton F. [3], Vivien D. [1], Young A. [1], Agin V. [1], Orset C. [1].

[1] INSERM, Caen, France
[2] CHU Caen, France
[3] CNRS, France

gauberti@cyceron.fr

Introduction: The lack of relevant stroke models in large animals is a limitation for the development of innovative therapeutic/diagnostic approaches. The aim of the present study was to develop an original and clinically relevant pre-clinical model of embolic stroke in the monkey.

Methods: During full physiological and biochemical monitoring, six monkeys underwent enucleation, the right MCA was exposed and alpha-thrombin was injected into the MCA. The monkeys were subjected to somatosensory evoked potentials (SEPs) and MRI studies (T2, FLAIR, DWI, PWI and MRA) prior to, and following the acute (2 h) and chronic stages (24 h to 3 months) of stroke.

Results: This feasibility study showed that, it is possible to induce ischemic lesions in the MCA territory of the monkey following the direct injection of thrombin into the lumen of the M1 segment of the MCA. This procedure leads to cortical or subcortical ischemic lesions and to a persistent impairment of somatosensory responses as evidenced by MRI and SEPs data, respectively.

Conclusions: In situ induction of an endogenous fibrin clot together with the lack of mortality make this original model of stroke in large non-human primates, highly relevant to determine the effectiveness of drug administration including thrombolytic therapy and to validate new imaging procedures.

Automated radiosynthesis of [^{18}F]MPPF derivatives for imaging 5-HT$_{1A}$ receptors

P-036

Goblet D. [1], Thonon D. [1], Plenevaux A. [1], Defraiteur C. [2], Wouters L. [2], Franci X. [2], Luxen A. [1].

[1] University of Liege, Liege, Belgium
[2] GE Healthcare Diagnostic Imaging, Belgium

david.goblet@ulg.ac.be

Introduction: Dysfunction of the central serotoninergic system is implicated in numerous neurodegenerative disorders such as Alzheimer's disease, dementia, depression, anxiety, schizophrenia, and Parkinson's disease. 5-HT$_{1A}$ receptors are involved in several physiological functions including sleep, mood, neurogenesis and learning [1]. Consequently, there have been huge efforts to find ligands for this receptor. [^{11}C]WAY-100635 is a high affinity radioligand used for quantifying 5-HT$_{1A}$ receptors with positron emission tomography. An ^{18}F-labeled radioligand would be advantageous because of higher specific activity and physical/nuclear properties ($t_{1/2}$= 109 min, 97% of positron decay and positron energy of 635 keV maximum). [^{18}F]MPPF, a selective 5-HT$_{1A}$ antagonist derived from WAY-100635, is currently one of the most successful PET ligands used for 5-HT$_{1A}$ receptor imaging [2]. However the affinity is lower than WAY-100635 and the amount of [^{18}F]MPPF reaching the brain is relatively low, as MPPF is a substrate for P-glycoprotein [3].

Methods: In order to improve the brain uptake of the radiotracer, a desmethylated analog has been developed in our lab and preliminary in vitro studies show positive results [4]. Nevertheless, the radiosynthesis takes place in two steps, as the removal of a protecting group is needed. A one step procedure with a MPPF derivative could be of very great interest. We have synthesized many MPPF derivatives in our lab (modification on the phenylpiperazine moiety) and developed an automated radiosynthesis procedure for the production of these radiotracers. [^{18}F]MPPF was chosen as the model compound. We used a GE Healthcare FASTlab™ module and made modifications to the [^{18}F]FDG synthesis sequence and cassette. [^{18}F]MPPF was synthesized by coupling of [^{18}F]FBA with the corresponding amine. After coupling, the crude solution was diluted with water and passed through a tC_{18} cartridge for prepurification. After elution, the [^{18}F]MPPF was purified by semi-preparative HPLC.

Results: Total synthesis time, including purification was approximately 100 min. [^{18}F]FBA and [^{18}F]MPPF were obtained at a corrected yield of 60% (n=20) and 45% (n=5) respectively. The radiochemical purity, checked by radio-TLC and UPLC, was >95%.

Conclusions: We have developed an automated method for [^{18}F]MPPF (and derivatives) production using a commercial synthesizer (FASTlab™ from GE Healthcare) and a conventional HPLC system resulting in good yields and high (radio) chemical purity. By simply switching the vial containing the modified amine, an ^{18}F-labeled MPPF derivative could be obtained. Radiosynthesis is still under optimization and the radiotracers synthesized need to be tested as suitable 5-HT$_{1A}$ radioligands.

Acknowledgement: This work was supported by the *Fondation Rahier* of the University of Liege. This work was supported by a GE Healthcare Diagnostic Imaging grant.

References:

1. Filip M., Bader M. et Al, Pharmacol Rep. 2009 Sep-Oct; 61(5):761-77
2. Aznavour N, Zimmer L. Et Al, Neuropharmacology. 2007 Mar; 52(3):695-707
3. Laćan G., Plenevaux A. et Al, Eur J Nucl Med Mol Imaging. 2008 Dec;35(12):2256-66
4. Defraiteur C., Plenevaux A. et Al., Br J Pharmacol. 2007 Nov; 152(6):952-8

P-037

The vitamine E analogue CR6 protects against the long-term microstructure damage induced by MCA occlusion: a longitudinal Diffusion Tensor Imaging study

Justicia C. [1], Soria G. [1], Tudela R. [2], Van Der Linden A. [3], Messeguer A. [4], Planas A. [5].

[1] Investigaciones Científicas (CSIC), Institut d'Investigacions Biomèdiques August Pi i Sunyer (IDIBAPS), Barcelona, Spain
[2] CIBER de Bioingeniería, Biomateriales y Nanomedicina (CIBER-BBN), Group of Biomedical Imaging of the University of Barcelona, Spain
[3] University of Antwerp, Antwerp, Belgium
[4] Institut de Química Avançada de Catalunya (IQAC), CSIC, ,Spain
[5] Institut d'Investigacions Biomèdiques de Barcelona (IIBB)-Consejo Superior de Investigaciones Científicas (CSIC), Institut d'Investigacions Biomèdiques August Pi i Sunyer (IDIBAPS), Spain

cjmfat@iibb.csic.es

Introduction: Oxidative and nitrosative stress are targets for intervention after ischemia/reperfusion. CR-6 is a synthetic analogue of vitamin-E, with the additional capacity to scavenge nitrogen-reactive species. Recently it has been demonstrated that CR-6 exerts a protective action against cerebral ischemia/reperfusion injury. The aim of this study was to investigate whether CR-6 can protect the brain microstructure after brain ischemia as assessed by longitudinal Diffusion Tensor Imaging (DTI).

Methods: Sprague–Dawley rats had the middle cerebral artery occluded for 90 mins to induce brain ischemia. CR-6 (100 mg/kg) or vehicle (oliva oil) was orally administered at 2 and 8 h after ischemia onset. Longitudinal MRI scans were performed under isofluorane anaesthesia in a BioSpec 70/30 horizontal animal scanner (Bruker BioSpin, Ettlingen, Germany), equipped with a 12 cm inner diameter actively shielded gradient system (400 mT/m). Receiver coil was a phased-array surface coil for rat brain. Animals were scanned before surgery and 1, 3 and 5 weeks later. The lesion was monitored by T2 mapping of coronal slices acquired with a MSME sequence by applying 16 different echo times (TE), repetition time (TR) = 4764 ms, Field of view (FOV) = 40 x 40 x 21 mm3, matrix size = 256 x 256 x 21 pixels, resulting in a spatial resolution of 0.156 x 0.156 mm in 1.00 mm slice thickness. DTI images were acquired by using a EPI DTI sequence applying TR = 3800 ms, TE = 30.85 ms, 4 segments, b-value = 1000, 30 different diffusion directions, 5 A0 images, slice thickness = 1 mm, number of slices = 14, FOV = 2.0 x 2.0 x 1.4 mm3, matrix size = 96 x 96 x 14 pixels, resulting in a spatial resolution of 0.21 × 0.21 mm in 1 mm slice thickness. T2 maps were analysed using ImageJ. DTI maps of the tensor diffusivities, fractional anisotropy (FA), apparent diffusion coefficient (ADC), axial diffusivity ($\lambda = \lambda 1$) and radial diffusivity ($\lambda = [\lambda 2 + \lambda 3/2]$), were calculated using Paravision 5.0 software (Bruker Biospin, Etlingen, Germany) and custom programs written in Matlab (The MathWorks, Inc., Natick, MA, USA). ROIs were individually drawn for each subject and hemisphere, by an experienced neurobiologist blinded to the treatments, overlaying the MRI images with the digital Paxinos and Watson rat brain atlas.

Results: DTI diffusion indices, particularly axial and radial diffusivities, demonstrated that microstructure was better preserved after brain ischemia in CR6-treated animals than in animals receiving the vehicle. The latter showed a significant increase of MD, axial and radial diffusivities in the ipsilateral anteroventral thalamus, caudate putamen, globus pallidus and internal capsula 3 and 5 weeks after ischemia versus pre-scan. However, CR6 treated animals did not show such increase of DTI indexes in any of the ROIs analysed revealing preserved microstructure of the brain tissue.

Conclusions: This work demonstrates that transient cerebral ischemia induces long-term microstructure alterations of brain tissue that are detected by DTI magnetic resonance imaging technique, and that the vitamin-E analogue CR6 attenuates these alterations.

Acknowledgement: S and RT are supported by CSIC (JaeDoc) and CIBER-BBN, respectively. We acknowledge the European Erasmus program supporting Sofie de Prins and Stephan Cools that helped in this study. Work supported by national grants (SAF2008-04515-C02-01, FIS PI081880), European Network of Excellence DiMI (LSHB-CT-2005-512146), and FP7/2007-2013 project (grant agreement n°201024).

Design and synthesis of fluorescent probes for serotonin 5-HT1A receptors

P-038

Leopoldo M. [1], Lacivita E. [1], Berardi F. [1], Perrone R. [1], Jafurulla M. [2], Saxena R. [2], Rangaraj N. [2], Chattopadhyay A. [2].

[1] Università degli studi di Bari "A. Moro", Bari, Italy
[2] Council of Scientific and Industrial Research, Hyderabad, India

leopoldo@farmchim.uniba.it

Introduction: The serotonin1A receptor subtype (5-HT1A) belongs to the large family of 5-HT receptors that comprises at least 14 receptor subtypes. 5-HT1A receptor is likely the most extensively studied serotonin receptor. The 5-HT1A receptor has been initially implicated in anxiety and depression. Recent studies have evidenced its implication in neuroprotection, cognitive impairment, and pain [1]. Many information are available about the molecular pharmacology of 5-HT1A receptor. However, the study of 5-HT1A pharmacology at the single cell and single molecule level by fluorescence-based techniques has not been possible due to the lack of an effective 5-HT1A fluorescent ligands. We here describe design, synthesis and preliminar pharmacological evaluation of two fluorescent probes for 5-HT1A receptor.

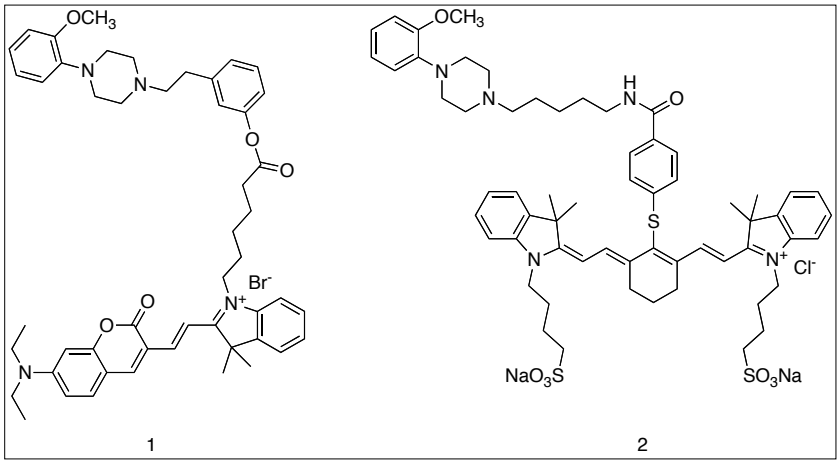

Methods: The new fluorescent probes have been designed following a classic approach [2]: a pharmacophore moiety, selected from the literature, has been conjugated through a linker to a fluorescent dye. One red-emitting and one near infrared dye were selected because such excitation wavelengths cause reduced light scattering and do not cause cell damage. The synthesis and purification of the target compounds was accomplished by standard methods. The compounds 1 and 2 underwent binding assays to test their ability to displace [3H]-8-OH-DPAT from 5-HT1A receptors overexpressed in HEK-298 cell membranes. The fluorescent ligand 1 was evaluated in visualization experiments of 5-HT1A receptor on CHO cells by confocal laser scanning microscopy.

Results: Compounds were obtained in good yields and in good quantities to allow further biological studies. Both compounds 1 and 2 possessed good 5-HT1A receptor affinities (Ki = 35 nM and 68.9 nM, respectively). The target compounds displayed the same fluorescent properties as the corresponding fluorophores. In visualization experiments by confocal laser scanning microscopy compound 1 was able to label 5-HT1A receptors on CHO cells overexpressing the receptor. This interaction revealed to be specific since the compound was unable to bind wild-type CHO cells and also because 5-HT significantly displaced competitively 1 from the binding site.

Conclusions: This study indicates that fluorescent probes for 5-HT1A receptor can be successfully designed on the basis of knowledge of structure-activity relationships of 5-HT1A receptor agents. The 5-HT1A fluorescent ligand that have been identified possess suitable characteristic for visualization of 5-HT1A receptors.

References:

1. Lacivita E et al; Curr Top Med Chem. 8:1024-1034 (2008)
2. Leopoldo M et al: Drug Disc Today 14:706-712 (2009)

POSTER

NEUROIMAGING from BENCH to BEDSIDE

P-039

Comparative evaluation of cerebral blood flow in a rat model of cerebral ischemia using ^{15}O-H_20 positron emission tomography and ^{99m}Tc-HMPAO single-photon emission tomography

Martin A. [1], Boisgard R. [1], Gervais P. [2], Thézé B. [1], Vuillemard C. [2], Tavitian B. [1].

[1] CEA, DSV, I²BM, SHFJ, Laboratoire Imagerie Moléculaire Expérimentale; INSERM U803, Orsay, France
[2] CEA, DSV, I²BM, SHFJ, France

abraham.martin-munoz@cea.fr

Introduction: Ischemic stroke occurs when cerebral blood flow is interrupted in a specific region of the brain. After ischemic stroke, cerebral parenchyma suffers perfusion changes over time which have been correlated with biological processes as compensatory growth of blood vessels to supply metabolic demand [1], underlying inflammation [2] and angiogenesis [3].Thereafter, a precise understanding of the cerebral blood flow evolution after ischemic stroke is essential for the comprehension of cerebral ischemia physiopathology. Here, a comparative imaging evaluation of cerebral blood flow using PET and SPECT during and after cerebral ischemia was performed in rats.

Methods: [^{15}O] H20 and [^{99m}Tc] HMPAO were used in a rat model of 2 hours transient middle cerebral artery occlusion (tMCAO) during occlusion, during early reperfusion and later on at 1, 2, 4 and 7 days. The tissue was analized *ex vivo* using histological (HE) and immunohistochemistry (CD31).

152

Results: *In vivo* PET imaging showed a significant decrease of the ipsilateral or lesioned area versus contralateral ratios during the occlusion in relation to control, days 4 and 7 after reperfusion ($P<0.001$), early reperfusion ($P<0.01$), and to day 2 ($P<0.05$). The ratios also showed a significant decrease at day 1 in relation to days 4 and 7 ($P<0.01$).

In vivo SPECT images showed a significantly decrease during the occlusion in relation to days 4 and 7 after reperfusion ($P<0.001$), at control, early reperfusion and at day 2 ($P<0.01$) and at day 1 ($P<0.05$). There was also observed a decrease of the signal at day 1 in relation to control and at day 7 ($P<0.05$). For all animals, [^{15}O] H20 with [^{99m}Tc] HMPAO ratios were showing a significantly correlation (r=0.7218). Furthermore, binding signal in both brain hemispheres showed increase of cerebral blood flow at seven days after reperfusion using both techniques compared to control animals.

Conclusions: This is the first study using [^{99m}Tc] HMPAO single proton emission tomography in order to study the cerebral blood flow in experimental stroke in rats. SPECT data showed a similar sensivity as Positron emission tomography using [^{15}O] H_20 to detect perfusion changes over time. Such perfusion changes observed in the present study probably reflect different physiopathological processes underlying cerebral ischemia.

Acknowledgement: This work was supported in part by the FP6 network DiMI (LSHB-CT-2005-512146) and by the FP6 European No EMIL (LSHC-CT-2004-503569).

References:

1. Plate KH; Journal of Neuropathological Experimental Neurology. 58, 313-20.
2. Martin A;.Journal of Cerebral Blood Flow and Metabolism. 30, 230-241.
3. Lin TN; Journal of Cerebral Blood Flow and Metabolism. 33, 2985-91.

Comparison of dopamine transporter density in Parkinson's disease patients with and without autonomic dysfunction using F-18 FP-CIT PET/CT

P-040

Park E. , Park K.W. , Hwang Y.M. , Oh S.Y. , Choe J.G. .

Korea University Anam Hospital, Korea University College of Medicine, Seoul

angela_ekpark@yahoo.co.kr

Introduction: Autonomic dysfunction is a common non-motor feature of Parkinson's disease (PD) which can severely impair the life quality of PD patients. However, evaluation of striatal presynaptic dopaminergic function with SPECT or PET imaging using various radiotracers has been limited in the differential diagnosis of parkinsonism and in the severity assessment of Parkinson's disease. We compared the dopamine transporter (DAT) density of PD patients with and without autonomic dysfunction using F-18 FP-CIT PET/CT, which has been approved recently by Korean FDA for clinical uses.

Methods: Twenty clinically diagnosed PD patients (mean age 68.6±8.1 y, M:F=5:15) and 8 age-matched healthy normal controls (65.1±4.7 y, M:F=2:6) were studied with F-18-FP-CIT PET/CT. Among 20 PD patients, 10 had no significant autonomic dysfunction (PD-AD) while the other 10 had autonomic dysfunction (PD+AD). F-18-FP-CIT PET/CT images were obtained 120 minutes after injection of 185 MBq F-18-FP-CIT. Semi-quantitative analysis was performed using manual ROI method. A DAT parameter V3", a measure directly related to the density of DAT, was calculated in striatal regions as (striatal ROI–cerebellar ROI mean radioactivity)/cerebellar ROI mean radioactivity on F-18-FP-CIT PET/CT images.

Results: PD patients demonstrated significantly lower DAT V3" in the striatum (2.29±0.69), caudate nucleus (2.56±0.67), and putamen (1.99±0.77) than those of healthy normal controls (4.02±0.55, 3.88±0.54 and 4.16±0.61, respectively) (p<0.05). The ratio of putamen-to-caudate nucleus V_3" of PD patients (0.76±0.16) was significantly lower than normal controls (1.07±0.09) (p<0.05), indicating that putamen is more affected than caudate nucleus in PD. The V3" in the caudate nucleus (2.33±0.52) and putamen (1.78±0.69) of PD+AD group were lower than those of PD-AD group (2.79±0.74 and 2.20±0.81, respectively), but this result was not statistically significant (p=0.06). Serotonin transporter density in the midbrain did not show significant difference between PD+AD and PD-AD.

Conclusions: The striatal DAT density of PD+AD tended to be lower than that of PD-AD patients, although not statistically significant. F-18 FP-CIT PET/CT imaging may be useful in the assessment of autonomic dysfunction in PD patients. Further investigations are needed with larger number of patients.

Acknowledgement: This work is supported by Korea University Grants (K0931131 and K0932081)

References:

1. Kim JS; Nucl Med Mol Imaging. 42(6):425-434 (2008)
2. Adler CH; Mov Disord. 20:S23-29 (2005)

POSTER

NEUROIMAGING from BENCH to BEDSIDE

P-041

Synthesis of tosylate and mesylate precursors for one-step radiosynthesis of [^{18}F]FECNT

Pijarowska J. , Jaron A. , Mikolajczak R. .

Insitute of Atomic Energy POLATOM, Otwock, Poland

j.pijarowska@polatom.pl

Introduction: Dopamine transporter (DAT) is critical to the regulation of dopamine neurotransmission and is decreased by Parkinson's disease. Several tropane analogues of cocaine have been developed and used in PET studies to evaluate the physiology and pharmacology of the dopamine transporter (DAT). However, low selectivity and unfavourable kinetics of most of the compounds limit their use in quantitive PET studies.

The fluorine-18 labelled ligand 2-beta-carbomethoxy-3--beta-(4-chlorophenyl)-8-(2-fluoroethyl)-nortropane (FECNT) has promising properties and appears to be an excellent imaiging PET agent. The development of automated [18F]FECNT synthesis system is a crucial because high amounts of radioactivity and availability of radiotracer for multiple PET study is necessary. A semi-automated synthesis of [18F]FECNT based on the two-steps has been developed at 16% decay corrected yield [1]. We hypothesize that N-[18F]fluoroalkylnortropane analogs could be synthesized at hight yield by direct [18F]fluorination from appropriate precursors: N-tosylate and N-mesylate derivatives. This compounds and non-radioactive FECNT as a standard in order to characterize [^{18}F]FECNT on HPLC are synthesized in accordance with requirements for Investigational Medicinal Product (IMP).

Methods: The synthetic approach which we adopted based upon the published procedures [2,3] with some modifications. The essential feature of this route was the reaction of Grignard reagent with the critical intermediate anhydroecognine methyl ester, which was obtained from cocaine hydrochloride by hydrolysis in HCl and esterification with methanol. 3-β-substituted tropane derivative obtained in Grignard reaction was subjected to demethylation, as described [4]. Non-radioactive FECNT was prepared by direct N-(2- fluoroethyl) alkylation of analytically pure 3-β-substituted nortropane precursor. The alkylating agent 2-fluoroethyl brosylate was prepared from 2-fluoroethanol and 4-bromobenzenesulfonoyl chloride. The crude product was purified by recrystallization. The tosylate (TsOECNT) and mesylate (MsOECNT) precursors were synthetised from 3-β-substituted nortropane precursor in two steps by N-hydroxyethylation with 2-bromoethanol and subsequent tosylation of the obtained alcohol with appropriate anhydride. The crude products were purified by preparative HPLC.

Results: In the present study we investigated and optimized synthetic route of non-radioactive FECNT, tosylate and mesylate analogs. Overall production yield were 74% for FECNT, 58% for TsOECNT and 81% for MsOECNT synthesis and a purity of this products were over 99% measured by the analytical HPLC(UV, 220 nm). The ^{1}H NMR and MS analysis confirmed a structure of this compounds.

Conclusions: The synthesis method of tosylate and mesylate precursors were established and an automated radiosynthesis of [18F]FECNT will be evaluated. We expect that the new one–step method will provide a facile and reliable procedure for [18F]FECNT preparation in routine clinical applications.

Acknowledgement: This work is supported by DiMI, LSHB-CT-2005-512146

References:

1. Voll R.J. et al. Appl. Rad. Isot. 2005 (63) 353
2. Zirkle C. L et al. J. Org. Chem. 1962 (34) 1269
3. Clarke R. L. et al. J. Med. Chem. 1973 (16) 1260
4. Meegalla S. K. et al. J. Med. Chem. 1997 (40) 9

Sex differences inDopamine D_2 Receptor Occupancy in the Amygdala using AMPT with PET and [^{18}F]fallypride

P-042

Riccardi P. [1], Park S. [2], Carroll X. [1], Anderson S. [3], Benoit D. [2], Li R. [2], Bauernfeind A. [4], Schmidt D. [2].

[1] Mercer University, Macon, United States
[2] Vanderbilt university, United States
[3] Georgia State University ,United States
[4] George Washington university, United States

riccardip@aol.com

Introduction: Dopaminergic neurotransmission plays an important role in many psychiatric disorders which show sex differences in incidence, clinical course, and treatment outcomes. We examined whether PET studies using [^{18}F]fallypride performed prior to and following alphamethylparatyrosine (AMPT) administration could be used to estimate sex differences in baseline Dopamine D_2 receptors (DAD2r) occupancy.

Methods: Four females and four males normal subjects were recruited with no history of psychiatric, neurological or medical illness. PET studies were performed using a GE Discovery LS PET scanner with 3-D emission acquisition and transmission attenuation correction. [^{18}F]fallypride PET scans (5.0 mCi, specific activity > 2,000 Ci/mmol) were performed prior to and following AMPT administration over 26 hours. Serial scans were obtained for 3.5 hours. Blood samples for HVA plasma levels were collected.

Results: Analysis of variance of the ROI data with treatment status, region, sex and laterality as factors revealed significant effects of sex in the right ($F = 9.403$, $P = 0.002$) and left amygdala ($F = 3.486$, $P = 0.05$). No difference in b.p was found in the left amygdala at baseline, but significant differences were determined at baseline and post treatment in the right amygdala ($p=0.005$ and $p=0.002$) and post treatment in the left amygdala ($p=0.019$) with females demonstrating lower levels of D_2/D_3 receptors compare to males. Effect of treatment was observed in females in the left amygdala with a percentage of change of 6.7%.

Conclusions: The amygdala has been shown to be functionally asymmetrical in animals and humans, is involved in stress and emotion processing, and is importantly modulated by dopamine. We report here for the first time a sex differences in the occupancy of DA D_2r by dopamine in vivo in the amygdala. Previous AMPT administration and [18F]fallypride PET studies to assess the baseline occupancy of DAD_{2r} by endogenous dopamine in-vivo reported no significant effects of treatment in the amygdala when males and females were grouped together. The results of this study underscore the importance of considering sex differences in the context of DAD_{2r} availability.

Acknowledgement: Funding for this reaserch was provided by a NIH grant entltled “PET imaging of Extrastriatal Dopamine levels” NIMH 5RO1 MH6898-03

References:

1. Verhoeff NP, Kapur S, Hussey D et al (2001). A simple method to measure baseline occupancy of neostriatal dopamine D2 receptors by dopamine in vivo in healthy subjects. Neuropsychopharmacology 25; 213-223
2. Riccardi P., Baldwin R, Salomon R., et al. (2008). Estimation of baseline Dopamine D2 receptor occupancy in Striatum and extrastriatal regions in humans with Positron emission tomography with [18F]fallypride.

P-043

Manual versus automatic delineation of VOIs for analysis of nuclear medicine images

Svarer C. [1], Hammers A. [2], Heckemann R. A. [2], Knudsen G.M. [1].

[1] Neurobiology Research Unit, Rigshospitalet,, Copenhagen, Denmark
[2] The Neurodis Foundation, Lyon, France

csvarer@nru.dk

Introduction: Quantification and analysis of nuclear medicine images is performed by visual inspection in most cases. More objective and less observer-dependent analysis often requires automatic identification of volumes of interest (VOIs) in the images. In this study we investigated the levels of precision achievable with manual delineation on high resolution MR images and compared them to the precision of a fully automatic method.

Methods: The method described in Svarer et al(1) has been refined to handle neighborhood voxels in labeled template volumes using a maximum-probability algorithm. We applied it to 19 MR data sets, each with 67 manually delineated VOIs(2). To test the precision of the automatic algorithm, we performed a leave-one-out cross-validation-comparison: using each data set in turn as the target, we automatically generated two independent VOI sets by randomly bisecting the template pool, leading to two independent segmentations of each target by nine atlases each, and calculated the average VOI voxel overlap (intersection divided by average labeled volume). To test the reproducibility/precision of the manually delineated VOI sets, a third VOI set was generated for each target using the entire template pool but itself, and its overlap with the manual VOI set were calculated.

Results: The voxel overlap for the two automatically generated VOI sets was 88.3±5.2%, whereas the voxel overlap between the automatically generated and the manually delineated VOI set was 76.3±9.8%.

Conclusions: Of the 24% non-overlap between manual and automatic methods approx. 12 percentage points may be attributable to variation in the automatic method using different VOI template sets whereas precision in manual delineation of the VOIs may largely underlie the other half of the difference between manual and automatically generated VOI sets. This variation will be removed using an automatic approach based on multiple template sets.

Acknowledgement: Supported by The Lundbeck Foundation, Rigshospitalet, and the Danish Medical Research Council. These studies were funded in part by the EC - FP6-project DiMI, LSHB-CT-2005-512146.

References:

1. Svarer C, Madsen K, Hasselbalch SG, Pinborg LH, Haugbøl S, Frøkjaer VG, Holm S, Paulson OB, and Knudsen GM (2005) MR-based automatic delineation of volumes of interest in human brain PET images using probability maps. Neuroimage 24: 969-979.
2. Hammers A, Allom R, Koepp MJ, Free SL, Myers R, Lemieux L, Mitchell TN, Brooks DJ, and Duncan JS (2003) Three-dimensional maximum probability atlas of the human brain, with particular reference to the temporal lobe. Hum Brain Mapp 19: 224-247.

PET Amyloid and Tau Ligand [18F]FDDNP uptake in early Alzheimer disease

P-044

Tauber C. [1], Beaufils E. [1], Kepe V. [2], Vercouillie J. [1], Venel Y. [1], Baulieu J.L. [1], Barrio J. [2], Hommet C. [1], Camus V. [1], Guilloteau D. [1].

[1] UMRS INSERM U930 - CNRS ERL3106 - University of Tours, France
[2] Dpt of Molecular and Medical Pharmacology, D. Geffen School of Medecine, UCLA, United States

clovis.tauber@univ-tours.fr

Introduction: The PET tracer [18F]FDDNP specifically binds amyloid-beta plaques and tau neurofibrillary tangles, which are typical in the development of the Alzheimer disease (AD). We evaluated the feasibility of a non-invasive quantification of [18F]FDDNP to detect these proteins and discriminate early AD patients from healthy controls (HC). This abstract presents the preliminary results on the currently included cohort of 4 AD and 2 controls.

Methods: All the potential subjects underwent Neuropsychological Assessment (MMSE, Trail Making Test, Semantic Fluency Task, Free and Cued Recall Test, 80 item Boston Naming Test). Patients meeting research criteria for AD and cognitively normal controls underwent PET imaging with 2-(1-{6-[(2-[F-18]fluoroethyl) (methyl)amino]-2-naphthyl}ethylidene)malononitrile (FDDNP) and [18F]FDG. All subjects underwent MR 3D axial T1 weighted imaging. FDDNP distribution volume ratios (DVR) parametric images were generated using Logan graphical analysis with the cerebellum grey matter as a reference region. Regions of interest (ROIs) were defined in the Posterior Cingulate, Parietal, Frontal and Temporal regions. The DVR scores were measured as the mean DVR values of each of these regions. A global score was calculated as the mean DVR scores of all these regions.

Results: All the AD patients had positive FDDNP scans by visual inspection, while all the HC had negative scans. Global values of the FDDNP-PET binding were significantly higher ($p<0.05$) in the AD group (1.18±0.06) than in the control group (1.06±0.03). Similar results were obtained in several individual ROIs, namely the Frontal (1.21±0.07 vs 1.06±0.01) and Temporal (1.17±0.03 vs 1.08±0.02) regions. A cross analysis with the results of the neuropsychological tests clearly indicates some correlations. The patient with the lowest MMSE score (15) has the highest global DVR score (1.27) among the group, and inversely the AD patient with the highest MMSE score (23) has the lowest global DVR score (1.12) among the AD group. Similar correlations were obtained individually between the verbal tests results and the corresponding ROIs results.

Conclusions: These data indicate that the [18F]FDDNP can be used to discriminate non invasively AD subjects from HC. The global fixation of the tracer is significantly higher for the AD than for the HC. Moreover, the specificity of the fixation seems to be correlated with the evolution of the pathology and the results of the neuropsychological tests.

Acknowledgements: Partly supported by FP6-project DiMI, LSHB-CT-2005-512146, PHRC STAFF FDDNP

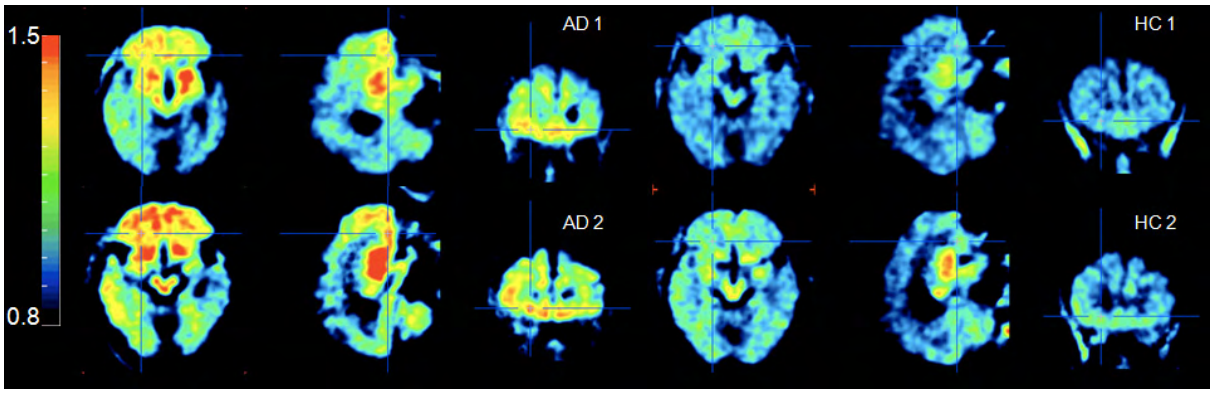

Fig1: DVR parametric images of 2 patients with Alzheimer disease (AD) and 2 healthy controls (HC).

POSTER

NEUROIMAGING from BENCH to BEDSIDE

P-045

Cryogenic brain injury as a model of brain trauma: Use of GFAP-luc mice to assess GFAP expression as an indication of neural injury

Van Beek E., Blankevoort V., Snoeks T., Kaijzel E., Löwik C.W.G.M. .

Leiden University Medical Center, The Netherlands

e.r.van_beek@lumc.nl

Introduction: Applying a cryogenic lesion of the cerebral cortex provides a simple and highly reproducible model of brain trauma without entering the intracranial cavity. In the present study we assessed and mapped the sequence of events that occur following induction of a cryogenic brain lesion using transgenic glial fibrillary acidic protein (GFAP)-luc reporter expressing mice. In these mice, the GFAP reporter is inducible following injury to the CNS and this model provides an easy model feasible for the study of transcriptional regulation of the GFAP gene and indications of possible neural injury.

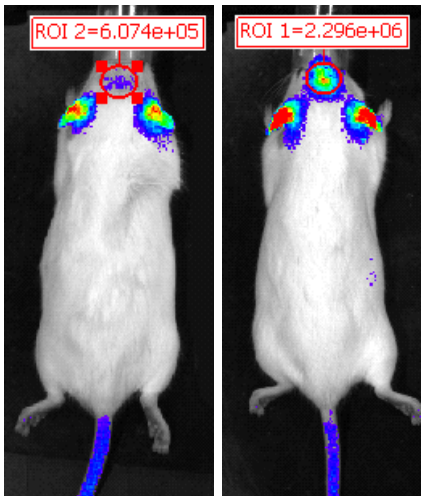

Control

GF AP–luc expression 24h after freeze injury

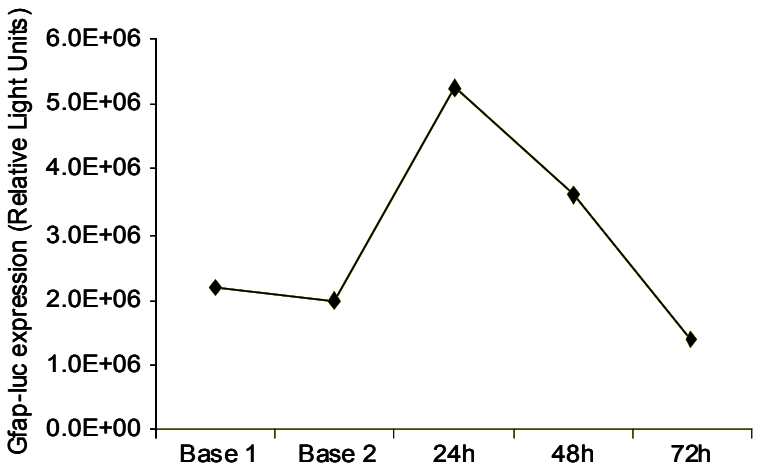

Methods: A brain lesion was induced by placing a liquid nitrogen cooled cone shaped copper device with a tip diameter of 1 mm for 1 min. onto the skin-free surface of the cranium of the cerebral cortex of a mouse. At different time points after lesion induction GFAP-luc activity was measured, mice were injected with Evans blue and brains were stained with 2,3,5-Triphenyltetrazolium chloride (TTC).

Results: 24h after induction of the cryogenic lesion, BLI measurement showed that, at the lesion site, GFAP-luc expression was increased 2-3 times over control level and gradually returned to basal after 72h. Evaluation of tissue viability using TTC staining showed that 24h after lesion, the primary lesioned cortex appeared as an unstained white area (dead tissue), whereas, the rest of the brain appeared red (living tissue). Moreover, at the lesion site, i.v. injected Evans blue leaked into the brain tissue, indicative for disruption of the blood brain barrier. This was also visualised in intact isolated brains by Fluorescence Imaging (FLI).

Conclusions: Cryogenic lesion in the GFAP-luc mouse model showed a transient induction of GFAP expression, indicative for astrocyte activation in reaction to neural injury. Brain injury was confirmed by TTC staining and leakage of Evans blue over the blood brain barrier. GFAP-luc mice provide an easy and convenient model to study cryogenic brain trauma.

Acknowledgement: This project was supported by EU-FP7 ENCITE (HEALTH-F5-2008-201842) and Volkswagen Stiftung.

Plaque burden in the APPPS1 mouse picked up with diffusion kurtosis magnetic resonance imaging

Vanhoutte G. , Geys R. , Pereson S. , Veraart J. , Van Broeckhoven C. , Kumar-Singh S. , Sijbers J. , Van Der Linden A. .

University of Antwerp, Belgium

greetje.vanhoutte@ua.ac.be

Introduction:Transgenic mouse models are essential in understanding the pathogenic role of the β-amyloidogenic pathway in Alzheimer(AD).*In vivo* detection of the amyloid deposits in the brain would be beneficial in terms of diagnosis and therapy follow-up.Therefore we investigated the sensitivity of a new method, diffusion kurtosis imaging (DKI), to detect amyloid burden, a correlate for brain damage in AD patients and transgenic $APP_{(swe)}$-$PS1_{(L166p)}$ mice. The use of this model was carefully chosen for its effective amyloidosis in the brain without the occurrence of neurodegeneration, tau-pathology or behavioural changes.All mice of 17months manifested amyloid burden in all brain regions(1).Since previous studies could show different *ex vivo* patterns for mean kurtosis in an APPPS1 mouse model, we hypothesize that the microstructural changes in the brain, due to extracellular amyloid deposits,can be measured *in vivo* by DKI(2). We investigated the neocortical and hippocampal regions linked to the cognitive impairment in AD. Further studies will be conducted to determine the longitudinal effects.

Methods:Experiments were conducted on a 9,4T MR system(Bruker Biospec, Ettlingen Germany). DKI scans were performed on $APP_{(swe)}$-$PS1_{(L166p)}$ mice(n=5) and control WT mice(n=5). The mice were anaesthetized with isoflurane and monitored to maintain physiological parameters. The DKI protocol included 7 b_0-images and 30 gradient directions with 7 b-values (400 to 2800s/mm²) acquired with multi-slice2-shotSE-EPI(TR/TE=7500/24ms,δ=5ms, Δ=12ms,acquisition=96*64, FOV=19,2*12.8mm², slice thickness=0,40mm, NEX=4). Realignment, was carried out by the vision lab (Univ. Of Antwerp) and diffusion kurtosis tensor and diffusion tensor derived parametric maps were computed (Matlab). These include mean kurtosis (MK), radial kurtosis (RK), axial kurtosis (AK), fractional kurtosis anisotropy (KA), fractional anisotropy (FA), mean diffusion (MD), axial and radial diffusion (AD, RD) maps. Regions of interest (cortex and hippocampus) were chosen based on the AD pathology and delineated on grey values of FA, MD and magnitude maps in AMIRA (Mercury Computer systems, San Diego, USA). Differences of diffusion parameters between WT and APPPS1 mice were computed by means of the Mann-Withney non-parametric statistical test in SPSS 16.0 (SPSS Inc. Chicago, USA).

Results: This is the first *in vivo* study on AD mouse models using DKI.Already with a small set of number of animals, we could detect differences according to genotype. MK($p<0.05$), AK($p<0,05$) and RK($p<0.05$) were significantly increased in the cortex of APPPS1 mice as compared to the WT mice. In the hippocampus only RK($p<0,05$) values were significantly increased.Other DTI and DKI derived parameters didn't show significant differences.

Conclusions: Increases in kurtosis parameters reflect the presence of amyloid leading to higher brain microstructural complexity Extracellular amyloid results in interstitial changes which can also lead to impairment of synaptic function(3).Our results reinforce the hypothesis that DKI, which is a characterization for non-Gaussian diffusion distribution, is a more sensitive technique then his predecessor diffusion tensor imaging(4;5). Next to AD, DKI holds further promises in the detection of other neurodegenerative diseases upon changes in brain microstructure.Validation of the link between the presence of amyloid and changes in kurtosis will be represented through immunohistochemical stainings of the same mice of which the analysis is ongoing now.

Acknowledgement: This work is funded by the EC-FP6-poject DiMI (LSHB-CT-2005-512146)

References:

1. Radde R et al., (2006)
2. Falangola MF et al., (2007)
3. Mueggler T et al., (2004)
4. Hui ES et al., (2008) 5) Jensen JH et al., (2005)

P-047

In vivo Imaging of Rat Glioma using the TSPO-ligand [^{18}F]DPA-714

Winkeler A. [1], Boisgard R. [1], Dubois A. [1], Awde A. [1], Zheng J. [1], Ciobanu L. [2], Siquier-Pernet K. [1], Jego B. [1], Dollé F. [1], Tavitian B. [1].

[1] CEA\DSV\I2BM\SHFJ, Orsay, France
[2] roSpinCEA\DSV\I2BM\NeuroSpin,France

alexandra.winkeler@cea.fr

Introduction: In the last years there has been an enormous increase in the development of radioligands targeted against the translocator protein TSPO (18 kDa). TSPO expression is nearly absent in the intact CNS parenchyma but increases rapidly upon inflammation in activated microglia and serves as a biomarker for imaging cerebral inflammation (1). In addition, TSPO has also been reported to be over-expressed in a number of cancer cell lines (2, 3) and human tumours including glioma (4). Here, we investigated the use of the PET-radioligand [^{18}F]DPA-714 (5) as new marker to image glioma *in vivo*.

Methods: 9L rat glioma cells have been stereotactically implanted in the striatum of Fisher, Wistar and Sprague Dawley rats. Dynamic [^{18}F]DPA-714 PET imaging was performed 11-14 days after implantation. The injected dosed was 1.24 ± 0.30 mCi (mean + std). T2w-MRI and/or [^{11}C]Methionine PET were acquired prior to the [^{18}F]DPA-714 PET imaging session in order to monitor tumor growth. The [^{18}F]DPA-714 PET images were then co-registered to the corresponding MRI. For quantitative analysis a volume-of-interest (VOI) analysis was performed on both the kinetic and summed image data sets. In addition, the expression of TSPO 9L rat glioma cells was investigated using Western Blot.

Results: 9L glioma tumors grown in Fisher (n=5), Wistar (n=4) and Sprague Dawley (n=6) rats were imaged by [^{18}F]DPA-714 PET. Tumors grown in Fisher and Wistar rats were also monitored by MRI. All rats showed significant [^{18}F]DPA-714 PET accumulation at the site of tumor implantation compared to the contralateral site. Tthe %ID/cc in Fisher, Wistar and Sprague Dawley rats is listed in the following table:

	control (mean±std)	tumor (mean±std)
Fisher	0.15 ± 0.02%	0.49 ± 0.05%
Wistar	0.13 ± 0.06%	0.35 ± 0.09%
Sprague Dawley	0.11 ± 0.05%	0.26 ± 0.06%

TSPO expression was confirmed by Western Blot in 9L cells *in vitro* and by immunohistochemistry *ex vivo*.

Conclusions: This study demonstrated the feasibility of using the TSPO-radioligand [^{18}F]DPA-714 to characterize 9L glioma *in vivo* in different rat models with PET imaging. [^{18}F]DPA-714 therefore has the potential to become a promising radiotracer to image human glioma.

Acknowledgement: This work has been supported by the 6th FW EU grant EMIL (LSHC-CT-2004-503569) and DiMI (LSHB-CT-2005-512146).

References:

1. Winkeler A, Boisgard R, Martin A, & Tavitian B (2009) J Nucl Med 51, 1-4.
2. Hardwick M, Fertikh D, Culty M, Li H, Vidic B, & Papadopoulos V (1999) Cancer Res 59, 831-842.
3. Starosta-Rubinstein S, Ciliax BJ, Penney JB, McKeever P, & Young AB (1987) Proc Natl Acad Sci U S A 84, 891-895.
4. Black KL, Ikezaki K, Santori E, Becker DP, & Vinters HV (1990) Cancer 65, 93-97.
5. Damont A, Hinnen F, Kuhnast B, Schollhorn-Peyronneau MA, James M, Luus C, Tavitian B, Kassiou M, & Dolle F (2008) Journal of Labelled Compounds & Radiopharmaceuticals 51, 286-292.

A novel 19F MRI-based migration assay: application to primary human dendritic cells

P-048

Bonetto F. [1], Srinivas M. [1], Weigelin B. [1], Cruz Ricondo L.J. [1], Heerschap A. [2], Figdor C. [1], De Vries I.J. [1].

[1] Nijmegen Center for Molecular Life Science, Radboud University Nijmegen Medical Centre, The Netherlands
[2] Radboud University Nijmegen Medical Centre, Nijmegen, , Netherlands

bonetto.fernando@gmail.com

Introduction: The decisive role of dendritic cells (DCs) in inducing immunity formed the rationale for DC immunotherapy: DCs loaded with tumor antigens are injected into cancer patients to stimulate T cells to eradicate tumors. However, success in clinical trials has been limited mainly due to an inefficient migration rate post-vaccination. As DC migration can be affected by several factors, a suitable in vitro assay is required to reproduce *in vivo* conditions. Here we present a novel ^{19}F MRI-based, quantitative assay to measure cell migration in varying chemokine environments in a 3D scaffold specially designed to mimic biological tissue. We obtained migration rates comparable with clinical results (using scintigraphy for quantification) [1] showing the potential application of this assay to simulate different *in vivo* migration conditions. Moreover, we observed that the percentage of migrating cells strongly depends on the initial cell density.

Methods: Primary human DCs were cultured, as per standard protocols for DC vaccination trials [2]. For ^{19}F-labeling, a biocompatible polymer currently in clinical use, poly(D,L-lactide-co-glycolide) (PLGA) was used to entrap a perfluorcarbon tracer. After maturation, cells were harvested, and viability and maturation marker expression determined. The presence of label within the cells was checked by optical microscopy. For migration assays, a variable number of cells were embedded in a fixed volume of a scaffold matrix (cell layer) and a chemokine gradient was created above it. A chemokine-free gel set below the cell layer served as a control. The sample was placed vertically in the MRI scanner and only upward migration was considered to exclude the effects of gravity. Temperature was maintained at 37°. All experiments were performed on a 7T horizontal bore MR system with a ^{1}H/^{19}F volume coil. ^{1}H 2D spin echo images and chemical shift spectroscopy (CSI) were used to track and quantify the migration of 1-15x10^{6} cells. Nine ^{19}F-CSI experiments (1.1 hours each) were sequentially performed in order to keep track of the migrating cells.

Results: Cell migration was assessed by measuring cell movement relative to their initial position above and below the cell-gel layer. Minimal migration was observed in samples with 10-15×10^{6} cells. However, with smaller cell numbers, 5×10^{4} from 5×10^{6} cells (1%) and 2.5×10^{4} from 1×10^{6} cells (2%) were found to migrate up. Migration was found to stop 10 hrs after the start of the experiment. No cell migration was found below the initial cell layer during the whole study for all cell layer numbers, indicating that the upward cell movement was truly caused by the chemokine gradient.

Conclusions: In the present study we showed that ^{19}F-CSI and ^{19}F-MRI can be used to track and quantify cell migration in 3D collagen scaffold assays. The number of cells in the initial cell layer was in the order of the typical cell bolus injection in patients [1] and the migration rates were measured to be in the order of 2%, similar to that obtained in clinical results. The study showed that the initial cell density plays a decisive role in DCs migration, which is important information to optimize cell migration in a clinical setting. Thus, this assay is suitably to simulate *in vivo* clinical conditions, giving the potential chance for detailed analysis of DC migration by MRI.

Acknowledgement: This work was partially supported by NWO (VISTA grant) and ZONMW (911-06-021) for investments.

References:

1. P. Verdijk, T. W. Scheenen, et al.. Int J Cancer 120(5): 978-84 (2007).
2. I. J. de Vries, W. J. Lesterhuis et. al.. Nat. Biotechnol. 23(11), 1407-1412 (2005).

P-049

In vivo magnetic resonance imaging reveals altered migration of endogenous neural progenitor cells following cuprizone-induced central nervous system demyelination

Guglielmetti C. , Praet J. , Vreys R. , Ponsaerts P. , Van Der Linden A. .

University of Antwerp, Belgium

carolineguglielmetti@hotmail.com

Introduction: The Cuprizone mouse model represents a highly reproducible tool to study *in vivo* demyelination and remyelination processes. The time course of demyelination-remyelination during Cuprizone administration has been well characterized and it has been suggested histologically that endogenous subventricular zone neural stem/progenitors cells (NSPC) are recruited during the remyelination process[1]. We tested whether the recently validated in situ NSPC labelling technique with micron-sized iron oxide particles in combination with the transfection agent Poly-L-lysine[2] (MPIOs-PLL) is suitable to visualize NSPC migration towards demyelinated areas.

Methods: 20 C57BL/6 mice (8 weeks old) were used. All mice were injected in the right lateral ventricle with 2 µl MPIOs-PLL (9.1 10^5 particles, 0.67 mg Fe/ml). 10 mice were fed a diet containing Cuprizone (0.2%) during a 4-week period post-injection (p.i). *In vivo* T_2*-weighted 3D-MGE (78 µm isotropic resolution) was performed at 4 weeks (peak of inflammation), 6 weeks (peak of proliferation of NSPC) and 12 weeks (complete remyelination) pi. All images were acquired on a 9.4T Bruker console. 5 animals of each group received an injection of 5-bromo-2'-deoxyuridine (BrdU; 50 mg/kg i.p.) twice a day over a period of 5 days before either the first or the second imaging time point.

Results: MRI revealed hypointense voxels along the rostral migratory stream (RMS) and in the olfactory bulb (OB) for controls. In contrast, for the Cuprizone treated mice, hypointense areas towards the OB were detected only in 2 mice at week 4. From week 6 onward they were detected in both groups. Hypointense voxels are also found in the region of the external capsule (EC) at the ipsilateral side of injection from 4 weeks onward in the Cuprizone treated group. Each MR image is a compilation of 5 consecutive MR slices. Histological analyses are being performed in order to confirm whether the hypointense voxels are MPIO particles in oligodendrocyte-differentiated NSPC.

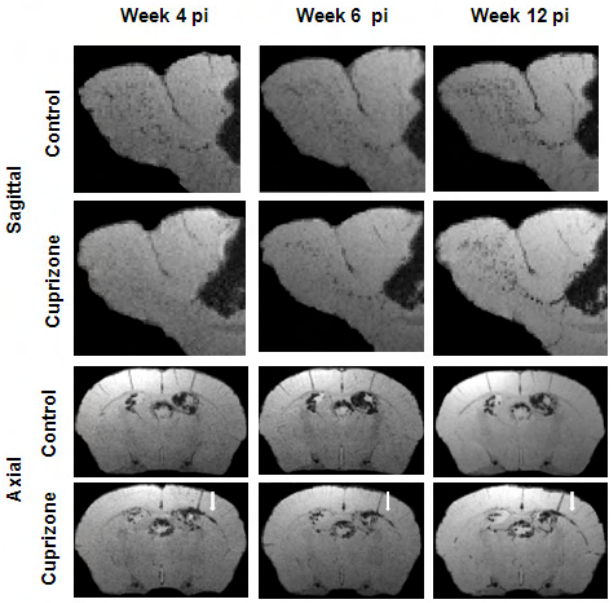

Conclusions: In situ labelling of endogenous NSPC by direct injection of MPIOs-PLL in the lateral ventricle revealed NSPC migration impairment towards the OB, as well as the presence of MPIOs in the EC in the Cuprizone mouse model. Histological analysis is ongoing in order to further characterise migrated MPIO-labelled cells.

Acknowledgement: This work is supported by IWT (SBO/030238), EC-FP6-project DiMI (LSHB-CT-2005-512146) and IUAP-NIMI-P6/38

References:

1. Matsushima G K et al; Brain Pathology, 11: 107-116 (2001)
2. Vreys R et al; NeuroImage 49, 2094-2103 (2010)

Evolution pathways of compartmentalization and distribution of labeling iron-oxide particles in tumor tissue

P-050

Kotek G. , Van Tiel S. , Wielopolski P. , Krestin G. , Bernsen M. .

Erasmus University Medical Center Department of Radiology, Rotterdam, Netherlands

g.kotek@erasmus.nl

Introduction: In our study we addressed the effects and the evolution of SPIO distribution on R2 and R2* values according to specific pathways, such as cell death, cell mixing and cell division. Also we investigated the effects of technical variations in labeling efficacy, cell density, imaging resolution and aggregation of labeling particles. We identify areas for improvement in cell labeling technique and imaging for quantitative cell tracking.

Methods: Brown Norway 175 (BN175) sarcoma cells were labeled with iron-oxide (SPIO) particles. Various intravoxel SPIO distributions were prepared by methods mimicking biologically relevant processes (compartmentalization, mixing, division). R2* and R2 relaxometry was performed at high resolution at 3.0T, iron concentration was measured by optical emission spectrometry. Effects of spatial distribution and compartmentalization of SPIO on relaxivity (dR/dcFe) was analyzed.

Results: We showed that relaxivity is sensitive to variations of cell labeling, cell density and imaging resolution. Our data suggest that intracellular variance of cell division rate potentially lead to breakdown of unique relaxation rate vs. iron concentration relationship. Our results indicate that cell death can be identified by parallel monitoring of R2 and R2* values, and we confirm that R2' differentiates between intracellular and extra-cellular SPIO. We found a unique relaxation rate vs. iron concentration relationship in case of dominance of cell division. Our results suggest that tighter control on labeling variance put in place for stem cell labeling.

Conclusions: We challenge labeled cell quantification by identifying sensitivity of the relaxivity to imperfections of labeling technique and imaging method; besides the numerous complications in quantification, with thorough consideration of limitations and monitoring of biologically relevant factors, quantification is feasible.

In case of mixing labeled and non-labeled cells (likely process in stem cell tracking) a strong control on labeling efficiency is required, since R2*(cFe) and R2(cFe) curves are sensitive to initial intracellular iron content and cell density.

References:

1. Bowen CV, Zhang X, Saab G, et al.
2. Application of the static dephasing regime theory to superparamagnetic iron-oxide loaded cells. Magn Reson Med 2002;48:52–61.
3. Rad AM, Arbab AS, Iskander AS, et al. Quantification of superparamagnetic iron oxide (SPIO)-labeled cells using MRI. J Magn Reson Imaging 2007;26:366–74.
4. Kuhlpeter R, Dahnke H, Matuszewski L, et al.R2 and R2* mapping for sensing cell-bound superparamagnetic nanoparticles: in vitro and murine *in vivo* testing. Radiology. 2007 Nov;245(2):449-57. Epub 2007 Sep 11.

P-051

Acupuncture Works on Endorphins via Activating Stretch-Activated Cation Channels

Liang J. [1], Zhong P. [2], Yang X. [3], Li G. [3], Yang E. [3], Cheung P. [1].

[1] The University of Hong Kong, Hong Kong, Hong Kong
[2] First Affiliated Hospital of Sun Yat-Sen University,
[3] Hong Kong Applied Science and Technology Research Institute Company Limited, Hong Kong

cmleung@eee.hku.hk

Introduction: Acupuncture has been in use for three thousand years in China but was not practiced in the West until the last three decades. Among acupuncture therapies, the acupuncture-induced analgesic effect has been used widely to alleviate diverse pains, particularly chronic pain. To shed light on the 2500-year-old acupuncture analgesia, pain control by acupuncture through Ca2+-regulated release of opioid peptides is proposed.

Methods: 4-week-old C57BL/6N mice were kept in a specially designed holder, with their hind legs and tails exposed during acupuncture. An acupuncture needle (Hwato) 0.4 mm in diameter, 50 mm in length was inserted into the right hind leg, between the tibia and fibula, approximately 5 mm lateral to the anterior tubercle of the tibia. The acupuncture needle was driven by a piezoelectric bending element at 1 Hz. After receiving acupuncture treatment for 40 minutes, animals were sacrificed. Blood samples were harvested from the left ventricle of the heart. Plasma was separated by centrifuging samples at 1000 × g for 15 minutes at 4 ˚C and diluted 1:10 in a sample diluent before assay. The levels of plasmaβ-endorphin were measured using a Mouse β-Endorphin ELISA kit from USCN Life Science. Method for *in vivo* monitoring of Ca2+ excitation in mouse skeletal muscle during acupuncture was described in [1].

Results: Acupuncture was initiated by the stimulation of needle driver describe above in the hind-limb muscle of the mouse. Plasma β-endorphin was measured 40 min after the acupuncture treatment by immunoassay. Elevation of β-endorphin levels is observed (Fig.1b) along with cytosolic Ca2+ activation in muscle fibers *in vivo* (Fig.1a) 40 min after the stimulation is applied. The acupuncture induced β-endorphin secretion is blocked by the intraperitoneal injection of Gd3+, thestretch-activated Ca2+ channels blocker.

Conclusions: These findings suggest that acupuncture analgesia depends on the physiological afferent signal elicited in the mechanosensation pathway. The acupuncture needle manipulation induces a Ca2+-dependent secretion of β-endorphin via interactions with stretch-activated Ca2+ channels. The depolarization-evoked opioid peptide β-endorphin then penetrates the fenestrated capil ary vessels in the pituitary by diffusion, and so enters the general circulation. Our results are in agreement with the studies on endogenous neuropeptide release during electroacupuncture [2] and may lead to new directions for acupuncture analgesia research by unveiling its cellular signal transduction pathways.

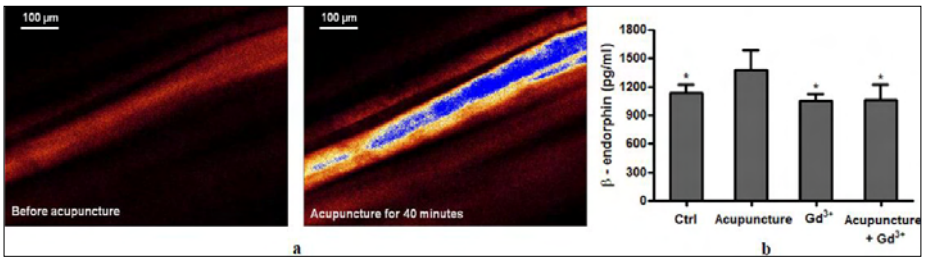

Fig1: Acupuncture stimulates ß -endorphin release via activating stretch-activated cation channels.

References:

1. Liang J.M., Li G., Yang E.S., Cheung P.Y.S. *In Vivo* Monitoring of Ca2+ Excitation in Mouse Skeletal Muscle during Acupuncture. WMIC 2009, p.527. [2] Han J.S. Acupuncture: neuropeptide release produced by electrical stimulation of different frequencies. Trends Neurosci. 26, 17-22 (2003).

Labeling protocols for MRI and optical imaging of human muscle cells precursors

P-052

Libani I.V. [1], Lui R. [1], Martelli C. [1], Clerici M. [1], Fiorini C. [2], Lucignani G. [1], Ottobrini L. [1].

[1] University of Milan, Rescaldina, Italy
[2] Politecnico of Milan, Italy

ilaria.libani@unimi.it

Introduction: The interest about cell-mediated therapy finalized to tissues regeneration research is increased in the last few years. Although numerous protocols which include extraction of stem cells from healthy animals and implantation in diseased models were set up, important parameters such as the distribution and localization of the injected cells, cell survival, proliferation and differentiation cannot be evaluated *in vivo*. Here we refined and tested specific labelling protocols for *in vivo* visualization by MRI, SPECT and Optical Imaging of a human muscle cells precursor cell line as a proof of principle for the application of these procedure to stem cells in the evauation of muscle stem cell mediated treatments.

Methods: Human Skeletal Muscle Cells (HSkMC) were labelled for 24 or 48h with different amounts of Endorem® (0-100–200 µg Fe/mL) in presence or not of Poly-L-Lysine (PLL), Protamine Sulfate (PrS), Polybrene (PB) or infected, with a lentiviral vector [1] carrying Luciferase gene under control of the muscle specific Myogenin promoter (pGZ.Myo.L vector). Labelled HSkMC were analized for viability, iron content (Perl's Staining and spectrophotometer analysis [2]), morphology, differentiation capability or intrarterially (i.a.) injected into NUDE mice for in-vivo imaging by means of MRI, FLI or BLI. Initial cell distribution was also followed with scintigraphy after cell labelling with 111Indium-oxime (60 µCi/106 cells) and gamma counting of explanted organ was performed to validate imaging data *ex-vivo*.

Results: HSkMC incubated for 24 or 48h with 0-100-200 µg Fe/mL did not show significant differences, in terms of viability, between labelled/non-labelled cells in the presence or absence of PLL, PB or PrS (n=3) remaining higher than 84+8% after 24h and higher than 80,6+4,6% after 48h. The percentage of Iron+ cells increased in proportion to the iron content in the medium even if there are not significat differences between CTRL and PLL. In particular we obtained more than 90% Iron+ cells in the samples incubated with 200 µg Fe/mL for 24 or 48h. Intracellular iron content reached the higest levels in the samples loaded with 200ug/ml+PLL: 61,5+2,8 pg/cells after 24h and 114,9+9,6 pg/cells after 48h. For this reason 200 ug/mL endorem+PLL was deemed as the ideal condition for cell labeling for *in vivo* visualisation by MRI. Loaded HSkMC were injected i.a. into NUDE murine model of muscle inflammation. MRI permitted to follow over time HSkMC distribution into the injured muscle. SPECT and BLI of HSkMC not only confirmed celldistribution to muscle but also revealed an early localisation into the lung. HSkMC infected with pGZ.Myo.L, i.a. injected in the same mouse model, were detectable in muscle up to 5 weeks after injection. Interestingly, at this timepoint, the signal is still present only near the lesion area while disappeared in the rest of the body suggesting that this construct could be used to evaluate not only localisation but also the differentiation *in vivo* by means of BLI.

Conclusions: We set up protocols to efficiently visualize human muscle cells precursors localization and differentiation by MRI, SPECT or *in vivo* optical imaging. These protocols will be useful to study the fate of cells once injected into recipient NUDE mice with different techniques and will make it possible to study their behaviour *in vivo* over time. Furthermore, it will be possible to use these instruments for the *in vivo* study of muscular stem cells in restoring skeletal muscles after damage.

Acknowledgement: This work was supported by a Cariplo Foundation grant, the FP6 Hi-CAM project (LSHC-CT-2006-037737) and from the Doctorate School of Molecular Medicine, University of Milan.

References:

1. Naldini L. et al; Science 272(5259):263-7 (1996)
2. Boutry N. et al; Contrast Media Mol Imaging 3(6):223-32 (2008)

POSTER

GENE and CELL based THERAPIES

P-053

Studying molecular processes *in-vivo*: A framework for quantifying variability in molecular MRI

Plenge E. [1], Kotek G. [1], Guenoun J. [1], Doeswijk G. [1], Krestin G. [1], Niessen W. [2], Meijering E. [1], Bernsen M. [1].

[1] Erasmus University Medical Center Rotterdam, Rotterdam, The Netherlands
[2] Erasmus University Medical Center, Rotterdam and Faculty of Applied Sciences, Delft University of Technology, The Netherlands

e.plenge@erasmusmc.nl

Introduction: Quantitative characterization of cellular and molecular processes in-vivo is dependent on consistent image data. To justify conclusions regarding observed biological changes over time, the changes should exceed those attributed to imaging artifacts and inconsistencies. The aim of this work is to establish a framework for quantifying the variability inherent to molecular magnetic resonance imaging (mMRI) protocols.

Methods: Our framework consists of variance maps, variance histograms, visualization and quantification of the precision of expert contouring. To demonstrate the efficacy of our framework we have compared the variability of two different acquisition protocols in the challenging environment of a rodent heart. SPIO labeled stem cells were injected into the myocardium

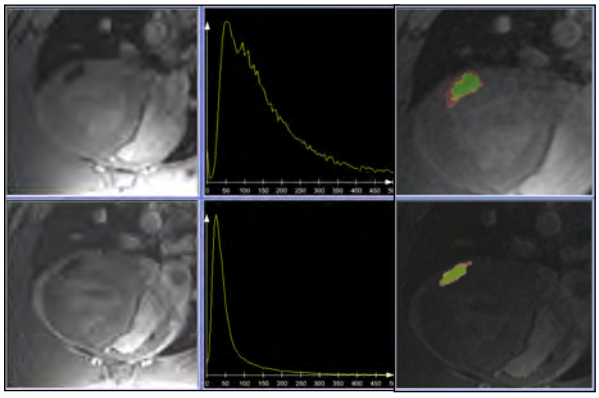

of a rat and cardiac MRI performed. Without moving the anesthetized rat at any point, seven 3D non-triggered images and seven 2D cine sequences were acquired intermittently to capture inevitable changes due to e.g. breathing, coil-heating etc. in both datasets. The assumption was made that no biological changes occur within the acquisition time. After rigid registration of the images in each dataset, the per-voxel variance over each dataset was calculated. Variance maps were generated for visualization, variance distributions for quantification. Three experts manually segmented the cell cluster in each slice/frame of each 3D/cine sequence. The inter- and intra-observer variability was visualized and quantified by a similarity index (SI) [1].

Results: The created framework allows objective quantification of the variability inherent to mMRI protocols. Fig. 1 and table 1 visualize and quantify the variance distribution of the datasets due to imaging inconsistencies, and the inter- and intra-observer variability of the expert segmentation. Through such a quantitative assessment a lower limit on the longitudinal changes in the biological process to be studied can be defined.

Conclusions: We have proposed a framework for evaluating mMRI protocols in terms of variability. The proposed framework allows anyone to objectively assess how well-suited an mMRI protocol is for a longitudinal study of a given biological process.

Acknowledgement: Supported by ENCITE, funded by the European Community under FP7.

	3D	2D cine
Inter-obs. variability, SI	0.70	0.79
Intra-obs. variability, SI	0.56	0.64

Fig1: Top and bottom row shows visualizations related to the 3D and 2D cine datasets, respectively. Left: Slice/frame of each dataset. Middle: Histograms of per-voxel variance of each dataset. Right: Variability among three expert's segmentations of cell cluster (colors represent the number of experts including the voxel in the cell cluster).

References:

1. Pohl KM et al; Med.Img.Analysis, 11:5:465-477 (2007)

Clinically applicable cell tracking by MRI in cartilage repair using Superparamagnetic Iron Oxide (SPIO)

P-054

Van Buul G. , Kotek G. , Wielopolski P. , Farrell E. , Uijtterdijk A. , Bos P. , Weinans H. , Verhaar J. , Krestin G. , Van Osch G. , Bernsen M. .

Erasmus MC, Rotterdam, The Netherlands

g.vanbuul@erasmusmc.nl

Introduction: Cell tracking is a useful tool for optimizing cell-based cartilage repair. Cell labeling using superparamagnetic iron oxides (SPIOs) enables non-invasive *in vivo* cell tracking by MRI, and has already been used experimentally in a clinical setting[1]. We investigated the clinical, intra-articular applicability of this cell tracking technique regarding safety, MRI traceability and label re-uptake.

Methods: Part 1: Human bone marrow stromal cells (hBMSCs) were labeled with SPIO (ferumoxides-protamine sulphate complexes) in a range of 0 - 250 µg/ml. Cell viability was asses-sed and metabolic cell activity was quantified up to seven days. Part 2: SPIO-labeled hBMSCs (100,000 to 5,000,000 cells) were injected ex vivo in pig knees, to mimic a clinically relevant sized model. Furthermore, SPIO-labeled cells (10,000 - 1,000,000 per 75 µl) were seeded in cartilage defects in vitro. Scanning was performed on a clinical 3.0 T MRI scanner. Part 3: To show possible SPIO re-uptake by synovial cells, viable and dead GFP-SPIO double-labeled chondrocytes were seeded on human synovium explants for five days. Samples were analyzed using fluorescence- and light microscopy.

Results: Part 1 Cell labeling and -behaviour: SPIO labeling resulted in labeling efficiencies of approximately 90% and did not negatively affect cell viability or cell proliferation for dosages up to 250 µg/ml. Part 2 MRI traceability: All SPIO-labeled cell dosages, both intra-articular injected or seeded in cartilage defects, were visualized by MRI (Fig. 1). The amount of signal voids was related to the used cell number. SPIO-labeled cells seeded in cartilage defects in vitro could be visualized and quantified using a T2* mapping MRI technique.

Part 3 SPIO re-uptake: GFP+-SPIO+ cells, indicating originally seeded cells, were seen in synovium samples containing living cells. GFP$^-$-SPIO+ cells, indicating SPIO re-uptake by synovial cells, were found in samples containing dead cells.

Conclusions: Although possible SPIO re-uptake by host cells might limit duration of accurate cell tracking, we showed promising results for the use of SPIO labeling for cell tracking in clinical cartilage repair procedures. This approach provides the extra advantage to simultaneously track cells and evaluate cartilage repair in one MRI session.

Acknowledgement: This work is supp. by the Smart-Mix Prog. of the Neth. Min. of Econ. Aff. & the Neth. Min. of Educ., Cult. & Science; and the EC-FP7 project ENCITE (HEALTH-F5-2008-201842).

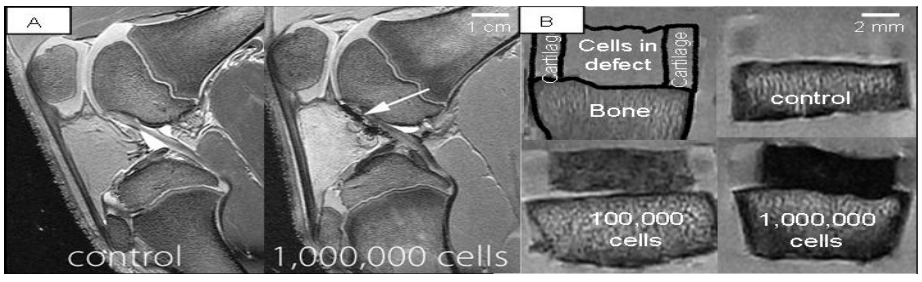

Fig1:Intra-articularinjectedSPIO-labeledcells(1A)andcellsseededincircularcartilagedefectsinavolumeof75 µl(1B)wereaccuratelyvisualizedbyMRI.Theamountofintensityofsignalvoidswasrelatedtousedcellnumber.

References:

1. Bulte JW; AJR Am J Roentgenol. 193(2):314-25 (2009)

P-055

Labeling of HUVEC with different iron oxide particles: An in vitro study about incorporation, distribution, retention and toxicity

Van Tiel S. , Wielopolski P. , Houston G. , Krestin G. , Bernsen M. .

ErasmusMC, Rotterdam, The Netherlands

s.vantiel@erasmusmc.nl

Introduction: For *in vivo* cell tracking it is essential that the cells have incorporated a label so that they can be distinguished from their surroundings in Magnetic Resonance Imaging (MRI)[1-3]. A vast amount of studies have been published dealing with labeling of various cell types with iron oxide nanoparticles. In these studies a large variety of labeling protocols have been described. While for every cell type tested efficient labeling and subsequent detection by MRI[4] has been reported, it is not clear how different labeling protocols may influence labeling efficiency. The purpose of this study was to systematically investigate the effect of variations in dose and duration of labeling on label incorporation, distribution, retention and toxicity using two commonly used types of iron oxide nanoparticles; the so-called SPIO and MPIO particles.

Methods: Primary culture Human Umbilical Vein Endothelial Cells (HUVECs) were grown to 80-90% confluence and labeled with SPIO or MPIO at concentrations ranging from 0 - 100 µg Fe and incubation times of 4-48hrs. Cellular iron load was measured by Inductible Coupled Plasma- Optical Emission Spectrometry (ICP-OES). Cellular localization and retention over time of iron oxide complexes was assessed on cytospin slides. Cell functionality of labeled cells was tested by a tube forming assay. MRI traceability of labelled cells was tested using a 3D-SPGR sequence with TR/TE 41.1/10.5 ms, and a flip angle (α) of 50° with a resolution of 38 µm x 38 µm x 100 µm and a FOV of 2 cm x 2 cm.

Results: Under the conditions tested a maximal iron load of 18.2 pg per cell was obtained for SPIO. A much higher iron load of 661 pg per cell was achieved with MPIO. Inter and intra cellular distribution of label are both strongly dependent on the labeling protocol used. Labeling with high doses and short incubation times may result in large intra-cellular vesicles with multiple iron-oxide complexes. Labeling with low doses and long incubation times may result in small intra-cellular vesicles with just one iron-oxide complex. A better retention of label was observed after short incubation times and high labeling doses. For both MPIO and SPIO higher doses were tolerated at shorter incubation times. At equal incubation times, MPIO was better tolerated than SPIO. In FACS studies, clear changes in forward scatter and side scatter plots, corresponding to changes in cell size and cell granularity respectively were observed following labeling. Both effects were more pronounced after labeling with MPIO than with SPIO. At the highest doses of MPIO tested cell sizes increased 4-7 times in cell volume compared to unlabeled control cells. The effects of SPIO and MPIO labeling on tube forming capacity of HUVECS was tested at all doses that did not significantly affect cell survival. For all these conditions tested HUVECs still displayed tube forming capacity. Sensitive imaging by MRI at the single cell level in vitro was possible for all conditions tested.

Conclusions: HUVECs can be labeled efficiently with SPIO and MPIO, but dose and duration of exposure of cells to the particles strongly influence label incorporation, distribution, retention and toxicity.

Acknowledgement: This research has been done in part through support from ENCITE - funded by the European Community under the 7th Framework program.

References:

1. Bulte JW. Methods Mol Med.124:419-439 (2006)
2. Modo M et al. Mol Imaging. 4:143-164 (2005)
3. Hoehn M et al. J Physiol. 584:25-30. (2007)
4. van Buul GM et al. Contrast Media Mol Imaging. 4:230-236 (2009)

Visualization of aberrant migration in the YAC 128 mouse model for Huntington's disease by *in situ* labelling of neural progenitor cells with iron oxide particles

P-056

Vreys R. [1], Blockx I. [1], Kandasamy M. [2], Nguyen H.H.P. [3], Verhoye M. [1], Aigner L. [2], Van Der Linden A. [1].

[1] University of Antwerp, Belgium
[2] Paracelsus Medical University Salzburg, Austria
[3] University of Tübingen, , Germany

ruth.vreys@ua.ac.be

Introduction: The outcome of a recent validation study of various *in situ* cell labelling strategies is that intraventricular injection of a small number of micron-sized iron oxide particles (MPIOs) in combination with the transfection agent Poly-L-lysine (PLL) is a successful method for the MRI visualization of endogenous neural progenitor cell (NPC) migration in the adult mouse brain[1]. As it was recently reported that NPC migration is impaired in a mouse model of Huntington's disease (HD)[2], we tested if the *in situ* labelling technique using MPIOs-PLL is suitable to visualize aberrant NPC migration in YAC128 mice, a mouse model of HD.

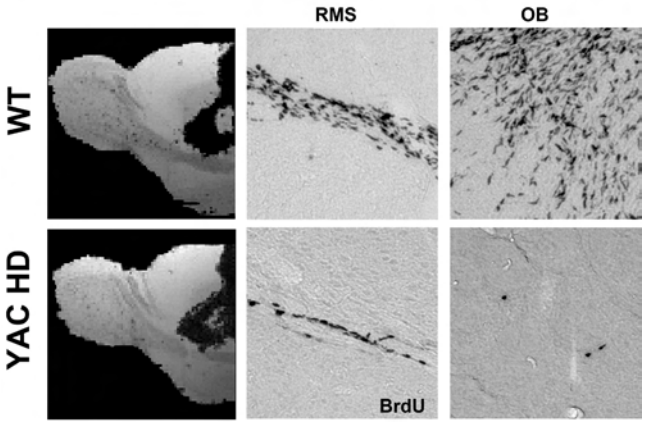

Methods: YAC128 transgenic mice (n=5; 66-69 weeks old) maintained on a FVB/N background and age-matched non-transgenic littermates (n=5; wild-types) were used. Mice were injected intraventricular with 1.5 µl MPIOs-PLL (9.1 x 10^5 particles, 0.67 mg Fe/ml). *In vivo* T_2*-weighted 3D-GE (78 µm isotropic resolution; 9.4T) was performed at 1 week up to 13 weeks post injection. *Ex vivo* T_2*-weighted 3D-GE (66 µm isotropic resolution; 9.4T) was performed on perfused and fixed brains in their skulls. Four days before perfusion, mice received 5 times (every 3 h) an injection of 5-bromo-2'-deoxyuridine (BrdU; 50 mg/kg i.p). Immunohistochemistry was performed for BrdU on 25 µm sagittal sections.

Results: MRI revealed hypointense pixels along the rostral migratory stream (RMS) and in the olfactory bulb (OB) for all wild-types (WT). In contrast, for the YAC 128 mice (YAC HD), hypointense areas towards the OB were detected in only two mice. As neurogenesis is reduced upon ageing, the fraction of MPIO-labelled NPCs was very limited. The first column in the figure shows for both groups minimum intensity projection (mIP) compositions of *ex vivo* MR images comprising the RMS of five animals. The mIP of YAC HD shows less hypointense areas in the RMS and OB compared to the WT. Histological staining for BrdU shows that there are less $BrdU^+$ cells present in the RMS and OB of the YAC HD compared to the WT (figure, second and third column).

Conclusions: In situ labelling of endogenous NPCs by intraventricular injection of MPIOs-PLL revealed aberrant NPC migration towards the OB in the YAC128 mouse model for HD.

Acknowledgement: Supported in part by: IWT (Ph.D. grant; SBO/030238), EC-FP6-project DiMI (LSHB-CT-2005-512146) and IUAP-NIMI-P6/38

References:

1. Vreys R et al; NeuroImage 49, 2094-2103 (2010)
2. Moraes L et al; Neuropathology 29, 140-147 (2009)

POSTER

GENE and CELL based THERAPIES

P-057

Optimization of *in vitro* radiolabeling of mesenchymal stem cells with ^{18}F-fluorodeoxyglucose

Wolfs E. [1], Bormans G. [2], Van Santvoort A. [3], Vermaelen P. [3], Mortelmans L. [3], Verfaillie C. [4], Van Laere K. [3], Deroose C. [3].

[1] K.U.Leuven, Leuven, Belgium
[2] Laboratory for Radiopharmacy, K.U.Leuven, Belgium
[3] Division of Nuclear Medicine, K.U.Leuven, Belgium
[4] Stem Cell Institute, K.U.Leuven, Belgium

Esther.Wolfs@med.kuleuven.be

Introduction: Because of their great differentiation potential and immunomodulatory properties, mesenchymal stem cells (MSCs) are considered to be a potential source for tissue regeneration and immunomodulatory therapy [1-4]. For the optimization of this type of stem cell therapy, novel methods are required to follow the *in vivo* fate of stem cells after injection [5]. Stem cells can be labeled with radioisotopes *in vitro,* such as ^{18}F-fluorodeoxyglucose (^{18}F-FDG), a positron emitting glucose-analogue which is taken up by cells in a similar manner as glucose. After phosphorylation, ^{18}F-FDG is trapped intracellularly, since it misses the 2'-hydroxyl group blocking further steps of the glycolysis pathway. The molecule stays in the cell until its decay [6]. The aim of this study is to optimize the radioactive labeling of MSCs *in vitro* with ^{18}F-FDG.

Methods: Mouse MSCs were obtained from the Stem Cell Institute Leuven, and were seeded in 24 well dishes for uptake experiments. ^{18}F-FDG (5µCi) was added to each well, in the presence of different insulin concentrations, and for uptake kinetics for up to 6 hours. In addition, ^{18}F-FDG washout after labeling was assessed. Additionally, 3 mice were injected with 500 000 ^{18}F-FDG-labeled MSCs, and stem cell biodistribution was investigated with a µPET scanner 10 minutes after injection. Furthermore, a µCT image was acquired for coregistration with the µPET images.

Results: ^{18}F-FDG uptake by MSCs was slightly higher with the addition of insulin (0,01 IU) but with only limited additional effect of higher concentrations. Furthermore, experiments also showed significantly higher ^{18}F-FDG uptake with longer incubation periods, slowly reaching a plateau after 6h of incubation. However, a significant tracer washout could be observed after 1 hour. In addition, *in vivo* µPET experiments with radiolabeled MSCs in mice showed almost exclusive pulmonary activity, confirming the intracellular location of the tracer.

Conclusions: This study demonstrates that mouse MSCs can be successfully labeled with ^{18}F-FDG *in vitro.* Labeling efficiency increases even when very low insulin concentrations are added. Uptake kinetics assessment showed a significantly higher uptake with increasing incubation time for up to 6 hours of incubation. Despite the tracer washout after one hour *in vitro*, *in vivo* µPET studies confirmed the intracellular location of the tracer through an almost exclusive pulmonary signal. Furthermore, *in vitro* labeling with the given dose (5µCi) permits solid imaging of stem cells injected in mice.

References:

1. Caplan A. Adult mesenchymal stem cells for tissue engineering versus regenerative medicine. J Cell Physiol 2007;213(2):341-7.
2. Jackson L, Jones D, Scotting P, Scottile V. Adult mesenchymal stem cells: differentiation potential and therapeutic applications. J Postgrad Med 2007;54(2):121-8.
3. Caplan A. Why are MSCs therapeutic? New data: new insight. J Pathol 2009;217(2):318-24.
4. Jiang Y, et al. Pluripotency of mesenchymal stem cells derived from adult marrow. Nature 2002;418(6893):41-9.
5. Lauwers E, et al. Non-invasive imaging of neuropathology in a rat model of a-synuclein overexpression. Neurobiol Aging 2007;28(2):248-57.
6. Caracó C, et al. Cellular release of [18F]2-fluoro-2-deoxyglucose as a function of the Glucose-6-phosphatase Enzyme system. J Biol Chem 2000; 275 (24): 18489-2000

Responsive MRI contrast agent for specific cell imaging of inhibitory, GABAergic neurons

P-058

Aswendt M. [1], Gianolio E. [2], Kruttwig K. [1], Brüggemann C. [1], Aime S. [2], Himmelreich U. [3], Hoehn M. [1].

[1] Max Planck Institute for Neurological Research, Cologne, Germany
[2] University of Turin, Italy
[3] Katholieke Universiteit Leuven, Belgium

Markus.Aswendt@nf.mpg.de

Introduction: γ-Aminobutyric acid (GABA) is the major known inhibitory neurotransmitter. The rate-limiting step in the synthesis of GABA is the decarboxylation of glutamate by the enzyme glutamic acid decarboxylase (GAD), which exists in two isoforms: GAD65 and GAD67 [1].

We exploited the feasibitity of cell specific contrast generation with the new smart contrast agent Gd-DOTAgad responsive to GAD activity. It consists of the chelate Gd-DOTA coupled to a long hydrocarbon backbone with glutamic acid residues. Upon cleavage of the glutamate moieties the hydration of the paramagnetic metal ion increases, leading to a higher relaxivity.

Methods: Postnatal day 14, Wistar rat tissues were mechanically homogenized, and lysed with cell lysis reagent M-PER (Pierce, USA). After protein determination, same amounts were incubated at 37°C for 24 hours with 1 mM Gd-DOTAgad together with the GAD activator pyridoxal-5'-phosphate. MR measurements were made at 4.7T (Bruker, Germany) using a custom made coil system. The MR phantoms consist of plastic tubes embedded in 1.5% agarose (Fluka, Switzerland). RAREVTR scans (TE=12.0ms, TR=30–250 ms, matrix=128x128; FOV=30.0 mm, resolution=0.234x0.234 mm; slice thickness=2.0 mm). CGR8 murine embryonic stem cells were differentiated in a 3 step protocol using chemically defined media.

Results: Tissue lysates of cerebellum, cortex and liver (as a negative control) were incubated with Gd-DOTAgad. Corresponding controls were Gd-DOTAgad in PBS and tissue lysates without contrast agent. T1 maps calculated from RAREVTR with an in-house software were used to evaluate the change in relaxation rate ΔR1 (Fig. 1A) identifying the highest changes with brain lysates. CGR8 cells were successfully differentiated in a 10 day-lasting protocol resulting in a high proportion of GAD65/67 positive cells, proven by immunocytochemistry (Fig. 1B).

Conclusions: Gd-DOTAgad incubated with tissue lysates leads to enhanced ΔR1 rates in highly expressing GAD65/67 brain regions. A differentiation protocol to obtain GABAergic neurons from ES cells was successfully established. Efficient labelling with Gd-DOTAgad of murine ES and neuronal precursor cells is in progress for evaluation of differentiation induced contrast. With this approach it will be possible to label cells prior to transplantation and to follow their differentiation fate *in vivo* with MRI.

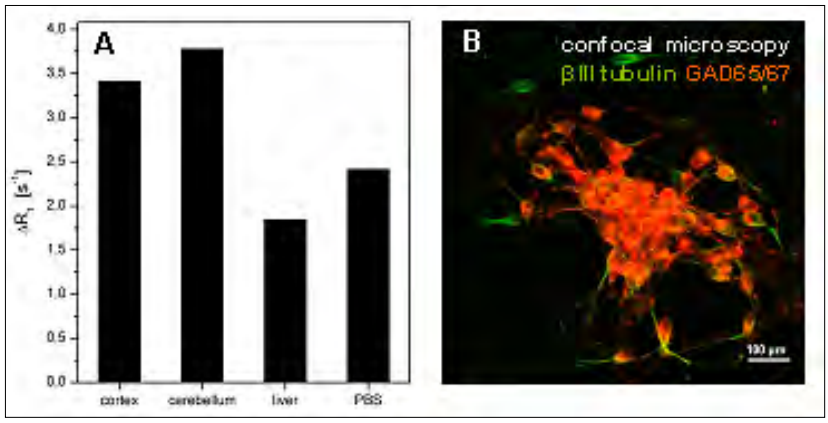

Acknowledgement: This work was supported in part by grants from the European Union under FP6 program (StemStroke, LSHB-CT-2006-037526) (DiMI, LSHB-CT-2005-512146), and under FP7 program (ENCITE, HEALTH-F5-2008-201842).

References:

1. Erlander, M.G., et al., Two genes encode distinct glutamate decarboxylases. Neuron, 1991. 7(1): p. 91-100.

POSTER

PROBE DESIGN

P-059

Novel ultrasound contrast agents for drug delivery

Berti R.P. [1], Freret L. [1], Haiat G. [2], Pisani E. [3], Díaz-Lópeza R. [3], Tsapis N. [3], Pucci B. [4], Fattal E. [4], Taulier N. [1], Urbach W. [1].

[1] Laboratoire d'Imagerie Paramétrique, PARIS, France
[2] Laboratoire de Biomécanique et Biomatériaux Ostéo-Articulaires, France
[3] Laboratoire de Pharmacie Galénique, France
[4] Laboratoire de Chimie Bioorganique et des Systèmes Moléculaires Vectoriels, France

romain.berti@upmc.fr

Introduction: We are working on novel Ultrasound Contrast Agents (UCA) to improve the signal for echographic diagnosis and at the same time to extend their applications as possible drug carriers.

Methods: We have investigated two types of agents:The first one is made of polymer PLGA (Poly Lactic Glycolic Acid) that encapsulates a liquid PFOB (PerFluoro-Octyl Bromide) core. The agent radius can be varied from 150 nm to 10 µm and it remains stable for weeks [1]. The second type is made of a telomer FTAC (fluorinated polymer) encapsulating a fluorinated liquid or gas core. It forms agent with a radius of about 100 nm and are stable over days. The size of both types of agent is weakly polydisperse. In addition, for a better understanding of the relationship between mechanical and ultrasound properties of the above contrast agents, we performed 2D and 3D time domain simulations to compute the acoustic wave propagation in an our UCA solution.

172

Results: We have measured *in vitro* the signal-to-noise ratio, backscattered signal, and destruction by ultrasound waves of the two nano-size ultrasound contrast agents, where the applied ultrasound signal has a frequency of either 5 or 50 MHz. In addition, the comparison between 2D numerical and experimental results shows a good agreement[3], the 3D simulations are still under ways and should permit an improvement of our predictions. Our first tests performed *in vivo* showed that our agents induce a significant enhancement in the backscattered signal. For targeting purpose, the surface chemistry of the first UCA particles type was modified by incorporating phospholipids (fluorescent, pegylated, and biotinylated phospholipids) in the organic phase before emulsification[2]. Microscopy shows that phospholipids are present within the shell and that the core/shell structure is preserved. The functionalization did not modify the echographic signal arising from capsules.

Conclusions: These results demonstrates that these nano and polymeric capsules are suitable ultrasound contrast agent and can be easily modified for targeted therapy or molecular imaging purpose.

Acknowledgement: This work is supported by a grant from ANR (n° NT05-3-42548) and EC-FP6-project DiMI (LSHB-CT-2005-512146)

References:

1. Pisani et al. Adv. Funct. Mater. 18 (2008) 1-9
2. Diaz-Lopez et al. Biomaterials 30 (2009) 1462-1472
3. Haiat & Al, J. Acoust. Soc. Am. 127 1, (2010)

Methods to study the interaction between aptamer probes and cell surface biomarkers

P-060

Cibiel A. , Pestourie C. , Gombert K. , Janssens I. , Thézé B. , Tavitian B. , Ducongé F. .

CEA,DSV,I^{2}BM,SHFJ,INSERMU1023, Orsay, France

agnes.cibiel@cea.fr

Introduction: Aptamers are specific nucleic acids-based ligands selected by an *in vitro* molecular evolution process (named SELEX). Recently, SELEX has been performed against living cells and allows for successful selection of aptamers against a specific transmembrane protein[1] or against cell surface biomarkers without prior knowledge of the target[2]. Here, we compared different techniques to study the interaction between aptamers and their target.

Methods: For the binding experiments, 10^5 cells were first incubated with 5'-^{32}P-labeled aptamers or control sequences for 15 minutes at 37°C and then washed. Bound sequences were recovered in 400µL of lysis buffer and the amount of radioactivity was counted. To optimise this protocol, we evaluated the number of washings and different combinations of unspecific competitors (tRNA, ssDNA and Polyinosine) at different concentrations. This allowed us to determine the protocol that yielded the highest signal/background ratio and to measure the affinity and the Cmax of different aptamers. In addition, an automation of the protocol has been performed. For microscopy analysis, aptamers were first labelled using Ulisys Alexa fluor 546. Then, they were imaged using epifluorescence microscopy (Axio Observer Z1 Zeiss) at different time points during incubation (up to 40 minutes).

Results:We observed that 5 washing cycles during the binding experiments were enough to decrease the background. In addition, we observed that the best combination of competitors seemed to be dependent on the cell type. In contrast, the optimal concentration of competitors was always around 100µg/ml. The use of higher concentrations did not have any effect suggesting that unspecific targets were saturated at this concentration. Finally, the use of competitor during pre-incubation and/or incubation of aptamers had the same impact on the signal/background ratio. Labelling aptamers with different amounts of Ulysis Alexa 546 showed that when the ratio of Alexa/aptamer was increased, fluorescence intensity decreased, due to self-quenching phenomenon. This labelling method has been optimised to study the cellular localisation of aptamers by microscopy. In addition to providing information on the membrane or intracellular location of aptamers (after internalisation), microscopy allowed for evaluation of the kinetics of association between the aptamer and the target.

Conclusions: The use of the above described two methods allowed us to obtain complementary results. Binding experiments led to the quantification of the kD or the number of targets on the cell surface whereas microscopy provided the localisation of the aptamer on the cell surface and its evolution over time. Aptamers selected against cell surface biomarkers could have many applications in the biomedical field (e.g. cell sorting, biomarker discovery, imaging, drugs design, etc.). Our methods can be used to rapidly assess their potential.

Acknowledgements: This work was supported by grants from the European Molecular Imaging Laboratory (EMIL) network (EU contract LSH-2004-503569), the FMT-XCT program (EU contract 201792) and l'Agence Nationale pour la Recherche (project ANR-Emergence ARTIC and ANR-TecSan DOT-IMAGER). AC was supported by a fellowship (Irtélis) from the CEA.

References:

1. Cerchia L et al. (2005) PLoS Biol 3(4)
2. Pestourie C, Tavitian B, Duconge F (2005) Biochimie 87(9-10): 921-930

POSTER

PROBE DESIGN

P-061

MRI intelligent contrast agents as enzyme responsive nanosystems

Figueiredo S. [1], Cittadino E. [1], Terreno E. [1], Moreira J.N. [2], Geraldes C. F. [3], Aime S. [1].

[1] Department of Chemistry IFM and Molecular Imaging Center, Torino, Italy
[2] cLaboratory of Pharmaceutical Technology, Faculty of Pharmacy and Center for Neurosciences and Cell Biology, University of Coimbra, , Portugal
[3] Department of Life Sciences, Faculty of Sciences and Technology, and Center for Neurosciences and Cell Biology, University of Coimbra, Portugal

Saharic@gmail.com

Introduction: When Magnetic Resonance is the imaging modality of choice it is necessary to design highly sensitive systems in order to overcome MRI relatively low sensitivity. We have envisaged an approach to enzyme-responsive agents based on the use of liposomes loaded in the aqueous cavity with a high number of paramagnetic complexes. Liposomes are self-assembled vesicles formed by saturated and unsaturated phospholipids commonly used in drug delivery. The overall relaxation enhancement of solvent water protons depends upon the permeability/disruption of the liposome membrane to water molecules. Our work has addressed the objective of i) modifying the permeability of liposome membrane thus pursuing an enhancement of the observed proton relaxation rate upon the enzymatic cleavage of peptides covalently bound to the phospholipid moieties or ii)promoting the disruption of low relaxivity aggregates formed by the binding capabilities of a macromolecular substrate that is selectively cleaved by the enzyme.

Methods: Paramagnetic liposomes were prepared using the proper membrane by the thin film hydration method followed by extrusion. The lipidic film was hydrated with a 200mM solution of GdHPDO3A, followed by dialysis to remove non-entrapped material. The T1 measurements in vitro were carried out at 0.5T on a Stelar Spinmaster, whereas the *in vivo* measurements were acquired at 7T on a Bruker Avance 300 spectrometer. The temporal evolution of T1 contrast was determined *in vivo* after intratumor injection to mice bearing xenografted B16 melanoma.

Results: i)The relaxometric properties of the liposomes loaded with the lipopeptide was tested in vitro measuring the r1 over time of three samples: a) the suspension of liposomes incorporating the lipopeptide in the presence (I) and absence (II) of MMP1 and b) liposomes incorporating the stearic acid in the presence of MMP1. The results reported indicated that sample I showed a slight increase in the relaxivity likely due to partial instability of the liposome. In the presence of MMP, a more pronounced enhancement was observed. Importantly, the liposomal sample in which the incorporated lipopeptide was replaced by stearic acid did not show any significant enhancement, confirming that the enhancement observed for sample a-I) is related to the MMP1 activity. This different behaviour can be well appreciated by looking at the different contrast exhibited in the corresponding T1weighted MR image. *In vivo* kinetic experiment following the intratumor injection of the lipopeptide-based paramagnetic liposome indicated a rapid washout of the imaging probe, consistent with a relevant release of the Gd(III) complex in the extracellular fluid, where MMPs accumulates. ii) The interaction of anionic liposomes and protamine yields supramolecular adduct with low relaxivity. The action of trypsin causes the digestion of protamine and the consequent de-assembly of the adduct. The process is accompanied by an overall relaxation enhancement as consequence of the recovering of the original permeability of the liposome membrane to water molecules. An illustrative example of the utilization of this responsive probe consists in the entrapment of the supramolecular assembly in alginate vesicles. The detected change in r1 due to trypsin is correlated to the one in the absence of alginate. Thus, an *in vivo* exploitation relies on the entrapment of micron-sized particles into an alginate matrix that has often been considered as a bio-compatible device in cell-based therapies.

Conclusions: We have now envisaged a molecular probe that work as an enzymatic substrate in a particular microenvironment, hence enhancing the MRI signal as a function of enzymatic activity. As further goal, an anti-tumoral drug will be co-encapsulated with the MRI probe, allowing supervise the tumoral therapy.

Standardization of molecular PBCA-microbubbles for routine use

P-062

Fokong S. , Liu Z. , Gätjens J. , Kiessling F. .

Helmholtz Institute, Aachen, Germany

sfokong@ukaachen.de

Introduction: To develop standardized highly monodisperse targeted polybutylcyanoacrylate (PBCA)-microbubbles for contrast enhanced molecular ultrasound imaging.

Methods: PBCA-microbubbles were produced by mechanical agitation and size isolated by centrifugation. Physical parameters of the size optimized microbubbles and regular (Sonovist) microbubbles were compared. Targeting of the microbubbles for molecular imaging was achieved by covalently binding streptavidin molecules onto the shell of surface activated PBCA-microbubbles and the subsequent attachment of biotinylated markers. The amount of targeting ligands on the surface of the microbubbles was quantified using a fluorescence activated cell sorter (FACS). The suitability of these microbubbles for destructive imaging methods like power Doppler ultrasound, used for the evaluation of the degree of angiogenesis and the effect of antiangiogenic therapy, was investigated in gelatin phantoms.

Results: Following a new protocol for the synthesis of PBCA microbubbles, highly monodisperse populations could be isolated. Curves obtained from particle sizer measurements showed size isolated microbubbles which are normally distributed with a narrower standard deviation (> 97% ± 1.0-3.0 µm) in comparison to regular Sonovist microbubbles (> 97% ± 0.2–10 µm). The high monodispersity was also confirmed by SEM (scanning electron microscopy) pictures. The population distribution remained constant even with prolonged storage in solution (over 4 months), indicating high stability. Comparison of the resonance frequencies and the persistence in an ultrasound field showed a significantly lower resonance frequency and a lower persistence in the ultrasound field for the monodispersed microbubbles compared to the polydispersed microbubbles. The high monodispersity was maintained even with covalent coupling of streptavidin molecules onto the shell of the microbubbles. A quantification of the number of streptavidin molecules on the surface by the use of a FACS gave approximately 2 x 10^4 streptavidin molecules per microbubble. This number can be tuned according to the degree of surface activation of the microbubbles. Destructive imaging using SPAQ (Sensitive Particle Acoustic Quantification) [1] was also possible with these monodispersed microbubbles showing a highly reproducible destruction with high mechanical index ultrasound waves.

Conclusions: Size optimized non modified PBCA-microbubbles are more suitable for use as ultrasound contrast agents in comparison to regular Sonovist microbubbles. The simplified synthetic protocol allows for a speed up in the synthesis and purification process (6 days vs. 3 h). The low resonance frequency and persistence lead to more efficient detection using power Doppler techniques. Also, given the relative high number of targeting ligands which can be easily attached to their surface, and the possibility to efficiently quantify their amounts in a region of interest, they are very suitable for molecular imaging of intravascular targets. In summary, the tuned properties of the microbubbles presented in this study, will make them very interesting as building blocks for tailoring of specific contrast agents for ultrasound.

Acknowledgement: This work is supported by the German Federal Ministry of Education and Research (BMBF-0315017).

References:

1. M. Reinhardt, P. Hauff, A. Briel, V. Uhlendorf, M. Schirner, Sensitive particle acoustic quantification (SPAQ), Investigative Radiology 40 (2005) 2-7.

POSTER

PROBE DESIGN

P-063

Novel Gd(III)-based probes for MR molecular imaging of matrix metalloproteinases

Gringeri C. [1], Catanzaro V. [2], Menchise V. [3], Digilio G. [1], Aime S. [2].

[1] Department of Environmental and Life Sciences, University of Eastern Piedmont "A. Avogadro", Alessandria, Italy
[2] Department of Chemisty IFM & Center for Molecular Imaging, University of Turin, Italy
[3] Institute for Biostructures and Bioimages (CNR) c/o Molecular Biotechnology Center (University of Turin), Italy

cgringeri@gmail.com

Introduction: The assessment of the activity of a selected panel of MMPs in a given tissue or anatomical district is very important for the typization and staging of cancer and autoimmune diseases, and for the evaluation of the efficacy of therapies. [1] "Molecular Imaging" is a relatively new and rapidly growing branch of diagnostic imaging devoted to visualize tissue specific patho-physiological processes on the basis of their cellular/biochemical molecular signatures. MRI is one of the most clinically relevant imaging techniques, because of its great spatial resolution (<100 μm with modern high field equipment). We are developing a new procedure for MR molecular imaging of MMP activity, based on β-cyclodextrin/poly-β˜ciclodextrin assemblies, carrying i) a suitably designed, MMP responsive Gd(III)-based MRI contrast agent, ii) a MMP-inhibitor (as the drug); and iii) a vector targeting the region of interest. In this communication, we report about the design, synthesis and characterization of Gd(III)-based MMP responsive probes.

176

Methods: The peptide based ligands have been prepared by solid phase peptide synthesis (SPPS) on an automated synthesizer equipped with a microwave reactor by using the Fmoc chemistry. The hydrolysis of the imaging probes by selected MMPs (MMP-1, MMP-12) has been asseyed by either a spectrophotometric method (based on the chromogenic substrate thiopeptolide) or a relaxometric method. Hydrolysis kinetics have been followed by measuring over time the relaxivity of the probe with/without poly-β˜cyclodextrin. After cleavage, peptide fragments bearing the Gd-chelate are released, and relaxivity is reduced as a consequence of the reduced molecular size.

Results: The CAs developed in this work are based upon a MMP-cleavable peptide functionalized with a Gd(III)-DOTA as the reporter unit, and with a hydrophobic alkyl chain for binding to poly-β-CD. Compound K11 contains the PLGLWAR peptide sequence ending with a C11 alkyl chain. K11 appeared to be poorly recognized by MMPs likely because of the steric hindrance of the DOTA macrocycle directly bound to the Proline residue, known to be essential for MMP recognition.

To make K11 a better substrate for MMP-1/MMP-12 the DOTA moiety has been moved far away from the proline by inserting a GVV tripeptide strip. Furthermore a polyethylenglycol-based spacer between the N-terminal of the peptide and the DOTA unit has been added to increase the hydrophilicity of the molecule (compound K11N). Both K11 and K11N interact with poly-β˜CD with association constants (K_a) of 300 M and 500 M, respectively. K11N can be cleaved by MMP-12/ MMP-1 either in the free form or as the inclusion complex with poly-β˜CD.

Conclusions: These results show that probe K11N can be easily recognized by MMPs, also when interacting with poly-β˜CD, making it possible to use the probe within targeted nanosystems based upon cyclodextrin.

Acknowledgement: This work is supported by FP6 Project NMP4-CT-2006-026668 (MediTrans)

References:

1. Shapiro SD Curr. Opin. Cell Biol. 1998, 10, 602-608.

Functionalization of nanoparticles for molecular imaging; a covalent approach

P-064

Herranz F. [1], Salinas B. [1], Rosell Y. [1], Desco M. [2], Ruiz-Cabello J. [1].

[1] Universidad Complutense de Madrid- CIBERES, Madrid, Spain
[2] Hospital Gregorio Marañón, Spain

fherranz@pdi.ucm.es

Introduction: The key point in the development of new nanoparticles (NPs) for imaging is the surface functionalization. By the attachment of new molecules one should, ideally, provide stability in physiological conditions, with a narrow size distribution and a functional group for the binding of biomolecules. These changes on the NPs surface can be made by weak non-specific interactions or by strong specific covalent bonds.

Methods: Iron oxide nanoparticles were synthesized by the decomposition of organic precursors redendering hydrophobic Fe_3O_4 NPs. These nanoparticles have oleic acid as surfactant, providing excellent size distribution, crystallinity and stability. To transfer the NPs to water the chemical structure of the oleic acid was modified by chemical methods, obtaining water stable NPs ready for further modification.

Results: Fe_3O_4 NPs were synthesized (7 ± 1 nm) by the decomposition of organic precursors. The surfactant of the NPs (oleic acid) was oxidized by means of potassium permanganate in a two phase system. This way we obtained water stable, carboxylic acid functionalized NPs, that were fully characterized (47 ± 4 nm, Zeta potential -46 mV, r_1=4 s^{-1} mM^{-1} and r_2= 115 s^{-1} mM^{-1}, FTIR and ^{1}H-NMR).[1] These NPs are stable in buffer conditions and are being used for *in vivo* MRI. Besides, we took advantage of the carboxylic acid on the surface to covalently funcionalize the NPs with different molecules and dyes, like glucose, EDANS,[2] and streptavidin-alexa647.

Conclusions: Here we report a new approach for the covalent functionalization of superparamagnetic nanoparticles. We demonstrate the usefulness of the method with several examples of covalent functionalization with different molecules and *in vivo* MRI use.

Acknowledgement: This work was supported in part by MAT2008-01489 and SAF2008-0512-C02-01.

References:

1. Herranz, F.; Morales, M. P.; Roca, A. G.; Desco, M.; Ruiz-Cabello, J., Chemistry A European Journal 2008, 14, (30), 9126-30.
2. Herranz, F.; Morales, M. P.; Roca, A. G.; Vilar, R.; Ruiz-Cabello, J., Contrast Media Mol. Imaging 2008, 3, (6), 215-22.

POSTER

PROBE DESIGN

P-065

Comparison of different chelating systems for the synthesis of Ga-68 labelled peptides for molecular imaging using RGD-peptides as model compound

Knetsch P. [1], Petrik M. [1], Rangger C. [1], Griessinger C. [2], Fani M. [3], Wester H.J. [4], Pichler B. [2], Pietzsch H.J. [5], Decristoforo C. [1], Haubner R. [1].

[1] Medical University Innsbruck, Innsbruck, Austria
[2] University of Tuebingen, Germany
[3] University of Freiburg, Germany
[4] Technische Universitaet Muenchen, Germany
[5] Research Center Dresden-Rossendorf, Germany

peter.knetsch@i-med.ac.at

Introduction: Due to its increasing availability Ga-68 attracts increasing interest in molecular imaging with PET. Moreover, due to the straightforward labelling protocols especially for labelling of peptides this is an interesting alternative to F-18 labelling strategies. Here the imaging properties of c(RGDfK) conjugated to different chelating systems are compared.

Methods: Peptides were synthesised using standard SPPS protocols. After cyclisation in solution and selective deprotection of the amino function of the lysine the chelating moieties were conjugated via in situ activation. The chelating systems include 1,4,7,10-tetraazacyclododecane-1,4,7,10-acetic acid (DOTA), a 1,4,7–triaaza-10-oxocyclododecane-1,4,7-acetic acid derivative (B505), 1,4,7-triaazacyclononane-4,7-acetic acid-1-2-glutaric acid (NODAGA), and a tris(2-mercaptoethyl) amine derivative (NS3). Labelling was carried out using the fractionated elution method in sodium acetate or phosphate buffer, respectively. In vitro evaluation included determination of the partition coefficient, protein binding properties, metabolic stability, binding affinity, and cell uptake characteristics. *In vivo* evaluation was carried out using nude mice bearing alpha(v)beta3-positive and alpha(v)beta3–negative tumours. For all tracer biodistribution data were collected. For the most promising also small animal PET imaging was carried out.

Results: All peptides could be labelled with Ga-68 in good radiochemical yields. Labelling of NODAGA-RGD could be achieved even at room temperature. Whereas labelling of NS3-RGD has to be followed by Seppak separation to obtain the product in high radiochemical purity. The compounds showed comparable partition coefficients, binding affinity for the alpha(v)beta3 integrin as well as receptor specific uptake. However, great differences were found in the protein binding properties. Out of the four peptides tested only NODAGA-RGD showed low protein binding. This is also reflected in the biodistribution data. Lowest activity concentration in blood and best tumour/background ratios were found for NODAGA-RGD. Subsequent small animal imaging showed best imaging properties for NODAGA-RGD, which seems to be comparable with F-18-Galacto-RGD.

Conclusions: In this series NODAGA-RGD revealed most promising properties for molecular imaging applications. Easy radiolabelling at room temperature, low amount of protein bound activity and the resulting lower activity concentration found in blood compared to the other compounds makes it to an interesting alternative to F-18-Galacto-RGD for imaging alpha(v)beta3 expression. However, the general advantage of NOTA derivatives for imaging purposes have to be confirmed by additional studies using other peptide structures.

GdDOTA-PIB: a potential MRI marker for Alzheimer's disease

P-066

Martins A. [1], Morfin J.F. [1], Hamplova A. [1], Kubicek V. [1], Suzenet F. [2], Salerno M. [3], Lazar A. [4], Duyckaerts C. [4], Geraldes C. [5], Toth E. [1].

[1] Centre de Biophysique Moléculaire,CNRS, Orléans, France
[2] Université d'Orléans, France
[3] Université Paris 13, France
[4] Hôpital de la Pitié-Salpêtrière, France
[5] University of Coimbra, Portugal

andre.martins@cnrs-orleans.fr

Introduction: Alzheimer's disease (AD) is the most frequent form of intellectual deterioration in elderly individuals, characterized by the brain deposition of amyloid plaques and neurofibrillary tangles. Early detection of the β-amyloid (Aβ) deposits *in vivo* is very difficult. Recently ^{11}C-radiolabeled small-molecules have been developed, capable of entering the brain and specifically targeting amyloid plaques for imaging with PET, such as several Thioflavin T derivatives [1-2]. In particular, the uncharged analogue 6-OH-BTA-1 (Pittsburgh compound B - PIB) is highly efficient both in crossing the BBB and in selective binding to AD amyloid aggregates. A major limitation of PET is the requirement for the markers to be labelled with short-lived isotopes. The use of Aβ marker linked to a MRI CA would constitute an attractive noninvasive *in vivo* imaging approach. Recently, Poduslo used CA aided MRI to image AD plaques with Gd(III)DTPA conjugated to a putrescine-modified human Aβ peptide able to cross the BBB and selectively target individual amyloid plaques in the brain of Alzheimer's disease transgenic mice. Nevertheless, due to its large size, several days (weeks) of incubation with the CA are necessary to obtain the labeling of amyloid plaques in transgenic mouse brain *in vivo*. In an attempt to label Aβ plaques using small metal complexes for the diagnostics of Alzheimer disease, we synthesized a PIB-derivative of DOTA.

Methods: DOTA-PIB was synthesized using a new, versatile strategy. The Gd^{3+} complex has been characterized by relaxometric methods. The compound forms micelles in aqueous solution; the critical micellar concentration has been measured. Experiments on human brain slices have been carried out to assess binding of the compound to the β-amyloid deposits.

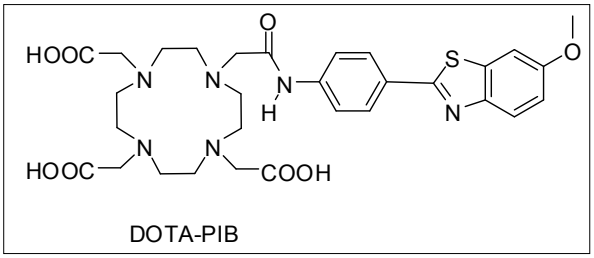

DOTA-PIB

Results: The ^{1}H NMRD profiles evidence aggregation of the GdDOTA-PIB complex in aqueous solution, with a cmc of ~1.5 mM. The preliminary experiments on human brain slices show good binding affinity of the LnDOTA-PIB compound towards the amyloid plaques.

Conclusions: We synthesized and investigated a novel Gd^{3+} complex with good binding properties to β-amyloid deposits.

Acknowledgement: We thank the support from the F.C.T. Portugal (project SFRH / BD / 46370 / 2008 and COST D38.

References:

1. Mathis CA, Bacskai BJ, Kajdasz ST, McLellan ME, Frosch MP, Hyman BT, Holt DP, Wang Y, Huang GF, Debnath ML, Klunk WE. (2002) Bioorg Med Chem Lett.12(3):295-8.
2. Nesterov EE, Skoch J, Hyman BT, Klunk WE, Bacskai BJ, Swager TM. (2005) Angew Chem Int Ed Engl. 26(34):5452-6.

POSTER

PROBE DESIGN

P-067

A comparative study of the self-elimination of *para*-aminobenzyl alcohol and hemithioaminal-based linkers. Application to the design of Caspase-3 sensitive pro-fluorescent probes

Meyer Y. [1], Richard J. A. [1], Delest B. [2], Noack P. [2], Renard P. Y. [1], Romieu A. [1].

[1] University of Rouen, Mont Saint Aignan, France
[2] Quidd: smart molecular imaging, Mont Saint Aignan, France

yvesmeyer@estvideo.fr

Introduction: This study focuses on the disassembly-behavior of self-immolative pro-fluorescent linkers under physiological conditions occurring via an enzyme-initiated domino reaction. The targeted linkers are based on para-aminobenzylalcohol (PABA) or hemithioaminal derivatives of para-carboxybenzaldehyde or glyoxilic acid. We found that a fine tuning of the kinetic properties can be obtained through the modulation of the linker structure, giving either a fast signal response or customizable systems suitable for the design of protease-sensitive fluorogenic probes or prodrug systems.

Methods: Five model compounds bearing specific self-immolative linkers were synthesised and all integrate both: (1) a phenylacetamide moiety to be cleaved by Penicillin G Acylase (PGA) functionning as the triggering agent, and (2) a masked umbelliferone (i.e., 7-hydroxycoumarin) unit to be released as the final product and to elicit turn-on fluorescence. All these fluorogenic probes were incubated at the same concentration (3 µM) at 37°C with PGA (0.12 U) in phosphate buffered saline (PBS, pH 7.5) and the corresponding fluorescence time-courses were recorded at λ = 460 nm.

Results: Comparison of the resulting fluorescence recovery curves clearly indicates that the decomposition of PABA-based self-immolative linkers was faster than with the hemithioaminal counterparts. No nonspecific cleavage of these pro-fluorescent probes was detected in control reactions when incubated only in PBS. These results demonstrate that the use of PABA or hemithioaminal based linkers affords enzyme-reactive pro-fluorophores with high chemical stability. Despite the slower release of umbelliferone from the hemithioaminal probe derived from glyoxylic acid, this linker presents a peptide-like structure able to be readily and widely functionalised.

Conclusions: PABA derivatives will be used for getting fast-response probes whereas the hemithioaminal spacers will be preferred for the construction of finely tunable (bio)functionalised probes. A first generation of Caspase-3 (apoptosis process) sensitive pro-fluorescent probes using PABA linkers has been obtained (AcDEVD-PABA-Umbelliferone) and in vitro fluorescence assay was performed with the corresponding recombinant human protease: 10-fold increase of the enzyme velocity was obtained as compared to the commercially available profluorophore AcDEVD-AMC.

Acknowledgement: This work is supported by CNRS, Quidd: Smart Molecular Imaging and La Région Haute-Normandie.

References:

1. R. Erez and D. Shabat, Org. & Biomol. Chem., 2008, 15, 2669-2672. H. Y. Lee, X. Jiang and D. Lee, Org. Lett., 2009, 11, 2065-2068.
2. C. Fossey, A.-H. Vu, A. Vidu, I. Zarafu, D. Laduree, S. Schmidt, G. Laumond and A.-M. Aubertin, J. Enzyme Inhib. Med. Chem., 2007, 22, 591. C. Fossey, N.-T. Huynh, A.-H. Vu, A. Vidu, I. Zarafu, D. Laduree, S. Schmidt, G. Laumond and A.-M. Aubertin, J. Enzyme Inhib. Med. Chem., 2007, 22, 608.
3. Y. Meyer, J. A. Richard, M. Massonneau, P. Y. Renard and A. Romieu, Org. Lett., 2008, 10, 1517-1520.
4. Y. Meyer, J. A. Richard, B. Delest, P. Noack, P. Y. Renard and A. Romieu, Org. & Biomol. Chem., 2010, In Press DOI: 10.1039/b926316k.

Olefin Metathesis for the functionalization of superparamagnetic nanoparticles

P-068

Salinas B. [1], Ruiz-Cabello J. [1], Desco M. [2], Herranz F. [1].

[1] Universidad Complutense Madrid- CIBERES, Madrid, Spain
[2] Hospital Gregorio Marañón, Spain

besalina@pdi.ucm.es

Introduction: One of the most important points in the synthesis of new nanoparticles (NPs) for molecular imaging is the functionalization of the surface with new molecules. There is a necessity for new approaches, allowing more versatile synthesis and the introduction of biomolecules for specific interactions. This modification of the surface should be done covalently in mild conditions. Olefin metathesis offers many of those features thanks to the new family of catalysts, especially Hoveyda-Grubbs 2nd generation.[1]

Methods: Iron oxide nanoparticles were synthesized by the decomposition of organic precursors redendering hydrophobic Fe_3O_4 NPs, with oleic acid as surfactant. We carried out the olefin metathesis between the double bond in oleic acid structure and methyl acrylate. After the hydrolysis of the ester, water stable dispersion of superparamagnetic nanoparticles were obtained.

Results: Fe_3O_4 NPs were synthesized (10 ± 2 nm) by the decomposition of organic precursors.[2] The NPs were reacted in dry conditions with methyl acrylate in the presence of catalytic amounts (4%mol) of Hoveyda-Grubbs 2nd generation catalyst. After hydrolysis of the ester water stable NPs, with narrow size distribution (30 ± 5 nm) and a Zeta potential corresponding to the introduced carboxylic acid (-46 mV) were obtained. The presence of the new diacid on the surface was confirmed by ^{1}H-NMR and FTIR.

Conclusions: Here we report, for the first time, the use of olefin metathesis for the synthesis of water stable Fe_3O_4 NPs with excellent yield and selectivity. This synthesis opens up the possibility for the attachment of new molecules in one step from the hydrophobic nanoparticles in a mild and selective way.

Acknowledgement: This work was supported in part by MAT2008-01489 and SAF2008-0512-C02-01.

References:

1. Rybak, A.; Meier, M. A. Green Chem. 2008, 1099-1104.
2. Herranz, F.; Morales, M. P.; Roca, A. G.; Desco, M.; Ruiz-Cabello, J., Chemistry A European Journal 2008, 14, (30), 9126-30.

POSTER

PROBE DESIGN

P-069

Pyridine-based lanthanide complexes : towards bimodal agents operating as near infrared luminescent and MRI reporters

Toth E. [1], Bonnet C. [1], Villette S. [1], Suzenet F. [2], Buron F. [2], Shade C. [3], Petoud S. [1].

[1] Centre de Biophysique Moléculaire, CNRS, Orleans, France
[2] Université d'Orléans, France
[3] University of Pittsburgh, USA

eva.jakabtoth@cnrs-orleans.fr

Introduction: Among the state of the art bioimaging modalities, some are characterized by high resolution but low sensitivity (magnetic resonance imaging, MRI) and others by high sensitivity but low macroscopic resolution (optical imaging). Luminescent/MRI bimodal imaging offers the advantage of combining the high resolution of MRI with the high sensitivity of luminescence and the development of contrast agents active for both techniques is of prime importance. Lanthanides offer unique opportunity to develop such bimodal contrast agents given their magnetic and optical properties. Nevertheless, it was long thought that the conditions required for both applications were non-compatible. Here, we report on a versatile pyridine-based scaffold for Ln^{3+} complexation where MRI and near infrared (NIR) luminescence requirements are both satisfied using the same ligand.

Methods: The synthesis of the ligands and the complexes will be briefly described. Potentiometric titrations have been performed to assess to thermodynamic stability of the complexes, together with kinetic measurements to quantify their inertness. To characterize the MRI properties, the exchange rate of the water molecules directly bound the Gd^{3+} was determined by measuring ^{17}O longitudinal relaxation times. Finally the NIR spectra of the corresponding Nd^{3+} and Yb^{3+} were recorded, as well as the lifetimes of the excited states and the quantum yield of the complexes to quantify their luminescent properties.

Results: The bishydrated complexes are found to be thermodynamically stable and the ligands show a significant selectivity for Ln^{3+} over endogenous cations such as Zn^{2+}, Ca^{2+} and Cu^{2+}. The kinetic inertness is also remarkable for such bishydrated complexes. The chelates do not form ternary complexes with endogenous donors which does not limit relaxivity in biological media. All the complexes give rise to NIR emission and the quantum yields are remarkable.[1] They are in the same range as those of non-hydrated complexes optimized for fully protecting the NIR emitting Ln^{3+} for aqueous applications. The modification of the pyridine into quinoline was successful in shifting the excitation wavelength of the system towards higher values.

Conclusions: The pyridine synthon is a prime candidate for the development of bimodal NIR/MRI imaging probes, as the bishydrated Ln^{3+} complexes are thermodynamically and kinetically stable and display a high NIR quantum yield. The successful modification of the pyridine into a quinoline did not modify the thermodynamic properties of the complexes, but it resulted in a shift of the excitation energy towards lower values preventing damages to biological samples and allowing deeper tissue penetration of the excitation photons. The pyridine platform offers also easy routes for coupling the probes to biological vectors and optimizing the MRI properties.

Acknowledgement: This work was financially supported by the Institut National du Cancer, La Ligue contre le Cancer, France, and was carried out in the frame of the COST action D38.

References:

1. L. Pellegatti, J. Zhang, B. Drahos, S. Villette, F. Suzenet, G. Guillaumet, S. Petoud, E. Toth, Chem. Commun., 2008, 6591-6593.
2. S. Comby, D. Imbert, C. Vandevyver, J.-C. G. Bünzli, Chem. Eur. J., 2007, 13, 936.

Delivery of multiple F-18 tracers from a single automated platform (FASTlab™ synthesizer)

P-070

Bhalla R. .

GE Healthcare, Amersham, United Kingdom

rajiv.bhalla@ge.com

Introduction: The majority of F-18 radiotracers prepared in the clinic are synthesized on be-spoke automated rigs, which require modifications (and time) in order to switch to the production of different tracers. The increasing demand to facilitate the production of multiple F-18 tracers from a single clinical site (and preferably from a single Hot Cell) has necessitated the need to develop an easy to use automated platform which can readily accommodate the production of multiple F-18 tracers.

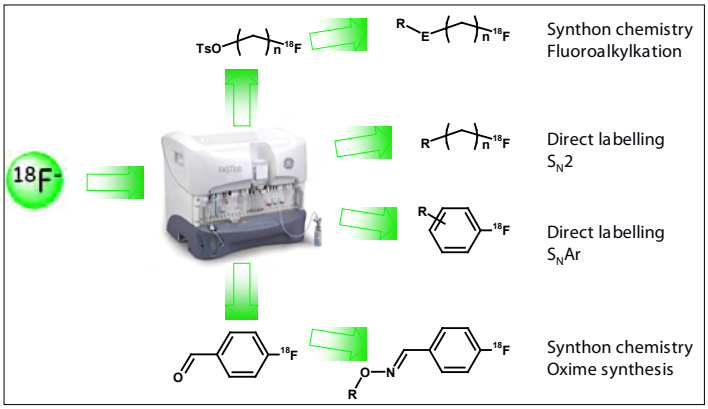

Fig1: Example of radiochemistry on FASTlabTM

Methods: The FASTlab™ is an automated PET radiochemistry synthesis platform incorporating a disposable cassette. The disposable cassette contains a reaction vessel, pre-filled reagent vials and SPE cartridge(s). The FASTlab™ performs transfers (of F-18, reagents, solvents etc) in and out of the reaction vessel using a combinations of syringe drivers, pressure and vacuum – this combination of processes provides a high degree of control, allowing manipulations to be carried out with a high degree of precision and accuracy. The F-18 labelling is preformed in the reaction vessel and subsequent purification is performed either on the cassette using SPE cartridges or externally via a HPLC.

Results: Figure 1 presents a snapshot of some the chemistry which has been successfully transitioned onto the FASTlab™, demonstrating that this platform is capable of accommodating a diverse range of chemistry. Examples of F-18 tracers transferred to the FASTlab™ and currently in use in the clinic will be presented.

Conclusions: FASTlab™ is an automated synthesizer which is capable of producing GMP quality F-18 tracers. We have demonstrated the versatility of FASTlab™ by transitioning a wide variety of chemistry onto the platform to produce a large number of F-18 tracers, many of which are now being assessed in the clinic. We are now focussing on expanding the range of chemistry and the number of tracers available on FASTlab™ (both GE Healthcare proprietary and non proprietary).

POSTER

TECHNOLOGY

P-071

Monte-carlo modelling of a silicon detector insert combined with a PET scanner

Brzezinski K. , Oliver J.F. , Llosá G. , Solevi P. , Linhart V. , Cabello J. , Lacasta C. , Rafecas M. .

Instituto de Física corpuscular, CSIC/Universidad de Valencia, Spain

brzezinski@ific.uv.es

Introduction: Recent works have explored the capabilities of insert devices to improve the performance of clinical [1,2] as well as small animal [3,4] PET scanners. The development of a high resolution probe to be mounted inside a conventional PET scanner to increase its spatial resolution and sensitivity is one of the goals of the EU project MADEIRA. This paper describes the modelling of the MADEIRA set-up using Monte-Carlo (MC) techniques. These techniques are vital for optimizing the configuration of the proposed system by maximizing efficiency and spatial resolution. Furthermore, simulations allow characterization of the system and are useful for modelling its physical response, which can be included in image reconstruction. In the probe-and-ring system, a pair of annihilation photons has several ways of being detected. This work focuses on the classification and quantification of the basic detection modes.

Methods: A preliminary study was conducted to validate the physics models of GEANT4 for the purpose of modelling the silicon (Si) detector probe. One layer of a Si detector was irradiated by a Ba-133 source and energy spectra measured. The full probe-and-ring system was modelled using the MC toolkit GATE (based on GEANT4). The model includes a probe consisting of ten layers of 26x40 pixel Si detectors, with 1x1x1 mm^3 pixels, in coincidence with an existing partial-ring PET scanner with two opposing groups of 12 block detectors. The scanner diameter is 1 m and each partial ring spans 67.5º out of 180º so that it must be rotated to three different positions to cover the full FOV. Each detector block consists of an array of 32 BGO crystals of 6x2x30 mm^3. Initial simulations were run with points sources of 0.1 and 1.5 mCi in the centre of the FOV and the probe at a 50 mm. A temporal resolution of 5 ns was applied. The coincidences were classified as ring-ring and ring-probe; for each type, the contribution of accidental coincidences (randoms) was estimated.

Results: The spectra measured with the Si detector were successfully reproduced by the GEANT4 code. For the full probe-and-ring system, coincidences where constructed using a 10 ns time window. The simulations permitted to quantify the kinds of coincidences as well as to evaluate the sensitivity and random fractions for each type (see table I).

		ring-ring	ring-probe
random fraction (%)	0.1 mCi	0.013	1.3
	1.5 mCi	0.2	15.5
Sensitivity (%)	0.1 mCi	9.7	0.42
	1.5 mCi	9.0	0.39

Table1: Random Fractions and Sensitivities

Simulations are now being carried out with more complex activity distributions. An iterative reconstruction algorithm, based on ML-EM, developed for previous two-dimensional simulations of the MADEIRA system is now being modified to reconstruct the new three-dimensional data.

Conclusions: The goal of a high resolution Si detector probe in coincidence with a conventional PET scanner is improving its spatial resolution and sensitivity. MC simulations of the proposed system have been performed and basic processes quantified. Other types of events such as those with various detections in the probe are now being studied and could potentially be exploited to increase the system sensitivity. The GATE toolkit will be shown to be useful in simulating such a non conventional scanner geometry. The coincidence data is now being applied to reconstruction.

Acknowledgement: Supported by TEC2007-61047

References:

1. Janecek M et al; IEEE Trans Nucl Sci. 53 No.3: 1143-1149 (2006)
2. Zhou J et al; Phys Med Biol. 54:5193-5208 (2008)
3. Wu H et al; J Nucl Med. 49:1668-1676 (2008)
4. Park SJ et al; Phys Med Biol. 52 4653-4677 (2007)

Autofluorescence corrected multispectral red-shifted fluorescent protein tomography

P-072

Deliolanis N. [1], Wurdinger T. [2], Tannous B. [2], Ntziachristos V. [1].

[1] Helmholtz Zentrum Muenchen, Neuherberg, Germany
[2] Massachusetts General Hospital, United States

ndeliolanis@yahoo.com

Introduction: The development of fluorescent proteins (FPs) that operate in the far-red and near-infrared part of the spectrum, enable the macroscopic visualization of FP activity deep in tissues. We demonstrate herein a multispectral fluorescence tomography method that allowed the visualization of labeled glioma tumors in animal brains operating with two-orders of magnitude better sensitivity compared to imaging GFP. We discuss how the detection sensitivity can be improved by at least an order of magnitude using further shifted FP's and the potential of the method for accelerating discovery associated with functional genomics, stem cell research and systems biology.

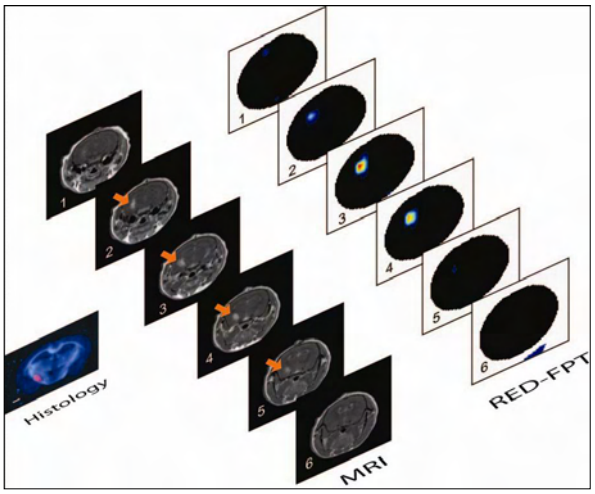

Methods: The method makes use of a novel spectral inversion scheme that integrates three-dimensional image reconstruction and auto-fluorescence correction that works seamlessly in the steep absorption transition from visible to near-infrared. The method is based on non-contact full angular projection Fluorescence Molecular Tomography.

Results: We have successfully imaged mCherry labeled glioma tumors located deep in tissue in animal brains. The results show almost perfect anatomical localization of the tumors that is verified by MRI and histology.

Conclusions: The approach offers therefore the ability for tomographically visualizing the emerging new class of red-shifted fluorescent proteins though entire animals. We discuss how the detection sensitivity can be improved by at least an order of magnitude using further shifted FP's and the potential of the method for accelerating discovery associated with functional genomics, stem cell research and systems biology.

Acknowledgement: This research is supported by a Marie Curie Intra-European Fellowship within the 7th European Community Framework Programme.

References:

1. Shaner, N. C. et al. "Improved monomeric red, orange and yellow fluorescent proteins derived from Discosoma sp red fluorescent protein". Nat. Biotechnol. 22, 1567-1572, 2004.
2. N. Deliolanis et al. "Free-space fluorescence molecular tomography utilizing 360° geometry projections", Opt. Lett. 32 382-384 (2007)

POSTER

TECHNOLOGY

P-073

Acquiring the sample surface from co-registered FMT/MR measurements of a murine tumor model

Dikaiou K. [1], Stuker F. [1], Vats D. [1], Ratering D. [1], Keist R. [1], Klohs J. [1], Ripoll J. [2], Rudin M. [1].

[1] Institute for Biomedical Engineering, Zurich, Switzerland
[2] Institute of Electronic Structure and Laser, Heraclion, Greece

dikaiou@biomed.ee.ethz.ch

Introduction: The combination of MRI and FMT is promising in preclinical imaging, combining the high spatial resolution and soft tissue contrast of MRI for deriving structural and physiological information with high sensitivity of fluorescence imaging for studying molecular targets/interactions. Moreover, MR information can be used as a prior in the FMT reconstruction. The necessary steps to this end are the co-registration of the two datasets, the acquisition and use of the sample surface for reconstructing fluorescence images, and the characterization of different tissue types within the sample. The first two steps are presented here for an *in vivo* measurement.

Methods: We measured nude mice bearing subcutaneous tumors on the thigh flank. 106 colon cancer-derived C51 cells had been injected 9 days prior to measurement. The protease-activatable probe ProSense 680 (VisEn Medical, Bedford, USA) was administered via the tail vein in two doses of 13nmol each, 48h and 24h prior to measurement.

We used a custom-made FMT/MR compatible animal support equipped with an MR transceiver surface coil. Each animal was fixed under anesthesia on the stage and measured on FMT. The optical signal from a 1.5x1.2cm2 ROI around the tumor was collected upon excitation with a 671nm cw laser at 680nm and 720 nm. Thereafter, the stage was inserted into a Biospec 94/30 MR scanner (Bruker BioSpin MR, Ettlingen, Germany) operating at 9.4 T. 14 transversal slices with a FOV of 3.8x1.5cm2 and 1.0mm thickness covering the tumor were acquired with a FLASH sequence (TE/TR = 5/250ms) for high sample/background contrast. The elapsed time between FMT/MR measurements was 30min.

The MR data was automatically segmented according to [1]. Iso-surfaces were determined in order to compute the top surface height map, which was interpolated to match the optical image pixel dimensions. As both the height map and the optical white light image are oriented along yz on the coordinate system, they were used for co-registration. Reference points on the tumor outline were interactively selected to compute an affine transformation between the two images. The co-registered surface was subsequently used in FMT reconstruction.

Results: The co-registered FMT/MR dataset for one mouse is shown, zoomed on the ROI for clarity. The reconstructed fluorescence is plotted on the white-light image. The top surface is shown in green.

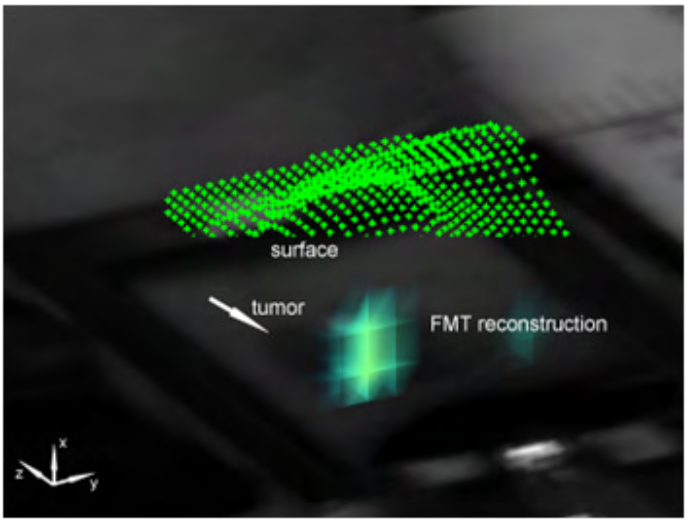

Conclusions: A framework for co-registering FMT/MR data and recording the sample surface was presented. It constitutes an essential step towards full FMT/MR data integration and future use of MR a priori information in the FMT reconstruction.

Acknowledgement: This work was supported financially by the EU FP7 FMT/XCT project.

References:

1. N.Otsu, A Threshold Selection Method from Gray-Level Histograms, Automatica, 1975

P-074

fDOT/ PET/CT imaging of biological processes in tumors

Garofalakis A. , Dubois A. , Kuhnast B. , Dupont D. , Jassens I. , Mackiewicz N. , Dollé F. , Tavitian B. , Ducongé F. .

CEA, Institut d'Imagerie BioMédicale, Service Hospitalier Frédéric Joliot, Laboratoire d'Imagerie Moléculaire Expérimentale, Orsay, France, Metropolitan

anikitos.garofalakis@cea.fr

Introduction: Small animal Fluorescence Diffuse Optical Tomography (fDOT) is a relatively new technology that can provide quantitative imaging of molecular processes. It allows using smart activatable probes which can measure biological processes that are inaccessible using nuclear probes. For instance, fluorescent sensors have been designed to monitor specific proteolytic activities using quenched NIRF probes that become fluorescent when they are cleaved by a protease of interest. In this work, we performed experiments aiming in integrating fDOT imaging of fluorescent probes with PET-FDG and a X-ray micro-CT imaging.

Methods: For performing combined fDOT/PET/CT measurements we have developed a simple approach that incorporates a multimodal mouse supporting system that can fit in all three modalities. We performed multimodal imaging of two processes in a tumour using the fluorine-18- FluoroDeoxyGlycose ([^{18}F]-FDG) and a fluorescent activatable probe. For optical monitoring we used probes for monitoring cathepsin activity and the localization of integrin alpha-v-beta-3 in tumor models by using different commercially available probes (Prosense680, Integrisense680, Visen Medical, USA and AngioStamp, Fluoptics, France). We used as models nude mice bearing a subcutaneous xenograft of two different cell lines, the MDA-MB-231 and the NIH-MEN2A. For the multimodal measurements we followed a protocol that allows for the optimal correlation of the fDOT and the PET data. Each mouse has been firstly measured by PET and was sequentially placed on the fDOT system for optical imaging. Once the mouse was placed in the PET, an intravenous injection of FDG with an activity of 200 µCi was performed and the dynamic PET scan was initiated. Optical measurements were performed 24h after the probe injection.

Results: We reconstructed the 3D cathepsin activity and the localization of Integrin with respect to the tumor volume as given by PET. In the all xenograft models, we observed that the glucose consumption and the fluorescent probes were just partially co-localized in the tumour. Indeed, the [^{18}F]-FDG labelled all the tumour xenograft whereas the fluorescence signal was predominantly located at the base and only partially overlapped with the tumor volume as imaged by µPET.

Conclusions: In this study we explored the potential of integrating information collected by nuclear and optical imaging taking advantage of the unique possibilities that each modality can provide. We found that the activatable probes used are concentrated underneath the tumor predominantly connected to the stroma while the highest glucose consumption appears to be uniformly distributed in the tumour tissue. Cathepsin activity is regulated by complex interactions between extracellular matrix components and cells populating the tumor like stromal cells and therefore it is expected to be reconstructed underneath the FDG signal. We proved that cancer imaging can benefit from the development of dual PET/Optical methods can act synergistically and that can provide complementary information enhancing thus the information collected from a single subject.

Acknowledgement: This work was supported by grants from the European Molecular Imaging Laboratory (EMIL) network (EU contract LSH-2004-503569 and the european program FMT-XCT "Hybrid Fluorescence Molecular Tomography (FMT) – X-ray Computed Tomography (XCT) method and system" contract No 201792.

References:

1. Ntziachristos, V., Ripoll, J., Wang, L.V. & Weissleder, R. Looking and listening to light: the evolution of whole-body photonic imaging. Nat. Biotechnol 23, 313-320 (2005).
2. Weissleder, R., Tung, C.H., Mahmood, U. & Bogdanov, A. *In vivo* imaging of tumors with protease-activated near-infrared fluorescent probes. Nat. Biotechnol 17, 375-378 (1999).

POSTER

TECHNOLOGY

P-075

Deep tissue molecular imaging with fluorescent biomarkers using multispectral optoacoustic tomography. A simulation study

Glatz J. , Deliolanis N. , Schulz R. , Razansky D. , Ntziachristos V. .

Helmholtz Zentrum Muenchen, Neuherberg, Germany

ndeliolanis@yahoo.com

Introduction: Fluorescent protein markers have established themselves as a valuable tool in biomedical research. Their applicability in multispectral optoacoustic tomography (MSOT) has recently been demonstrated with fluorochromes and fluorescent proteins [1,2].

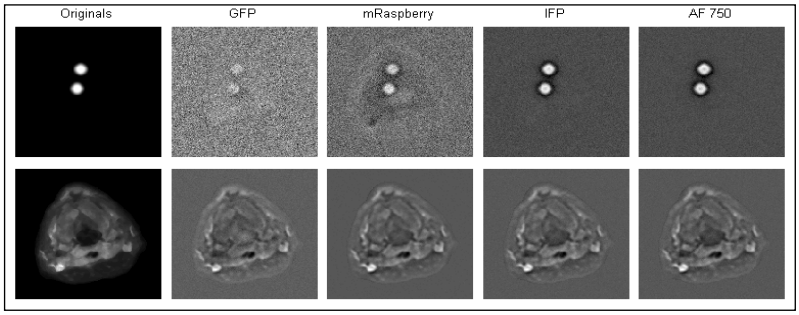

Fig. 1: Unmixing of tissue and protein distribution for simulated data

Methods: A simulation study was conducted for the proteins GFP, mRaspberry, IFP and AF750. Theoretical calculations, based on light and sound propagation models suggests that IFP and AF750 yield an acoustic signal that is acoustic signal that is three orders of magnitude higher than that of GFP. Two protein inclusions of a concentration of 1 μM were simulated in a cervical mouse structure and reconstructed by the backprojection algorithm.

Results: It was shown that the protein concentration can be unmixed using only three multispectral measurements. Using blind source separation techniques this could even be achieved without prior spectral information. The unmixed components of the different proteins are shown in Figure 1. The distinctively weaker signal strength from GFP and mRaspberry is a consequence of the strong tissue absorption in their spectral region.

In order to obtain a stronger signal from the center the reconstructions were normalized for the light fluence inside the sample. From the simulation study the optimal measurement wavelengths could be determined for each protein. Their usage, as well as the blind source separation, was verified in a practical experiment using a tissue mimicking phantom with fluorochrome inclusions.

Conclusions: The new red-shifted proteins can boost the acoustic signal intensity by over three order of magnitude. Protein concentrations can be unmixed in deep tissue and correcting for the light attenuation is an important step towards quantitative unmixing.

Acknowledgements: This research is supported by a Marie Curie Intra-European Fellowship within the 7th European Community Framework Programme.

References:

1. D. Razansky et al. Multispectral photoacoustic imaging of fluorochromes in small animals Opt. Letters, 32, 2891-2893, 2007
2. D. Razansky et al. Multispectral opto-acoustic tomography of deep-seated fluorescent proteins *in vivo* Nat. Photonics, 3, 412-417, 2009

Microfluidic [^{11}C]-carbonylation reactions for the rapid synthesis of radiolabelled compounds for PET

P-076

Miller P. [1], Audrain H. [2], Bender D. [2], Demello A. [1], Gee A. [3], Long N. [1], Vilar R. [1].

[1] Imperial College London, London, United Kingdom
[2] Arhus University Hospital PET Centre, Denmark
[3] GSK, United Kingdom

philip.miller@imperial.ac.uk

Introduction: The synthesis of 11C compounds for PET requires fast and specialised chemical techniques owing to the short half-life of the 11C radioisotope (t1/2 = 20.4 min) and sub-micromolar reaction scales. [1] Microfluidic reactors are emerging as a valuable technology for the rapid and small scale synthesis of short-lived radiopharmaceuticals for PET imaging. [2] The palladium mediated 11C-carbonylation reaction is a highly versatile route for the preparation of a wide range of 11C-carbonyl compounds[3], however, the low molecular concentrations of 11CO coupled with its poor solubility in organic solvents make this a particularly challenging transformation. Here we report the application of a microfluidic reactor for improving the synthesis of 11C labelled amide and ester molecules via the palladium mediated 11C-carbonylation reaction.

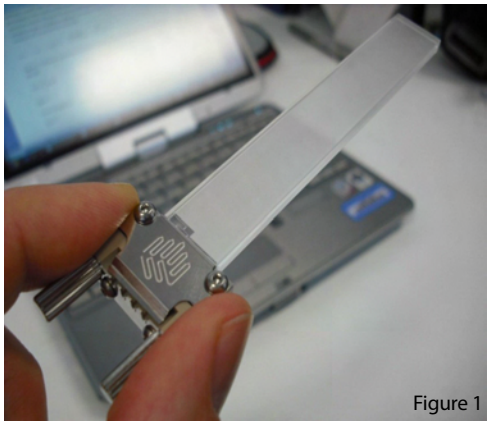

Figure 1

Methods: The microfluidic reactor (figure 1) was fabricated from glass using chemical wet etching techniques and contains two inlets, one outlet and a 5 metre long reaction channel. A simple mixing tee motif is used bring the gas and liquid reagents into contact with each other. The palladium mediated 11C-carbonylation reaction of a range of aryl halides was investigated (scheme 1). In a typical 11CO labelling experiment the coupling reagents (aryl halide, palladium catalyst and amine) were premixed and loaded into a 50 uL loop on an injector port. 11CO, produced via the high temperature reduction of 11CO2 over Mo, was preconcentrated and trapped onto molecular sieves. The coupling reagents were injected into the microfluidic device while at the same time 11CO was released from the molecular sieves and passed into the device for reaction.

Results: The total reaction and processing times for a typical reaction, including trapping and release of 11CO, was 15 min from end of bombardment. A series of amide and ester molecules were labelled with 11C using our microfluidic reaction system (scheme 1). Radiochemical yields (RCY) of labelled products were found to be dependent on the type of aryl halide and nucleophile used for the reaction. Generally, iodoaryl substrates with activating groups (CF3 or CN) gave consistently higher RCYs (>80%) and radiochemical purities (>95%) than aryl halide substrates with deactivating groups (OCH3).

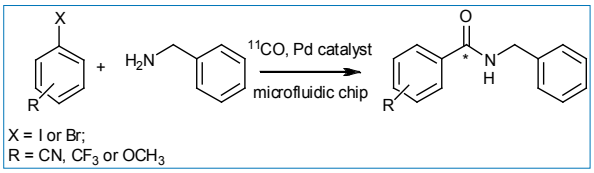

Scheme 1

Conclusions: A glass fabricated microfluidic device has been used to effectively perform high speed 11CO radiolabelling reactions. The larger surface area-to-volume ratio within the microfluidic reactor improves the gas liquid contact area and is thought to enhance the problematic CO insertion step of this reaction.

Acknowledgement: PWM is grateful to the EPSRC for the awardofaLifeSciencesInterfacefellowship(EP/E039278/1).

References:

1. P. W. Miller et al., Angew. Chem. Int. Ed., 2008, 47, 8998.
2. P. W. Miller, J. Chem. Technol. Biotechnol. 2009, 84, 309.
3. B. Langstrom et al., J. Labelled Compd. Radiopharm., 2007, 50, 794.

POSTER

TECHNOLOGY

P-077

Boosting image quality in low-dose RC-gated 5D cone-beam micro-CT

Sawall S. [1], Bergner F. [1], Lapp R. [2], Mronz M. [2], Karolczak M. [1], Kachelrieß M. [1].

[1] Institute of Medical Physics (IMP), Erlangen, Germany
[2] CT Imaging GmbH, Erlangen, Germany

stefan.sawall@imp.uni-erlangen.de

Introduction: Micro-CT imaging of the animal heart typically requires respiratory and cardiac (RC) gating. This can either be done prospectively or retrospectively. For functional imaging, and for multi-modality imaging, it is often desired to obtain the full 5D information (volumetric + respiratory + cardiac) and retrospective gating is the method of choice. The amount of information available to reconstruct one volume for a given respiratory and cardiac phase is significantly lower than the total amount of information acquired. For example the reconstruction of a volume from a 10% wide respiratory and a 20% wide cardiac window uses only 2% of the data acquired. Achieving a similar image quality as a non-gated scan would typically require to increase the dose by a factor of up to 50. Our aim is to provide similarly high image quality at low dose levels (100 to 500 mGy).

Methods: We implemented a two-step iterative image reconstruction algorithm based on the McKinnon-Bates approach. The first step, aiming at R gating only, uses a prior image consisting of the reconstruction of all data. The RC gating step uses the image of the first step as a prior. An edge-preserving anisotropic diffusion filter is applied to the volume data after each iteration to perform spatial and temporal resolution-preserving noise reduction in up to five dimensions. We demonstrate our new reconstruction approach using mouse data scanned with a dedicated in-vivo micro-CT scanner (TomoScope Synergy, CT Imaging GmbH, Erlangen, Germany). We derived an intrinsic gating signal (kymogram) from the rawdata to synchronize our reconstruction. The scan itself consisted of ten rotations with 7200 projections in total. The scan time was five minutes, the tube voltage 65 kV. The gating window widths were set to 10% in the respiratory and to 20% in the cardiac cycle.

Results: Although the mouse data available to us shows only an untypically low enhancement of about 110 HU (blood vs. myocardium) our approach yields an image noise of as low as 35 HU while preserving the spatial resolution of about 100 µm. We also performed a standard RC-gated reconstruction. Its high noise levels of about 170 HU are prohibitive and significant artifacts are observed due to sparse view sampling.

The dose of our protocol is about 500 mGy. Reconstructions using less than the available 10 rotations show that one can achieve good image quality in RC-gated micro-CT with about 100 mGy, provided that the contrast agent delivers sufficient contrast.

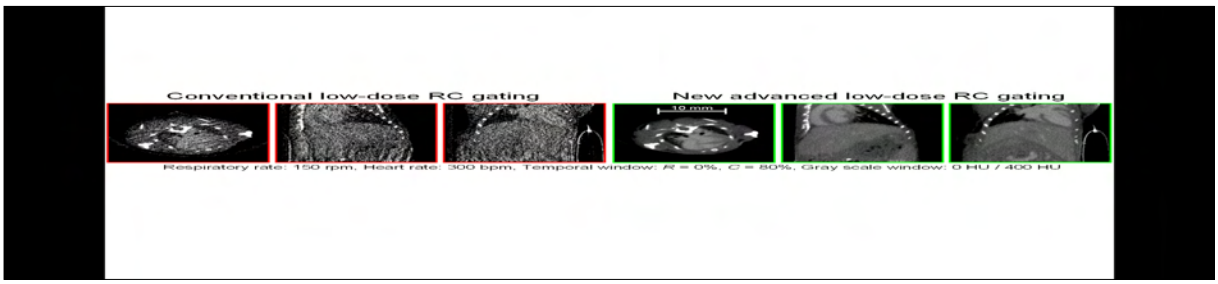

Conclusions: Using advanced image reconstruction techniques enables us to perform high fidelity low-dose double-gated imaging of free breathing small animals.

Acknowledgement: This work was supported by the Deutsche Forschungsgemeinschaft (DFG) under grant FOR 661.

Methodological approach using microscopy for quantitative evaluation of neo-angiogenesis and tumour progression in pre-clinical cancer models

P-078

Thézé B. , Beynel A. , Chapotot L. , Boisgard R. , Tavitian B. .

CEA /Inserm 1023, Orsay, France

benoit.theze@cea.fr

Introduction: *In vivo* molecular imaging methods can localize sites of angiogenesis and obtain functional data, whereas microscopic methods provide their highest resolution on preserved tissue specimens. To bridge the gap between molecular imaging methods and microscopy, we developed a method to evaluate neo-angiogenesis and tumour volume on formalin-fixed tissues samples.

Methods: In order to visualize the mammary tumour vessels density in the MMTV-PyMT transgenic model of mammary carcinoma, mice were injected i.v. with Horse Radish Peroxidase (HRP)– tomato lectin (at 6.66 g/kg), which binds surface glycoproteins of red blood cells and endothelial cells inside the vascular lumen. Tumours were immediately sampled, fixed in formalin and frozen. For this pilot study, four tumours from each of two mice were sectioned every 300 µm . For every section, HRP-lectin was revealed with 3,3´-diaminodbenzidine (DAB) and the tissues were counterstained with haematoxylin. Panoramic views of each tissue section were acquired in bright-field with a motorized AxioObserver Z1 Zeiss microscope. Tissue staining and image acquisition parameters were standardized for quality control. Using imageJ image analysis software, a macro was developed: (i) to separate blue and brown colours from the RGB original image using the colour deconvolution plugin in batches of images, and (ii) to evaluate the area occupied by the tumour in the whole sample. A treatment pipeline was designed with the Cellprofiler software for threshold and segmentation of vessels (brown) versus tumour masses (blue). Object-based filtering was applied to vessels according to their size and to their localization inside or outside of the tumour masses in order to separate neo-vessels from pre-existing vessels and areas of necrosis.

Results: Using this approach, we were able to measure areas occupied by vessels and tumours and, (i) to obtain an estimate of neo-angiogenesis defined as the ratio between tumour blood vessels' volume and tumour volume (1.27% ± 0.61%), (ii) to determinate the real volume of tumour in the sample (75% ± 7%), which also contain muscular, adipose and conjunctive tissue, (iii) to obtain the ratio between total blood volume and total sample volume (5.99% ± 0.42%), and (iiii) to discriminate between small (55% ± 9.6%), medium (32% ± 2.8%), and large (12.9% ± 7.8%) blood vessels.

Conclusions: The data from this feasibility study provides morphological information about the vascular network in the PyMT model. Further validation steps should now allow correlating the results with functional information obtained by PET imaging, and provide a method for the evaluation of anti-angiogenic drugs in animal tumour models.

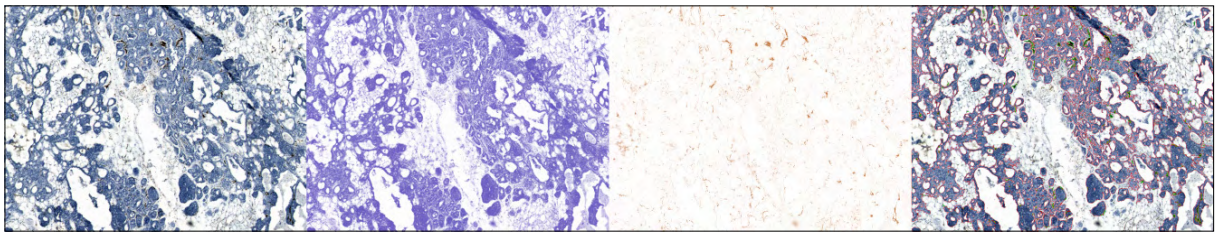

Fig1 from left to right: original image, blue and brown colour deconvolved images and final segmented image

Acknowledgement: This work was supported by the 6th FW EU grants EMIL (LSHC-CT-2004-503569) and DiMI (LSHB-CT-2005-512146)

References:

1. Rasband, W.S., ImageJ, U. S. National Institutes of Health, 1997-2009
2. Jones TR et al. (2008) CellProfiler Analyst: data exploration and analysis software for complex image-based screens. BMC Bioinformatics

POSTER

TECHNOLOGY

P-079

Changes of heart stroke volume index established by ^{99m}Tc MIBI GSPECT scintigraphy after radioiodine treatment of patients with subclinical hyperthyroidism

Kaminski G. , Podgajny Z. , Szalus N. , Bilski M. , Dziuk M. .

Military Institute of Health Services, Warsaw, Poland

gkam@wim.mil.pl

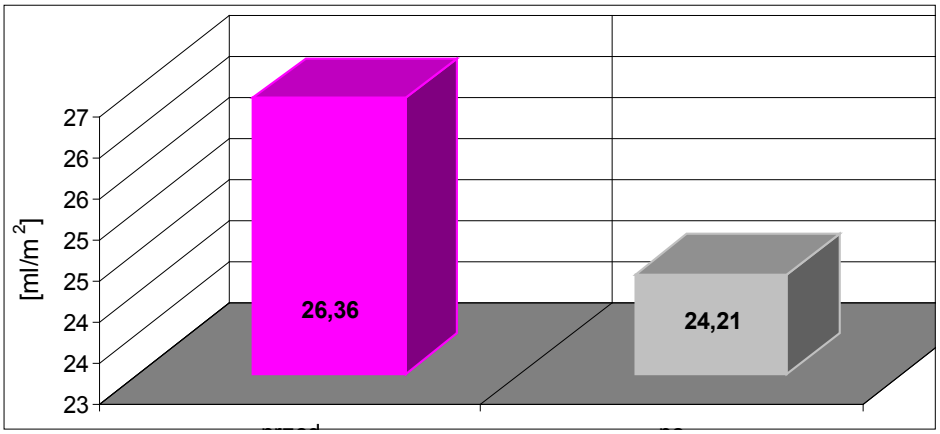

Fig.1. Mean values of SVI before (left) and after (right) radioiodine treatment p = 0,042)

192

Introduction: Stroke volume index (SVI) is an indicator of heart load. Increased heart load is one of causes of cardiac death. Subclinical hyperthyroidism (SH_{yper}) increases mortality mostly due to cardiovascular events. SH_{yper} affects about 1% of population including patients with cardiovascular diseases. The aim of the investigation was to estimate an influence of cure with radioiodine of SH_{yper} on heart stroke volume index (SVI) measured by heart scintigraphy - ^{99m}Tc MIBI GSPECT.

Methods: 44 patients (37 women, 7 men) aged 45.9±11, with 12.8±9.8 month history of only autonomous SH_{yper} (TSH=0.16±0.1 IU/l), were examined with ^{99m}Tc MIBI GSPECT twice: before and 5.7±4.2 months after TSH normalization (TSH=1.32±0.1 IU/l) after radioiodine treatment (at dose 12.1±5.7 mCi) . The radioiodine (^{131}I) and ^{99m}Tc MIBI were carried by POLATOM/Poland. The average time between examinations was 12.5 ± 6 months. The Local Ethical Committee approval for this investigation has been obtained.

Results: The cure of SH_{yper} caused decrease of SVI from 26.36 to 24.21 ml/m^2 (p=0.042)

Conclusions: Cure of autonomous subclinical hyperthyroidism with radioiodine decreases heart load. This finding indicates to treat subclinical hyperthyroidism, especially in patients with cardiovascular diseases.

References:

1. Parle J.V., Maissoneuve P., Sheppard M.C., Boyle P., Franklyn J.A.: Prediction of all- cause and cardiovascular mortality in elderly people from one low serum thyrotropin result: a 10 -year cohort study.
2. Lancet, 2001, 358: 861 - 865.

PET/CT investigations with 68Ga-DOATATE in neuroendocrine tumors - first clinical experience

P-080

Kunikowska J. [1], Krolicki L. [2], Pawlak D. [3], Kobylecka M. [2].

[1] Medical University of Warsaw, Poland
[2] Medical University of Warsaw, Poland
[3] IEA POLATOM, Świerk, Poland

jolanta.kunikowska@wum.edu.pl

Introduction: Neuroendocrine tumors (NETs) have distinct biological and clinical characteristics, in particular a high density of somatostatin receptors at the cell membrane. It is this property that allows the use of radiolabeled somatostatin analogs for imaging of these tumors. Novel techniques PET/CT with 68Ga-DOTATATE open new possibilities in the diagnosis of patients with NET. Sensitivity of that techniques is depending on SSTR expression, but average range is 60-94%.

The aim of this study was to evaluate the diagnostic usefulness of a new somatostatin analog, 68Ga-DOTATATE, for PET/CT in patients with diagnosis of neuroendocrine tumors.

Methods: 55 patients with NET were examined (24 men, 31 women; age range, 18-86 y; mean age +/- SD, 51.4 +/- 12.5 y). For analysis, patients were divided into 3 groups: detection of unknown primary tumor (n = 13 patients), follow-up after surgery (n = 23 patients), staging of disease (n= 19). PET imaging was performed on PET/CT scanner Biograph 64, 60 minutes post injection of 120-185 MBq 68Ga-DOTATATE.

Results: In the group patients with unknown primary tumors, 68Ga-DOTATATE revealed 9 primary foci. 7 were not visible in CT (4 in intestinum, 3 in pancreas) and 2 foci observed in CT and PET/CT - small nodule in lung. In 4 cases primary tumors were not found.

In the cases of patients after surgery, examination shown new foci in 5 patients (liver-3, lymph nodes in abdominal cavity-2, peritoneum-1, pancreas-1).

In the group of staging of disease in 12/19 cases PET and CT shown the same foci. In 7/19 (37 %) patients in 68Ga-DOTATATE examination was revealed new lesions (intestinum-1, liver-3, bone-1, pancreas-4, lymph nodes in abdominal cavity-2)

Conclusion: Results of our study shown that 68Ga-DOTATATE PET/CT is very useful non-invasive techniques in diagnosis of patients with NET. 68Ga-DOTATATE PET/CT examination should be performed for staging and restaging of disease and it gives more clinically useful information than CT.

POSTER

ENDOCRINE DISEASES

P-081

Influence of number of subsets and iterations of Ordered Subsets Expectation Maximization (OSEM 3D Flash) reconstruction on quantitative assessment of small and medium detected lesions in SPECT study with used in ^{99m}Tc[EDDA/HYNIC]Octreotate for patients with GEP-NET

Lenda-Tracz W. .

Nuclear Medicin Unit, Krakow, Poland

wtracz@su.krakow.pl

Introduction: The algorithm OSEM 3D Flash generally is the most appropriate available method of reconstruction. The choice of appropriate sets of OSEM 3D Flash reconstruction is crucial in interpretation of scintigraphy images. The number of subsets and iterations significantly influences the lesion to noise ratio. Therefore the aim of the study was to find the optimum number of subsets and iterations which present the most effective lesion to noise ratio in quantitative assessment of small and medium lesions detected with the use of ^{99m}Tc[EDDA/HYNIC]Octreotate.

Methods: The results of 20 patients with confirmed neuroendocrine tumors (GEP-NET) were analyzed. SPECT studies, acquisition 3-4 h after injection of 740 MBq ^{99m}Tc[EDDA/HYNIC] Octreotate, were performed. The E.CAM 180 (Siemens), double-head gamma-camera, was equipped with parallel, low-energy, high-resolution collimators. Data were acquired with 180 rotation with 128 non-circular projections (30s per view) using a 128x128 matrix with 1.23 zoom. OSEM 3D Flash reconstruction (subsets number 8, 16, 32 for 2-30 iterations) was performed.

Results: Lesion to noise ratio in voxels was analyzed for different setting combinations (n,m) of number of subsets (n) and iterations (m) of OSEM 3D Flash reconstruction. An increasing number of subsets and iterations influences the increasing values of lesion to noise ratio. No difference for settings (16,m) and (32,m) was observed for quantitative assessment of small and medium lesions detected. Differences between lesion to noise ratio were observed in a group with 8 subsets (8,m). However, the quality of images is variable for all setting combinations (n,m).

Conclusions: The high number of subsets improves the image quality and the images are smoother. The increasing number of iterations on the one hand gives a little better contrast but on the other hand the shape of the lesions and organs is sharper. In spite of the fact that the image quality is changed with the increasing number of subsets and iterations, for quantitative assessment only (8,m) setting is changed significantly. Therefore, for quantitative assessment the best choice is setting with 8 subsets and 2-30 iterations but at least 6 and no more than 22 iterations with step equal at least 4 iterations. The appropriate number of iterations depends on the image quality assessment.

The precise localization of metastatic lesion with used SPECT/CT with CoDe system after 131I – MIBG therapy in patients with disseminated pheochromocytoma

P-082

Szalus N. [1], Podgajny Z. [2], Kaminski G. [3], Mazurek A. [1], Giżewska A. [1], Dziuk E. [1].

[1] Department of Nuclear Medicine,Military Institute of Medicine, Warsaw, Poland
[2] Department of Endocrinology and Radioisotope Therapy2 - Military Institute of Medicine, Warsaw, Poland
[3] Department of Endocrinology and Radioisotope Therapy - Military Institute of Medicine, Warsaw, Poland

nszalus@wp.pl

Introduction: Pheochromocytoma is a rare tumor that originates from chromaffin cells such as the adrenal medulla and sympathetic ganglia. Malignant pheochromocytoma is uncommon, and metastases typically affect the bones, liver, lungs, and lymph nodes. Meta-iodo-benzyl guanidine (MIBG) is a norepinephrine analog, and 131I- and 123I-MIBG have been widely used for the diagnosis of pheochromocytoma. This technique has high specificity and detectability not only for primary tumors but also metastatic lesions when compared with morphologic imaging such as computed tomography (CT) and magnetic resonance imaging (MRI). Co-registered data have been shown to be useful in the evaluation of patients with cancer at diagnosis and staging, in monitoring the response to treatment, and during follow up, for early detection of recurrence. Gamma camera with CoDe system is a new modality to the PET/CT and SPECT/CT imaging to the precise localization metastatic lesions.

Aim of study: The aim of this study is to investigate the precise localization 131-MIBG with used SPECT/CT CoDe system for metastatic diseases in patients with malignant pheochromocytoma.

Material and methods: Two patients with disseminated pheochromocytoma (the first patient with metastases to the liver, bones and lung; the second with metastases to the bone) were referred for study. Routine whole body scan with I-131 was performed with a dual head gamma camera (Infinia Hawkeye General Electric Milwaukee with CoDe system, USA) using a large field of view with high energy collimator a 20 % energy window centered at 364 keV and, 1024 x 512 matrix. The data acquisition was performed 72 hours after 131-MIBG therapy. Whole body anterior and posterior views were obtained. SPECT images of thorax and abdomen were obtained with 45 sec/frame, 60 projections, 20 % window centered at 364 keV, matrix size of 128 x 128 and zoom factor of 1.0. This was followed by CT acquisition using single slice (1 cm thickness). Using volumetrix software in Xeleris, fused images in coronal, sagittal and transaxial views were then obtained. Whole body planar images were first interpreted alone. Then, they were reassessed with the addition of SPECT/CT coregistered images.

Results: 1. In these patients SPECT/CT revealed 30 % more pathological lesions than planar studies alone. 2. SPECT/CT provided precise anatomical localization not clearly evident in planar images alone. 3. It also enabled exclusion of disease in sites of physiologic tracer deposition found suspicious in planar studies alone

Conclusion: SPECT/CT allows more precise localization and interpretation of 131I-MIBG whole body scan thereby improving its diagnostic accuracy. It also has impact on correct restaging after therapy with 131I-MIBG preparation.

References:

1. Bas Havekes at al. Clinical Endocrinology (2010) 72, 137–145
2. Akie Takano at al. Ann Nucl Med (2008) 22:395–401

P-083

Multimodal *in vivo* imaging of pancreatic beta-cells via antibody mediated targeting of beta-cell tumors

Vats D. [1], Dikaiou K. [1], Stuker F. [1], Honer M. [2], Wang H. [3], Schibli R. [2], Rudin M. [1].

[1] Institute for Biomedical Engineering, ETH Zurich, Zurich, Switzerland
[2] Institute of Pharmaceutical Sciences, ETH Zurich, Switzerland
[3] F.Hoffman La-Roche, Basel, Switzerland

vats@biomed.ee.ethz.ch

Introduction: Pancreatic beta-cells regulate glucose metabolism by producing and secreting insulin in sufficient amounts. Progressive loss of beta-cell mass and function surmounts to acute diabetes. Diagnosis of diabetes and the evaluation of potential therapeutics suffer from lack of established methods for *in vivo* imaging of beta-cells. This study demonstrated the *in vivo* targeting of a novel antibody to a beta-cell surface protein in beta-cell tumor models. The pilot study evaluated the binding capacity of ^{89}Zr-lableled and alexa680 labeled monoclonal antibody against hTMEM27, a human beta-cell surface glycoprotein (1), for targeted imaging of beta-cell tumors in nude mice using positron emission tomography (PET) and fluorescence imaging.

Methods: Insulinoma cell-line (beta-cells), Ins1E, was taken as the parental cell-line for generating stable cell lines (2) over-expressing hTMEM27 (Ins-TM) while blank Ins1E cells (Ins-only) were taken as controls. Ins-TM and Ins-only cells were used to generate subcutaneous tumors in nude mice. 1.5MBq of ^{89}Zr-anti-hTMEM27 monoclonal antibody (^{89}Zr-TM-mAb) and 2mg/kg alexa680-anti-hTMEM27 monoclonal antibody (alexa680-TM-mAb) and alexa680-anti-HA control monoclonal antibody (alexa680-HA-mAb) were injected i.v. in tumor bearing nude mice. The animals were *in vivo* imaged three days after antibody administration: PET for ^{89}Z-TM-mAb and fluorescence imaging (both near infrared fluorescence reflectance imaging and near infrared fluorescence molecular tomography (NIR-FMT)) for alexa680-TM-mAb and alexa680-HA-mAb. The antibody retention was quantified using gamma counting of excised tumors for the ^{89}Zr labeled antibody and the fluorescence intensity was derived from region of interest (ROI) quantification for reflectance mode and NIR-FMT data (using MATLAB tools). The data was compared between the hTMEM27 over expressing insulinomas (Ins-TM), control insulinomas (Ins-only) and control antibody in hTMEM27 over expressing tumors (TM-HA), for antibody specificity over a period of 6 days. Individual tumors from optical study were further subjected to histological analysis for accurate localization of the dye distribution within tumor tissue.

Results: We found 6-7 times higher retention of the antibody in TMEM27 over expressing beta-cells, when compared to control beta-cells or with control antibody by both ^{89}Zr-PET and NIR-imaging (Figure 1). The fluorescence microscopy results confirmed antibody retention to TMEM27 in target insulinomas (Ins-hTMEM-tumors).

Conclusions: The pilot study could demonstrate the dual modal imaging of beta-cell mass, in a beta-cell tumor model, and identified a novel antibody for image-guided targeting of a beta-cell surface glycoprotein.

Acknowledgement: This work is funded by F.Hoffmann La-Roche Ltd.

Figure 1.

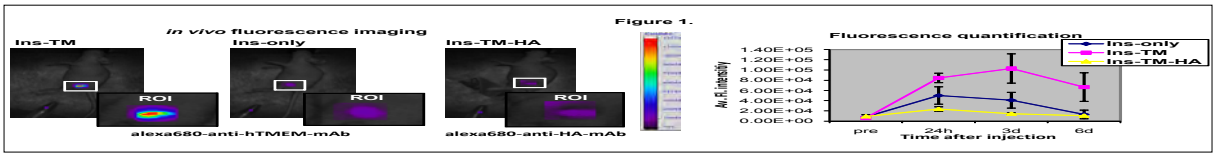

References:

1. Akpinar P et al.; Cell Metab. 2(6):385-97 (2005)
2. Wang H and Iyenedjian P B.; PNAS. 94: 4372-4377 (1997)

6-[^{18}F]Fluoro-PBR28, a novel TSPO 18 kDa radioligand for imaging neuroinflammation with PET

P-084

Boisgard R. [1], Damont A. [1], Blossier A. [1], Jego B. [1], Siquier K. [1], Kassiou M. [2], Dolle F. [1], Tavitian B. [1].

[1] CEA, Orsay, France
[2] Sydney University, Australia

raphael.boisgard@cea.fr

Introduction: The peripheral benzodiazepine receptor (PBR or TSPO 18 kDa) is expressed by microglial cells in many neuropathologies involving neuroinflammation. [^{11}C]PK11195 is today the most widely used radioligand for the *in vivo* imaging of PBR using PET, and this in spite of its low brain uptake and its high level of non-specific binding. Numerous PK11195 challengers are currently under investigation [1,2], and of particular interest are the *N*-benzyl-*N*-(2-phenoxyaryl)-acetamides, a series which includes [^{11}C]PBR28 [3]. A fluorine-containing analogue, namely 6-fluoro-PBR28 (*N*-(2-methoxybenzyl)-*N*-(6-fluoro-4-phenoxypyridinyl-3-yl)acetamide), has been labeled with the longer half-life positron-emitter fluorine-18 and pharmacologically evaluated in a rat model of neuroinflammation (unilaterally, AMPA-induced, striatum-lesioned rats) with PET.

Methods: 6-Fluoro-PBR28, as well as the corresponding precursors for labeling, were synthesized from 4-chloro-3-nitropyridine. 6-Fluoro-PBR28 was labeled with fluorine-18 by nucleophilic *hetero*aromatic substitution using K[^{18}F]F-Kryptofix®222, purified by HPLC (Waters Symmetry® C-18) and formulated for *i.v.* injection. The AMPA rat model was used to study *in vitro* and *in vivo* specific and non-specific binding using autoradiography and µPET imaging on a Concorde Focus P220 PET camera, including displacement with PK11195 and non-labeled 6-fluoro-PBR28 (1 mg/kg).

Results: Starting from a 37 GBq cyclotron-produced [^{18}F]fluoride batch, 3.3-3.7 GBq of 6-[^{18}F]fluoro-PBR28, > 99% radiochemically pure and ready-to-inject, were obtained within 90 minutes (Figure 1A). In PET experiments, 6-[^{18}F]fluoro-PBR28 showed a higher contrast between the lesioned area and the corresponding area in the intact contralateral hemisphere (ratio ipsi/contra at 60 min post-injection: 6-[^{18}F]fluoro-PBR28 : 2.2) (Figure 1B). Furthermore, 6-[^{18}F]fluoro-PBR28 was displaced by PK11195 or 6-fluoro-PBR28. Finally, modelisation of the PET data using the "simplified-reference-tissue-model" showed increased binding potential (BP) in comparison to the BP of [^{11}C]PK11195 measured in the same model (2.0±0.6 versus 1.1±0.2). Immunohistochemical analyses correlate with PET-imaging and showed strong activation of microglia in and around the lesion.

Conclusions: Dynamic µPET studies in rats demonstrate the potential of 6-[^{18}F]fluoro-PBR28 to image neuroinflammation.

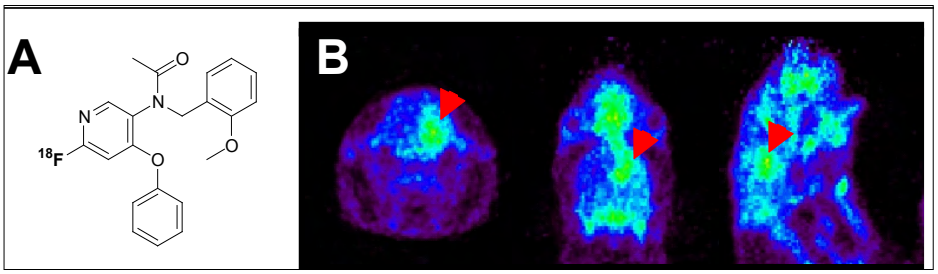

Fig1: Structure of 6-[18F]fluoro-PBR28 (A) and microPET images (B) obtained in AMPA lesioned rat (60 min p.i.)

Acknowledgements: Supported in part by the EC - FP6-project DiMI (LSHB-CT-2005-512146) and EMIL (LSH-2004-503569).

References:

1. Chauveau F et al; Eur J Nucl Med Mol Imag 35: 2304-2319 (2008)
2. Dollé F et al; Curr Med Chem 16: 2899-2923 (2009)
3. Briard E et al. J Med Chem 51: 17-30 (2008)

P-085

Neuroinflammation is increased in the brain of ageing corpulent (JCR:LA-cp) rats: a positron emission tomography study

Boutin H. [(1)], Drake C. [(1)], Denes A. [(1)], Mccoll B. [(1)], Prenant C. [(1)], Brown G. [(1)], Kassiou M. [(2)], Herholz K. [(2)], Rothwell N. [(2)].

[(1)] University of Manchester, United Kingdom
[(2)] University of Sydney, Australia

herve.boutin@manchester.ac.uk

Introduction: Despite intense research and development of several animal models, drugs efficient in preclinical model of cerebral ischaemia so far have failed when reaching clinical trial[1]. One striking feature of the animal models is the lack of co-morbidities and risk factors when compared to clinical set-up, in which patients have atherosclerosis, high blood pressure, chronic and/or acute inflammation due to chronic inflammatory diseases and infections. Inflammation and neuroinflammation in particular are known aggravating factors of stroke outcome[2]. Here we investigate the impact of known risk factors of stroke such as obesity and atherosclerosis in JCR:LA-cp (corpulent) rats on neuroinflammation as measured by TSPO expression in activated microglia.

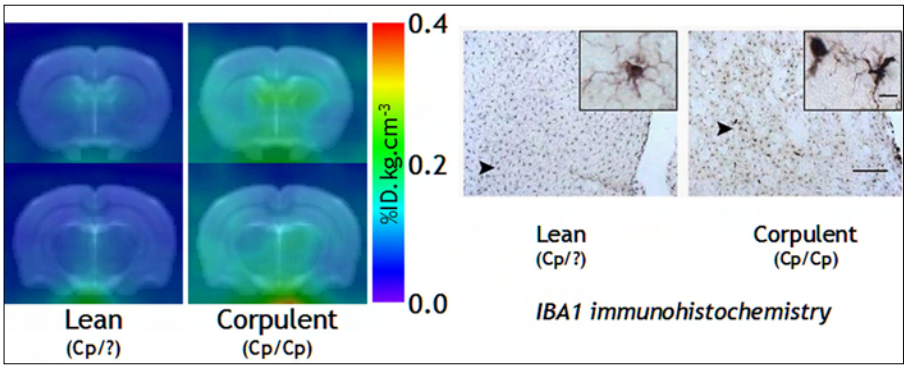

Methods: Neuroinflammation was assessed with [^{18}F]DPA-714 by PET in Lean (control: Cp/?)) and JCR:LA-cp (corpulent: Cp/Cp) rats PET imaging. 2 groups of rats were scanned at 9 months or 12 and 15 months of age (n=4 per group). PET images were co-registered with a MRI template[3] for analysis and automatic segmentation performed for user-independent ROI determination[4,5]. Euthanasia was performed at 9 months and 15 months of age 3 to 7 days after PET imaging to assess various neuroinflammation biomarkers (GFAP, IBA1, VCAM) by immunohistochemistry (IHC).

Results: Our results show an increase (+38%) in neuroinflammation in the brain of corpulent rats when compared to control. In older rats (12 and 15 months old), neuroinflammation was even further increased but in both lean and corpulent rats. Neuroinflammation, as quantified by PET, was mainly localised in peri-ventricular and thalamic areas of the brains. IHC for microglial activation confirmed the PET data in 15 months old animals (Figure below).

Conclusions: Our data show here the importance of including risk and co-morbidity factors in preclinical models of stroke as they have a significant impact on neuroinflammation. This study shows the crucial role of molecular imaging with the high translational value of PET imaging to investigate such paradigms. A more detailed study of the localisation of neuroinflammation as localised by PET and IHC is now ongoing. Further investigation either in animals with spontaneous stroke or with induced cerebral ischaemia will be required to compare the impact of co-morbidity and risk factors in this animal model.

Acknowledgement: Prof. N. Rothwell and Dr H. Boutin are funded by MRC. This study was carried out within the EC-FP6 project DiMI (LSHB-CT-2005-512146) framework.

References:

1. Dirnagl U. (2006) J Cereb Blood Flow Metab. 26:1465-1478;
2. McColl B.W. et al. (2009) Neuroscience. 158:1049-1061;
3. Schwarz A.J. et al. (2006) Neuroimage. 32:538-550;
4. Maroy R. et al. (2008) IEEE Trans.Med.Imaging. 27:342-354;
5. Maroy R. et al. (2010) J Nucl Med (submitted).

Detection of inflammatory diseases by NIRF imaging with specific probes targeting leukotriene receptor $CysLT_1R$

Busch C. [1], Passon M. [1], Lehmann F. [2], Socher I. [1], Kaiser W.A. [1], Hilger I. [1].

[1] University Hospital Jena, IDIR, Jena, Germany
[2] DYOMICS GmbH, Jena, Germany

Corinna.Busch@med.uni-jena.de

Introduction: Leukotriene synthesis occurs early in inflammatory processes and plays a major role for the recruitment of leukocytes to the inflamed region (1). A key representative of these eicosanoids, leukotriene D4 (LTD4), shows high affinity to G-protein coupled cysteinyl leukotriene receptor 1 ($CysLT_1R$). Detection of $CysLT_1R$ by molecular imaging (2) with near-infrared (NIR) fluorophores could be a suitable diagnostic tool for early identification of inflammatory processes. Aim of this study was the design and characterization of NIRF-based contrast agents specifically targeting $CysLT_1R$ in order to develop future diagnostic tools for inflammatory diseases, particularly in early stages.

Methods: Polyclonal rabbit $CysLT_1R$ antibody ($CysLT_1R$*DY-734) or polyclonal rabbit-IgG (IgG*DY-734) as well as the corresponding Fab fragments (Fab-$CysLT_1R$*DY-734, Fab-IgG*DY-734) were bound to activated NHS ester of NIR-fluorophore DY-734 (Dyomics, Jena, Germany). Probes were characterized by determining dye/protein ratios. After verification of $CysLT_1R$ expression (PCR, flow cytometry) in HL-60 cells, binding of the synthesized probes *in vitro* was assessed by flow cytometry. *In vivo,* an ear edema was induced in mice (3), and NIR fluorescence was measured with whole body imaging system Maestro™2.2 after i.v.-probe administration. *Ex vivo* biodistribution studies were performed.

Results: Flow cytometry proved binding of $CysLT_1R$*DY-734 and IgG*DY-734 to $CysLT_1R$-expressing HL-60. *In vivo*, all probes revealed stronger binding to the edematous than to the corresponding healthy region. 6 h post injection, specific $CysLT_1R$*DY-734 and Fab-$CysLT_1R$*DY-734 demonstrated 1.9 and 1.2 fold higher binding than IgG*DY-734 and Fab-IgG*DY-734, respectively. Investigation of isolated organs revealed that full length IgG´s are eliminated via liver, while Fab fragments additionally accumulated in kidney.

Conclusions: A novel NIRF-based probe specifically targeting Leukotriene D_4 receptor $CysLT_1R$ allows detection of inflammatory processes in ear edema-induced mice in early stages.

Acknowledgement: The present investigations were supported by the "Deutsche Forschungsgemeinschaft" within the DFG program Hi 689/6-1.

References:

1. Hui Y, Funk C. Cysteinyl leukotriene receptors. Biochem. Pharmacol. 2002;64:1549-57.
2. Weissleder R, Mahmood U. Molecular Imaging. Radiology 2001;219:316-33.
3. Kurnatowska I, Pawlikowski M. Anti-inflammatory effects of somatostatin analogs on zymosan-induced earlobe inflammation in mice: comparison with dexamethasone and ketoprofen. Neuroimmunomodulation 2001;9:119-24.

P-087

PET imaging of Hypoxia by ^{18}F-Fluoromisonidazole ([^{18}F]FMISO) to detect early stages of experimental arthritis

Fuchs K. [1], Grießinger C. [1], Fischer K. [1], Mannheim J. [1], Wiehr S. [1], Judenhofer M. [1], Reischl G. [2], Röcken M. [3], Pichler B. [1], Kneilling M. [3].

[1] Laboratory for Preclinical Imaging and Imaging Technology of the Werner Siemens-Foundation, Department of Radiology, Eberhard- Karls University, Tübingen, Germany

[2] Radiopharmacy, Department of Radiology, Eberhard- Karls University, Tübingen, Germany

[3] Department of Dermatology, Eberhard- Karls University, Tuebingen, Germany University Hospital Tübingen - Department of Radiology, Tübingen, Germany

Kerstin.Fuchs@med.uni-tuebingen.de

Introduction: Early detection of autoimmune diseases such as rheumatoid arthritis is essential for early interventional anti-inflammatory treatment to prevent cartilage- and bone deterioration. Hypoxia can induce angiogenesis via stabilization of the transcription factor hypoxia inducible factor (HIF)-1α/2α in resident and infiltrating cells by induction of pro-angiogenic mediators. Also, hypoxia is hypothesized to be one of the early indicators of inflammation. The aim of our study was to examine initial phases of hypoxia-induced angiogenesis and inflammation in rheumatoid arthritis, by *in vivo* small animal PET, even before clinical symptoms or histological joint inflammation are detectable. Therefore, we used the hypoxia tracer ^{18}F-Fluoromisonidazole ([^{18}F]FMISO), which selectively accumulates in hypoxic tissue, and [^{18}F]Fluordesoxyglucose ([^{18}F]FDG).

200

Methods: We induced arthritis in BALB/c mice via intraperitoneal injection of serum containing autoantibodies against glucose-6 phosphate-isomerase (GPI). Mice underwent [^{18}F]FMISO-, or [^{18}F]FDG - PET investigations, 6 - 52 hours after induction of GPI-arthritis. Additionally, we performed H&E-staining, Western Blot (HIF-1α/2α) and real-time PCR analysis of gene expression patterns (bFGF, VEGF, IL-1β, TNF, IL-6, and COX-2) in joint tissue 6 and 12 hours after initiation of arthritis.

Results: Starting 6 hours after induction of GPI-arthritis we detected an enhanced [^{18}F]FMISO uptake in arthritic joints compared to healthy joints. Differences in [^{18}F]FMISO uptake between arthritic and healthy joints reached a level of significance 13 hours after induction of GPI-arthritis. In contrast to [^{18}F]FMISO, no increase in [^{18}F]FDG-uptake was detectable at these early time points (6-13 hours). Comparable to the *in vivo* [^{18}F]FDG-PET data, no histological visible signs of arthritis were examined in H&E-stained slices of arthritic joint tissue. In line with the *in vivo* [^{18}F]FMISO-PET-data, RT-PCR analysis performed 6 hours after GPI-serum injection showed a 7.5-fold enhanced expression of HIF-2α mRNA. Interestingly, mRNA-levels of pro-angiogenic and pro-inflammatory mediators such as bFGF and VEGF, TNF, IL-6, and COX-2 were not elevated 6h after induction of GPI-arthritis. Starting 54h after induction of GPI-arthritis we detected significant differences in [^{18}F]FDG uptake in arthritic ankles, and a 6.5-1550 fold enhanced expression NF-$_k$B induced genes such as COX-2, IL-6, IL-1β and, TNF.

Conclusions: Non invasive *in vivo* examination of hypoxia-induced angiogenesis using [^{18}F]FMISO is a powerful tool to detect initial phases of angiogenesis in autoimmune diseases such as rheumatoid arthritis even before joint inflammation becomes detectable by other methods.

P-088

Intracellular [^{64}Cu]PTSM and extracellular [^{64}Cu]DOTA-antibody labelling of ovalbumin-specific Th1 cells for *in vivo* PET investigations of Th1 cell trafficking in OVA-specific lung inflammation

Griessinger C.M. [1], Wiehr S. [1], Bukala D. [1], Kesenheimer C. [1], Röcken M. [1], Ehrlichmann W. [3], Reischl G. [3], Pichler B. [1], Kneilling M. [2].

[1] Laboratory for Preclinical Imaging and Imaging Technology of the Werner Siemens-Foundation, Department for Radiology, Eberhard Karls University of Tübingen, Germany

[2] Department for Dermatology, Eberhard Karls University of Tübingen, Germany

[3] Radiopharmacy, Eberhard Karls University of Tübingen, Germany

Christoph.Griessinger@med.uni-tuebingen.de

Introduction: T helper cells play an important role in the development of autoimmune diseases. For detailed in vivo analysis of the migration properties of Th1 cells, high sensitive imaging modalities, such as small animal PET are powerful tools. So far basic migration properties like kinetics, homing, and sites of T cell proliferation in animal models for autoimmune diseases are still poorly understood. The aim of our study was to establish new T cell labelling strategies to gain new insights in Th1 cell trafficking in vivo using small animal PET. In our studies Th1 cells were in vitro labelled intracellularly with the lipophilic tracer [^{64}Cu]PTSM or extracellularly with [^{64}Cu]DOTA-linked antibodies prior to injection into diseased mice and tracking by small animal PET.

Methods: To investigate whether intracellular [^{64}Cu]PTSM labelling or extracellular [^{64}Cu]DOTA-antibody labelling impair ovalbumin (OVA)-specific Th1 cells, we analysed cell viability and functionality. OVA-T cell receptor (TCR) transgenic CD4+ T cells were isolated from spleen and lymph nodes of DO.11.10 mice and cultured together with irradiated antigen presenting cells (APC), Oligo 1668 peptide, anti-IL-4, and IL-2 for 12-14 days. 10^6 OVA-Th1 cells were labelled with 0.7 MBq [^{64}Cu]PTSM for 3 hours or with 0.7 MBq radiolabelled OVA-TCR-specific antibody (KJ1-26), which was linked to [^{64}Cu] via the chelator DOTA, for 0.5 hours. Th1 cell viability was assessed by trypan blue staining after incubation with increasing amounts of activity. Specific Th1 cell functioning was analyzed through interferon-gamma (ELISA) levels in supernatants of specific activated OVA-Th1 cells (T cells + irradiated APC + OVA peptide). In vivo T cell migration was investigated in an animal model for OVA-induced lung inflammation. Mice were sensitized with OVA (i.p.) and challenged intranasally twice after four weeks to induce OVA-specific lung inflammation. A total of 10^7 [^{64}Cu]PTSM or [^{64}Cu]DOTA-KJ1-26 antibody labelled OVA-Th1 cells were injected i.p. into diseased and healthy mice. Static PET-scans in combination with CT, biodistribution, and autoradiography were performed 24 and 48 hours after OVA-Th1 cell transfer.

Results: In vitro investigations revealed an activity dependent impairment of OVA-Th1 viability and functionality after [^{64}Cu]PTSM or [^{64}Cu]DOTA-KJ1-26 antibody labelling. After a time period of 24 hours post labelling, the cell viability sunk to 80% and functionally was decreased by 20% compared to unlabelled control cells. Analyzing OVA-specific Th1 cell migration in the mouse model for lung inflammation, we detected an accumulation of [^{64}Cu]PTSM labelled OVA-Th1 cells in lung tissue and the thymus already 24h after the final challenge. Detection of [^{64}Cu]DOTA-KJ1-26 antibody labelled OVA-Th1 cells was even possible for up to 48 hours. In vivo PET data were further confirmed by ex vivo biodistribution and autoradiography. Compared to [^{64}Cu]PTSM labelled OVA-Th1 cells we gained a more defined distribution of extracellularly [^{64}Cu]DOTA-KJ1-26 labelled cells in the peritoneum (the site of injection), draining lymphatic tissue and the sites of OVA-specific lung inflammation. Furthermore we detected a significant accumulation of OVA-Th1 cells in the omentum majus.

Conclusions: Both [^{64}Cu]-based labelling methods cause an impairment of Th1 cells viability and functionality. However, both labelling strategies are applicable for in vivo PET-imaging, revealing a detection limit of 500 OVA-Th1 cells in draining lymph nodes and sites of OVA-specific lung inflammation over a time period of 48 hours.

P-089

[18F]DPA-714, [18F]PBR111 and [18F]FEDAA1106: Radiosyntheses on a TRACERLAb FX-FN synthesizer

Kuhnast B. , Damont A. , Demphel S. , Le Helleix S. , Boisgard R. , Tavitian B. , Dollé F. .

CEA, Orsay, France

bertrand.kuhnast@cea.fr

Introduction: Neuroinflammation is involved in acute and chronic neurological disorders through the activation of microglial cells or the recruitment of peripheral macrophages. Both microglia and macrophage activation results in the notable over-expression on the outer mitochondrial membranes of the so-called translocator protein (TSPO 18 kDa), supporting today extensive efforts in the design of radioligands for the *in vivo* imaging of this pharmacological target by Positron Emission Tomography [1]. Of particular interest are DPA-714 [2], PBR111 [3] and FEDAA1106 [4], three ligands belonging to different chemical classes (the pyrazolo[1,5-*a*]pyrimidineacetamides, the imidazo[1,2-*a*]pyridineacetamides and the *N*-benzyl-*N*-(2-phenoxyaryl)-acetamides, respectively) but all designed for a labelling with the positron-emitter fluorine-18 via a tosyoxy-for-fluorine nucleophilic aliphatic substitution. Production of [18F]DPA-714, [18F]PBR111 and [18F]FEDAA1106 on the advanced, commercially available, automated module TRACERLab™ FX-FN synthesizer is presented.

Methods: The automated process implemented on the TRACERLab™ FX-FN synthesizer involves: (A) the preparation of the K[18F]F-Kryptofix®222 complex in two heating steps, first at 60°C for 7 min under a stream of N_2 and then at 120°C under reduced pressure for 5 min, followed by (B) reaction of K[18F]F-Kryptofix®222 with the appropriate tosyl-precursors (4 to 5 mg) at 165°C for 5 min in DMSO (0.7 mL), then (C) SepPak®Plus Alumina N cartridge pre-purification after dilution of the reaction mixture with HPLC solvent (4 mL) and finally (D) semi-preparative HPLC purification. HPLC purifications were performed on a X-Terra® column for [18F]DPA-714 (Solvent : NH_4OAc 0.1M pH 10 / MeCN : 60/40 (v/v), Flow rate : 5 mL/min, Rt = 11-12 min), on a Symmetry® C-18 column for [18F]PBR111 (Solvent : H_2O / MeCN / PicB7 : 60/40/2 (v/v/v), Flow rate : 5 mL/min, Rt = 14-15 min) and on a Symmetry® C-18 column for [18F]FEDAA1106 (Solvent : H_2O / MeCN / TFA : 60/40/0.1 (v/v/v), Flow rate : 5 mL/min, Rt = 21-22 min). The HPLC-collected fraction containing pure [18F]DPA-714, [18F]PBR111 or [18F]FEDAA1106 were automatically formulated using a SepPak®Plus C-18 cartridge ((i) HPLC-collected fraction dilution and loading on the cartridge, (ii) cartridge washing with 10 mL of water, (iii) cartridge elution with 2 mL of EtOH, and (iv) final dilution with 8 mL of saline). The process was programmed on the TRACERLab™ FX-FN synthesizer in one single "method" divided in three "time-lists".

Results: Starting from a 37.0 GBq cyclotron-produced [18F]fluoride batch, 6.7 to 8.5 GBq (18-23% non decay corrected yields) of [18F]DPA-714 or [18F]PBR111 or [18F]FEDAA1106, > 99% radiochemically pure and ready-to-inject, were obtained within 50-60 min. The overall decay corrected radiochemical yield reached up to 30%. Specific radioactivities ranged from 74 to 222 GBq/µmol (2-6 Ci/µmol).

Conclusions: Radiosynthesis of [18F]DPA-714, [18F]PBR111 and [18F]FEDAA1106 has been successfully implemented on a TRACERLab™ FX-FN synthesizer.

Acknowledgements: Supported in part by the EC - FP6-project DiMI (LSHB-CT-2005-512146) and EMIL (LSH-2004-503569).

References:

1. Dollé F et al; Curr Med Chem 16: 2899-2923 (2009)
2. Damont A et al; J label Compds Radiopharm 51: 286-292 (2008)
3. Dollé F et al; J label Compds Radiopharm 51: 435-439 (2008)
4. Zhang MR et al; J Med Chem 49: 2735-2742 (2006)

In vivo near-infrared fluorescence imaging of lung matrix metalloproteinases in an acute cigarette smoke-induced airway inflammation model in different mice strains

P-090

Perez-Rial S., Del Puerto-Nevado L., Giron-Martinez A., Gonzalez-Mangado N., Peces-Barba G. .

Instituto de Investigacion Sanitaria-Fundacion Jimenez Diaz-CIBERES, Madrid, Spain

sperezr@fjd.es

Introduction: Recent studies have suggested that pulmonary macrophage-derived metalloproteases (MMPs) are the critical mediators of cigarette smoke exposure (CSE)-induced emphysema, but it has never been seen via imaging techniques [1]. The purpose of this study was to visualize and quantify acute pulmonary inflammation by real-time near-infrared fluorescence (NIRF)-mediated molecular imaging [2] in the lung tissue evaluating MMPs activity in response to CSE in mice strains with different susceptibility to develop smoking-induced emphysema.

Methods: To accomplish this task, susceptible (C57BL/6j) and resistant (129S2/SvHsd) mice [3] were exposed to acute CSE using a whole-body exposition. 24h after CSE MMPs activity was assessed via optical imaging system by a MMPs-sensitive activatable fluorescence probe in order to characterize the distinctive profile of CSE-induced acute inflammation. Furthermore MMPs protein levels in the lung tissue were analyzed by Western blot analysis.

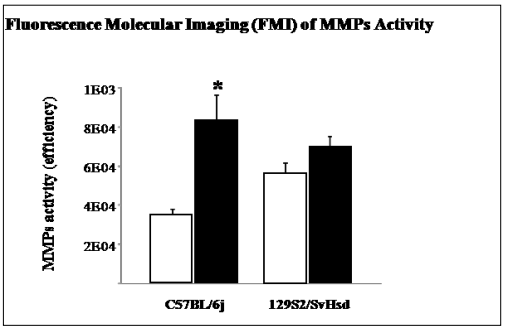

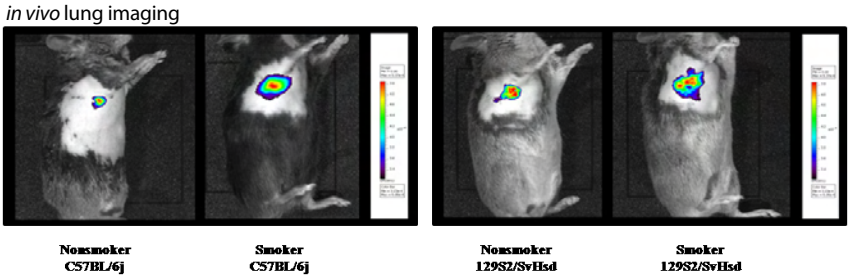

Results: In vivo semiquantitative optical imaging analysis of MMPs activity in the lung revealed increased acute-CSE-associated MMPs activity in C57BL/6j but not in 129S2/SvHsd. Only in susceptible mice most important MMPs protein levels were significantly increased in the lung tissue of smokers compared with the non-smokers group.

Conclusions: Optical imaging via NIRF offers a simple, effective, and rapid technique for noninvasive monitoring and semiquantitative analysis of lung inflammation and MMPs expression. We are able to distinguish between susceptible and resistant mice strains in terms of the profile of MMPs activity in the early stages of pulmonary disease. The results of our study suggest that mechanisms underlying different susceptibilities to CSE can be detected at the beginning of the disorder. They produce different response to acute tobacco smoke.

Acknowledgement: This work is supported in part by the Spanish "Ministerio de Ciencia e Innovación" (SAF2008-05412-C02- 02) and CIBERES (CB06/06/0009).

References:

1. Churg A et al; Am J Respir Crit Care Med. 167(8):1083-9 (2003)
2. Haller J et al; J Appl Physiol. 104(3):795-802 (2008)
3. Morris A et al; J Pharmacol Exp Ther. 327(3):851-62 (2008)

POSTER

INFECTION and INFLAMMATION

P-091

Development and pre-clinical evaluation of a novel class of ^{18}F labelled PET ligands for evaluation of PBR/TSPO in the brain

Trigg W. , Ahmad R. , Arstad E. , Avory M. , Hirani E. , Jones P. , Khan I. , Luthra S. , Morisson-Iveson V. , O'shea D. , Passmore J. .

GE Healthcare, Amersham, United Kingdom

william.trigg@ge.com

Introduction: The peripheral benzodiazepine receptor (PBR; otherwise known as TSPO (18kDa)) is a well-established target for imaging activated microglial cells and macrophages in inflammatory diseases such as MS, Alzheimer's disease and a wide range of both peripheral and brain diseases[1]. Starting from a core tetracyclic indole pharmacophore[2], which displayed high affinity for the PBR, we have designed a series of molecules to assess the SAR around the pharmacophore and to determine the best site to introduce the radiolabel.

Methods: Compounds have been assessed for PBR affinity in a radioligand binding assay and in a range of *in vitro* ADME assays. Following on from the *in vitro* assessments, promising compounds were radiolabelled and assessed *in vivo* for biodistribution and metabolism profiles. The compounds with the most appropriate profiles were assessed using autoradiography in the Facial Nerve Axotomy (FNA) model described by Banati *et al.*[3]

The corresponding data for the archetypal PBR ligand PK11195 was generated for comparison.

Results: The olfactory bulb (OB) has high expression of PBR and is used to measure specific uptake, with the striatum used as a low expression area for comparative purposes. Key data obtained are summarised in the table below.

Compound (Ki)	Initial brain uptake (%ID/g)	OB @ 2 min (%ID/g)	OB @ 30 min (%ID/g)	2:30 Striatum ratio	OB : Striatum ratio (30 min)	Metabolism Profile - % Parent in brain at 60 min p.i.	FNA Model lesion : non lesion ratio (in vitro)
[^{11}C]PK11195 (1.24nM)	0.28-0.48*	0.42	0.21	3.20	2.10	100	2.8**
[^{18}F]AH114011 (0.37nM)	0.32	0.39	0.31	1.73	2.07	96.0	2.3
[^{18}F]AH114629 (0.40nM)	0.42	0.51	0.28	4.75	3.50	97.6	NT

* Whole brain value not calculated

** [3H]PK11195 used for autoradiography studies

Conclusions: Preclinical evaluation of the 18F labelled tetracyclic indole class of ligands for PBR shows that this class of molecules represents a promising class of PET ligands that should be further evaluated.

References:

1. Cagnin et al., Neurotherapeutics, Vol. 4, No. 3, 443-452 (2007)
2. Okubo et al., Bioorg Med. Chem. 12(2):423-438 (2004)
3. Banati et al., J. Neurocytol. 26:77-82. (1997)

Local administration of adeno-associated virus into the mammary gland ductules

P-092

Hamm J. [1], Cojoca R. [1], Iezzi M. [2], Mautino A. [1], Turco E. [1], Silengo L. [1], Musiani P. [2], Forni G. [1].

[1] University of Turin, Italy
[2] University of Chieti Pescara, Italy

jorg_hamm@yahoo.com

Introduction: Adeno-associated virus (AAV) is a single-stranded DNA parvovirus with charateristics that render it attractive for gene therapy applications (1). More than 14 AAV serotypes have been characterized which differ in efficiency of infection and tissue tropisms. Cell entry seems to occur by AAV receptor mediated endocytosis, the receptors recognised by the capsid proteins vary in different serotypes and might be an determinant for tissue tropism. The DNA remains mainly extrachromosomal, does not replicate, and is unable to produce infectious particles, features desirable for gene therapy vectors. In the majority of the applications AAV2 vector is used for gene transfer experiments, but other serotypes have been explored recently because they can offer superior transduction efficiencies or different cell tropisms. Furthermore, neutralising antibodies against AAV2 are frequently found in human sera and can compromise efficiency of gene transfer. AAV9 has been reported to allow a robust expression in heart and muscle, but other expression sites have also been indicated.

Methods: AAV9 vectors expressing luciferase as a reporter gene driven by the cytomegalo virus promoter (AAV9-CMV-luc) or by the murine EF1alpha promoter (AAV9-EF1a-luc) were administered locally into the mammary gland network by intraductal injection (2) into BALB/c female mice. Expression profile and body distribution were determined by *in vivo* and *ex vivo* optical imaging, and by histological analysis.

Results: AAV9-CMV-luc migrates from the injected gland to ipsilateral glands, but not to contralateral glands. Luciferase expression is observed predominantly in muscle cells and is stable for months. The observed expression of luciferase in the ipsilateral lymph nodes indicate that the virus might use the lymphatic system to reach all of the five ipsilateral mammary glands.

Conclusions: AAV9 vectors appear to be well suited for targeted, long-lasting gene expression in muscle tissue. Mammary epithelia cells are apparently not infected efficiently, not even after site specific injection into the duct of mammary glands.

POSTER

TARGETED THERAPY

References:

1. Büning et al.; J Gene Med 2008; 10: 717–733.
2. Murata et al.; Cancer Res. 2006 Jan 15;66(2):638-45.

P-093

Copper-64- and Gallium-68- NODAGA-conjugated bombesin antagonists as new PET tracers

Mansi R. , Dumont R. , Jamous M. , Tamma M. , Nicolas G. , Fani M. , Cescato R. , Reubi J.C. , Weber W. , Maecke H. .

Nuclear Medicine, Freiburg, Germany

rosalba.mansi@uniklinik-freiburg.de

Introduction: The gastrin-releasing peptide or bombesin receptor (GRPr) is frequently overexpressed in several human cancers including prostate, breast, small cell lung and pancreatic cancer [1,2]. Specific radiolabeled ligand for this receptor offer new opportunities for the diagnosis and treatment of these diseases. Many bombesin antagonists have shown high affinity for the GRPr [3]. In this study, we evaluated the potential of a statine-based bombesin antagonist, conjugated to NODAGA through a polyethyleneglycol spacer, to specifically target GRPr expressing cancer cells. We determine the effect of two different radioisotopes Ga-68 and Cu-64 on the tumor targeting efficacy and in vivo pharmacokinetics. Moreover we evaluated the PET imaging properties of the two radiotracers.

Methods: The peptide assembling and NODAGA-conjugation were accomplished on solid phase. The conjugate MJ5 was radiolabeled with Ga-68 and Cu-64 and the radioconjugates were evaluated in vitro and in vivo in tumor-bearing nude mice, using the GRP-receptor positive prostate carcinoma cell line PC-3. To study the bombesin antagonistic properties of MJ5 cells were treated either with 10 nmol/L bombesin, or with 1 µmol/L MJ5 or, with 10 nmol/L bombesin in the presence of a 100-fold excess MJ5 for 30 min at 37°C. GRPr internalization was studied by immunofluorescence.

Results: The immunofluorescence assays confirmed the strong antagonist properties of the conjugates: MJ5 failed to induce significant internalisation of GRPr and when given at a concentration of 1 µmol/L together with 10 nmol/L bombesin, MJ5 was able to antagonize bombesin-induced receptor internalisation. Biodistribution studies revealed high and specific uptake of both conjugates in PC-3 tumors and in GRPr positive tissues such as pancreas and intestine. The Ga-68-MJ5 biodistribution data showed a good tumor uptake at 1h (4.54±0.52% I.A./g) and good tumor to kidney and tumor to blood ratios (4.1 and 10.9 respectively). These promising data prompted us to investigate the biodistribution of MJ5 with a longer lived radionuclide. The tumor uptake of the Cu-64-MJ5 was 3.7 times higher than the Ga-68-labeled analog at 1h (16.80±3.22% I.A./g) and remained high at 4h (13.97±3.68% I.A./g). At 4 h higher tumor to kidney (8.6), tumor to blood (36.2) and tumor to pancreas (18.2) ratios were achieved than for Ga-68-MJ5 at 1 h. The PET/CT images demonstrated exellent visualization of the PC3 tumors by Ga-68- and Cu-64 MJ5.

Conclusions: The labeling with the two radionuclides distinctly influences the pharmakokinetics of the radiopeptides in particular in regard to the uptake in the tumor and receptor positive organs. The high tumor uptake and the good tumor to background ratio of the Cu-64 labeled analog at 4h warrant clinical testing of this probe for PET imaging in humans.

Acknowledgement: We acknowledge COSTD38 and the Swiss National Science Foundation for the financial support.

References:

1. R.Markwalder, J.C. Reubi, Cancer Res., 155 (1999) 1152.
2. J.C. Reubi, M. Korner, et al., Eur.J.Nucl.Med.Mol.Imaging, 31 (2004) 803
3. R.T. Jensen, D.H. Coy, Trends Pharmacol. Sci., 12 (1991) 13

A novel indocyanine green nanoparticle probe for non invasive fluorescence imaging *in vivo*

P-094

Mérian J. [1], Navarro F. [1], Josserand V. [2], Texier I. [1].

[1] CEA LETI MINATEC, Grenoble, France
[2] CRI INSERM U823, France

juliette.merian@cea.fr

Introduction: Fluorescence imaging, a non invasive, non ionizing and sensitive technology, is opening a new era in medical application such as image-guided surgery. Indocyanine Green (ICG), the only Near InfraRed optical contrast agent approved by the FDA [1], is encapsulated in lipidic nanoparticles (LNP). Using LNP as nanocargo presents advantages such as improvement of the dye chemical stability, biocompatibility and passive targeting, as well as suitable properties for fluorescence detection of tumors [2].

Methods: LNP are composed of a lipid core, stabilized by phospholipids and pegylated surfactants and are dispersed in aqueous buffer. ICG (Infracyanine™) is incorporated into the lipid mixture as a concentrated solution in ethanol. Solvent is evaporated and this oily phase is mixed with aqueous phase before sonication is performed at 40°C for a whole 5min period (VCX750 Ultrasonic processor). Particle size, size distribution, and surface charges are evaluated by dynamic light scattering (DLS). Optical properties

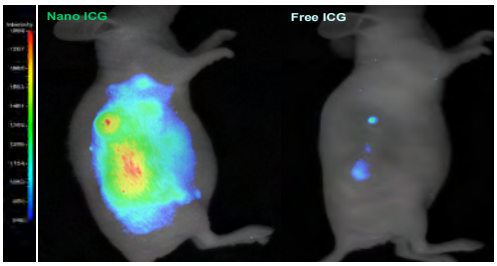

characterizations are performed using visible absorbance and fluorescence spectrometries. MTT assay is performed using 3T3 fibroblasts to assess LNP cytotoxic index. The in vivo distribution of ICG-loaded LNP is investigated in Nude mice bearing xenografted sub-cutaneous TS/Apc tumors using a NIR whole animal imaging device (Fluobeam 800), and compared to that of free ICG in aqueous solution.

Results: ICG loading does not modify the size (30nm diameter, one population) and the polydispersity index (from 0.11 to 0.13) of the LNP, but decreases the zeta potential, which becomes more negative (-5.8±2.5mV for nude LNP, versus -18.2±2.1mV for ICG loaded LNP). The dye encapsulation within LNP induces a 16nm red-shift of its absorption and emission (maximum at 820nm); as well as an improvement of its fluorescence quantum yield and a longer lifetime in comparison to free dye in water. LNP carrier is well tolerated in vitro (IC50~1 mg/mL of lipids). Furthermore, ICG loaded LNP injection in Nude mice implanted with subcutaneous Ts/Aps tumors, shows a better fluorescence signal in tumor site in comparison of free ICG at the same dose.

Conclusions: LNP vectorization provides ICG a modification of its pharmacokinetics in addition to an improvement of its optical properties. These characteristics are suitable for long term and sensitive in vivo imaging required for efficient tumor detection. ICG loaded LNP, thanks to their low size, takes advantages of the Enhanced Permeability and Retention (EPR) effect and are passively accumulated with time into the tumor.

Acknowledgement: J.Mérian1, F. Navarro[1], V. Josserand[2], I. Texier[1]: 1CEA LETI Minatec, 2 CRI-INSERM U823

References:

1. Frangioni, J.V. *In vivo* near infrared fluorescence imaging. Curr. Opinion Chem. Biol. 7, 2003:626-634
2. Texier, I. Goutayer, M. and al Journal of Biomedical Optics, 14(5), 2009: 054005

POSTER

TARGETED THERAPY

P-095

Evaluation and optimization of the concept of an antibody directed enzyme-prodrug therapy using noninvasive imaging technologies

Napp J. [1], Dullin C. [2], Krewer B. [3], Von Hof J.M. [3], Schmuck K. [3], Mathejczyk J. [4], Hartung F. [4], Stühmer W. [4], Tietze L. F. [3], Alves F. [4], Pardo L. A. [4].

[1] MI for exp Medicine, Göttingen, Germany
[2] University Medicine Göttingen, Germany
[3] University Göttingen, Germany
[4] MPI for exp Medicine, Göttingen, Germany

jnowako1@gwdg.de

Introduction: Relatively low selectivity to tumor versus normal cells challenges virtually all cancer chemotherapies. Site-specific activation of prodrugs in tumors is one strategy to achieve high efficacy and specificity of treatment, decreasing toxicity in normal tissues. Here, we present the design and validation of an Antibody Directed Enzyme-Prodrug Therapy (ADEPT) in which an antibody against Eag1 is used to carry the drug-activating enzyme, ß-galactosiase (ß-gal) to the tumor tissue. Eag1 (ether-à-go-go1) voltage-gated potassium channel has been chosen as a tumor-specific target since this plasma-membrane protein is easily accessible to extracellular interventions and Eag1 is aberrantly expressed (>75%) in tumors from diverse origin but basically not detected in healthy tissue outside the central nervous system.

Methods: Two monoclonal anti-Eag1 antibodies, mAb62 and mAb56, a humanized 56 antibody, as well as a single chain fragment of the mAb62, scFv62, were tested for their feasibility to deliver the drug-activating enzyme ß-gal to the tumor. Near infrared fluorescence (NIRF) imaging was used to study the biodistribution and binding characteristics of the anti-Eag1 antibodies *in vivo* in a subcutaneous Eag1-expressing MDA-MB-435S tumor model in nude mice. Fluorescence intensity, lifetime and location of Cy5.5 labeled antibodies *in vivo* was measured with the time-domain NIRF imager, Optix MX2 (ART, Advanced Research Technologies; Canada), at certain time points. Fluorescence lifetime (the average time during the molecule stays in its excited state) was used to discriminate between non-specific and probe-derived signals. Distribution of the fluorescent probe in tumor sections *ex vivo* was further investigated by the Odyssey infrared imaging system (LI-COR Biosciences, Germany) as well as by NIRF microscopy (Axiovert 200M, Carl Zeiss, Germany). For the tumor-specific activation of the prodrug, the mAb62 was conjugated to ß-gal, resulting in 62-gal. The ß-gal activity of the 62-gal conjugate and its ability to bind to the Eag1 epitope were tested *in vitro* on Eag1-expressing MDA-MB-435S cells and control AsPC-1 cells using a colorimetric CPRG (chlorophenolred-ß-D-galactopyranoside) assay. The ß-gal activity in mice was analyzed by NIRF imaging using the fluorescent activatable probe, DDAOG (9H-(1,3-dichloro-9,9-dimethylacridin-2-one-7-yl) β-d-galactopyranoside) by NIRF imaging.

Results: All tested antibodies targeting Eag1 bound specifically to MDA-MB-435S tumors with maximal intensity peaks at 24-48 h after application; fluorescence was still detectable for at least 1 week *in vivo*. We confirmed specific binding of the antibodies to the tumors by *ex vivo* NIRF imaging of tumors isolated from mice injected with fluorescently labeled antibodies 24 h prior to section, as well as by NIRF microscopy of tumor slices. Moreover, we show that monoclonal antibodies against Eag1, but not the scFv62 fragment, resulted in strong fluorescence signals in the area over liver, detectable for at least 4 days *in vivo*. Similar fluorescence signals over liver were also observed in tumor-bearing mice injected with Cy5.5-labeled control IgGκ2B, confirming that the liver signals did not result from Eag1-mediated binding of those antibodies to cells within liver. Furthermore, we show that the 62-gal conjugate specifically binds *in vitro* to Eag1-expressing MDA-MB-435S, but not to control Eag1-non expressing AsPC-1 cells and that 62-gal possess high ß-gal activity, when bound to MDA-MB-435S cells. Moreover, 24 h after application of the 62-gal to the tumor bearing mice we detected ß-gal activity *in vivo* over the tumor area.

Conclusions: Here, we successfully applied NIRF imaging to evaluate anti-Eag1 antibodies as tools for a novel concept of targeted cancer therapy. Since *in vivo* 62-gal 1) specifically binds to Eag1-expressing tumors and 2) shows measurable ß-gal activity at the tumor site, this conjugate can further be applied in the ADEPT for specific activation of cytotoxic prodrugs at the tumor site.

A novel [^{18}F] PET imaging agent for the epidermal growth factor receptor

P-096

Pisaneschi F. [1], Shamsaei E. [1], Nguyen Q.D. [1], Glaser M. [2], Robins E. [2], Kaliszczak M. [1], Smith G. [1], Spivey A.C. [1], Aboagye E.O. [1].

[1] Imperial College London, London, United Kingdom
[2] Medical Diagnostic Discovery (part of GE Healthcare), United Kingdom

f.pisaneschi@imperial.ac.uk

Introduction: The Epidermal Growth Factor Receptor (EGFR/c-ErbB1/HER1) is overexpressed in many cancers including breast, ovarian, endometrial and non-small cell lung cancer.[1, 2] An EGFR specific imaging agent could facilitate clinical evaluation of primary tumours and/or metastases.

Methods: We designed and synthesized a small array of fluorine containing compounds based on a 3-cyanoquinoline core.[3] The compounds were screened in vitro for their affinity in cell-free EGFR autophosphorylation assay and for their activity in the inhibition of the EGFR tyrosine kinase in EGFR overexpressing A431 cell lines.

Results: A lead compound, incorporating 2'-fluoroethyl-1,2,3-triazole was selected for evaluation as a radioligand based on its high affinity for EGFR kinase (IC_{50} = 1.81 ± 0.18 nM), good cellular potency (IC_{50} = 21.97 ± 9.06 nM), low lipophilicity and good metabolic stability. 'Click' labelling[4] afforded [^{18}F]-2'-fluoroethyl-1,2,3-triazole derivative in 7% end of synthesis (EOS) yield from aqueous fluoride in a total synthesis time of 3 h and >99% radiochemical purity. The compound showed good stability in vivo and a 4-fold higher uptake in A431 tumour xenografts relative to muscle. Furthermore, the radiotracer could be visualized in A431 tumour bearing mice by small animal PET imaging (NUV_{60} = 0.13±0.02).

Conclusions: The novel [^{18}F]-imaging agent constitutes a promising radiotracer for further evaluation for imaging of EGFR status.

Acknowledgement: This work was funded by Cancer Research UK programme grant C2536/A7602 and UK Medical Research Council core funding grant U.1200.02.005.00001.01.

References:

Bazley, L. A.; Gullick, W. J. Endoncr. Relat. Cancer 2005, 12, S17.
Marmor, M. D.; Skaria, K. B.; Yarden, Y. Int. J. Radiat. Oncol. Biol. Phys. 2004, 58, 903.
Wissner, A.; Overbeek, E.; Reich, M. F.; Floyd, M. B.; Johnson, B. D.; Mamuya, N.; Rosfjord, E. C.; Discafani, C.; Davis, R.; Shi, X.; Rabindran, S. K.; Gruber, B. C.; Ye, F.; Hallett, W. A.; Nilakantan, R.; Shen, R.; Wang, Y.-F.; Greenberger, L. M.; Tsou, H.-R. J. Med. Chem. 2003, 46, 49.
Glaser, M.; Årstad, E. Bioconjugate Chem. 2007, 18, 989.

POSTER

TARGETED THERAPY

P-097

Structural methods in subcellular image analysis

Dietlmeier J. , Whelan P.F. .

Centre for Image Processing and Analysis, Dublin, Ireland

julia.dietlmeier@ieee.org

Introduction: From a computer vision perspective subcellular imaging is an extremely complex and dynamic environment as can be inferred from Fig.1(a). Mitochondria form an important category of membrane enclosed, on average 200nm large organelles which reside inside every living cell. Mitochondrial morphology is crucial to the understanding of apoptosis mechanisms and the subsequent development of therapies targeting age- and cancer-related diseases[1],[2]. There is a high demand in automated segmentation which can provide an objective quantitative information in a reasonable time frame[2]. However, the state-of-the-art is dominated by manual tools. Early attempts to automate the segmentation are based on the machine-learning framework[3].

Methods: Instead of pursuing the machine-learning pathway we approach the segmentation and localization problem from the structural point of view which also has an appealing theoretical aspect. Here, we apply the well developed and widely acknowledged framework of Mathematical Morphology. Our multistage segmentation targets (i) specific challenges of image acquisition such as low contrast, non-uniform illumination and speckle noise; (ii) structural challenges such as cluttered scene, clustered and deformed mitochondria and deformed cristae.

Results: We outline our preliminary results by examining Fig.1. The first and the key step is localization which is based on the analysis of mitochondrial morphology. After extracting localiza tion markers we apply a seeded region grow algorithm which fills the inner-membrane space of each organelle, as can be seen in Fig.1(e). Gap-free control boundary is currently achieved by using morphological thickening and thinning operators on the binary image. In order to separate clustered mitochon-dria we apply a seeded watershed algorithm. The results of extracted sha-pes are provided in Fig.1(f)-(g). We verify that our segmentation works well on small-scale images containing a small number of mitochondria as can be seen in Fig.1(f)-(l). The other technique to obtain mitochondrial contour is recon-struction-by-dilation. Here, we correlate the localization markers with extracted contours in order to yield correct result.

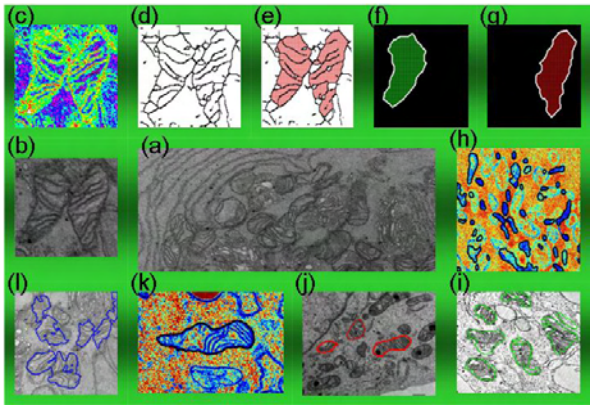

Fig.1 (a) TEM image of STS-treated DU-145 prostate cell. (b). Example of two clustered mitochondria. (c)-(l) Selected segmentation results.

Conclusions: The major challenge is firstly to extract the mitochondrial shape within reasonable accuracy. Secondly, we attempt to expand our detection approach to a larger scale problem such as the whole cell image. We plan to validate this on a larger representative mitochondria image database and in doing so compare our approach to existing machine-learning algorithms.

Acknowledgement: This research was supported by NBIP Ireland funded under the Higher Education Authority PRTLI Cycle 4, co-funded by the Irish Government and the European Union - Investing in your future. Special thanks to Royal College of Surgeons in Ireland (RCSI) for sample preparation and acquisition of TEM images. We would like to thank American Society for Cell Biology (ASCB) and Nature Publishing Group3 for the permission to use selected micrographs.

References:

1. Perkins GA et al; Methods in Enzymology. 456:29–52 (2009)
2. Sun MG et al; Nature Cell Biology. 9:1057–1065 (2007)
3. Narasimha R et al; Pattern Recognition. 42:1067–1079 (2009)

In vivo-post mortem multimodal image registration in a rat glioma model

Dubois A. , Boisgard R. , Jego B. , Lebenberg J. , Hérard A. S. , Dollé F. , Lebon V. , Delzescaux T. , Tavitian B. .

CEA-I2BM, Orsay, France

albertine.dubois@cea.fr

Introduction: Histological staining techniques can identify the regulation of specific biomarkers in small animal models of glioma and provide indicators of cellular dysfunction. The correlation of *in vivo* imaging signal changes and molecular indicators of tissue damage in histological brain sections represents an important means of understanding the cellular mechanisms responsible for these changes under pathological conditions. This requires an accurate image registration that can compensate the distortions that occur in the brain during the extraction, fixation, and staining process. Here, we present the preliminary results obtained by applying an overall registration strategy for the fusion of *in vivo* PET and MRI data with *post mortem* brain images in a rat 9L-glioma model.

Methods: Experiments were conducted on male Wistar rats. Twelve days after intrastriatal injection of 9L rat glioma cells, we acquired T2-weighted MRI and 60 min dynamic PET using [18F]DPA-714 [1] for *in vivo* evaluation of peripheral benzodiazepine receptor (PBR) expression. Following *in vivo* imaging, animals were euthanized. The entire brains were cut into 20 μm-thick coronal sections and processed for H&E staining and PBR immunohistochemistry. A blockface photograph was also recorded prior to each section. The overall co-registration strategy relied on using the blockface photographs as an intermediate reference, onto which the *in vivo* MRI and PET images and the digitized histo- and immunohistochemical brain sections were registered separately and superimposed so as to obtain *in vivo-post mortem* registration [2;3].

Results: By way of feasibility study, the co-registration strategy was only performed on one rat's right hemisphere. As illustrated in Figure 1, after each registration task, both the external contours, the outer edges of the cortex and inner structures such as the corpus callosum, the hippocampus, the striatum and even the tumor were correctly superimposed whatever the modality.

Conclusions: We obtained promising registration results of T2-weighted MRI and [18F]DPA-714 PET with *post mortem* brain volumes. Once results from additional animals had been provided, our approach could be used to evaluate, quantify and compare tumor volume, pharmacokinetic and physiological parameters (e.g. ligand differential uptake areas within the tumor) measured from *in vivo* MRI and PET data with those derived from corresponding *post mortem* histo- and immunohistochemistry.

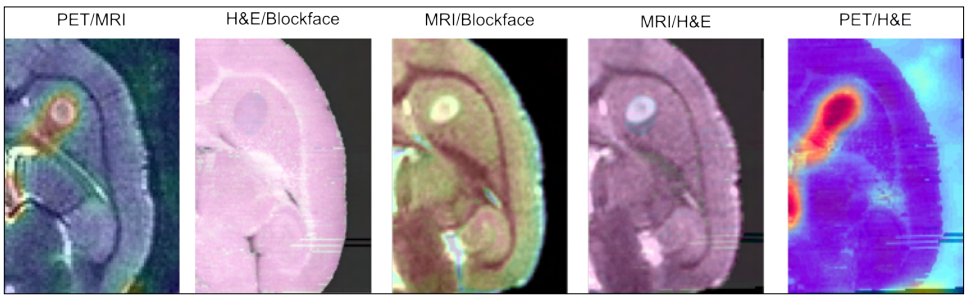

Fig1: Fusion of (A) PET (rainbow) and MRI (black and white), (B) Blockface (black and white) and H&E (pink) volumes, (C) MRI (black and white) and blockface volume (rainbow), (D) MRI (black and white) and H&E volume (pink) and (E) PET (rainbow) and H&E volume (black and white)

References:

1. Damont A et al; J label Compds Radiopharm. 51 (7): 286-292 (2008)
2. Dauguet J et al; J Neurosci Methods. 164 (1): 191–204 (2007)
3. Lebenberg J et al; Neuroimage. In press (2010)

P-099

Feasibility and success of Independent Component Analysis of resting state fmri data from the rat

Jonckers E. , Van Auderkerke J. , Van Der Linden A. , Verhoye M. .

Bio-Imaging Lab, Sint Lenaarts, Belgium

elisabeth.jonckers@ua.ac.be

Introduction: Resting state fMRI is used with growing interest with the purpose to spot age1 or pathology2 induced abnormalities in functional connectivity (FC) in the human brain. Only recently resting state FC measurements were acquired in rats3, opening the potential of assessing FC in the rat brain in several neuropathologies (e.g. schizophrenia). The human resting state networks are identified using a seed-based approach or independent component analysis (ICA)4. Since ICA analysis of resting state fMRI of rodents is up to now not published, we performed a pilot study, implementing the technique in rodents and testing the reproducibility of the ICA outcome.

Methods: A group of 5 male rats was imaged 4 times. On 2 time points with one week in between 2 consecutive resting state data were acquired using single shot gradient echo EPI. Rats were anesthetized with Medetomidine. Imaging was done on a 9.4T scanner using TR 2s and TE 16ms. 12 slices of 1 mm were acquired with a FOV of (3x3) cm and matrix size of 128x128. ICA was implemented on the dataset using GIFT (Group ICA of fMRI toolbox), working in matlab2008. The number of components for the ICA of the individual subjects or group (5 rats x 4 repetitions) was set at 15.

Results: The outcome of our ICA analysis, clearly revealed different brain regions within 10 of the 15 components. Figure 1 demonstrates 3 components of clearly functional different cortical regions.

Each ICA component was evaluated over the different time points. Mean components (for the 5 animals) were very reproducible both for measurements on the same day as measurements with one week in between. Also single subject components were similar over time. Although the differences are bigger between measurements with one week in between, indicating that there could be an influence of scanner variability and physiological state of the animal.

Fig 1: 3 Components resulting from ICA of rat resting state data. Colors representing z-values, higher z-values meaning a higher convergence between time course of the voxel and mean time course for the component.

Conclusions: This study implementing ICA on rat resting state data proves the usability of the technique for studying FC in the rat brain in a reproducible way. This paves the way to use this tool for assessing FC changes under different circumstances such as both physiological changes and pathologies. Implementing the technique in animal models can help to unravel the underlying processes.

References:

1. Damoiseaux JS et al (2008) Cereb Cortex. 18(8), 1856-1864.
2. Greicius MD et al (2004) Proc Natl Acad Sci U S A. 101(13), 4637-4642.
3. Pawela CP et al (2008) Magn Reson Med. 59(5), 1021-1029.
4. Beckmann CF et al (2005) Philos Trans R Soc Lond B Biol Sci. 360(1457), 1001-1013.

A fast and robust acquisition scheme for CEST experiments

Longo D. , Cittadino E. , Terreno E. , Aime S. .

University of Torino, Italy

dario.longo@unito.it

Introduction: Chemical Exchange Saturation Transfer (CEST) agents are a new class of MRI contrast agent based on the selective irradiation of a mobile proton pool in slow/intermediate exchange with water[1]. Long irradiation pulses at the resonant frequency (Δω) are needed to obtain a complete saturation of the CEST pool and a correct saturation transfer (ST%) quantification requires the acquisition of many images at different frequency offsets (Z-spectrum), thus making a CEST experiment a time-consuming procedure depending on the number of sampled frequency offsets[2]. A trade-off between the number of frequency offsets and the accuracy of ST% determination has to be found in order to distinguish the characteristic ST% time course for individual voxels. The development of fast and robust methods are therefore mandatory to correctly detect CEST molecules in Molecular Imaging applications.

In this work a computational procedure has been developed to evaluate the accuracy of ST% quantification as a function of the number of frequency offsets centered around the resonant frequency of the mobile proton pool with different levels of noise and of B_0 inhomogeneities. We also proposed a different acquisition procedure, by acquiring first a complete Z-spectrum followed by the sampling of a limited number of frequency offsets and then replacing these points in the first Z-spectrum, thus improving the temporal resolution of CEST contrast quantification, without sacrifying the ST% accuracy.

Methods: Z-spectra were simulated by using a two-pool model solving the Bloch equation (T_{1A}= 2 s, T_{2A}= 0.1 s, T_{1B}= 1 s, T_{2B} = 0.015 s, Δω = 4.2 ppm, k_{ex} = 160 s^{-1}, 30 mM diacest agent, saturation pulse 3 μT for 5 s). Gaussian noise was added both in the signal intensities and in the frequency axis and zero shifts were introduced in the range 0.1-1 ppm. Z-spectra were interpolated by smoothing spline (with zero shift correction) by different number of points around the resonant frequency (with step of 0.1 ppm) both at positive (Δω) and negative offsets (-Δω): i) 7 points, ii) 5 points, iii) 3 points, iv) 3 points with 0.2 ppm step, v) 1-(Δω/-Δω) (ON/OFF scheme) with and vi) without zero-shift correction, compared to a full Z-spectrum in the range ±10 ppm with steps of 0.1 ppm. In *in vivo* CEST images were acquired on a 7 Tesla Bruker spectrometer with a complete Z-spectrum (single-shot RARE spin-echo, TR 6 s, centric encoding, MTX 64, saturation pulse: 3 μT for 5 s) followed, upon injection of a CEST agent by the dynamic acquisition of only 3 points around the resonant frequency (Δω = 4.2 ppm) for 30 min (50 scans, temporal resolution: 36 s).

Results: The ON/OFF scheme with and without zero-shift correction showed the highest mean ST errors, up to 2 % and 5%, respectively and with high standard deviation values. The method iv) with 3 points spaced of 0.2 ppm, in comparison with the more accurate but also time consuming i) and ii) methods, displayed mean ST errors lower than 1%, but with a drastic reduction in acquisition time. In *in vivo* the continous acquisition of only 3 frequency offsets around the resonant frequency and the correction for zero shifts by using the pre-contrast Z-spectrum allowed to evaluate the ST% time course with a temporal resolution of few seconds and to discriminate between enhancing and not-enhancing pixels in kidneys.

Conclusions: The acquisition of 3 points spaced of 0.2 ppm around the resonant frequency of the mobile proton pool resulted to be sufficient enough to provide a robust and accurate ST% quantification, with a fast temporal resolution by using a modified Z-spectrum acquisition.

Acknowledgement: Economic support from regional government (NanoIGT project - CIPE 2007) and EC-FP7 project (ENCITE: FP7-HEALTH-2007A).

References:

1. Ward KM, et al.; J Magn Reson. 2000; 143: 79
2. Liu G, et al.; Magn Reson Med. 2009; 61: 399

P-101

Binding potential estimation in 11C-PE2I PET brain striatal images: impact of partial volume correction under segmentation errors

Maroy R. , Dusch E. , Comtat C. , Leroy C. , Trebossen R. .

CEA, Orsay, France, Metropolitan

renaud.maroy@cea.fr

Introduction: Numerous methods have been proposed for the correction of the Partial Volume Effect (PVE) that hampers striatal PET studies. While their quantification accuracy is known for most, their ability to recover correct pharmacokinetic parameters in case of segmentation errors is less clear. The work proposes to compare the binding potential estimations using 4 distinct Time Activity Curve (TAC) estimation methods.

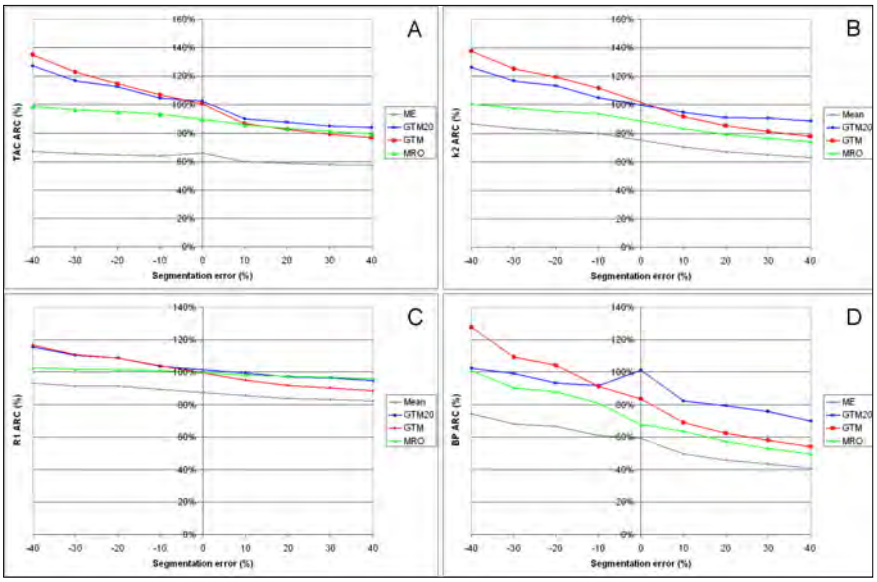

Methods: A phantom based on the Zubal phantom of a 11C-PE-2I PET exam with kinetics generated using the simplified tissue model of Lammertsmaa[1] (R1=1.28, k2=.09, BP=17) was analytically simulated on a ECAT HRRT (Siemens, 2.4mm intrinsic resolution). PET images were reconstructed with 1.2 1.2 1.2mm^3 voxels and 20 frames using both RM-OP-OSEM[2], which compensate for PVE, and OP-OSEM.

Twenty realizations of caudate segmentations containing errors ranging between 40% volume underestimation (-40%) and 40% volume overestimation (40%) were defined[3]. Four TAC estimation methods were compared for the caudate: the mean TAC measurement in the standard OP-OSEM image (ME) and in the RM-OP-OSEM image (MRO), the Geometric Transfer Matrix method (GTM) and an improved GTM[3] method using voxel selection (GTM20). The R1, k2 and binding potential (BP) estimated with the estimated TACs using[1] were compared based on the Apparent Recovery Coefficient (ARC).

Results: Unlike k2 and R1, the BP is globally underestimated by the methods. The lowest performances are obtained without correction, using ME. The best ARC for the TACs (Fig 1.A) and R1 (Fig 1.C) are achieved using MRO, but the use of MRO leads to suboptimal BP (Fig 1.D), which is the model parameter of major interest. The best ARC for BP and k2 (Fig 1.B) are achieved using GTM20, which provides better TACs than GTM, leading also to better ARC than GTM.

Conclusions: Our improved GTM method with voxel selection achieves the TAC estimation in terms of binding potential and k2 recovery.

References:

1. A A Lammertsma et al. Neuroimage, 1996
2. F C Sureau et al. JNM, 2008
3. R Maroy et al. SNM, 2009

Automated quantification scheme based on an adapted probabilistic atlas based segmentation of the brain basal nuclei using hierarchical structure-wise registration

Maroy R. [1], Leroy C. [1], Douaud G. [2], Trebossen R. [1].

[1] CEA, Orsay, France, Metropolitan
[2] Radcliffe Hospital, Oxford, United Kingdom

renaud.maroy@cea.fr

Introduction: The work proposes: 1) a new basal ganglia segmentation method based on probabilistic atlas construction and compared to manual segmentation, 2) a validation method for segmentation of structures using a co-acquired PET image.

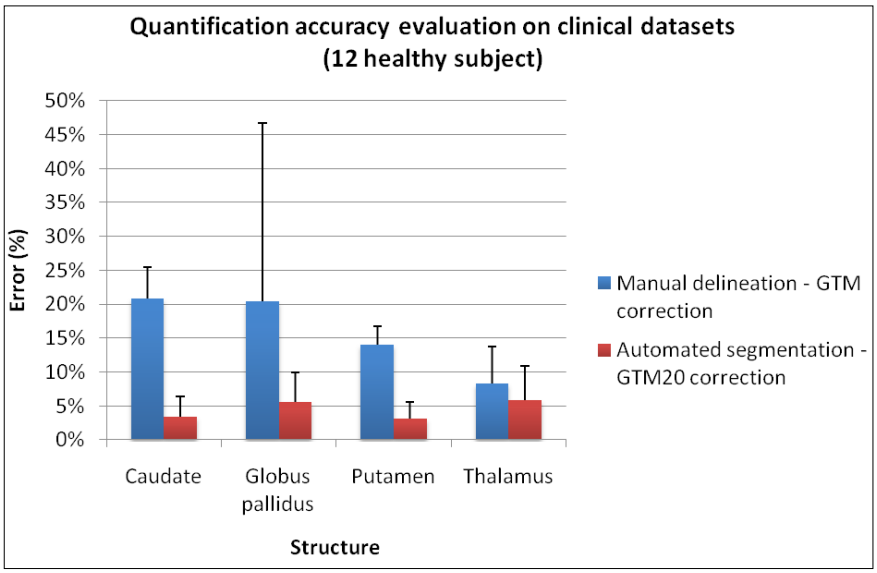

Methods: T1 MRI (T1) and 18F-PEII PET images were acquired in 12 healthy adults and co-registered. The PET images, acquired on the HRRT PET system, were reconstructed with both the AWOSEM (NoPSF) and the 3D-OP-OSEM PSF (PSF) methods. The basal nuclei were segmented manually in a knowledge base (KB) of 24 T1 and in the 12 acquired subjects T1 (IS). A probabilistic atlas adapted to IS was constructed using a structure-wise hierarchical registration of each KB image on IS. Segmentation was obtained simply through atlas probability maximization.

A GTM correction was applied on the NoPSF using as spatial domain 1) the manually drawn structures or 2) the automatically drawn structures, with A) ROI defined as in [Frouin, 2002] or B) with adequate selection of 20% (GTM20) of the corresponding spatial domain voxels. The estimated values were compared for 1)+A) and 2)+B) to the mean TAC in PSF, considered as the reference, inside manually drawn eroded regions using the estimation error (E).

Results: GTM20 performed significantly better than GTM for both the manual and automated delineation. Besides, the gain using together the automated segmentation and GTM20 (E1)+A)/E2)+B)) was 6.1 for the caudate, 3.6 for the globus pallidus, 4.6 for the putamen and 1.4 for the thalamus for an increased reproducibility.

Conclusions: We have proposed a quantification scheme using an adapted probabilistic atlas based segmentation of the basal nuclei and a partial volume correction method that enhances both the precision and the reproducibility of the PVE corrected measures.

POSTER

MI DATA ANALYSIS METHODS

P-103

VHISTdiff - comparing workflow histories (VHIST/VINCI)

Vollmar S. , Hüsgen A. , Sué M. , Nock J. , Krais R. .

Max Planck Institut for Neurological Research, Köln, Germany

vollmar@nf.mpg.de

Introduction: VHIST [1] has been developed to document workflows in multi-modality imaging (however, it is not at all limited to this field). The VHIST file format is PDF compatible and it can be displayed with any PDF viewer ("human readable"). However, VHIST files also contain structured information on each workflow step (embedded XML) suitable for automated processing. In one current project, we are integrating VHIST into VINCI [2], our package for visualization and analysis of tomographical data. This enables us to natively create VHIST files which can store meta data of original file formats, filter operations, "image arithmetics" and registration parameters.

Methods: An interesting application of VHIST files is the comparison of workflow histories belonging to similar but subtly different image data, e.g. image data of one subject which has been aquired by the same scanner but which has been processed in a different way (type and order of filter steps; thresholding; application of masks; different types of normalization, different reconstruction parameters; different approaches when converting raw data). For this kind of comparison we are currently developing a new tool, *VHISTdiff*, which allows to automatically find corresponding workflow steps and report the differences.

The figure depicts a graphical representation of the "macroscopic" differences between two VHIST files (A.vhist, B.vhist) as they were found by the VHISTdiff algorithm: each tree represents the workflow history of one image. Dotted lines denote corresponding workflow steps, white text marks workflow steps that do not have a pendant. VHIST files can contain other VHIST files: in this example, the registration step of the A-tree contains file C.vhist, and likewise D.vhist is contained in the other registration step. The report of differences between corresponding workflow steps (e.g. different filter parameters) are not part of this particular graphical representation which has been rendered fully automatically using Graphviz [3].

VHISTdiff's algorithm uses some ideas of the traditional UNIX *diff* command for comparison of text files. However, the concept has been generalized to tree structures: VHISTdiff uses Dijkstra's algorithm [4] to optimize a cost function which favours association strings of similar workflow steps.

Outlook: First results of this new tool look promising. We will investigate strategies to define cost functions that try to be useful for a wide range of real-world use cases.

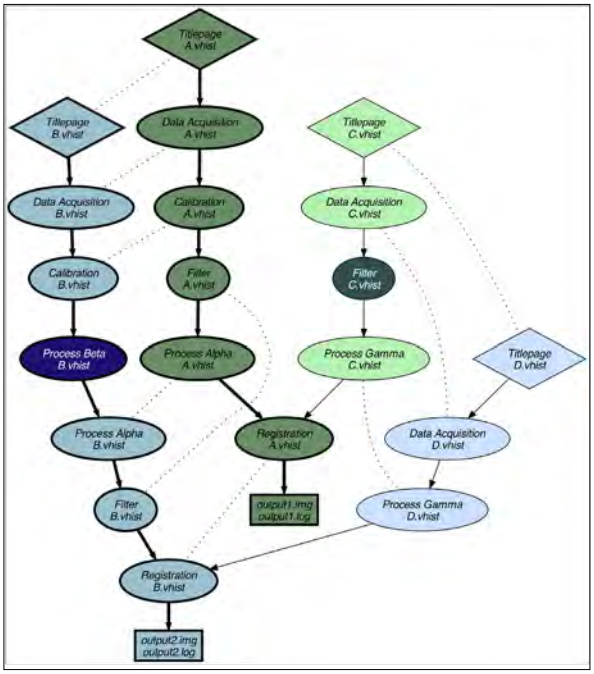

References:

1. VHIST, http://www.nf.mpg.de/vhist
2. VINCI, http://www.nf.mpg.de/vinci
3. The Graphviz software package, http://www.graphviz.org
4. Dijkstra, E. W. (1959). "A note on two problems in connexion with graphs". Numerische Mathematik 1: 269–271

Fast matrix-free method for fluorescence imaging

Zacharopoulos A. [1], Garofalakis A. [2], Ripoll J. [1], Arridge S. [3].

[1] FORTH IESL , Heraklion, Greece
[2] CEA, I2BM , France
[3] UCL CS, United Kingdom

azacharo@iesl.forth.gr

Introduction: In non-contact Fluorescence Molecular Tomography, the large number of measurements poses a challenge since the reconstruction methods used rely on the inversion of a derivative operator and the explicit formulation and storage of this operator in a matrix is generally not feasible. We test a matrix-free method that addresses the problems of large data sets and reduces the computational cost and memory requirements for the reconstructions. More specifically we challenged the Matrix-Free method with in-vivo measurements from mice where fluorescence tubes of different but controlled concentrations are inserted, to assess the quantification performance of the method.

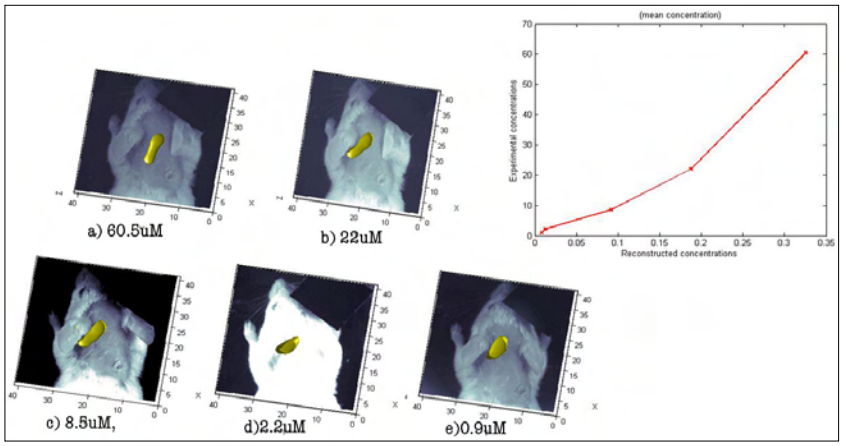

Methods: Our approach initially presented in [1], is based on a formulation of the diffusion approximation for the fluorescence case and the TOAST Image Reconstruction in Optical Tomography FEM package, [2] and uses a matrix free formulation. The explicit calculation and storage of the Jacobian is avoided by replacing it by a vector times matrix operator and a vector times adjoint matrix operator. Since we wanted to assess the quantification properties of the matrix-free method we aquired in-vivo measurements using a balb/c mouse where capillary of Alexa Fluor 647 of controlled concentrations a)60.5uM, b)22uM, c)8.5uM, d)2.2uM and e)0.9 uM. was inserted hypodermically in the ventral side. For the reconstructions, a slab-like geometry of dimensions 41mm x 41mm x 12mm was used with 5733 nodes and 4800 voxel-elements. For the optical parameters we assumed μa =0.06 mm-1 and μs =1. mm-1 for the 615nm excitation and μa =0.05 mm-1 and μs =1.5 mm-1 for the 700nm emission wavelengths. We set 1458 detectors positions by sampling the images, which for the 36 sources created two vectors of 48285 measurements each.

Results: The results for the five different experiments are presented as iso-surfaces in 3D in the figure where the white light image of the mouse is rendered in the background as a reference. The average time for the reconstruction was 50sec, in a Pentium 2Ghz machine with 2GB of memory.

Conclusions: Using the Matrix-free method we managed to reconstruct for the positions of the fluorescent tubes and a relative quantification accuracy and sensitivity. More specifically the algorithm demonstrated an almost linear response between the controlled concentrations and the reconstructed ones.

Acknowledgement: This work was funded by the EC Seventh Framework Grant, FMT-XCT, grant 201792.

References:

1. Zacharopoulos A, et al (2009) Opt. Express , 17, 3042--3051.
2. Arridge R S (1999) Inverse Problems, 15, 41--93 .

TOPIC: Cancer Biology

P-105

PET and MRI studies applied on characterization of Fisher/F98 rat glioma model

Valtorta S. (1), Ronchetti F. (2), Lo Dico A. (3), Politi L.S. (4), Masiello V. (5), Matarrese M. (5), Zara G. (6), Zenga F. (7), Scotti G. (4), Mauro A. (2), Moresco R.M. (5).

(1) Università degli Studi di Milano; IBFM-CNR, Segrate, Italy
(2) Istituto Auxologico Italiano, Italy
(3) San Raffaele Scientific Institute; IBFM-CNR; L.A.T.O., Italy;
(4) San Raffaele Scientific Institute, Italy;
(5) San Raffaele Scientific Institute; IBFM-CNR; Università degli Studi di Milano-Bicocca, Italy;
(6) Università di Torino, Italy;
(7) Università di Brescia, Italy

silvia.valtorta@unimi.it

Introduction: Preclinical brain tumor models have provided a wealth of information on the biology, imaging and experimental therapeutics of brain tumors[1],[2]. The aim of our study is characterized Fisher/F98 rat glioma model using Positron Emission Tomography (PET) and Magnetic Resonance (MR) analysis to set up an experimental model useful to study the efficacy of new colloidal vectors for chemotherapy.

Methods: Syngenic rat brain-glioma models (Fisher/F98) was obtained by stereotactic (x=2; y=5; z=3) implantation of different cell concentrations (10^2, 10^3, 10^4 and 10^5). To monitor tumor growth progression, rats underwent once a week Gadolinium enhanced T1-MRI studies followed by [^{18}F]FDG PET studies, starting from 7 days after surgery. A group of animals performed also [^{18}F]FAZA PET studies to evaluate regional tissue hypoxia. To improve quantification, PET and MRI images were fused using PMOD 2.7 software. Max radiotracers uptake was calculated for tumor, frontal cortex, cerebellum and background using region of interest (ROI) analysis. Radioactivity concentration values expressed in MBq/g were then transformed into percentage of injected dose per gram of tissue (%ID/g). Moreover, histological analysis of proliferation, apoptosis, differentiation, neoangiogenesis and hypoxia markers were performed.

Results: Mean survival time of rats injected with 10^4 and 10^5 cells was nine days. One week after surgery, MRI revealed a rapid growth that reached 0.11 cm^3 mean tumour volume. Animals injected with 10^3 and 10^2 cells showed a mean survival time of 18 and 24 days respectively. In rats injected with 10^3 cells, tumor was revealed 14 days after surgery at MRI and [^{18}F]FDG PET and successively tumors rapidly increased. Disease course in 10^2 cells injected rats was slower. Tumors were characterized by high [^{18}F]FDG uptake and hypoxic subareas which only partially overlapped. Hypoxic areas were mainly localized in correspondence to Gd-enhanced regions whereas hyper glucose metabolic areas were localized in the outer part of the tumors. At histological analysis tumoral masses showed an infiltrative pattern of growth and moderate neoangiogenesis. Tumors obtained at animals death showed diffused necrotic areas. HIF1 was clearly expressed by glial and neuronal cells in oedematous and hypoxic areas.

Conclusions: Our study indicates that Fisher/F98 rat glioma model reproduce s the characteristic of aggressiveness of human glioblastoma. Tumor was characterized by high glucose metabolism and by hypoxic sub-areas. The concentration of 10^2 cells permits to better monitor disease onset and progression and to plan experiments to test new anti-neoplastic therapies efficacy.

Acknowledgement: This work was supported in part by grants from: Regional AIRC 2008 n°6278 and FIRB-CNR n°RBIP06M8ZA.

References:

1. Spaeth N et al; Eur J Nucl Med Mol Imaging. 33:673-682 (2006)
2. Brioschi AM et al; J Nanoneurosci. 1:65-74 (2009)

TOPIC: Cancer Biology

Non-invasive "E2F sensing" system for monitoring DNA damage alteration induced by BCNU

P-106

Monfared P.[(1)], Rudan D.[(1)], Viel T. [(1)], Waerzeggers Y.[(1)],Hadamitzky M.[(1)], Schneider G.[(1)], Rapic S.[(1)],Neumaier B.[(1)], Backes H.[(1)], Winkeler A.[(1)], Jacobs A.H..[(1,2).]

[(1)]Max Planck Institute for Neurological Research, Cologne,
[(2)]European Institute for Molecular Imaging (EIMI), University of Muenster, Germany

Parisa.Monfared@nf.mpg.de

Introduction: Imaging transcriptional regulation of endogenous genes in living animals using noninvasive imaging techniques provide a clear perception of normal and cancer-related biological processes. Radiolabeled reporter probes and PET imaging can be translated into human studies in the near future. In our preliminary study, the endogenous expression of E2F, a gene that affects several important biological processes, has been imaged *in vivo* with bioluminescence imaging. A retroviral vector, Cis-E2F/LUC-IRES-TKEGFP, was generated by placing the reporter genes under control of an artificial cis-acting E2F-specific enhancer element. Following retroviral transduction of tumor cells in established xenografts, DNA damage induced alteration of E2F transcriptional activity, which correlated with the expression of E2F-dependent downstream genes as assessed by biolumencsnce imaging.

Aim: To verify whether the *cis*-reporter system (Cis-E2F/LUC-IRES-TKEGFP) is sufficiently sensitive to image endogenous transcriptional gene regulation by [^{18}F] FHBG PET imaging.

Methods: U87dEGFR-E2F-LITG cells were injected subcutaneously in nude mice and the development of the tumours was followed by Multimodal imaging. Two weeks after implantation, bioluminescence imaging, FLT and FHBG were performed before and 24h after treatment with low and high doses of BCNU.

Results: Here, we validate the utility of [^{18}F]FLT-PET to image proliferation rate of the tumor in response to DNA damage and compare with [^{18}F] FHBG uptake which is associated with E2F transcriptional activity. In keeping with in *vitro* findings, after 24 h post-treatment, low dose of BCNU induced an increase in [^{18}F]FHBG uptake as compared to non-treated mice. However, with high dose of BCNU [^{18}F]FHBG uptake decreased in E2F xenografts. [^{18}F]FLT accumulation in E2F xenografts decreased with low and high doses of BCNU at 24 and 48 hours. Quantitative changes in tumor [^{18}F]FLT uptake were associated with decreased tumor proliferation and tumor [^{18}F]FHBG uptake correlated with transcriptional gene regulation of E2F in response to DNA damage

Conclusions: We show the utility of [^{18}F]FHBG-PET to image DNA damage induced by BCNU and shown the tumor-specific activity of E2F. We propose that these types of reporter systems, will allow a detailed insight into the kinetics of cell cycle control and for the development of new cell cycle targeted molecular therapies.

Acknowledgement: This work is supported in part by the EC-FP6 European DiMI, (LSHC-CT-2004-503569) LSHB-CT-2005-512146 and Clinigene (LSHB-CT-06-018933).

POSTER

LATE BREAKING

TOPIC: Neuroimaging

P-107

Multi-tracer PET imaging of a mouse model of Alzheimer´s disease to assess microglial activation related to ageing and anti-inflammatory treatment

Rapic S.[1], Backes H.[1], Viel T.[1], Hadamitzky M.[1], Monfared P.[1], Rudan D.[1], Vollmar S.[1], Neumaier B.[1], Hoehn M.[1], Van der Linden A.[2], Heneka M.T.[3], Jacobs A.H.[1,4]

[1]Max Plank Institute for Neurological Research, Cologne, Germany
[2] Bio-Imaging Lab, University of Antwerp, Belgium
[3]Department of Neurology, University of Bonn, Germany
[4]European Institute for Molecular Imaging (EIMI)

Sara.Rapic@nf.mpg.de

Introduction: Alzheimer´s disease (AD), the leading cause of dementia in elderly people, is characterized by the deposition amyloid-β plaques in the brain surrounded by activated microglia. Activated microglia play an important role in amyloid clearance but also secrete pro-inflammatory molecules that lead to chronic neuroinflammation, and toxins that trigger cell death cascades in neurons, both eventually resulting in neurodegeneration. The nuclear peroxisome proliferator-activated receptor gamma (PPAR-γ) plays an important role in inflammatory processes. Agonists that bind and activate PPAR-γ, suppress inflammation by inhibiting the expression of pro-inflammatory molecules at transcriptional level. Determination of the contribution of neuroinflammation to the progression of AD can provide new insights in the development of therapy.

Aim: To assess with in vivo positron emission tomography (PET) whether microglial activation is correlated with age in APP/PS1 transgenic mice and wild-type mice and if anti-inflammatory treatment with a PPAR-γ agonist can reduce neuroinflammation.

Methods: Multi-tracer micro-PET imaging was performed in 13 months old $APP_{Swe}/PS1_{dE9}$ transgenic mice (n = 5) and C57BL/6J wild type mice (n = 7). Dynamic imaging was performed after intravenous injection of [^{11}C]PK11195, a radioligand for the translocator protein-18 kDa which is upregulated in activated microglia and [^{18}F]FDG for the quantification of cerebral glucose metabolic rate. [^{18}F]Fluoride bone imaging was performed after every scan for co-registration purposes. The animals were imaged at baseline and treated for 4 weeks with a PPAR-γ agonist. Right after treatment and 4 weeks off treatment, all animals were investigated again using the same imaging protocol to assess the effect of the therapy.

Results: Preliminary results show that uptake of [^{11}C]PK11195 is upregulated in transgenic mice compared to wild-type mice in the cortex (SUV of 75.15 and 57.20 respectively), thalamus (SUV of 78.90 and 63.63 respectively) and cerebellum (SUV of 82.12 and 65.47 respectively). Uptake of [^{18}F]FDG in transgenic mice is elevated as well, compared to wild-type mice, in the cortex (SUV of 162.10 and 106.78 respectively), thalamus (SUV of 172.07 and 115.33 respectively) and cerebellum (SUV of 166.50 and 114.46 respectively). Data were corrected for the total injected dose (ID). First image processing of the data obtained after treatment shows decreased brain retention of both tracers in transgenic mice.

Conclusions: The higher uptake of [^{11}C]PK11195 in the brain of transgenic mice compared to wild-type mice indicates the presence of activated microglia, suggesting neuroinflammation of the Alzheimer brain. Reduction of [^{11}C]PK11195 brain retention after treatment with the PPAR-γ agonist reflects its anti-inflammatory effect.

With the help of animal models for Alzheimer's disease and in vivo molecular imaging, longitudinal detection of microglial cells is made possible and may be of vital importance in defining their role in the progression of the disease and in the development of therapeutic strategies.

Acknowledgement: This work is supported in part by EC-FP6-project and DiMI LSHB-CT-2005-512146.

GE Healthcare

Discover GE's pre-clinical imaging solutions for your biomedical research and drug development process. Our offering in PET, SPECT and CT based on all new full digital APD-PET and CZT-SPECT detector technologies will enable you to:

- Quantify and visualize drug distribution and transport over time with SPECT and PET.
- Measure the delivery and action of agents. Lower the cost and the time of drug development.
- Validate animal models in weeks instead of months
- Verify your compound hits the target in-vivo with longitudinal studies.
- Establish dosing and kinetics in longitudinal studies
- Use clinically relevant imaging biomarkers to validate efficacy longitudinally

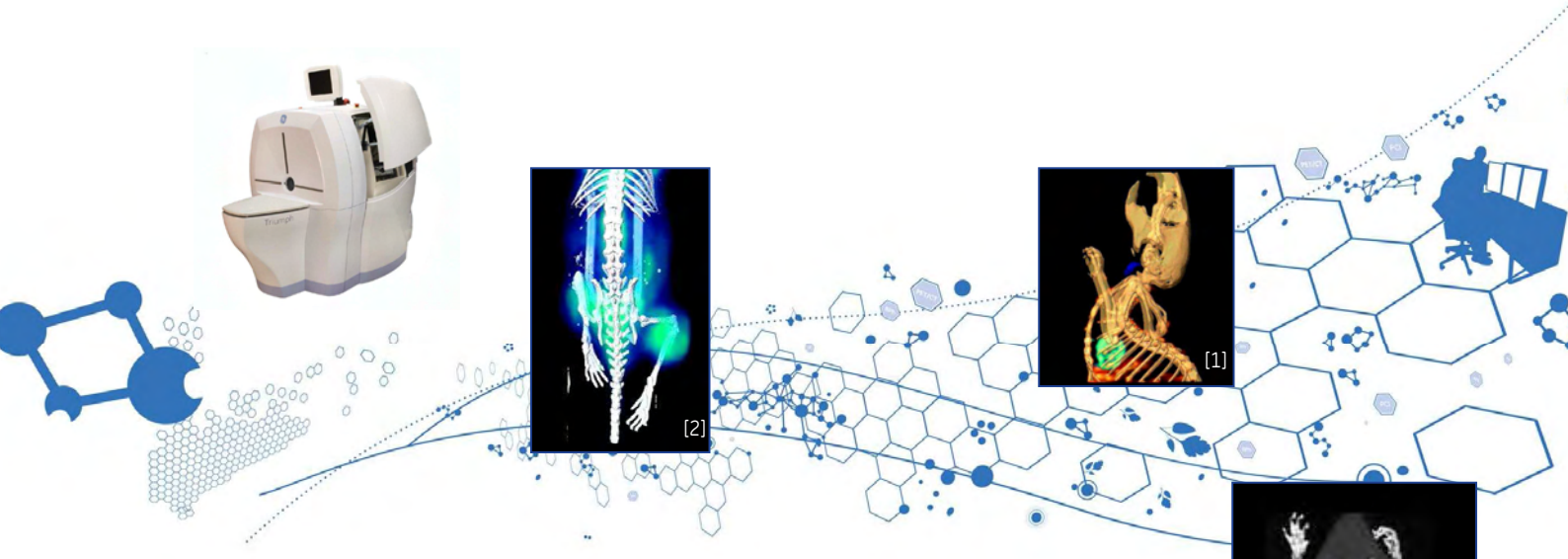

[2]

[1]


[3]

[1] Image courtesy of Timothy Doyle, Ph.D., Stanford University, USA
[2] Image courtesy of Prof. S. Staelens, Prof. S. Vandenberghe, and Dr. W. Ceelen Ghent University - IBBT Ghent, Belgium
[3] Image courtesy of Dr. P. Choquet Hôpital de Hautepierre, Strasbourg, France

GE imagination at work

index

INDEX

ANIMASCOPE

High TECHNOLOGY for High TRANSPARENCY

- **High Technology for High Transparency**
  - Non invasive imaging technologies
  - Small animals Preclinical imaging
  - Multimodality imaging services (Ultrason, MRI, Optical, PET, SPECT, CT Scan)
- **Reduce, Refine, Replace**
  - Quantitative, Precise, Predictive
  - Reduces experimental Artifacts
  - Longitudinal Studies - Reduce Animal Usage (minus 70-80%)
  - Reduction and Refinement of animal works are Cost and Time-effective on R&D
- **Bridge the gap between preclinical and clinical research**
  - **Drug Delivery and Liberation** (drug to target)
  - **Efficacy**, **Safety**, **Pathology** (desiderable and undesirable effects)
  - **Ligand-Target** interaction (receptors, enzymes, transporters) including **Dose Occupancy** relationships
  - **Dynamic Biodistribution and Kinetics**
- **One stop shop for :**
  - biology,
  - cardiovascular,
  - cell therapy, gene therapy, immunization,
  - musculoskeletal,
  - neurology, nephrology,
  - oncology,
  - reproduction, development,
  - nutrition (nutraceuticals, dietary supplements and functional food).

Give to your study a new look

Contact : Daniel CHRISTIAEN
ZI EUREKALP 38660 St Vincent de Mercuze (F)
d.christiaen@animascope.eu
Tel +33 (0)476 97 94 87
www.animascope.eu

Index

M

N

O

P

Q

R

S

230

ESMI/DiMI management office
c/o MPI for neurological research
Gleueler Str. 50
50931 Köln

T ++49 2 21 4 78 8 72 44
++49 2 21 4 78 8 79 60
E office@e-smi.eu

Layout: Doris Kracht
Binding and Printing: Hundt Druck GmbH